



HYBRID NANOSTRUCTURED SUPPORTS FOR MAGNETIC HYPERTHERMIA- MEDIATED ACTIVATION OF ENZYMES.

A DISSERTATION SUBMITTED TO THE
UNIVERSIDAD DE LA REPUBLICA
FACULTAD DE QUIMICA

AUTHOR

MSc. SONALI CORREA

ADVISORS

DR. LORENA BETANCOR

(Laboratorio de Biotecnología, Universidad ORT, Uruguay)

DR. VALERIA GRAZÚ

(Instituto de Ciencia de Materiales de Aragón (ICMA), CSIC/Universidad de Zaragoza, España)

ACADEMIC SUPERVISOR

DR. LAURA FRANCO FRAGUAS

(Área de Bioquímica, DepBio, Facultad de Química)

2019

Resumen

La nanobiotecnología se ha beneficiado recientemente del uso de nanobiocatalizadores inmovilizados aplicados a la biorremediación, bioprocesos sintéticos y biomedicina, entre otros campos. La integración enzimática en materiales híbridos permite capitalizar las ventajas sinérgicas de los diferentes materiales estructurales para mejorar las propiedades del biocatalizador. En esta tesis, hemos estudiado la síntesis de nanopartículas nanohíbridas [silica biomimética + nanopartículas magnéticas (MNPs)] como un vehículo de peroxidasa de rábano picante (HRP) para su uso en la terapia dirigida de profármacos de enzimas (DEPT). DEPT usa enzimas exógenas introducidas artificialmente en el cuerpo con el objetivo de convertir profármacos en su forma activa en el sitio deseado del organismo y, por lo tanto, tiene una ventaja sobre las terapias estándar no específicas por su selectividad potencial. El uso de enzimas encapsuladas o unidas a nanopartículas (NPs) ha ganado interés en este tipo de terapia ya que permite mejorar la estabilidad y reducir la inmunogenicidad de la enzima terapéutica, a la vez que mejorar la bioacumulación y retención de la enzima en el tejido tumoral. Esto es debido al efecto de retención y permeabilidad aumentada (EPR) por la presencia de una abundante vascularización inmadura en el tumor que hace que de forma pasiva se acumulen mayor cantidad de NPs que en tejidos sanos. Por tanto, las enzimas terapéuticas transportada por NPs tienen una mayor facilidad en acumularse en tejidos tumorales que la misma enzima administrada en forma libre. Sin embargo, las NPs no pueden evitar la distribución no selectiva en el cuerpo, sobre todo en órganos que para filtrar la sangre también usan el efecto EPR (hígado, bazo)., Por lo tanto, el uso exitoso de modalidades de DEPT que utilicen nanomateriales como vehículos de la enzima terapéutica depende de la implementación de estrategias que puedan proporcionar un control espaciotemporal sobre su actividad enzimática.

Para esto, en esta Tesis se ha optimizado la co-encapsulación de MNP junto con la enzima terapéutica HRP en nanopartículas de sílica biomimética. Se eligió HRP debido a su capacidad para convertir el ácido indol-3-acético (hormona vegetal) en radicales peroxilados con actividad citotóxica en varias líneas celulares tumorales. Sin embargo, la HRP tiene una temperatura óptima de 45°C y a la temperatura corporal su actividad biocatalítica no es máxima. Debido a que las MNPs pueden absorber energía en presencia de un campo magnético alterno externo (AMF) y liberarla al medio ambiente en forma de calor, nuestra hipótesis de trabajo se centra en lograr utilizar este calor para

alcanzar la temperatura óptima de la HRP de forma localizada (en una escala nanométrica), y así incrementar su actividad enzimática. Tradicionalmente, el desencadenar el aumento macroscópico de la temperatura de tejidos tumorales ha sido la estrategia más difundida para utilizar el gradiente muy alto de temperatura que se genera por calentamiento magnético en pocos nanómetros desde la superficie de las MNPs. Esto ha permitido el desarrollo de una nueva terapia para el tratamiento del cáncer, conocida como hipertermia magnética (MHT), ya que las células tumorales tienen una mayor sensibilidad al calor que las células normales. En esta Tesis sin embargo proponemos aprovechar este gradiente de temperatura localizado alrededor de las MNPs no para desencadenar que se eleve de forma macroscópica la temperatura de un tejido tumoral sino para modular la actividad de enzimas co-entrapadas con las MNPs en nanohíbridos de sílica biomimética.

El uso de sílica biomimética en el nanohíbrido se planteó bajo la premisa de utilizar un medio para estabilizar la enzima, que permita su probable inmunoaislación y, como se demostró más tarde, alcanzar a su vez un posible efecto de aislamiento térmico que disminuya la rápida disipación de calor que ocurre a pocos nm de la superficie de las MNPs y así sea posible modular la actividad de enzimas que no se encuentren unidas a la superficie de las MNPs. Es así que efectivamente la estrategia de co-encapsulación facilitó un aumento selectivo en la actividad biocatalítica de HRP al alcanzar localmente su temperatura óptima. Para llegar a esta conclusión, hemos optimizado la síntesis de los nanohíbridos variando diferentes parámetros tales como: i) tamaño del catalizador aminado requerido para la formación de NP de sílica (polietilimina MW ~ 1300, 2000, 25000, 60000 Da), ii) metodología de inmovilización de la HRP (adsorción / unión covalente en MNP antes de la encapsulación, co-encapsulación con MNP), iii) relación HRP/ MNP. La inmovilización de HRP y los rendimientos de actividad después del atrapamiento son similares con o sin MNP ($\sim 60 \pm 4\%$ y 78 ± 1 , respectivamente). Sin embargo, la estabilidad térmica de la enzima (50°C) aumentó 532 (Factor de estabilización) cuando la HRP se co-encapsula con MNP. El uso de PEI de diferentes tamaños no afectó los rendimientos de la inmovilización de HRP ni el tamaño (diámetro hidrodinámico) de los híbridos. Sin embargo, las MNP parecen actuar como plantillas para la deposición de sílice ya que su co-encapsulación con HRP reduce el tamaño radio de los biohíbridos (de ~ 800 -1000 a 500-600 nm). Todos los nanohíbridos obtenidos pudieron oxidar IAA, pero no se observó citotoxicidad en

ausencia del profármaco usando diferentes líneas celulares. También hemos estudiado el efecto del tamaño del catalizador aminado requerido para la formación del nanobiocatalizador (polietilenimina MW ~ 1300, 2000, 25000, 60000 Da), en su eficiencia de calentamiento magnético macroscópico (SAR, Specific Absorption Rate o tasa de absorción específica) y nanoscópico (activación enzimática). Los nanohíbridos (500-600 nm) mostraron activación enzimática (250-300%) sin un aumento significativo de la temperatura macroscópica y conservaron su actividad completa después de la aplicación de un ciclo de AMF (829 kHz, 25.2 mT) durante 20 min. Sin embargo, para que los nHs desarrollados puedan tener potencial para ser utilizados en DEPT es clave que presenten buena estabilidad coloidal en medios biológicos complejos. Para ello fue necesario bloquear grupos amino primarios presentes en la superficie de los mismos con glucosa. Este monósacaríido no solo permitió mejorar la estabilidad coloidal de los nHs en medio de cultivo completo, pero también sirve de biomolécula para vectorización activa de células tumorales. Los nanohíbridos funcionalizados con glucosa lograron diferencias significativas en la reducción de la viabilidad celular de una línea celular de cáncer de colon humano (HCT-116) después de la exposición a un ciclo de AMF (80% versus 30% de reducción en controles sin aplicación de AMF). Estos resultados muestran por primera vez que es posible controlar de forma remota la actividad de HRP co-atrapada con MNP mediante calentamiento magnético para una potencial aplicación en terapia antitumoral DEPT.

Acknowledgements

It takes two flints to start a fire and, in this case, they are my advisors Dr. Lorena Betancor and Dr. Valeria Grazú who kept the flame ablaze for the past five years.

First and foremost, I want to thank my advisor Dr. Lorena Betancor who has introduced me to the world of enzymes, biocatalysis and nanoparticles. I came to Universidad ORT intending to join her group, for two primary reasons: the areas of research in which she was involved, and what I had read about her. I have not been disappointed in either regard. It has been an honour to be her Ph.D. student. I truly appreciate her contributions of time, ideas and funding to make my Ph.D. experience industrious and inspiring. The joy and enthusiasm she has for research is absolutely infectious and motivational, and even through the toughest times she stood by me. I am grateful for the exceptional example she has set as a successful woman and researcher.

I would also like to thank my advisor Dr. Valeria Grazú, who has taught me about the world of magnetic nanoparticles and cellular oncology. Her unique style and contagious laughter always brightens up even the dullest of days. I truly appreciate all the invaluable time she has put in and hours of brain-wracking to ensure the best possible results. Her ambition, enthusiasm and passion for research is a quality I very much admire.

Together they are a force to reckon with. The both of you have been a tremendous mentor for me. I would like to thank you for encouraging me and for allowing me to grow as a research scientist. Your advice on both research as well as on my career have been vital in the development of my character.

I would like to thank my Academic tutor Laura Franco for her help from the very beginning and being ever so kind. Because of the research environment sustained by Prof. Lorena and Prof. Valeria, I have crossed paths with many graduate and post-graduate students and postdocs who have influenced and enhanced my research. I would like to thank Carlos Sanguinetti for accepting me as part of his team at Laboratory of Biotechnology. I would like to thank the all my colleagues at the who have borne with me through the initial moments when my Spanish was incomprehensible and for having patience and learning to understand me.

I would like to thank the BioNanoSurf group in Zaragoza, for all the memorable times and for welcoming me. It was a pleasure being part of the group though it was short one.

My parents, they did provide me with more than just my genetic material, after all. My interest in science started early in my life, when my mother would take me to the laboratory with her and show me the wonders of the microbiological world. And my father who would explain the side effects of pharmaceutical drugs (clearly, they had my career planned out). They encouraged and educated me in ways both straightforward and devious. I owe them everything.

Finally, I would like to thank my fiancé, Alejandro, who ensured that I had a home to come to when I arrived. When life threw curve balls at me his love and support has made it a lot easier for me to move on and I'm grateful for what we have. His faithful support during the final stages of this Ph.D. is so appreciated. I would like to thank his family for making me part of theirs and for showing interest in my work and encouraging me. And to all the people who have made my life here complete with their never-ending love and support.

Abstract

Nanobiotechnology has recently benefited from the use of a number of immobilized nanobiocatalysts applied to bioremediation, synthetic bioprocesses and biomedicine among other fields. Enzyme integration in hybrid materials capitalizes the synergic advantages of the structural builders for improved biocatalyst properties. In this thesis, we have studied the synthesis of nanohybrid nanoparticles (biomimetic silica + magnetic nanoparticles (MNPs)) as a vehicle of horseradish peroxidase (HRP) for its use in Directed Enzyme Prodrug Therapy (DEPT). DEPT uses foreign enzymes artificially introduced in the body with the aim of converting prodrugs into their active form at the desired site of the organism and therefore has an edge over standard non-specific therapies for their potential selectivity. However, nanoparticles cannot avoid unselective distribution in the body and consequently, the successful use of DEPT depends on the implementation of strategies that could provide spatio-temporal control over the activity of the therapeutic enzyme. For this, the co-encapsulation of MNPs together with HRP in biomimetic silica nanoparticles has been optimized. HRP was chosen because of its ability to convert indole-3-acetic acid (IAA) (vegetable hormone) into peroxy radicals with cytotoxic activity in several tumour cell lines. However, HRP has an optimum temperature of 45°C and at body temperature the biocatalytic activity is not at its maximum. MNPs can absorb energy in the presence of an external alternating magnetic field (AMF) and release it to the environment in the form of heat¹. This property has led to the development of a therapy for the treatment of cancer, known as magnetic hyperthermia (MHT) since tumour cells have a higher sensitivity to heat which makes them more susceptible than normal cells². In this thesis, we proposed that the heat generated by AMF is used to locally reach an optimal temperature that triggers the activity of the therapeutic enzyme. The use of biomimetic silica in the nanohybrid provided a means to stabilize the enzyme, putative immuno-isolation and as later proved, a thermal insulated effect that decreased heat loss and allowed for modulation of the enzymatic activity. Therefore, the co-encapsulation strategy facilitated a selective increase in HRP biocatalytic activity by reaching locally its optimum temperature. To arrive to this conclusion we have optimized the synthesis of the nanohybrids by varying different parameters such as: *i*) size of the required aminated catalyst for the formation of silica nanoparticles (polyethyleneimine MW~1300, 2000, 25000, 60000 Da), *ii*)

HRP immobilization methodology (adsorption/covalent binding onto MNPs before encapsulation, co-encapsulation with MNPs), *iii*) HRP/MNPs ratio. HRP immobilization and activity yields after entrapment are similar with or without MNPs ($\sim 60 \pm 4\%$ and 78 ± 1 , respectively). However, the enzyme thermal stability (50°C) showed a stabilization factor (SF) of 532 when HRP was co-encapsulated with MNPs. The use of PEI of different sizes did not affect the yields of HRP immobilization neither the hydrodynamic size of the NPs. However, MNPs seem to act as templates for silica deposition as their co-encapsulation with HRP reduces the hydrodynamic radius of the biohybrids (from ~ 800 - 1000 to 500 - 600 nm). All the obtained nanohybrid NPs were able to oxidize IAA but in the absence of the prodrug cytotoxicity using different cell lines was not observed. We have also studied the effect of the size of the required aminated catalyst for the formation of the nanobiocatalyst (polyethyleneimine MW ~ 1300 , 2000 , 25000 , 60000 Da), on their magnetic heating efficiency (SAR and enzyme activation). The nanohybrids (~ 500 - 600 nm) showed enzyme activation (250 - 300%) without a significant rise of the “overall” temperature and preserved their full activity after application of an AMF (829 kHz, 25.2 mT) for 20 min. Surface engineered nanohybrids, for better colloidal stability in cell culture media, achieved significant differences in the reduction of cell viability of a human colon cancer cell line (HCT-116) after the exposure to the AMF (80% versus 30% reduction in controls). Our results demonstrated that it is possible to remotely increase the activity of HRP co-entrapped with MNPs.

General Introduction

Surgery, chemotherapy and radiotherapy are currently the most used strategies in the treatment of cancer, a disease whose worldwide incidence and mortality had risen to 18.1 million new cases and 9.6 million deaths in 2018. In turn, these numbers will increase considerably over previous projections as 27.5 million new cases of cancer are expected each year by 2040 (61.7% increase from 2018)³. Recent investigations on cancer treatment gravitate towards the use of alternative therapies that overcome the problem of classical ones *viz.* insufficient concentration of the drug at the tumour site, limited biodistribution, systemic toxicity, lack of selectivity or differentiation between cancer and normal cells, and development on cancer therapy resistance⁴. Among those alternative therapies, strategies modelled on the use of enzymes and prodrugs, known as directed enzyme prodrug therapy (DEPT) gives enzyme therapy an edge over standard non-specific therapies for their potential selectivity. DEPT uses foreign enzymes artificially introduced in the body with the aim of converting prodrugs into their active form at the desired site of the organism. DEPT strategies may allow to reduce the systemic toxicity of drugs, being produced mainly at the site of interest which could potentially increase its selectivity and minimize unwanted side effects^{5,6}. Moreover, DEPT presents an amplifying effect since a single enzyme can activate many prodrug molecules which enables high drug concentrations in the tumour area generating cell death on adjacent tumoral cells (bystander effect) with no need of enzymatic internalization⁷. However, the success of this therapeutic approach depends on a highly selective delivery vehicle for the enzyme to the tumour site that ensures sufficient binding of enzymes to targeted cells.

Differently from the sole use of the therapeutic enzyme or the direct attachment of the enzyme to vectorizing agents (ex. antibodies, lectins), enzyme encapsulation emerged as an approach that improves accumulation and retention of the therapeutic enzyme within the tumour⁸. The size of the particles generated by encapsulation is advantageous for exploiting the well-known enhance permeability and retention (EPR) effect that provokes the accumulation of particulates due to a combination of fenestration in the vasculature and poor lymphatic drainage from tumours⁹. Additionally, immunoisolation provided by encapsulation aids the treatment by decreasing the clearance of

the enzyme from plasma, also a known cause of low concentrations of the enzyme at the tumour site. Last but not least, encapsulation improves proteolytic stability preserving the enzyme activity *in vivo* and provides a means to generate high volumetric activity nanocomposites¹⁰. It also provides a cover shell that may serve as a surface for anchoring active targeting agents such as glucose, folic acid, antibodies, etc, that could potentially improve the interaction with target cells.

Nevertheless, nanoparticles cannot avoid non-selective distribution. Particularly, liver/spleen accumulation is a predominant problem of therapeutic nanovehicles as fenestration in endothelial cells is the mechanism to remove foreign material in a similar manner to the EPR effect¹¹. Therefore, therapy activation outside the target site is unavoidable when using encapsulated enzymes, as mesophilic enzymes that are highly active at body temperature, are the choice for DEPT. The implementation of strategies that could provide spatio-temporal control over the activity of the therapeutic enzyme through external stimuli is, therefore, a new ground-breaking concept to surpass the current paradigm in DEPT¹².

MNPs can absorb energy in the presence of an external alternating magnetic field (AMF) and release it to the environment in the form of heat. This effect is called magnetic hyperthermia (MHT) and has emerged as a potential treatment for cancer. The main mechanism in hyperthermia is the ablation of tumour cells by destroying the protein and cell structure by heat which results in the shrinkage of the tumour size. Hyperthermia (HT) in different approaches has been combined with radiotherapy during the last decades, however, its implementation as a clinically relevant treatment has been restricted by its inability to effectively and preferentially target malignant cells. The importance of an effective and homogenous delivery of hyperthermia is highlighted by the fact that even half a degree rise in temperature can have a significant impact on cell viability¹³. The temperature reached is influenced by evident factors such as duration of the HT, frequency and force of the field. However, it is also affected by inherent properties of the NPs such as size, shape, functionalization or integration of MNPs into other materials. HT is not restricted to cell ablation for cancer treatment as it can be also utilized as an external stimulus to trigger drug payload release from nanocarriers¹⁴, as a mean of biosensing¹⁵ and biocatalysts control¹⁶.

In this thesis, we have studied a new strategy based on magnetic heating to increase the activity of an encapsulated therapeutic enzyme to gain spatio-selectivity control that could serve for a more effective DEPT treatment. For that, we have co-encapsulated horseradish peroxidase (HRP) and MNPs in biomimetic silica under the hypothesis that the heat generated by AMF could be used to locally reach an optimal temperature that triggers the activity of the therapeutic enzyme. HRP was chosen because of its ability to convert indole-3-acetic acid, a vegetable hormone, into peroxy radicals with cytotoxic activity in several tumour cell lines¹⁷. HRP has an optimum temperature of 45°C and therefore at body temperature the biocatalytic activity is not at its maximum. The selected co-encapsulation strategy could facilitate a localized “on and off” modulation of HRP activity by locally reaching its optimum temperature when the AMF is applied.

Therefore, the general hypothesis of this thesis is that a new material based in silica, MNPs and an entrapped HRP will be able to increase the activity of the immobilized enzyme after AMF application for the conversion of a pro-drug into its active form.

In order to achieve our objective, we have conducted a methodological approach and obtained results that have been divided in this work in three different chapters:

In chapter I, an introduction to the world of biocatalysis and directed enzyme prodrug therapy (DEPT) was covered with a focus on the development of a stable, efficient and versatile nanohybrid for its use in nanomedicine. The process for solely physically entrapping the enzyme through different immobilization strategies that involved pre and post modifications were applied in order to co-entrap the enzyme with MNPs within a biomimetic material, in turn enhancing the stability, reusability and efficacy of the enzyme compared to the soluble enzyme.

In chapter II, we characterised the nanohybrids with an aim to understand the physico-chemical properties, magnetic behaviour, surface properties and the ability to bioconvert a prodrug into toxic radicals. It focused on the applicability of the MNPs in nanomedicine combined with biocatalysis.

In chapter III, we studied the cytotoxicity of the nHs in the presence of prodrug on the viability of the two different cancerous cell lines. Following which the effect of hyperthermia mediated cytotoxicity was studied in a selected cell line.

Abbreviations

°C- degree Celsius

µg-Microgram

µL- microliters

Abs-Absorbance

ABTS - 2,2'-azino-bis (3-ethylbenzothiazoline-6-sulphonic acid)

AMF-Alternating Magnetic Fields

BET-Brunauer-Emmett-Teller

cm- centímetros

Da- Dalton

DEPT- Directed Enzyme Prodrug Therapy

DLS-Dynamic Light Scattering

DMEM- Dulbecco's Modified Eagle Medium

DNA-Deoxyribonucleic acid

EDC-1-Ethyl-3-(3-dimethylaminopropyl) carbodiimide

EDX-Energy Dispersive X-Ray Analysis

ESEM-Environmental Scanning Electron Microscopy

f - Frequency

FBS-Fetal Bovine Serum

GA-glutaraldehyde

H-Gauss Magnetic field

h-Hour

HAADF-High-Angle Annular Dark-Field Imaging

HPLC-High Performance Liquid Chromatography

HRP- Horseradish peroxidase

HRTEM-High-resolution transmission electron microscopy

HT-Hyperthermia

IAA-Indole-3-acetic acid

IONPs-Iron oxide Nanoparticles

IU-International unit for enzyme

kDa- kilo Dalton

kHz-kilo Hertz

M-Molar

mg-Milligram

MHT-Magnetic hyperthermia

min-Minute

mM-Millimolar

MRI- Magnetic Resonance Image

mT-milliTesla

mV-MilliVolt

MW-Molecular weight

nH-Nanohybrid

NHS-N-hydroxysuccinimide

nm-Nanometer

NP- nanoparticle

PAA-Poly-aspartic acid

PDI-Polydispersity Index

PEI-Polyethyleneimine

RNA-Ribonucleic acid

RT-Room Temperature

SAR-Specific Adsorption Rate

SF-Stabilization Factor

Si-Silica

SLP-Specific Loss Power

SNP-Silica NanoParticle

SPIONs-Superparamagnetic Iron Oxide Nanoparticles

SQUID-Superconducting Quantum Interference Device

STEM-Scanning Transmission Electron Microscopy

TMOS-Tetramethyl orthosilicate

XRD-X-Ray Powder Diffraction

ZP-Zeta Potential

$\mu\text{mol}/\text{min}$ – micromol per minute

Table of Contents

Resumen.....	2
Acknowledgements.....	5
Abstract.....	7
General Introduction.....	9
Abbreviations.....	12
<u>Chapter 1: Introduction</u>	20
Enzymes as nanobiocatalysts.....	20
Strategies for the immobilization of enzymes.....	22
Biomimetic silica as a support for enzyme immobilization.....	23
Post-immobilization modifications in enzyme immobilization.....	24
General properties of the enzyme horseradish peroxidase.....	24
Mechanism of action.....	26
Magnetic Nanoparticles (MNPs) in biocatalysis and biomedicine.....	29
Hybrid materials for enzyme immobilization.....	31
Objective.....	32
Specific Objectives.....	32
Materials and Methods.....	33
Materials.....	33
Methods.....	33
Determination of HRP activity.....	33
Oxidation of HRP.....	33
Immobilization strategies.....	34
Entrapment of HRP in biomimetic Si nanoparticles.....	34
Cross-linking with glutaraldehyde (GA).....	35
Immobilization of HRP onto MNPs.....	35
Covalent three-dimensional immobilization of the entrapped HRP.....	36
Co-entrapment with magnetic nanoparticles.....	36
Co-entrapment with in-house laboratory synthesised MNPs.....	37
General procedures for nHs characterization.....	37
Kinetics parameters of the nHs and free enzyme.....	37
Temperature profile of the nanoabiocatalysts.....	38
pH stability analysis of the nanobiocatalysts.....	39
Thermal Stability of the nanobiocatalysts.....	39
Reuse of nanohybrid by magnetic separation.....	40
Results and discussion.....	41
Co-entrapment of enzyme and MNPs within biomimetic silica.....	45

Characterization of the nHs	49
Effect of pH on the activity and stability of the nHs.....	49
Thermal stability of the nHs	50
Repeated uses of the nHs	52
Kinetic parameters of free and encapsulated HRP.....	53
Conclusions.....	54
<u>Chapter 2: Chapter Summary</u>	56
Introduction.....	57
Biomedical application of nanomaterials.....	57
Magnetic nanoparticles	59
SPIONs and magnetic Hyperthermia.....	62
Bioconversion of pro-drugs: Oxidation of IAA by HRP	64
Objective	68
Specific Objectives	68
Materials and Methods.....	69
Physicochemical characteristics of the nanohybrids (nHs).....	69
Analysis using Environmental Scanning Electron Microscopy (ESEM).....	69
Dynamic Light Scattering (DLS) and Z-potential measurements.....	69
Analysis using Scanning Transmission Electron Microscopy (STEM).....	69
Analysis using Transmission Electron Microscopy (TEM) and EDx.....	69
Porosimetry by Brunauer-Emmett-Teller (BET) Surface Area	70
Physical characterization of the nHs.....	70
Alteration of the order during synthesis.....	70
Inertisation of surface of nHs with Glucose.....	70
Magnetic characterization of the nHs	71
Analysis using Superconducting Quantum Interference Device (SQUID).....	71
Quantification of Fe in the nHs.....	71
Analysis the Specific absorption rate (SAR).	72
Activation of the enzyme using hyperthermia.	72
Thermal stability of the enzyme using hyperthermia.....	73
Biochemical characterization of the nHs	73
HPLC analysis of the conversion of 3-IAA by HRP.	73
Results and Discussion	74
Analysis using Scanning Electron Microscopy (SEM) and Dynamic Light Scattering (DLS)	74
Analysis using Transmission Electron Microscopy (TEM), Scanning Transmission Electron Microscopy (STEM) mode and EDX.....	78

Quantification of Fe in the nHs.....	79
BET surface analysis.....	80
Inertisation of the surface with Glucose 1 M.....	81
Bioconversion of the pro-drug by nHs.....	84
SQUID analysis	85
Analysis of Specific absorption rate (SAR).....	87
Activation of the enzyme using hyperthermia.	90
Stability with HT.....	92
Conclusions.....	93
<u>Chapter 3: Chapter Summary</u>	95
Introduction.....	96
Cancer and hyperthermia	96
Molecular mechanisms involved in cellular damaged triggered by Hyperthermia	97
<i>In vitro</i> and <i>in vivo</i> effects of Magnetic Hyperthermia.....	101
Other Therapeutic Strategies based on the non-conventional use of Magnetic Heating. ..	104
Gaining Spatio-Temporal over DEPT by Magnetic Heating.....	106
Objective.....	107
Specific Objectives	107
Materials and Methods.....	108
Materials	108
Methods	108
Cell viability studies of different concentrations of nHs using MTT in HaCat, HCT116 and HT29 cell lines.....	108
HPLC analysis of the adsorption of IAA on BSA	109
nHs-mediated cell cytotoxicity using MTT assay.....	109
Hyperthermia-mediated cell cytotoxicity.....	110
Statistical analysis.....	111
Fixation and Dehydration Protocol for TEM analysis	111
Results and Discussion	112
Cell Cytotoxicity Studies at Different Concentrations Of nHs.....	112
Cytotoxicity in the presence of nHs and the prodrug.....	115
Cell cytotoxicity mediated by magnetic heating.....	122
Conclusions.....	128
References.....	133
Acknowledgments.....	152
<u>Annexe of Theoretical basis of techniques: Dynamic Light Scattering</u>	155
Zeta Potential	157

SEM	158
TEM	160
Superconducting QUantum Interference Devices (SQUIDs)	161
Specific Power Absorption	163
Publications	166
Book Chapters	166
Cellulose-Based Nanosupports for Enzyme Immobilization	166
<i>In situ</i> immobilization of enzymes in biomimetic silica	166
Paper	166
Design of stable magnetic hybrid nanoparticles of Si-entrapped HRP	166

Chapter 1

Development Of A Hybrid Nanobiocatalyst Of HRP

Introduction

Enzymes as nanobiocatalysts

The use of enzymes as catalysts offers several advantages compared to classical organic-chemical synthesis. As enzymes are highly substrate- selective the formation of unwanted side products can be reduced or even prevented and cost- intensive purification processes can be simplified. Moreover, as enzyme reactions mostly occur in aqueous media, preferring mild reaction conditions, their application can be a substantial contribution to green and sustainable production processes.¹⁸ Therefore, enzymes are biocatalysts with outstanding prospects as catalysts in industrial and biomedical processes^{19,20} They also provide advantages over the use of microorganisms as biocatalysts, such as greater specificity, better standardization, easy handling and storage and are independent of bacterial growth rates. However, there are many drawbacks that impede their practical use such as lack of long-term operational stability and shelf-storage life and their unwieldy or impossible recovery and re-use. Scientists have developed several strategies to overcome these drawbacks among which integration of enzymes to different materials stand out as one of the most widespread²¹. The possibilities for practical applications of immobilized enzymes are continuously growing and a steady number of immobilization methods have been recently developed to preserve the activity of biotechnologically important enzymes in unnatural environment^{22,23,24,25}.

Enzyme association to insoluble materials, commonly called as enzyme immobilization, provides a number of advantages to the applied use of enzymes: immobilized enzymes can be reused, it minimizes costs and time of analysis, it facilitates the continuous use of the biocatalyst and may improve enzyme properties such as operational or thermal stability^{26,27}.

A wide variety of techniques are now available for the preparation of immobilized enzymes that may include chemical or physical mechanisms, addition of aiding agents during immobilization or combination of different strategies to obtain more active and stable preparations²¹. Moreover, investigations on material science have contributed

with a plethora of new supports compatible with enzyme activity, with better physical and mechanical properties. Such is the case of nanosupports, rapidly adopted for enzyme immobilization as they reduce diffusion limitations and maximize the functional surface area to increase enzyme loading. Active immobilized enzymes in nanomaterials, also known as nanobiocatalysts, have been studied for a wide variety of applications in biosensing and biotransformations²⁸. As intensive research in these fields developed, it became clear that integration of the enzyme to the different materials and through different interactions affected significantly the performance of the nanobiocatalysts while they impact aspects such as stability, storage, reusability in industrial and biomedical applications (**Table 1**)²⁹.

Table 1. Summary of enzyme immobilization techniques investigated showing their advantage, disadvantages, and various applications²¹. Adapted from Homaei, A. A *et al.*

Immobilization Principle	Advantages	Disadvantages	Applications	References
Deposition on solid	Retaining most of its activity	Low enzyme loading	Inversion of carbohydrates	30
Immobilization on polyketone by hydrogen bonds	Easy immobilization, high binding capacity, high stability	Negligible increase in Km value	Applicable for large enzyme viz peroxidases, amine oxidases	31
Classic covalent immobilization	Moderately stable to hydrolysis at neutral pH	Esters unstable in aqueous solutions	Immobilization of antibodies, proteases and oxidases	32, 33
Physical entrapment	Avoid negative influence on enzyme surface, thermally and mechanically stable	Diffusion and partition of substrate and product is restricted	Applicable for most enzymes, antibodies and development of biosensor	34
Adsorption on mesoporous silicates	Support is chemically and mechanically stable and resistant to microbial attack	Variable pore size preparation in harsh conditions causing denaturation of enzyme	Scaffold of mesoporous carbon materials	35, 36
Immobilization using affinity tag	In-situ immobilization possible	Low activity	Capture of proteins during purification in affinity chromatography	37
Immobilization on biodegradable polymers	Longer circulation in blood stream	Low entrapment efficiencies, burst release and instability of enzyme	Biomedical control release for enzyme replacement therapy	38
Encapsulation with lipid vehicles	High reproducibility	Enzyme inactivation by shear force	Medical, biomedical, enzyme replacement therapy, ripening process	39

Strategies for the immobilization of enzymes

Organic solvents and harsh conditions in biotechnological applications result in the deactivation or denaturation of the enzyme which significantly reduces the catalytic activity and enzyme efficiency. Enzyme stability is one of the most important requisite for a potential biocatalyst and stabilization may be achieved by medium engineering, chemical crosslinking, protein engineering or enzyme immobilization⁴⁰. When using

immobilization, the main goal is to develop an enzyme compatible support, to provide a higher surface area to increase the enzyme loading, achieve high stability and reusability of the biocatalyst with a simple and mild methodology. In principle, enzymes are immobilized via three major routes: *(i)* binding to a support; *(ii)* encapsulation or entrapment⁴⁰; or *(iii)* cross-linking⁴¹.

A wide variety of techniques are now available for enzyme attachment to a variety of supports^{42,43,44}. Immobilization techniques generally include chemical or physical mechanisms. Chemical immobilization methods mainly include enzyme attachment to the matrix by covalent bonds or other interactions and cross-linking between the enzyme and the matrix. Physical methods involve the entrapment of the enzymes within an insoluble matrix. A combination of chemical and physical methods has facilitated in certain occasions for the immobilization of different enzyme species in the same composite^{45,46,47,48}. The requirements of different enzymes are inherently varied and specific conditions are often needed for a defined application. Unfortunately at the present time, although *in silico* tools may help predict a certain behaviour of an enzyme towards a support, there is no generic method for enzyme stabilization that will be optimal for all enzyme systems, but a toolbox of versatile methodologies are now well documented in the literature⁴⁸.

Biomimetic silica as a support for enzyme immobilization

Physical entrapment is defined as an irreversible method of enzyme immobilization where enzymes are entrapped in a support or inside of fibres, either the lattice structure of a material or in polymer membranes that allows the substrate and products to pass through but retains the enzyme⁴⁹. Physical entrapment in biomimetic silica can yield nanostructured material with divergent morphologies within minutes under mild and green conditions. The use of silaffin proteins by unicellular diatoms, has inspired several studies to identify alternate aminated molecules as candidates for inducing silica precipitation from precursor compounds *in vitro*⁵⁰. The influence of templates in silica biomineralization has been studied *in vitro* using biological and nonbiological molecules⁵¹. The use of biomimetic silica has various advantages such as it is a mild and fast reaction wherein the formation of the nanoparticles takes place within minutes and under neutral pH and ambient temperatures. Due to its rigid structure it provides stability and enables the reuse of enzyme. Any material contained in the synthetic

mixture may become entrapped within the biomimetic Si nanoparticles⁵⁰⁻⁵³. The mild synthetic approach (room temperature, neutral pH, free of organic solvents) is compatible with a range of enzymes for which the strategy has also resulted in stabilization⁵⁴⁻⁵⁶. Moreover, for biomedical applications such as enzyme replacement therapies or direct enzyme prodrug activation, encapsulation of enzymes in a Si nanocarrier could reduce the immunogenicity of the enzyme. However, synthetic strategies for biomimetic Si nanobiocatalysts are not universal as they provide distinct properties to different enzymes and may be tailored to improve a desired attribute⁵⁷.

Post-immobilization modifications in enzyme immobilization

Chemical modification of enzymes after immobilization such as chemical cross-linking is a widely used strategy to gain stability of insoluble biocatalysts as well as reduce enzyme leakage overcoming a common problem in non-covalently attached enzymes to supports⁴¹. The enzyme is generally immobilized onto a support and then cross-linked with a bifunctional agent such as glutaraldehyde (GA) or a polymer⁵⁸. In particular, GA may react with different enzyme moieties, mainly involving primary amino groups of proteins, although it may eventually react with other groups (thiols, phenols, and imidazoles)⁵⁹. This approach can improve the enzyme stability.

General properties of the enzyme horseradish peroxidase.

The enzyme horseradish peroxidase (HRP) (E.C. 1.11.1.7), found in the roots of horseradish, is a plant grown in the temperate regions of the world mainly for the culinary value of its roots. It is a metalloenzyme with many isoforms, of which the most studied type is C. It contains a heme group and uses hydrogen peroxide to oxidize a wide variety of organic and inorganic compounds. The production of this enzyme from the roots of horseradish occurs on a large scale because it is widely used for commercial purposes, for example as a component of clinical diagnostic kits and in immunoassays⁶⁰.

A variety of physiological roles have been assigned to the horseradish peroxidase isoenzymes, including 3-indole acetic acid metabolism, lignification, cross-linking of cell wall polymers, suberin formation and resistance to infections^{61,62,63}. However, very little is known about their specific functions in the plant.

Welinder K. determined the dominating HRP amino acid sequence of HRP which constituted of a single polypeptide chain of 308 amino acids with a molecular mass of 33890 Da⁶⁴. The N-terminus is blocked by a pyroglutamate residue and peptides at the C-terminus can occur with or without the C-terminal serine residue. The enzyme also contains a heme prosthetic group, eight carbohydrate side chains and two calcium ions, so the total molecular mass is close to 44,000 Da⁶⁴.

From literature, it is known that HRP exists as group of distinctive peroxidase isoenzymes which are classified into three major groups- acidic, neutral and basic, depending on their respective isoelectric points. The most abundant isoenzyme, HRP-C, has a neutral pI, and accounts for more than half of peroxidase activity in horseradish roots and is used in most clinical and analytical applications⁶⁰. This was confirmed by Maehly 1955 wherein the isoelectric point was determined to be 7.2⁶⁵. From the general enzyme database, the pI of HRP isoenzymes depends on the species it is derived from and thus can vary between 3.0–9.0.

As mentioned above, eight of the nine potential N-glycosylation sites that can be recognized in the primary sequence of the enzyme are occupied. The total carbohydrate content of the HRP depends on the source from which the enzyme is obtained and typically varies between 18 and 22%⁶⁰.

The three-dimensional structure of HRP C, reported by Gajhede M. et al.⁶⁶, was elucidated by X-ray crystallography using crystals of the recombinant enzyme produced in *E. coli*, in its non-glycosylated form. The structure of the enzyme is constituted mainly by α -helices, with a small region of β sheets (**Fig. 1**). Two domains are distinguished, distal and proximal, among which is the heme group. The HRP has an active centre in which a heme b group (protoporphyrin IX) is found as a prosthetic group, to which the metal cation Fe^{3+} and two Ca^{2+} ions are coordinated; together, they are essential for the functional and structural integrity of the enzyme^{60,67}.

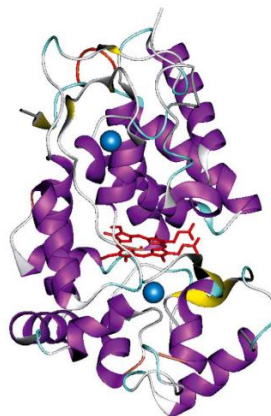
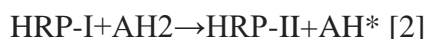
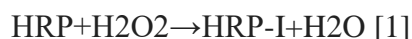


Figure 1. Three-dimensional representation of the X-ray crystal structure of horseradish peroxidase isoenzyme C (Brookhaven accession code 1H5A).

The heme group (coloured in red) is located between the distal and proximal domains which each contain one calcium atom (shown as blue spheres). α -Helical and β -sheet regions of the enzyme are shown in purple and yellow, respectively. The F0 and F00 α -helices appear in the bottom right-hand quadrant of the molecule.⁶⁰

Mechanism of action

Majority of the reactions catalysed by HRP can be expressed according to the reaction presented in the following equations:



Wherein, AH_2 y AH^* represent a reducing substrate and its radical product.

HRP catalyses the oxidation of a large variety of substrates in the presence of H_2O_2 which include reducing substrates such as aromatic phenols, acid phenols, indoles, amines and sulfonates. The detection of HRP activity is widely used in marking systems and a variety of procedures have been developed for that purpose. Although H_2O_2 is the natural substrate of HRP, several reducing molecules are available that can be used to monitor enzymatic activity. The reaction is a three-step cyclic process, in which the enzyme is first oxidised by H_2O_2 and then reduced back to the native form in two

sequential steps involving the formation of two enzyme intermediates, Compounds I and II. In the first step, the cleavage of the H_2O_2 molecule, results in the concomitant production of water and incorporation of one of the oxygen atoms of H_2O_2 into Compound I. Compound I contains two oxidising equivalents and an iron(V) state compared to the native enzyme and Compound II one equivalent. It is now known that Compound I contains an oxoferryl group ($\text{Fe}^{\text{IV}}=\text{O}$), in which the iron is in +4 oxidation state, and a porphyrin p-cation radical⁶⁹.

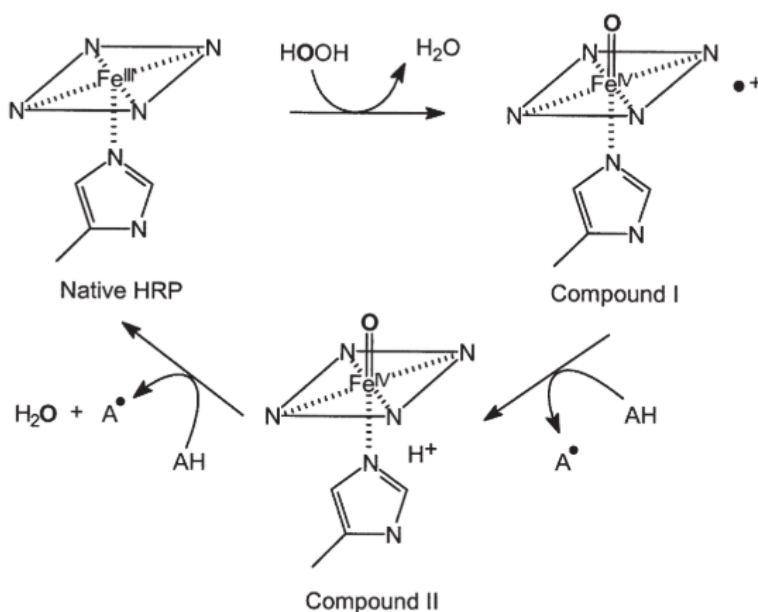


Figure 2. Reaction cycle of HRP, showing the enzyme intermediates, Compounds I and II⁶⁹. Adapted from Azevedo, A. *et al*

Compound I is now capable of reducing a variety of substrate molecules (AH equation and Fig) by transferring a single electron. The π -cation radical is first discharged, leading to the formation of the second enzyme intermediate, Compound II. Compound II, with an oxoferryl group ($\text{Fe}^{\text{IV}}=\text{O}$), undergoes a single electron reduction by the second substrate (AH) to a native ferric enzyme. The ferryl iron returns to its ferric state, whereas the oxygen accepts two protons to form a water molecule and is released from the heme⁶⁹.

H_2O_2 is the usual oxidizing substrate of HRP⁷⁰. Many chromogenic substrates can also be used in colorimetric and fluorimetric assays. These substrates are hydrogen donors that upon oxidation form a coloured product that can be monitored spectrophotometrically. Almost all phenol and aniline derivatives (e.g. alkyl, halo) are able to reduce HRP Compound I to the native enzyme⁶⁹. Chemiluminescent assays

commonly involve the oxidation of luminol or its derivatives, to give rise to 3-amino-1,2-benzenedicarboxylic acid and light molecules; these are particularly sensitive and widely used. Regarding colorimetric assays, it is common to use the TMB substrate (3,3', 5,5'-tetramethylbenzidine), a colourless substance that when oxidized gives rise to the formation of a blue product or [2,2'-azino-bis-(3-ethylbenzthiazoline-6-sulfonic acid)] ABTS that regenerates peroxidase giving a radical-cation (ABTS \cdot^+) with an absorption maximum at 414 nm (**Fig. 3**)⁷¹. The rate of oxygen production by peroxidases is greatly enhanced by the addition of ABTS, which is oxidized to cation radicals by peroxidases. It generates a green soluble product when oxidized and can be read in a spectrophotometer at 405 nm.

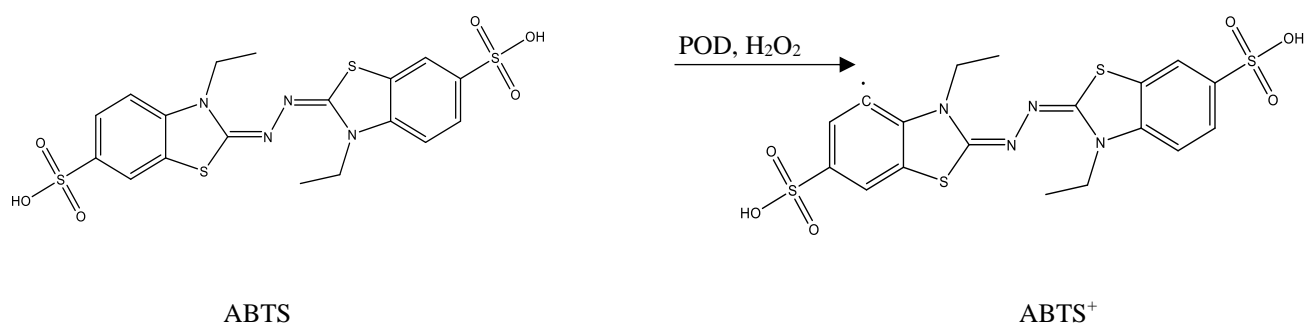


Figure 3. Colorimetric assay of the oxidation of ABTS by HRP in the presence of H₂O₂⁷¹. Adapted from Schulte-Ladbeck R. *et al.*

Immobilization of HRP

From literature, it is known that the HRP has been applied in the various fields of medicine, biotechnology and life sciences. It was traditionally used as a reporter enzyme in histochemical staining's and various diagnostic assays⁶⁸. Immobilization onto appropriate carriers has not only facilitated reusability but also has known to have a direct effect on the activity and the stability of the enzyme and therefore, optimization will certainly play a role in its future. A recent patent application issued, demonstrated the use of immobilized recombinant HRP and its variants for the treatment of wastewater, for the removal of endocrine-disruption compounds such as synthetic estrogens⁷².

The absence and presence of glycan structures determines the convenience of enzyme immobilization⁷³ and in turn its effect on enzyme stability⁷⁴. Surface lysine residues, on the other hand, play a role in directed enzyme immobilization *via* covalent linkages.

Hiner *et al.* observed that on the surface of HRP isozyme C1A, three (Lys174, Lys232, Lys241) out of six lysine residues were found to be accessible to chemical modifications⁷⁵. Whereas in another study, arginine residues, opposite to those of the active site, were mutated to lysine to form a batch of reactive groups suitable for increased and directed enzyme immobilization. Notably, the stabilities of the studied mutants in combination with stabilizing mutations resulted in a link favourable for immobilization behaviour with high enzyme stability⁷⁶.

Magnetic Nanoparticles (MNPs) in biocatalysis and biomedicine

According to the definition provided by the European Union Commission (recommendation of 18 October 2011), nanomaterial is any natural, incidental or manufactured material containing particles, where for 50% or more of the particles in the number size distribution one or more external dimensions is in the size range 1 nm-100 nm. It can occur in an unbound state, as an aggregate or as an agglomerate.⁷⁷ In the case of nanomaterials designed for biomedical applications, most of the existing ones as well as those that are currently under clinical studies correspond to 0D compounds, where all the dimensions are below 100 nm. Among the most commonly used nanomaterials for biomedical applications are liposomes, polymer NPs, gold NPs, magnetic NPs, silica NPs and quantum dots (**Fig. 4**)⁷⁸.

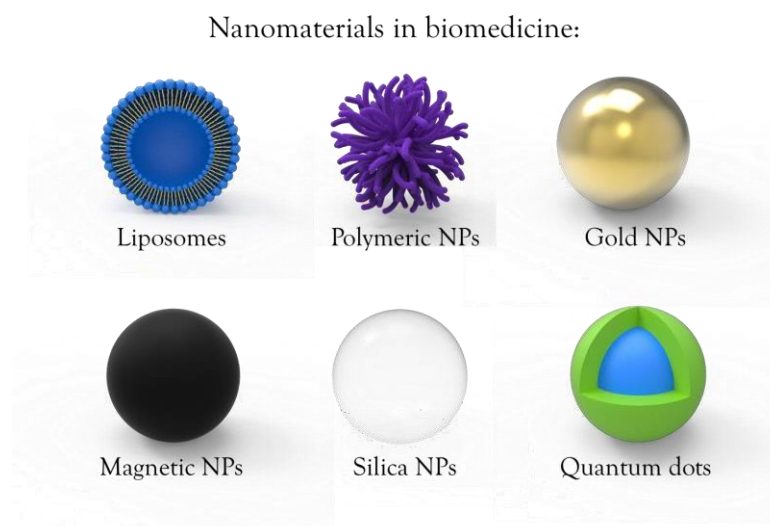


Figure 4. Most commonly used nanomaterials for biomedical applications: liposomes, polymeric nanoparticles, gold nanoparticles, magnetic nanoparticles, silica nanoparticles and quantum dots.

MNPs can be divided into pure metals, metal alloys and oxides, the most common composites are iron, nickel and cobalt. Among all of them iron oxide NPs are the most

extensively studied. The main advantages are their unique magnetic properties and are considered biocompatible as well as to their unique size and physicochemical properties. Because of the widespread applications of MNPs in biotechnology, biomedical, material science, engineering, and environmental areas, much attention has been paid to the synthesis of different kinds of MNPs.⁷⁹ For biomedical uses, the application of particles that present superparamagnetic behaviour at room temperature is preferred⁸⁰. From literature, we know that superparamagnetism appears in small ferro- or ferrimagnetic NPs and in sufficiently small NPs the magnetization can randomly flip direction under the influence of temperature. The time between two flips is known as the Néel relaxation time and in the absence of an external AMF the value of magnetization of these MNPs will be zero thus said to be in a superparamagnetic state. Normal ferri- and ferromagnetic are dependent on the Curie temperature for their transition to the superparamagnetic state but superparamagnetism is different from this standard transition since it occurs below the Curie temperature of the material⁸¹. This allows superparamagnetic nanoparticles to significantly avoid magnetic aggregation due to lack of net magnetization in the absence of field thus making them tuneable and in turn invaluable for biomedical applications⁸¹. Currently, MNPs are widely studied for their applications in biology and medicine, including magnetic bioseparation and detection of biological entities (cell, protein, nucleic acids, enzyme, bacterial, virus, etc.), clinic diagnosis and therapy, such as MRI (magnetic resonance image), targeted drug delivery and biological labels, RNA and DNA purification, magnetic cell separation and purification and magnetically controlled transport of anti-cancer drugs, as well as hyperthermia generation. The maghemite particles are preferred because of their greater saturation magnetization⁸². Maghemite (γ -Fe₂O₃) are biocompatible superparamagnetic materials that have low toxicity and strong magnetic properties. They have been widely used for *in vivo* examination including magnetic resonance imaging, contrast enhancement, tissue specific release of therapeutic agents, hyperthermia, magnetic field assisted radionuclide therapy, as well as *in vitro* binding of proteins and enzymes⁸³. Most of the studies with MNPs have been dedicated to the improvement of enzyme activity and loading. Additionally, many studies the inclusion of MNPs have contributed to the enhancement of the stability and the ease of separation from the medium which is an added attribute. Kouassi GK et al⁸³ demonstrated that when glucose oxidase was covalently immobilized on MNPs it enhanced its binding

efficiency 94-100% as well as improved its kinetic and stability when subjected to thermal denaturation and various pH conditions.

Hybrid materials for enzyme immobilization.

As previously discussed, selection of the support material for enzyme immobilization is a critical aspect due to its major impact on the properties of the biocatalyst. Its shape and textural characteristics of hydrophilicity/hydrophobicity properties, biocompatibility, toxicity or physicochemical stability can directly influence the performance and utility of the immobilized enzyme^{53,84,85}. Consequently, the discovery and use of new support materials with desired properties has become extremely important in the design of immobilized biocatalysts.

In this regard, scientific attention has been directed towards hybrid and composite materials, which combine properties of both composite precursor and maximize their advantages^{86,87}. Upon integration of the different materials, it is desired that the intrinsic characteristics of each individual component are preserved, exhibiting new additional properties due to the synergetic effect between the structural builders. When immobilizing an enzyme in composite supports, scientists aim for a combined benefit of the materials on the properties of the biocatalyst. Cao *et al.* demonstrated this in their work, wherein, a novel biocompatible magnetic cellulose nanocrystal (MCNC) composite was *in situ* prepared *via* a simple co-precipitation-electrostatic-self-assembly technique. This resulted not only an increased thermal stability of the immobilized preparation in comparison to its counterpart but also enhanced catalytic efficiency, ease of separation through magnetic forces, thus possessing all the prerequisites for a potent composite for biocatalysis⁸⁶. Similarly, Pavlovic *et al.* demonstrated that highly stable dispersions of enzyme-clay HRP nanohybrids using double layered hydroxide nanoclay synthesized and functionalized with heparin polyelectrolyte to immobilize the horseradish peroxidase enzyme. It resulted in greater affinity through electrostatic and hydrophobic interactions of the enzyme to the surface of the modified platelets preventing leakages but no hindering its functional integrity and enhanced colloidal stability²⁵.

Objective

Preparation of an active and stable immobilized nanohybrid of horseradish peroxidase.

Specific Objectives

Study different strategies for the entrapment of HRP in biomimetic silica

Study the co-entrapment of MNPs within the Si-HRP immobilized preparation

Evaluate the activity and stability of the different immobilized preparations.

Materials and Methods

Materials

Horseradish peroxidase (HRP) Type VI (EC 1.11.1.7), polyethylenimine (PEI) (MW 1300, 2000, 25000 and 60000), 2,2'-Azino-bis (3-ethylbenzothiazoline-6-sulfonic acid) diammonium salt (ABTS) and hydrogen peroxide were from Sigma Aldrich (St. Louis, MO). Tetramethyl orthosilicate (TMOS), trehalose and potassium phosphate monobasic were from MERCK (Whitehouse Station, NJ). Dibasic sodium phosphate and sodium acetate were from Biopack (Buenos Aires, Argentina). Gel filtration PD10-Columns were from GE Healthcare (Buckinghamshire, UK). Magnetic nanoparticles (MNPs) fluidMag-PAA (200 nm of aggregate size) were from Chemicell (Berlin, Germany). All other chemicals used were analytical grade reagents.

Methods

Determination of HRP activity

The activity of the free and entrapped enzyme preparations was measured by a colorimetric assay using 9.1 mM ABTS, ($\epsilon_M = 36.8 \text{ mM}^{-1}\text{cm}^{-1}$), as a substrate. The final assay contained 1.7 mL of 0.1 M potassium phosphate, pH 5.0 at 25°C, 0.1 mL of 9.1 mM ABTS, 0.2 mL 0.3% (w/w) hydrogen peroxide solution (H_2O_2) in deionized water and 10 μl of the soluble and nanohybrid preparations. The oxidation of ABTS was measured in a spectrophotometer at a wavelength of 405 nm for 2 minutes (Unico SQ-2800 UV-Vis).

One enzyme unit was defined as the amount of HRP able to oxidize 1 μmol of ABTS in the above-mentioned conditions.

Oxidation of HRP

To enhance the stability of the soluble HRP it was oxidized using a modification of Zalipsky's PEGylation protocol⁸⁸. Peroxidase (3 mg) was dissolved in 1.8 mL of 10 mM sodium phosphate containing 154 mM sodium chloride, pH 7.2. Simultaneously, 8.6 mg of sodium periodate was dissolved in 200 μL of distilled water and protected from light. The sodium periodate solution was immediately added to the enzyme

solution, and the sample was gently agitated. The mixture was incubated in the dark for 1 h at 25°C with constant agitation. The reaction was then quenched by the addition of 2.5 µL of glycerol and the oxidized enzyme was then purified by using a desalting PD10 column equilibrated with 100 mM sodium phosphate pH 6.0 containing 154 mM sodium chloride yielding a concentration of 1mg/mL of soluble enzyme. The oxidised enzyme is noted as HRPox.

Immobilization strategies

Entrapment of HRP in biomimetic Si nanoparticles

HRP stock solution (1 mg/mL) was prepared in 0.1 M sodium phosphate buffer, pH 8.0. A stock solution of PEI of different MW (PEI, 10%) was prepared in deionized water. Silicic acid was prepared by hydrolysing 154 µL of tetramethyl orthosilicate (TMOS) 1 M in 1 mL of 1 mM hydrochloric acid. The precipitation mixture consisted of 0.4 mL 0.1 M sodium phosphate dibasic buffer pH 8.0 (containing 300 mM trehalose when stated in the text), soluble enzyme (10 IU/mg), 0.1 mL PEI 10% and 0.1 mL hydrolysed TMOS. Initially, the enzyme, buffer and PEI were mixed and gently agitated in an end-over-end roller for 15 min at 25°C. Then, the hydrolysed TMOS was added and this mixture was kept standing for 5 min at 25°C. The resultant entrapped HRP preparation was then centrifuged (13 500 rpm) for 5 min, washed five times by centrifugation and resuspension with sodium phosphate buffer 0.1 M and sonicated in an ultrasonic cleaner with the power and frequency of 130 W and 20 kHz, respectively, (SONICS & MATERIALS, INC.) for 5 min. The immobilized nanobiocatalysts entrapped in Si are noted as BioSi@HRP.

Immobilization percentage was defined as:

$$\% I = \frac{(Initial\ activity - Activity\ in\ supernatant) * 100}{Initial\ activity}$$

Immobilization yield was defined as:

$$\% Y = \frac{(Activity\ in\ immobilized\ preparation) * 100}{Initial\ activity - Activity\ in\ supernatant}$$

Cross-linking with glutaraldehyde (GA)

To the previously entrapped HRP, 0.1 g (wet weight) of pellet, 2 ml of 0.5% glutaraldehyde solution (v/v) in sodium phosphate buffer 0.25 M, pH 7.0 and was agitated for 1 h at room temperature (RT). It was then washed thrice with sodium phosphate buffer 0.025 M, pH 7.0 and left in agitation overnight at RT. From here on, referred to as BioSi@HRP_GA.

Immobilization of HRP onto MNPs

100 μ l MNPs (2.5 mg/mL) of commercial MNPs fluidMAG-PEA and fluidMAG-Amine were incubated with 50 μ l HRPox (1 mg/mL) for 60 min. Aliquots were measured at spectrophotometrically at 420nm for 2 min at time intervals of 0, 15, 30, 45 and 60 min. The final solution was separated using a magnetic rack and resuspended in buffer of sodium acetate 0.25 M, pH 5.0 and measured spectrophotometrically.

Aminated MNPs were functionalized using the glutaraldehyde. 250 μ l of sodium phosphate buffer 0.2 M, pH 7.0 containing 15% (v/v) of glutaraldehyde was incubated overnight with 250 μ l of MNPs. The next day it was washed thrice with the sodium phosphate buffer 0.025 M to remove the excess glutaraldehyde. To the 450 μ l of MNP-GA solution, 50 μ l of the soluble HRPox (1 mg/mL) was added and aliquots of the supernatant were measured at 0, 15, 30, 45 and 60 min spectrophotometrically at 420 nm. After 60 min the MNPs were separated using a magnetic rack and the final suspension containing the soluble HRPox was measured spectrophotometrically.

Similarly, MNPs were activated using carbodiimide. Equal parts of 100 mM 1-Ethyl-3-(3-dimethylaminopropyl)-carbodiimide (EDC) and 150 mM N-hydroxysuccinimide (NHS) were mixed to form an activator solution and were left in agitation at RT for 10 min. Following which 40 μ l of MNPs in 1 mL of MES buffer 100 mM pH 5.5 were washed using a magnetic rack and was kept standing for 1 min. To this 1 mL of the activator solution was added and kept on an end-to-end roller in agitation of 30 min at RT. Using a concentrator (MWCO 30 kDa, Vivaspin, GE Healthcare) at 4000 rpm for 10 min at 25°C the mixture was filtered to remove the excess EDC-NHS. To this filtered mixture of MNPs, 10 μ l of HRPox (1 mg/mL) was added incubated at 24°C for 2 h. The reaction was quenched using ethanolamine. Following which the MNPs with the adsorbed enzyme were separated using a magnetic rack and the suspension and

supernatant were measured spectrophotometrically at 405 nm. The conjugate was further used in the entrapment within Si procedure mentioned above.

Covalent three-dimensional immobilization of the entrapped HRP

Soluble HRP was oxidised using a modification of Zalipsky's PEGylation protocol⁸⁸ as mentioned above. The oxidised enzyme was then entrapped within Si using the above-mentioned protocol. Following the entrapment, the enzyme was incubated in 0.25 M sodium bicarbonate, pH 10.0 (R 1:10) overnight at 4°C to facilitate the formation of Schiff's bases between the aldehyde groups generated in the enzyme and unreacted amino group from the support. The Schiff's bases were finally reduced using sodium borohydride (1mg/mL, 1:10) during 30 min at 25°C. The nanoparticles were then washed by centrifugation thrice and resuspended in 0.1 M sodium phosphate buffer pH 8.0. From here on, referred to BioSi@THRPox.

Additionally, a stabilizing agent, trehalose, known for its ability to provide added stability to protein was added. The 10 µL of HRPox was preincubated with 400 µL of sodium phosphate buffer 0.1 M, pH 8.0 containing 300 mM of trehalose. Following which the above-mentioned protocol was carried out. The obtained nHs were referred to as BioSi@THRPox.

Co-entrapment with magnetic nanoparticles

10 µL of a 25 mg/mL solution of MNPs (Chemicell FluidMAG-PAA, 200 nm) were brought to a magnetic separation rack during 5 min. The supernatant was removed and the MNPs were washed thrice and resuspended in the same volume of 0.1 M sodium phosphate buffer, pH 8.0. The co-entrapment procedure was the same as described above for the entrapment of HRPox with the addition of the washed 10 µL MNPs suspension just before the addition of TMOS. The resultant immobilized preparation BioSi@HRP_MNP was washed five times by centrifugation (13 500 rpm) for 5 min, and resuspended in sodium phosphate buffer 0.1 M and sonicated in an ultrasonic cleaner with the power and frequency of 130 W and 20 kHz, respectively, (SONICS & MATERIALS, INC.) for 5 min and finally reduced using the above-mentioned protocol. From here on, shall be referred to as BioSi@THRP_MNP_PEI (1300, 2000, 25000, 60000)

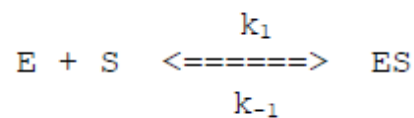
Co-entrapment with in-house laboratory synthesised MNPs.

The MNPs used were poly (maleic anhydride-alt-1-octadecene) with a diameter of 7-8 nm (PMAO), dimercaptosuccinic acid with a diameter of 6-8 nm (DMSA) and Nano-flower with a diameter of 15 nm (NF-4) nanoparticles from the Instituto de Nanotecnologia Aragon (INA), Zaragoza. The co-entrapment procedure was the same as mentioned above.

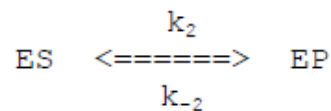
General procedures for nHs characterization

Kinetics parameters of the nHs and free enzyme

First proposed by Michaelis and Menten, the catalytic event that converts substrate to product involves the formation of a transition state. The complex that forms, when substrate and enzyme combine, is called the enzyme substrate (ES) complex.



Reaction products arise when the ES complex breaks down releasing free enzyme



Between the binding of substrate to enzyme, and the reappearance of free enzyme and product, a series of complex events must take place. For example, the ES complex must pass to the transition state (ES*); and the transition state complex must advance to an enzyme product complex (EP).



K_m and V_{max} are determined by incubating the enzyme with varying concentrations of substrate; the results can be plotted as a graph of rate of reaction (v) against

concentration of substrate ([S]), and will normally yield a hyperbolic curve, as shown in the graphs above.

The relationship is defined by the Michaelis-Menten equation:

$$v = \frac{V_{max}}{(1 + \frac{K_m}{[S]})}$$

The Lineweaver-Burk double reciprocal plot rearranges the Michaelis-Menten equation as:

$$\frac{1}{v} = \frac{1}{V_{max}} + \frac{K_m}{V_{max}} * \frac{1}{[S]}$$

Where, plotting 1/v against 1/[S] gives a straight line

The measurements of the basic kinetic parameters maximum reaction rate (V_{max}) and Michaelis constant (K_M) were performed using different concentrations of ABTS in the assay (0.325, 0.350, 0.380, 0.400, 0.455 mM) and 0.03% of H_2O_2 . These concentrations are the concentrations in the final assay of 2 mL. For the assay, 1.7 mL of potassium phosphate 0.1 M pH 5.0, 100 μ L of ABTS (6.5, 7.0, 7.6, 8.0, 9.1 mM), 200 μ L of 0.3% H_2O_2 and finally 10 μ L of HRP and the immobilized preparations was added. Changes in absorption were detected in a spectrophotometer (UV- 1800, Shimadzu Duisburg, Germany) at 420 nm and 30°C for 120 sec.

Temperature profile of the nanoabbiocatalysts

To study the **optimum temperature**, the reactants were heated in a water bath to a range of temperatures (20°C to 60°C). For the lower temperatures the spectrophotometer temperature was controlled to the desired temperatures up to 40°C. For the higher temperatures, the reactants were incubated in a water bath and up on reaching the temperature were immediately added to the cuvette and the measurement was carried out. 10 μ L enzyme was added to the reactant mixture and measured spectrophotometrically at 405 nm for 2 min.

To analyse the **thermal stability**, 10 μ l of the enzyme was incubated in 0.1 M sodium phosphate pH 8.0 for 1 h at the aforementioned temperatures (20 to 60°C) after which the activity was measured spectrophotometrically at 405 nm for 2 min.

pH stability analysis of the nanobiocatalysts

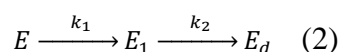
HRP preparations were incubated in 0.1 M sodium phosphate buffer pH 7.0 and 8.0, 25 mM sodium acetate pH 3.0, 4.0, and 5.0, and 25 mM sodium bicarbonate pH 10.0. Aliquots of soluble and entrapped suspensions were withdrawn, and their residual activity was measured as previously described after 1 h of incubation.

Thermal Stability of the nanobiocatalysts

The thermal stability was carried out at 50°C, wherein, aliquots of soluble and entrapped suspensions were withdrawn at different time intervals and their residual activity was measured as previously described. Residual activity was defined as:

$$\text{Residual Activity} = \frac{a}{a_0} \quad (1)$$

Where a are the IU at a time point and a_0 is the initial activity in IU. Biocatalysts inactivation was modelled based on the deactivation theory proposed by Henley and Sadana⁸⁹ using Graph Pad Prism. Inactivation parameters were determined from the best-fit model of the experimental data which was the one based on two-stage series inactivation mechanism without residual activity, as represented in the following scheme:



where k_1 and k_2 are first-order transition rates constants. E, E_1 and E_d are the corresponding enzyme species of progressively less specific activity, being the last one completely inactive. The mathematical model that represents this mechanism is:

$$\frac{a}{a_0} = \left(1 + \alpha \left(\frac{k_1}{k_2 - k_1}\right)\right) e^{-k_1 \times t} - \left(\alpha \left(\frac{k_1}{k_2 - k_1}\right)\right) e^{-k_2 \times t} \quad (3)$$

where α is the enzyme specific activity. Inactivation parameters were determined from the best-fit model of the experimental data. Half-life (time at which the residual enzyme activity is half of its initial value; $t_{1/2}$) was used to compare the stability of the different biocatalysts, being determined by interpolation from the respective model described by Eq. 2. The stability factor (SF) was the parameter used for a quantitative comparison of the stability of the biocatalysts and was found by

$$\text{Stabilization factor} = \frac{t_{1/2}}{t_{1/2_0}} \quad (4)$$

Where $t_{1/2}$ is the half life time of the more stable sample and $t_{1/2_0}$ is the half life time of the less stable sample.

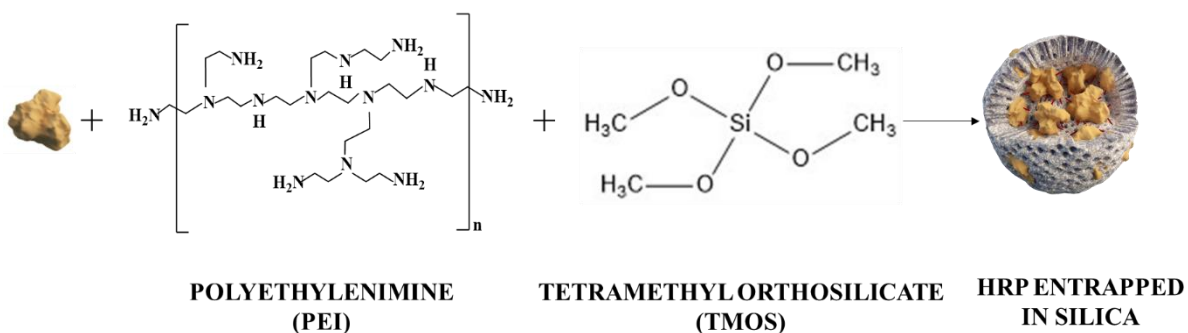
Reuse of nanohybrid by magnetic separation

The reusability of the immobilized enzyme nanohybrids was studied by repeated usage for 10 enzymatic cycles. Enzymatic reactions using 9.1 mM of ABTS and 0.3 % hydrogen peroxide as substrates were performed in a 2 mL reaction volume containing potassium phosphate buffer pH 5.0, and a fixed amount of immobilized enzyme (20 IU). Between each cycle, the nanohybrids were carefully separated using a magnetic separator (Chemicell- MagnetoPURE BIG SIZE) and then resuspended in the reaction mixture. The reactions were measured spectrophotometrically at 405 nm for 2 min. The activity determined during the first cycle was considered 100% for the calculation of remaining percentage activity after each use.

Results and discussion

Sol-gel and functionalized mesoporous Si have been previously used for enzyme immobilization. These methods have some inherent limitations such as harsh synthetic conditions or poor retention of the immobilized enzyme different from biomimetic Si synthesis^{44,90}. The immobilization approach follows a one-pot procedure, wherein, Si synthesis and the entrapment of the enzyme in our case HRP, occurs simultaneously⁹¹. As a first approach we study the behaviour of the enzyme immobilized in a biomimetic Si environment in order to evaluate further possible strategies for stabilization of the enzyme.

The entrapment of HRP solely in biomimetic Si and the properties of the obtained immobilized preparation was studied using the poly aminated catalyst polyethyleneimine (PEI) (MW ~ 1300 Da) and derivatives of silicic acid in mild reaction conditions (**Scheme 1**). PEI is a polymer containing primary, secondary and tertiary amino groups, having a strong anion exchange capacity, and the capability to chemically react with different chemical groups on either an enzyme or a support.⁹².



Scheme 1. Schematic representation of the synthesis of silica and the entrapment of the HRP.

The procedure resulted in an immobilized preparation (BioSi@HRP) with percentages of immobilization and yield of $52 \pm 4\%$ and $100 \pm 2\%$, respectively (**Table 3**). No enzyme leakage was detected as measured in the supernatant of a suspension incubated at 4°C for 1 month while the immobilized nanobiocatalyst retained $74 \pm 2\%$ of its initial activity.

A range of starting HRP concentrations were used to evaluate its impact in the immobilization parameters in silica entrapment (**Table 2**). A concentration of 1 mg/mL

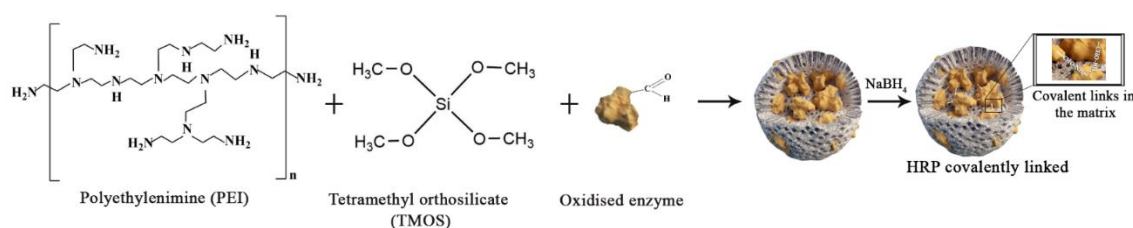
of enzyme was the minimal amount of enzyme that allowed a preparation with a high specific activity (IU/mg) and therefore it was selected for further experiments.

Table 2. Entrapment of different concentrations of HRP in biomimetic silica nanoparticles.

HRP (mg/ml)	Immobilization (%)	Immobilization yield (%)	Specific activity (IU/mg)
0.5	94 ± 3	50 ± 2	1.042 ± 4E-03
1	85 ± 2	59 ± 2	1.025 ± 2E-03
3	83 ± 2	53 ± 3	1.286 ± 4E-03
5	82 ± 4	49 ± 6	1.700 ± 7E-03
7.5	63 ± 4	42 ± 2	2.125 ± 5E-03
10	54 ± 3	12 ± 3	1.887 ± 8E-03
20	34 ± 5	10 ± 5	1.900 ± 7E-03

In order to improve the stability of the immobilized enzyme, pre and post-entrapment strategies were carried out seeking to achieve covalent attachment of the enzyme to the support. Considering the degree of glycosylation of this enzyme⁹³, we performed a standard mild oxidation via NaIO₄ of the enzyme. This treatment generates aldehyde groups on HRP sugar residues that could form Schiff's bases with amino groups of the PEI used as a catalyst for the Si deposition. Similar to the chemistry used to immobilize proteins on glyoxyl activated supports⁹⁴, a further reducing step via Na₂BH₄, would transform the first reversible interaction between the enzyme and the matrix into a three dimensional multiple covalent attachment of HRP within the Si particles (**Scheme 2**). This strategy managed to immobilize 74 ± 3% of HRP in compared to the first strategy and recovered 100 ± 1% (**Table 3**) of the activity in the preparation. Differences in the amount of enzyme immobilized within the particles could be due to the chemical changes generated on the surface of the enzyme after the oxidation treatment.

Variations in the isoelectric point or the interaction of surface residues with the PEI could alter the integration of the enzyme during silica matrix polymerization.



Scheme 2. Schematic representation of the entrapment of the enzyme (HRP) and further covalent attachment in biomimetic silica.

A second post-immobilization strategy was studied wherein the enzyme trapped in silica nanoparticles was incubated with glutaraldehyde. This incubation was intended to generate covalent bonds between amino groups from the surface of the enzyme and unreacted amino groups from the PEI in the vicinity of the enzyme within the nanoparticle. We were able to recover only 30 ± 5% of the activity after glutaraldehyde crosslinking and therefore, as the other strategies yields were higher, we discarded this strategy for further experiments (Table 3).

Table 3. Immobilization parameters of nHs with different immobilization strategies.

	Immobilization strategy	% Immobilization [(IU Applied-IU Supernatant) * 100 /IU Applied]	% Yield [(IU Applied-IU Supernatant) * 100 /IU Applied]
BioSi@HRP	Physical	52 ± 4	100 ± 1
BioSi@HRP_GA	Cross-linking	89 ± 2	30 ± 5
BioSi@THRP	Stabilizer	78 ± 3	69 ± 2
BioSi@THRPox	Covalent	74 ± 3	100 ± 1

Seeking a further improvement in the properties of the nanobiocatalysts, we included trehalose during the entrapment process, a common additive to gain protein stability⁹⁵. A direct correlation between the surface tension of trehalose solutions and the thermal stability of various proteins has been established and it is also known that trehalose

significantly increases the half-life of HRP²³. The immobilization parameters were improved after the addition of using trehalose, as immobilization and yield were $78 \pm 3\%$ and $69 \pm 2\%$, respectively.

The size of the aminated catalysts for the deposition of biomimetic silica has proven in the past to play a role in the physical properties of the final material formed⁹⁶. Under the premise that this could also affect the properties of the immobilized enzymes we performed the synthesis using PEI with different MW (MW ~ 2000, 25 000 and 60 000 Da). Except for PEI 25000 Da, which has been declared by the supplier is branched) all other PEIs are linear. Except for the BioSi@THRP_60000, the immobilization percentage (%I) and immobilization yield (%Y) of the different HRP were above 70%. The nH obtained with PEI MW 1300 displayed the higher results for %I and %Y (**Table 4**). The lower yield for the BioSi@THRP_60000 could be due to the higher molecular weight which could change the formation of Si during the synthesis forming a denser cover around the enzyme making it inaccessible to the substrate or decreasing the enzyme kinetics due to partition of substrates and products problems.

Table 4. Immobilization parameters of nHs with different sizes of PEI.

Immobilized preparation	Immobilization (%)	Yield (%)
BioSi@THRP_1300	60 ± 4	78 ± 1
BioSi@THRP_2000	61 ± 3	77 ± 2
BioSi@THRP_25000	64 ± 2	70 ± 5
BioSi@THRP_60000	70 ± 2	33 ± 5

*BioSi@THRP is the immobilized preparation in the presence of trehalose with different PEI

Co-entrapment of enzyme and MNPs within biomimetic silica

We first studied the immobilization of HRP on the surface of MNPs that could serve as an initial step in their integration within the biomimetic silica matrix.

We investigated various strategies such as ionic adsorption on the MNPs and the functionalization of the MNPs with EDC and activation with NHS for covalent attachment of the enzyme on the nanoparticle surface. We initially used aminated commercial MNPs (fluidMAG-PEA and fluidMAG-Amine) with our previously oxidised enzyme. We were able to achieve an adsorption of 14% of the applied enzyme (1 mg/mL, 10 IU) onto the MNPs but no enzymatic activity was found after adsorption (**Table 5**). We also used carboxylated commercial MNPs (fluidMAG-PAA) and achieved an adsorption of 6% with no remnant enzyme yield. We noted that on increased incubation time with the free enzyme the remnant activity in the supernatant decreased with no yield in the immobilized suspension.

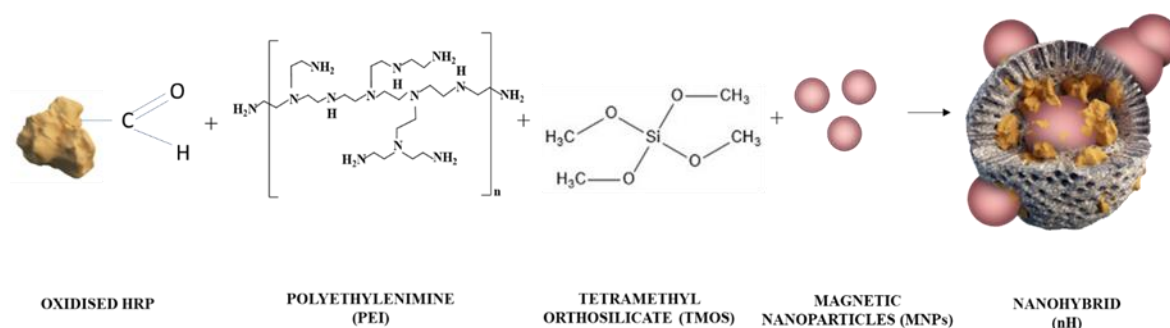
Following these results, we thought that an additional functionalization of the surface could aid in the recovering of the enzymatic activity. We used carboxylated commercial MNPs (fluidMAG-PAA), a coupling agent EDC, a zero-length crosslinking agent used to couple carboxyl or phosphate groups to primary amines, and the addition of -NHS which stabilizes the amine-reactive intermediate by converting it to an amine-reactive sulfo-NHS ester, thus increasing the efficiency of EDC-mediated coupling reactions. We were able covalently bind of $87 \pm 3\%$ with a final enzymatic yield of $15 \pm 4\%$ but after synthesis of Si we lost all enzymatic activity (**Table 5**). From the literature it is known that HRP on immobilization with EDC-coupled MNPs has not resulted in favourable results due to the inactivation of the enzyme. In the study of F. Kazenwadel et al.⁹⁷ it was shown that the coupling process with HRP lead to a partial inactivation of HRP yielding an activity of less 6% after optimization of the protocols. The main reason for the unusually low activity yield is the tendency of HRP to be inactivated by simple physical adsorption to the particle surface. This strategy was not used in further investigations.

Finally, we attempted to functionalize aminated MNPs with GA. It was possible to achieve a $68 \pm 2\%$ of the enzyme was cross-linked with the MNPs but the yield of the enzyme recovered was only $0.48 \pm 0.04\%$ and consequently entrapment in silica was not feasible.

Table 5. Immobilization parameters of HRP onto MNPs

MNPs	Technique	% I of HRP onto MNP	% Yield (Y)
MNPs_Amine	Adsorption	14	-
MNPs_PAA	Adsorption	6	-
MNPs_PAA	EDC coupling	87	15
MNPs-Amine	Glutaraldehyde	68	0.48

As the strategy of a covalent attachment of the enzyme to the surface of the MNPs were not successful we tested a one-pot procedure in an attempt to co-entrap the enzyme and MNPs within biomimetic silica while the silica matrix was being formed (**Scheme 3**).



Scheme 3. Schematic representation of the co-entrapment of MNPs and HRP in biomimetic silica.

Using PEI MW 1300, we studied the effect of various concentrations of MNPs of (fluidMAG-PAA, 200 nm) in the synthesis and on the final yield observing a direct correlation with the enzymatic activity of the immobilized preparations (**Table 6**). With increasing concentration of MNPs in the synthesis there was a decline in the final activity observed. Thus, from the results we chose 0.25 mg/mL of MNPs for all further experiments.

Table 6. Effect of concentrations of MNPs in the synthesis of nHs

Concentration of MNPs (mg/mL)	Yield (%)
0.25	74 ± 2
0.62	50 ± 1
1	31 ± 2
1.25	35 ± 1
2	29 ± 2
2.5	22 ± 1

The strategy was studied using PEIs of different sizes. Except for the BioSi@THRP_60000, the immobilization percentage (%I) and immobilization yield (%Y) for all the preparations were above 60%. The nH obtained with PEI MW 1300 displayed the higher results for %I and %Y (**Table 7**). None of the immobilized preparations obtained showed enzyme leakage as measured in the supernatant of a suspension incubated at 4°C for 1 month.

Table 7. Immobilization parameter of nHs.

Entrapment	Immobilization (%)	Immobilization yield (%)
BioSi@THRP_MNP_1300	83 ± 5	71 ± 2
BioSi@THRP_MNP_2000	76 ± 2	69 ± 4
BioSi@THRP_MNP_25000	77 ± 2	70 ± 5
BioSi@THRP_MNP_60000	69 ± 2	57 ± 5

When adding MNPs to the synthesis mixture, we observed that for the nH with PEI MW 60000 there was an increase in the %Y from 33±5% to 57±5% compared to the experiments where HRP was entrapped without MNPs. The presence of MNPs could

act as a template in directing the Si deposition in a more compact polymeric shell, reducing mass transfer limitations.

To understand the effect of the type of MNPs on the final yield of the nHs, a co-entrapment of the enzyme with laboratory synthesised, single domain and varying in size was performed.

Table 8. Immobilization with laboratory synthesised MNPs.

MNPs	Conc. of Iron (mg of Fe/ml)	Diame ter (nm)	Iron in Syn-thesis	I%	R%	Iron in Syn-thesis	I%	Y%
DMSA	2.6	7-8	0.0025	91 ± 3	15 ± 2	0.0005	91 ± 1	21 ± 3
PMAO	4.3	6-8	0.0025	80 ± 1	10 ± 1	0.0005	80 ± 3	20 ± 1
NF-4	5.6	15	0.0025	90 ± 2	13 ± 2	0.0005	90 ± 3	19 ± 2

The MNPs used were PMAO poly (maleic anhydride-alt-1-octadecene), DMSA dimercaptosuccinic acid and NF-4 Nano-flower nanoparticles from the Instituto de Nanotecnologia Aragon (INA), Zaragoza. The results showed a drastic decrease (**Table 8**) in the final enzymatic yield compared to the commercial MNPs. The yield was directly proportional to the concentration of MNPS in the synthesis (**Table 8**). This decrease could be attributed to the diameter of the MNPs which are 10 times smaller than the commercial MNPs. The MNPs could be blocking the active site of the enzyme causing a reduction in the yield. This could be corroborated with the above table when there a is reduction in the amount of MNPs offered to the synthesis there is an increase in the yield. Similar results were observed when we tried to ionically absorb the enzyme onto the MNPs. In the light of these and previous results, we selected the commercial MNPs for future experiments.

Characterization of the nHs

Effect of pH on the activity and stability of the nHs

Enzymes are affected by changes in pH. For any biocatalytic study it is of utmost importance to study the pH at which the enzyme is optimally active. pH stability is also important to study as it often restrains the applicability of enzymatic preparations due to its profound impact on the loss of structural integrity of many proteins. All the immobilized preparations resulted more stable than the soluble enzyme at acidic pH (**Fig. 5A**) and there was no observed effect of the MNPs on the pH stability (**Fig. 5B**). No loss of integrity of the nanoparticles was observed after 1 h of incubation at the different pH. From literature it is known that the linear PEI despite its simple structure displays intricate solution dynamics. Solution conditions affect the balance between inter- and intra-chain repulsion eg. pH increases the charge of the polymer, while added salt reduces charge repulsion due to screening the electrostatic interaction⁹⁸. The ramification of the PEI could play an important role in the inter and intra chain repulsion on account of pH changes.

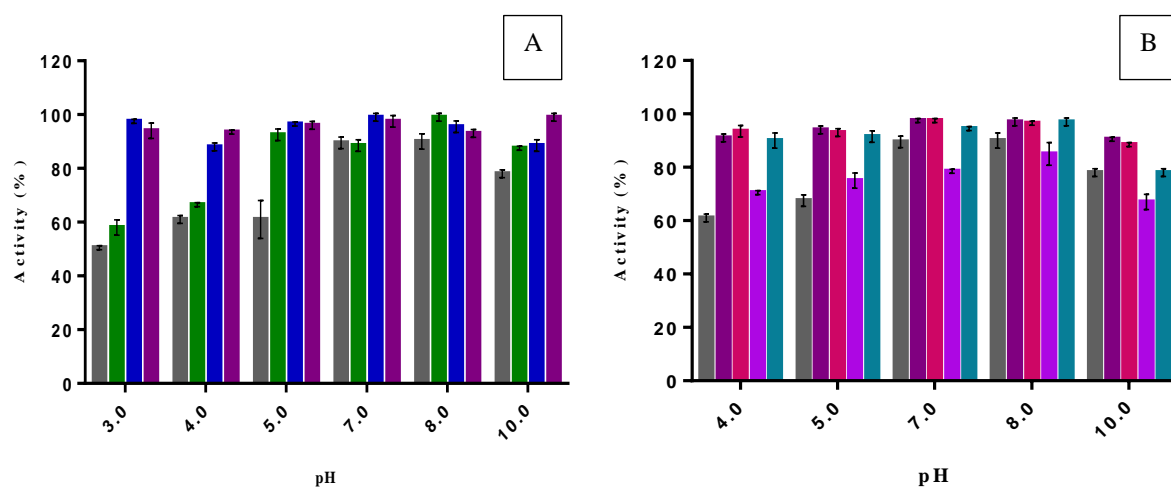


Figure 5. A) Effect of pH on the stability of HRP preparations: A) pH stability of the different soluble and entrapped HRP: soluble enzyme (■), BioSi@HRPox (■), BioSi@T_HRP (■) and BioSi@T_HRP_1300 (■). B) pH stability of the co-entrapped nHs with MNPs and distinct PEI: soluble enzyme (■), BioSi@THRP_MNP_1300 (■), BioSi@THRP_MNP_2000 (■), BioSi@THRP_MNP_25000 (■), BioSi@THRP_MNP_60000 (■). After 1 h incubation at the different pH 3, 4, 5, 7, 8, 10.

After entrapment and chemical modifications, the enzyme maintained its optimal activity at pH 4.0. The nHs with different PEI also showed the same optimal pH with an exception of BioSi@THRP_MNP_25000 which was optimally active at pH 5.0 (**Fig. 6B**).

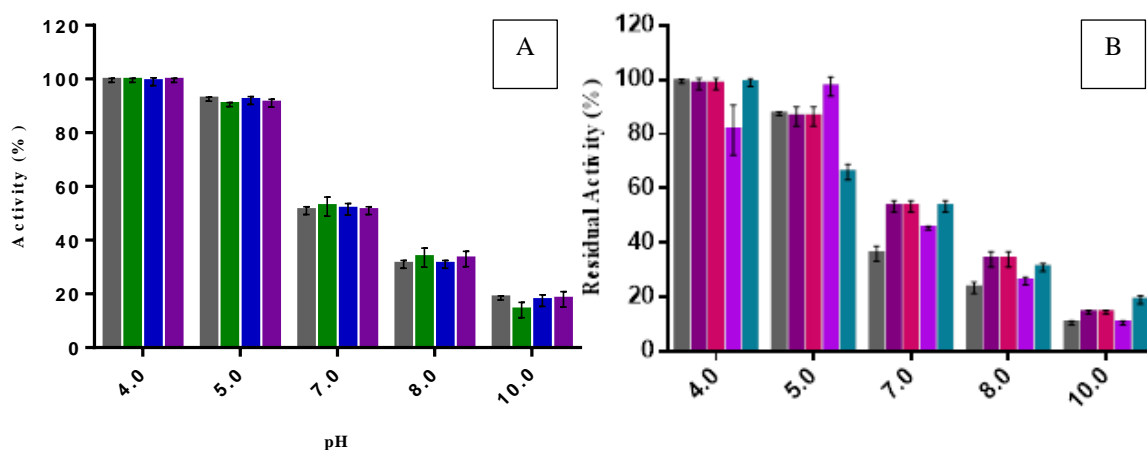


Figure 6. A) Optimum pH of the different nHs. A) Optimum pH of the different nHs: soluble enzyme (■), BioSi@HRPox (■), BioSi@T_HRP (■) and BioSi@T_HRP_1300 (■). **B) Optimum pH of the co-entrapped nHs with MNPs and distinct PEI:** soluble enzyme (■), BioSi@THRP_MNP_1300 (■), BioSi@THRP_MNP_2000 (■), BioSi@THRP_MNP_25000 (■), BioSi@THRP_MNP_60000 (■).

Thermal stability of the nHs

Stabilization of enzymes is a key factor to determine their full potential as biocatalysts. Our studies on thermal stability of the entrapped enzyme demonstrated that, after fitting the experimental data to the exponential model from Henley and Sadana⁸⁹, the physically entrapped HRP (BioSi@HRP) had a half-life time of 65.4 min at 50°C compared to the soluble enzyme that reached 50% of its initial activity after only 2.4 min (**Fig. 7A**). Thermal stabilization improved considerably after chemical modification of the nanobiocatalysts (**Fig. 7B**). When using PEI MW 1300, modified nanoparticles showed a half-life time of 150 min compared to 65.4 min of the unmodified entrapped HRP. The effect of trehalose and the chemical crosslinking on the thermal stability of the immobilized HRP was additive, as the preparation had a stabilization factor (SF) of 176 (**Fig. 7B**). Since the Si NP is a porous material, we excluded the possibility of trehalose leakage by incubating an immobilized preparation in suspension at 4°C for 1 month and determination of reducing sugars in the supernatant. No trehalose was detected under these conditions in the supernatant.

Moreover, a suspension of BioSi@THRP_MNP_1300 containing 12.5 ± 0.3 IU/mL in sodium phosphate buffer 0.1 M pH 8.0, retained $84\% \pm 3$ (10.5 ± 0.4 IU/mL) of its initial activity after 6 months of shelf storage at 4°C .

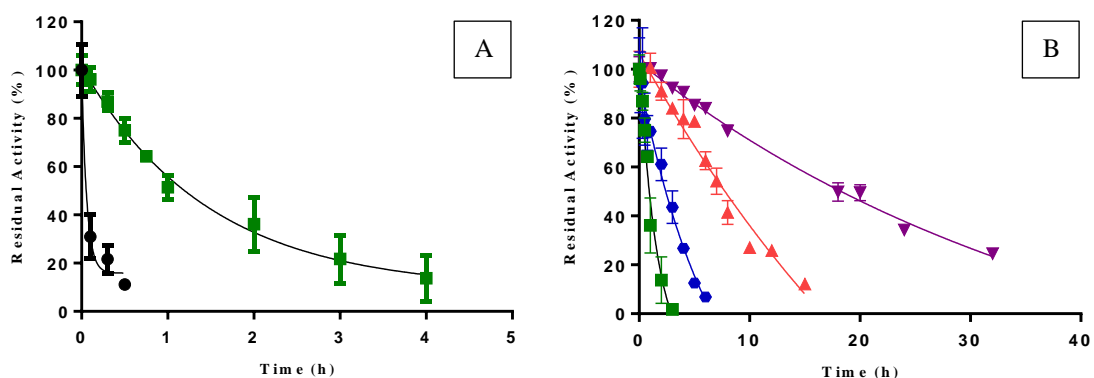


Figure 7. Thermal stability at 50°C of different HRP preparations. **A)** Soluble enzyme (HRP) (\bullet), BioSi@HRP (\blacksquare). Aliquots were taken at mentioned time intervals and measured spectrophotometrically at 405nm. The half-lives were determined as 0.04 h and 1.09 h for the soluble and immobilized preparations, respectively. **B)** Thermal stability of the BioSi@HRP (\blacksquare), BioSi@HRPox (\bullet), BioSi@THRP_1300(\blacktriangle) and BioSi@THRP_MNP_1300 (\blacktriangledown) showing half-lives 1.09 h, 2.5 h, 7.02 h, 21.3 h using Graphpad Prism v6.0.

We believe these results demonstrate that a three-dimensional rigidification of the enzyme structure is a determinant factor to a drastic improvement in its stability. Some indications of this effect had been previously obtained by immobilization of enzymes on matrixes modified with polymeric molecules in which it was believed that regions of the biomolecules were embedded within the support, improving their stability⁹⁹. However, an entrapment process assures that most of the enzymatic molecules lay within the matrix which is fundamental to reinforce our three-dimensional stabilization hypothesis. When stability of nanohybrids including MNPs was studied at 50°C , we observed a 532 SF of the enzyme entrapped in Si with MNPs (BioSi@THRP_MNP_1300) compared to the soluble enzyme (**Fig. 7B**).

Considering that the MNPs contain primary amino groups that could further react with the aldehyde generated upon mild oxidation in the HRP, we believe the presence of the MNPs provided an additional source of functional groups for multi-point covalent interaction. Moreover, the MNPs offer a more rigid surface to the enzyme to the flexible Si network formed as a shell of the nanohybrid. This may restrain enzyme distortion and contribute to a greater stabilization.

The nanohybrids with distinct PEIs showed an increase in the half-life similar to nanohybrids with PEI MW 1300 respect to the soluble with an exception of PEI MW 25000 which showed a SF of 20 with respect to the soluble enzyme (**Fig. 8**). The branched nature of this PEI amplifies the loading enzyme but could leave the enzyme more exposed to degradation caused by temperature increase¹⁰⁰.

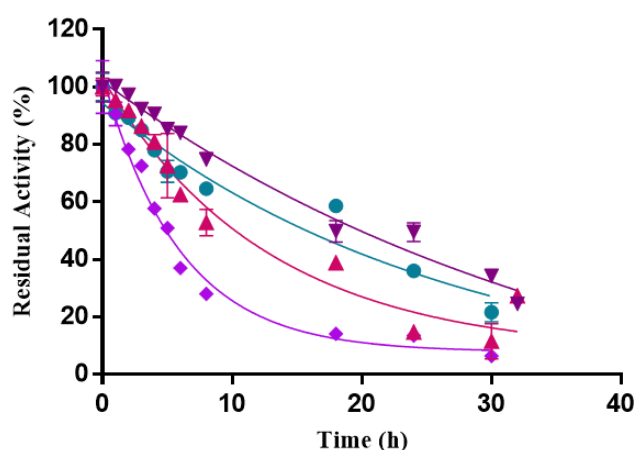


Figure 8. Thermal stability of the enzyme preparations with distinct polyethyleneimines (PEI). (BioSi@THRP_MNP_1300 (▼), BioSi@THRP_MNP_2000 (▲), BioSi@THRP_MNP_25000 (◆), BioSi@THRP_MNP_60000 (●) entrapped in silica with a magnetic core. The half-lives were determined as 21 h, 20 h, 8 h, 22 h, respectively using Graphpad Prism v6.0.

Repeated uses of the nHs

Operational stability is a key factor in the design of a nH. The activity of BioSi@THRP_MNP_1300 was assessed after several enzymatic cycles using the chromogenic substrate ABTS and hydrogen peroxide. In all studied cycles, the immobilized enzyme was magnetically separated and was assessed for its remnant catalytic activity. After 5 reuses the nanohybrids maintained 30% of its initial activity. (**Fig. 9**) Depending on the support and chemical modifications the cycles of reuse may vary from enzyme to enzyme or even within the same enzyme.

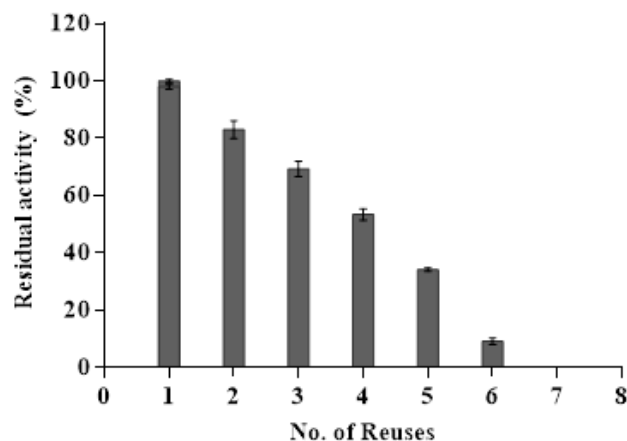


Figure 9. Operational stability of BioSi@THRP_MNP_1300. Residual enzyme activity after 6 reuses with substrates (ABTS and H₂O₂) and separation using a magnetic separator.

Kinetic parameters of free and encapsulated HRP

The kinetics parameters of the free and encapsulated HRP were investigated. Kinetics analysis of HRP activities in the immobilized suspensions revealed that the apparent K_m of the nHs for H₂O₂ was slightly higher than that of the soluble enzyme (**Table 9**). Modifications of K_m values for immobilized enzyme preparations can be attributed to substrate diffusion limitations and steric hindrances compared to the soluble forms¹⁰¹. The V_{max} values were approximately three times lower for all the immobilized preparations compared to the $0.033 \pm 7e-03$ mmol/min of the soluble HRP. Despite the differences in the kinetic parameters of the immobilized and soluble enzyme, the dramatic thermal and operational stabilization achieved by the strategy followed herein for immobilization would balance any negative effect of these parameters on the reaction.

Table 9. Kinetic parameters of the nHs and free enzyme.

Preparation	K_m (mM)	V_{max} (mmol/min)	k_{cat} (s ⁻¹)
HRP	3.4 ± 1.71	$0.033 \pm 7e-03$	6.68
BioSi@THRP_MNP_1300	4.4 ± 1.09	$0.013 \pm 1e-03$	2.57
BioSi@THRP_MNP_2000	5.8 ± 1.03	$0.014 \pm 5e-03$	2.82
BioSi@THRP_MNP_25000	4.5 ± 0.79	$0.013 \pm 2e-04$	2.71
BioSi@THRP_MNP_60000	5.7 ± 0.43	$0.015 \pm 4e-03$	3.00

Conclusions

In this Chapter, we demonstrated the preparation of a new nanosized hybrid material that combined MNPs, biomimetic silica and the enzyme HRP after exploring various strategies of immobilization. The addition of the disaccharide trehalose and a post immobilization chemical modification of the organic/inorganic material provided exceptional stability to the enzyme without compromising its activity surpassing previous reports for HRP stabilization^{102,103}. The immobilization did not affect the magnetic properties of the MNPS which facilitated the nHs separation in repeated batch transformations of a synthetic substrate. In summary, the unprecedented approach for the preparation of a nanohybrid biocatalyst provided excellent properties that could facilitate its applied use. Although out of the scope of this Thesis, further experiments on conversion of alternate substrates of immobilized HRP would broaden the range of applications of the system.

Chapter 2

Physico-chemical Characterization and Remote
Magnetic Heating Activation of Biohybrids

Chapter Summary

It is well known that there is clear relationship between the biological behaviour of nanoparticles and their physicochemical properties. Therefore, we performed an **extensive physicochemical characterization** of the optimized biohybrid nanoparticles (biomimetic silica+magnetic nanoparticles (MNPs)) which should act as a vehicle for the entrapped horseradish peroxidase (HRP) for its application in Directed Enzyme Prodrug Therapy (DEPT). For all the optimized biohybrids (Chapter 1), a number of techniques have been used in order to determine their: *i*) **size** by Dynamic Light Scattering (DLS), Transmission & Scanning Electron Microscopy (TEM&SEM), *ii*) **porosity** by Brunauer, Emmett and Teller (BET), *iii*) **net surface charge** by zeta-potential, and *iv*) **magnetic properties** by Superconducting Quantum Interference Device (SQUID) magnetometry.

The **final aim of this thesis** is the use of this biohybrids to **trigger, by magnetic heating, the conversion** of the non-toxic plant hormone indole-3-acetic acid (IAA) to toxic agents able to induce cell killing. Therefore, besides their characterization in buffered aqueous media, the **behaviour of the biohybrids in complex biological environment** (complete cell cultured media) was also studied. This is a key aspect to be considered as molecular interactions of nanomaterials with biological environments are highly complex on a molecular scale. Thus, in this Chapter, we also have focused on the colloidal stability of the developed biohybrids in cell culture media as well as on the formation and characteristics of protein coronae that have recently been shown to significantly modify the properties of pristine particles. In this line, their surface modification with glucose was optimized as this monosaccharide could act not only as a blocking agent for increasing the biohybrids colloidal stability but also as a targeting agent of cancerous cells.

Finally, we have also clearly demonstrated that is **possible to increase enzyme activity** by exposing the biohybrids to **alternating magnetic fields (AMF)**. While the global temperature of the media where the biohybrids were suspended does not significantly increased, their exposure to AMF triggered the local heating of HRP molecules microenvironment up to its optimal temperature (45°C). So, this is the **first time it has been shown that** it is possible to tune by magnetic heating the activity of enzymes that are not directly attached to magnetic nanoparticles (MNPs) surface but co-entrapped within a silica shell. The demonstration of this concept and the optimization of AMF application conditions were carried out using 2,2'-azino-bis (3-ethylbenzothiazoline-6-sulphonic acid) (ABTS) as substrate, as HRP facilitates the reaction with hydrogen peroxide, turning it into a green and soluble end-product. Altogether the obtained results show a great potentiality of the obtained biohybrids for DEPT anti-tumour therapy.

Introduction

Biomedical application of nanomaterials

The use of nanomaterials in biomedicine in the past decade has exponentially increased. The most important biomedical applications of nanoparticles (NPs) are in disease diagnostics and treatment. Nanoparticles (NPs) are solid colloidal particles (1 to 100 nm) and are comparable with those of cells, viruses, proteins, and genes, and have opened the potentiality of interacting with fundamental biological processes¹⁰⁴ (**Fig. 1**). The potential of these new generation NPs in targeted drug delivery has revolutionized safe and effective pharmacotherapies for complex diseases. Associated with nanometre sizes is there is a large surface area to mass ratio that improves loading capacity of drugs. The same nanoscale properties also increased propensity to diffuse across biological membranes, overcome several anatomic barriers that usually hampers drug biodistribution, and finally, crossing the fenestrations of the blood capillaries in order to penetrate tissues. Indeed, not only their size but also their shape, and surface features of NPs determine their biological distribution. Other advantage on improving drug delivery, is that different specific molecules, ligands or linkers could be attached to their surface to reach the target tissue decreasing the cytotoxicity in healthy cells (multi-functionalization). Indeed, the control of their surface characteristics is also decisive to obtain a non-toxic and stable colloidal suspension in physiological solutions, and to ensure a well sustained cellular uptake¹⁰⁵. Furthermore, nanocarriers are interesting as therapeutic agents improving properties as poor solubility, instability, pharmacokinetics and adverse side effects of drugs that are encapsulated or conjugated to their surface¹⁰⁶.

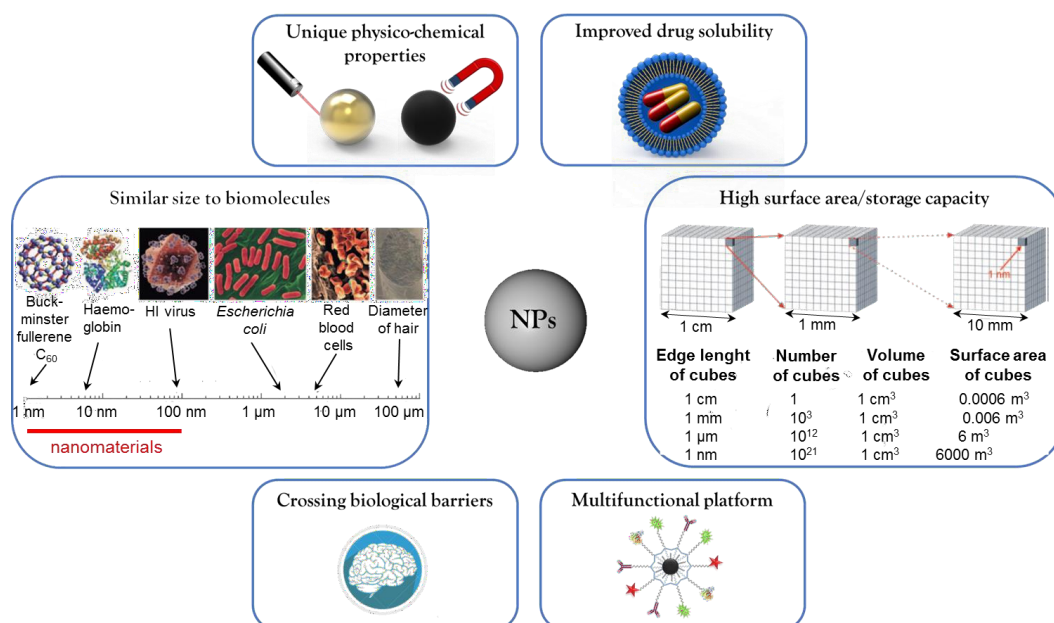


Figure 1. Key features of NPs for their use in biomedical applications. Adapted from Goesmann and Feldmann¹⁰⁷.

Tremendous efforts have been made in the past decades in the development of several therapeutic platforms that have been approved for cancer treatment, mostly organic ones such as liposomes and albumin nanoparticles. In comparison with these organic NPs, inorganic nanoparticles have more diverse and distinct physical properties closely correlated to their size and composition¹⁰⁸. Among the many nanomaterials in biomedicine, magnetic nanoparticles (MNPs) has taken the lead as they exhibit not only high biocompatibility but also an integrated design capability for cell targeting, imaging and therapy¹⁰⁹. MNPs are interesting due to their magnetic properties (magnetic moment, remanence and coercitivity) that make them interesting for the development of novel therapeutics strategies safer and more effective for cancer treatment. Indeed they present several advantages as theragnostics (treatment + diagnosis) agents: *i*) they could be visualized by Magnetic Resonance Imaging (MRI), *ii*) MNPs could be guided by controlled magnetic field gradients, and *iii*) they could be heated in the presence of an alternating magnetic field (AMF). However, one of the most challenging goals is the development of new strategies to finely tune the unique properties of MNPs, in order to improve their effectiveness in the biomedical field¹¹⁰.

Magnetic nanoparticles

MNPs can be divided into pure metals, metal alloys and oxides, whereas the most common composites of those are iron, nickel and cobalt but iron oxide NPs (IONPs) are the most extensively studied. That which sets them apart, other than their unique magnetic properties, is their biocompatibility and their capability of being injected into the body and with time their incorporation into the natural metabolic pathways¹¹¹. Whereas, materials such as cobalt or nickel are of less interest for *in vivo* applications as there are considered potentially toxic¹¹². The most common biocompatible MNPs are iron oxides, such as maghemite and/or magnetite ($\gamma\text{-Fe}_2\text{O}_3$ and Fe_3O_4). A key feature of MNPs that enables their application in biomedicine is related with their magnetic properties due to the electron orbital and spin angular moments. The response to an applied magnetic field (H) is measured by the magnetization, that is, the density of generated magnetic dipoles (M). The relation between the two magnitudes is defined as the magnetic susceptibility: $\chi = M/H$. Depending on the magnetic behaviour in response to magnetic field, magnetic materials can be classified into: paramagnetic, ferromagnetic, diamagnetic, antiferromagnetic, superparamagnetic and ferrimagnetic materials¹¹³. The following can be represented in the following diagram.

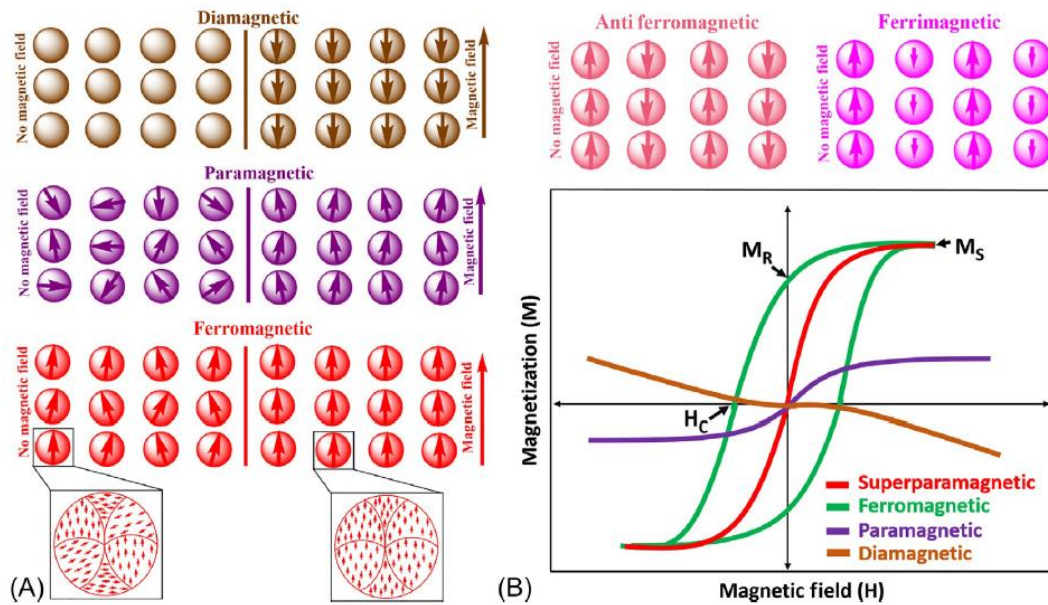


Figure 2. (A) Schematic illustration of the arrangement of the magnetic dipoles of various types of magnetic materials (diamagnetic, paramagnetic, ferromagnetic, antiferromagnetic, and ferrimagnetic), and their response in the absence and in the presence of an external magnetic field. (B) Representative hysteresis loops that illustrate the magnetic behaviour of materials when an external field is applied (H_c , coercive field; M_r , remnant magnetization; M_s , saturation magnetization). Adapted from Christos Tapeinos¹¹⁴.

All materials in nature display a type of weak repulsion to a magnetic field known as diamagnetism. Diamagnetic materials have a negative susceptibility ($\chi < 0$) and weakly repel an applied magnetic field (e.g., quartz SiO_2)¹¹⁵. For paramagnetic materials, there exist magnetic dipoles as illustrated in **Fig 2**, but these dipoles are aligned only upon application of an external magnetic field. For the balance of the magnetic properties, the magnetization in the absence of an applied field reveals their fundamental character¹¹⁶. Ferromagnetic materials have net magnetic dipole moments in the absence of an external magnetic field. Ferrimagnetic and ferromagnetic materials are the most interesting ones, as they exhibit remarkable magnetic properties. Ferromagnetic materials show a high magnetization M during the interaction with the applied field H . The magnetization does not increase indefinitely, but reaches asymptotically the saturation magnetization M_s . After turning off the external field H a little amount of residual magnetization, M_r remains, and the applied magnetic field required to reduce to zero the magnetization of the material is called coercive field or coercivity H_c . This relationship between

H and M is explained above (**Fig. 2**), showing the magnetic hysteresis loop. In contrast to dia- or paramagnetic ones, ferro- or ferrimagnetic materials retain a memory of an applied field once it is removed. Magnetic properties are highly dependent on the size and temperature thus when the size of a ferro- or ferri- magnet decreases to a certain critical value (D_c), the particles change from a state where they are composed by multiple magnetic domains to a single domain state. Further decrease in the size (D_0), implies that the thermal energy becomes comparable with that required for spins to flip directions, leading to the randomization of the magnetic dipoles in a short period of time. In such small particles the reversal of magnetization is spontaneous, therefore, in the absence of an external field they lose their magnetism but can rapidly respond once it is reapplied. Frenkel and Dorfman (1930) suggested this very same principle of the superparamagnetism theory, stating that ferromagnetic materials transfer from multi-domains to a single-domain state by particle resizing to nanoscale ^{117,118} (**Fig. 3**). Nanoparticles that present these unique magnetic properties are called superparamagnetic iron oxide nanoparticles (SPIONs) and are extremely attractive in the biomedicine field.

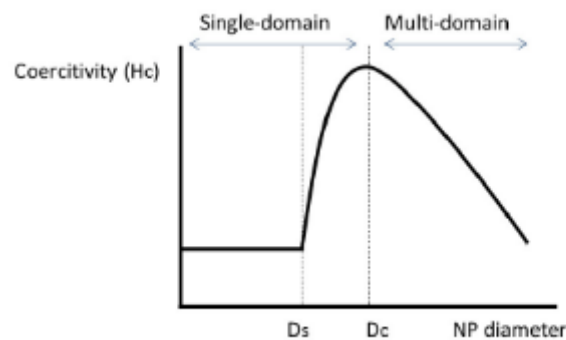


Figure 3. Magnetization behaviour of ferromagnetic and superparamagnetic NPs under an external magnetic field. Adapted from Ansari *et al* ¹¹⁷.

Domains of a ferromagnetic NP align with the applied fields. The magnetic moment of single domain superparamagnetic NPs aligns with the applied field. In the absence of an external field, ferromagnetic NPs will maintain a net magnetization, whereas superparamagnetic NPs will exhibit no net magnetization due to rapid reversal of the magnetic moment. The relationship between NP size, the magnetic domain structures, and coercive field is shown. D_s and D_c are the ‘superparamagnetism’ and ‘critical’ size threshold.

SPIONs and magnetic Hyperthermia

Hyperthermia (HT) is a way to improve the efficiency of chemotherapy or radiotherapy by raising the temperature of a tumour to 41–45°C using different physical mechanisms (eg. microwave irradiation applied via radiofrequency antennas, optical laser irradiation via fibres, water bath heating, etc)¹¹⁹. However, in clinical oncology, hyperthermia is currently regarded as the fourth line of therapy and is mainly applied as an adjunct, ranked below surgery, chemotherapy and radiotherapy. The technical challenges that are associated with the currently available hyperthermia modalities mainly include the difficulty of uniform heating within the tumour region until the required temperature is reached, without damaging the adjacent normal tissues. The use of MNPs in magnetic hyperthermia HT has become increasingly common in the treatment of cancer, and indeed had supposed a recent breakthrough in the field. Indeed, magnetic-mediated hyperthermia (MHT) may bring new alternatives for cancer locoregional hyperthermia by confining the heat to within the tumour site¹²⁰.

MHT uses a combination of alternating magnetic fields (AMF) and MNPs as heating agents. The objective is specifically and exclusively heating the region of a local tumour by means of the magnetic losses of magnetic nanoparticles in an external, alternating magnetic field, without damaging the surrounding healthy tissue. The confinement of the dissipated heat is a key factor and can be controlled using SPIONs and their ability to “switch-off” on removal of AMF. The energy loss in the magnetic material can be defined by two different effects: Magnetic losses through domain wall displacements (in multi-domain particles) called Neel losses; and energy loss from mechanical rotation of the particles, acting against viscous forces of the liquid medium (Brown losses). These effects add-up, converting the lost energy into heat. Many techniques involving hyperthermia are laser, ionizing radiation, and microwaves to heat up body (malignant) tissues. They can rise the intracellular temperature causing cell ablation, but they have unwanted collateral effects such as ionization of genetic material (radiation) or lack of selectiveness (microwaves) that affect the surrounding healthy tissues. In the recent years, MNP mediated hyperthermia has gained importance.

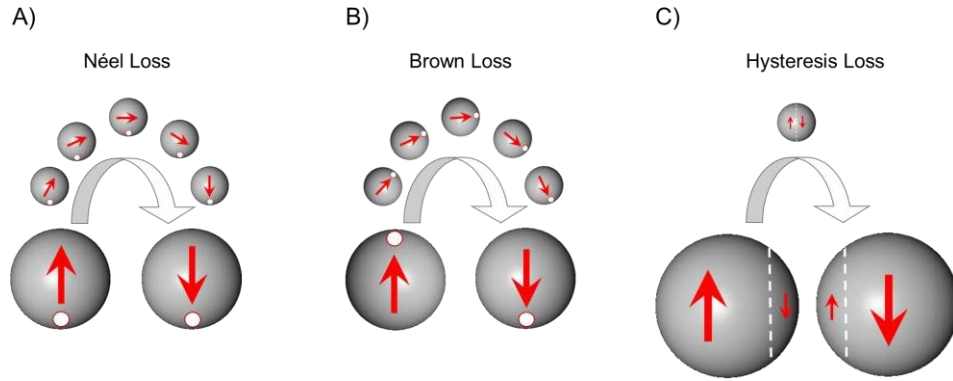


Figure 4. The major mechanisms of heat generation by MNPs. (A) Rotation of the moment within the MNPs overcoming their anisotropy energy barrier that leads to Néel Loss. (B) Mechanical rotation of the MNPs creates frictional losses with the environment and leads to Brown loss. (C) Movement of domain walls in multidomain MNPs leads to hysteresis loss. Adapted from Colombo *et al*¹²¹.

Though MH seems simple there are many factors that contribute to achieving the desired therapeutic effect. The employed MNPs should present a saturation magnetization high enough to efficiently heat on application of AMF and is related to the particle size and distribution of the SPIONs. The efficiency of the transformation of magnetic energy into heat can be described using the specific absorption rate (SAR) which is measured in terms of the rise in temperature per unit time and per gram of magnetic material, multiplied by the calorific capacity of the sample

$$\text{SAR [W/g]} = C \cdot (dT/dt) \cdot 1/m,$$

Where, 'C' is the specific heat capacity (eg. water 4185 W*s/l*K) (assuming 1 L=1 kg water), (dT/dt) is the heating rate in Kelvin per second, and 'm' is the concentration of the nanoparticles in g/L.

SAR depends not only on the amplitude (H) and frequency (f) of the AMF, but it is also closely correlated to the particle size and shape¹²². Besides, the increasing polydispersity of NPs implicates SAR reduction due to a decrease in the proportion of particles contributing to total heat generation¹²³. The nature of the coating is important, as it might significantly reduce the magnetic properties of the core, by influencing on the relative thickness of the shell and the overall size of the NP¹²⁴. The SPIONs physio-chemical properties are also tightly connected with the *in vivo* performance. Therefore, a suitable balance between the NPs optimal magnetic properties and the desired behaviour *in vivo* should be found.

DeNardo *et al.* demonstrated decreased tumour growth rates after applying AMFs to nude mice injected with antibody tagged, dextran- and PEG-coated, 20 nm diameter, superparamagnetic, iron oxide particles. It is worth noting that the applied fields used were quite large at 700,1000 or 1300 Oe (56, 80, 104 kA/m). The study also demonstrated that the nanoparticles had no observable toxicity¹²⁵.

Additionally, Munir T. et al. demonstrated using different capped iron oxide nanoparticles, the HRTEM, XRD, and DLS analysis showed that the average diameter around 20 nm, 20.5 nm, and 30 nm, respectively, and the particles were highly monodispersed with spherical morphology and additionally on exposure to alternating magnetic field of 15 mT and frequency 100 kHz for 1 h caused rise in temperature from 37 to 48 °C and resulted in cellular damage with subsequent apoptotic cell death. In an overall assessment, functionalized MNPs exhibited reduction in particle size, increased magnetization properties and enhanced efficacy for carcinoma treatments by hyperthermia¹²⁶.

Although, MNPs as nanoheaters has been mostly being developed for MHT application, it is gaining momentum non-traditional applications of magnetic heating such as triggering drug delivery or modulation of cell functions and responses by activating signal transduction mechanisms through stimulation of cells or sub-cellular entities¹⁰⁵. In this sense, this Thesis want to explore a completely novel use of magnetic heating that is to gain spatio-temporal control over bioconversion of pro-drugs by therapeutic enzymes, such as the use of horseradish peroxidase in the conversion of indole-3-acetic acid into cytotoxic radicals.

Bioconversion of pro-drugs: Oxidation of IAA by HRP

Over the past decade, the combination of indole-3-acetic acid (IAA) and horseradish peroxidase (HRP) has recently been proposed as a novel cancer therapy. 3-indole acetic acid (IAA), which is the main form of plant growth factor, is capable of producing cytotoxic species when oxidized by the action of the HRP enzyme¹²⁷. This system gives rise to an enzyme / prodrug combination with potential to be used as a basis in the development of new anti-cancer therapies. 3-indole acetic acid is a phytohormone involved in plant growth that is present in plants in picomolar quantities, but which influences multiple properties of plant growth, such as cell elongation, division and

differentiation, and also on senescence and abscission of the leaves. IAA is a derivative of indole, containing a carboxymethyl substituent. The activity of IAA in plant metabolism is regulated by the irreversible elimination of the molecule, which can occur through two alternative routes: the first depends on oxidation by peroxidases that cause decarboxylation and the second consists of non-decarboxylating reactions that form non-reactive compounds¹²⁸.

In the past decade, the decarboxylation pathway catalysed by HRP, which is known to be highly complex, has been extensively studied. P. Wardman *et al.* describes a 10-step mechanism in which HRP compound I and II will oxidise IAA (**Fig. 5.1**) at neutral pH to an indolyl radical cation (**Fig. 5.2**). This cation dissociates to form an indolyl radical (**Fig. 5.3**) with a radical pKa of 5.1 for dissociation of the indole N-H group. The radical cation (**Fig. 5.2**) but not the dissociated radical (**Fig. 5.3**) decarboxylates to form a skatoyl radical (**Fig. 5.4**). This carbon centered radical is very reactive towards oxygen, rapidly forming a peroxy radical (**Fig. 5.5**). The peroxy radical decays in two ways. Reduction and protonation form skatole hydroperoxide (**Fig. 5.8**), which reacts further with HRP compound I to form indole-3-carbinol (**Fig. 5.7**). The hydroperoxide can also decompose non-enzymatically to oxindole-3-carbinol (**Fig. 5.9**) and 3-methylene-2-oxindole (**Fig. 5.10**). In addition, combination and elimination by the Russell mechanism, in which two peroxy radicals combine, form indole-3-aldehyde (**Fig. 5.6**), indole-3 carbinol (**Fig. 5.7**), and singlet oxygen, although this may not occur at physiological pH. The reactivity of various indoles with HRP compound I has been shown to be closely related to the reduction potentials of the indolyl radical with an increase in rate constant of approximately 300-fold for a decrease in reduction potential (radical/ground state) of only 0.1 V¹²⁹.

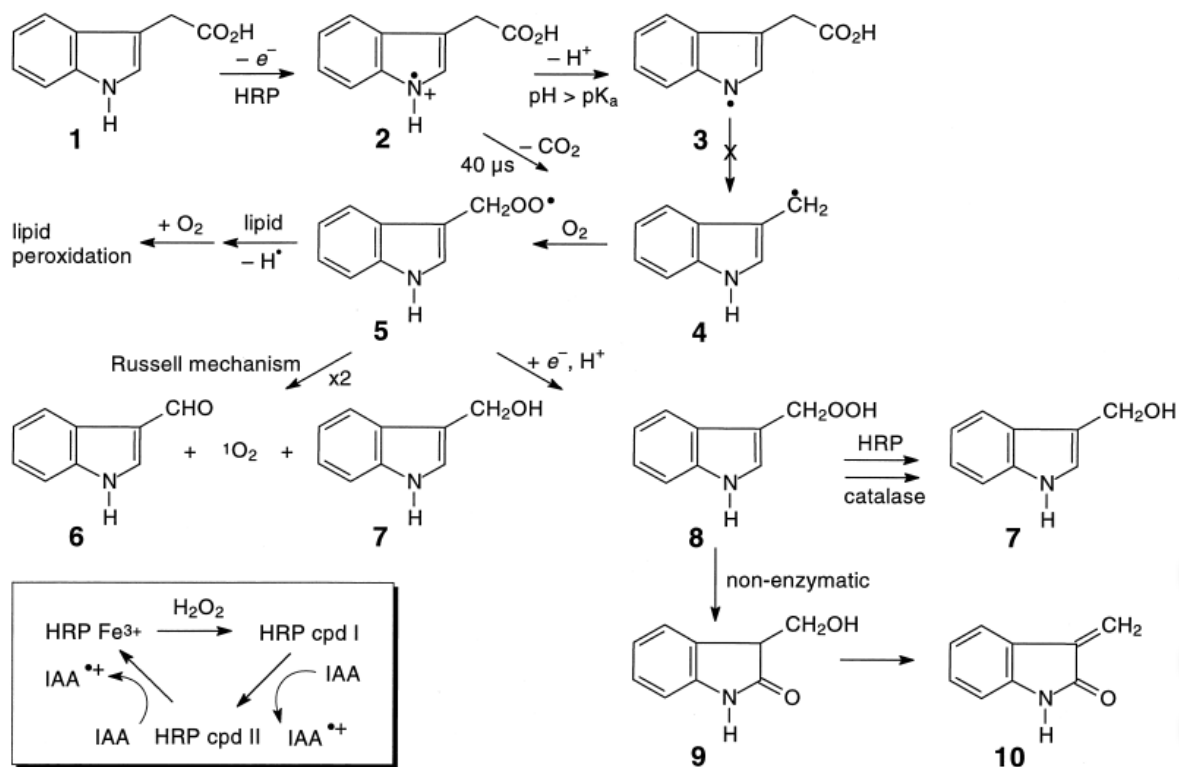


Figure 5. Reaction pathways involved in oxidative activation of IAA to toxic species. Adapted from Wardman *et al*¹²⁹.

In literature, there are many reports showing that the hormone, when activated by the action of HRP, gives rise to a potent cytotoxic drug that can be used as an anti-cancer agent. Gupta *et al.* demonstrated that using magnetic iron oxide NPs encapsulating HRP, the enzyme entrapment efficiency of HRP was found to be as high as 92%, and in the presence of solely IAA in two cell lines there was no cytotoxic effect, however, it was active only after oxidative decarboxylation by HRP. The benign substrate IAA reaches the cells and is then oxidized by HRP. IAA, on reacting with HRP, forms free radicals such as indolyl, skatole and peroxy radicals. This creates severe oxidative stress in the cancer cells, resulting in cell death.

However, HRP optimal temperature is 45°C, that means that at the corporal temperature HRP is not working at its maximum efficiency. That is why we proposed the use of magnetic heating generated by MNPs, co-encapsulated with HRP within biosilica NPs, to increase enzyme activity without raising the macroscopic temperature of the targeted tumoral tissue.

In this chapter, the characterization of the developed nanohybrids (Chapter 1) determining their magnetic properties is being studied. Even entrapped the HRP

molecules were capable to bioconvert IAA. Besides, local magnetic heating of co-entrapped HRP is demonstrated using an artificial colorimetric substrate for the proof of concept. Last by not least, thinking on their in vitro/potential in vivo use for DEPT, their stabilization in complex biological media (complete cell culture media) has been achieved by neutralization of their positive surface charge by blocking primary amine groups with glucose. Glucose has the advantage of not only being used as blocking agent but also could act as active-targeting molecule for tumoral cells.

Objective

To study the physicochemical properties of the nanohybrids obtained in Chapter 1 and showed that by magnetic heating is possible to tune the enzyme activity of co-entrapped HRP.

Specific Objectives

Determine the size, porosity, net surface charge and magnetic properties of the nHs.

Study the colloidal stability of the nHs in complex media and developing solutions to mitigate possible aggregation due to protein corona formation.

Study the effect of AMF on the enzyme activity entrapped in the nHs

Materials and Methods

Physicochemical characteristics of the nanohybrids (nHs)

Analysis using Environmental Scanning Electron Microscopy (ESEM).

The morphology and particle size distribution of the resulting nanoparticles (NPs) were characterized by Environmental Scanning Electron Microscopy (ESEM) images were obtained using a QUANTA-FEG 250 microscope in “wet-mode” using a Peltier stage and a gaseous secondary electron detector (GSED). The secondary electron images were taken at a voltage range between 10-15 keV, low temperature (1°C), high chamber relative humidity (100%) and high Pressure (659 Pa) to maintain the wet sample hydrated avoiding the sample damage during the observation. The sample was prepared in milliQ water in a dilution of 100 µg and sonicated prior to measurements for 3 min to improve its polydispersity.

Dynamic Light Scattering (DLS) and Z-potential measurements.

The measurements were performed on a Malvern ZS nano instrument at 25°C. Each sample was prepared by diluting the sample 100 µg with milliQ water of which 1 mL was added to a cuvette. The measurement was repeated 10 times, with a combination of 3 runs per measurement. The data was analyzed using Zetasizer software. Similarly, the z-potential was measured using the same sample in a Folded Capillary Zeta Cell and the sample was measured 10 times and analyzed using the software.

Analysis using Scanning Transmission Electron Microscopy (STEM).

Using a QUANTA-FEG 250 microscope an aliquot of the sample was centrifuged and resuspended in distilled water and sonicated for 3 min. The sample was mounted on a stub of metal with adhesive, coated with 40-60nm of gold and fixated. The measurements were carried out at RT and in solution.

Analysis using Transmission Electron Microscopy (TEM) and EDx.

Transmission Electron Microscopy (TEM) micrographs were acquired using a Tecnai F30 (FEI). TEM grids were prepared by drying a 10 mg of nHs suspended in water onto

a carbon coated copper grid at room temperature. Iron oxide cores were easily identified by STEM-HAADF (scanning transmission electron microscopy - high-angle annular dark-field imaging), due to the higher contrast of iron in comparison with the rest of the elements forming part of the nanoparticles.

Porosimetry by Brunauer-Emmett-Teller (BET) Surface Area

Textural properties of the nHs were characterized by nitrogen adsorption isotherms at -196°C of the samples using automatic adsorption equipment (ASAP2010 micromeritics). Before the measurements, samples were lyophilized and then calcined under air flux in a HOBERSAL oven at 600°C for 6 h using a heating rate of $7^{\circ}\text{C} \cdot \text{min}^{-1}$. Lyophilized and calcined samples were then outgassed under vacuum at 150°C until the pressure was stable and lower than $5 \mu\text{mHg}$. The apparent BET surface area (S₀BET) was calculated by fitting nitrogen adsorption data to the BET equation. The micropore volume (V_m) was calculated by the t-plot method. The Barrett–Joyner–Halenda (BJH) method was also applied in order to determine the pore size distribution in the mesopore range (2–50 nm). The total pore volume was directly recorded from the isotherm. The free space measurements were performed using helium gas. Nitrogen and helium gases used in the experiments were 99.9995% pure.

Physical characterization of the nHs

Alteration of the order during synthesis.

To study if the order of reagents used would affect the synthesis, kinetics and conformation of the nHs we altered the order in which they would be added to the synthesis. We added to buffer with trehalose the MNPs and the enzyme and incubated it for 10 min in agitation at RT. Following which the PEI (MW 1300 and 60 000) was added and incubated for 15 min at RT in agitation. And finally, the TMOS was added and the protocol followed the as before.

Inertisation of surface of nHs with Glucose.

To the previously optimized synthesis, mentioned in **Chapter 1**, for the co-entrapment of the MNPs and enzyme in silica to counter the problem of aggregation observed in the nHs a blocking with glucose 1 M was carried out. Prior to reduction with sodium

borohydride, the particles were washed, and a solution of 1 M glucose dissolved in distilled water was added (R1:10) and was placed on a roller shaker at RT for 1 h.

Magnetic characterization of the nHs

Analysis using Superconducting Quantum Interference Device (SQUID).

100 μ l of each sample were placed inside a polycarbonate capsule and sealed with vacuum grease for their magnetic characterization. The magnetic characterization was performed in a Quantum Design (USA) MPMS-XL and MPMS-5S SQUID magnetometers equipped with an AC (Alternating current) magnetic susceptibility option. Both DC (direct current) and AC measurements were performed.

For the DC measurements, field dependent magnetization was recorded at 300 K under decreasing field starting from 5 T, and at 10 K in the field range between -5 T and 5 T. These measurements allow the evaluation of the magnetic properties of the material, in particular to verify if the particles are superparamagnetic at room temperature, if their hysteresis loop is close, with negligible coercivity. This kind of measurements also allow comparing the saturation magnetization with that of the bulk material (around 80 emu/g for magnetite), to evaluate if there is any effect of the particle size on the magnetic properties of the material.

AC measurements were performed with AC amplitude of 0.41 Oe, in the temperature range between 2 and 300 K and at a frequency of 11 Hz. These measurements are useful to verify the aggregation of the particles and the impact that this process could have on their magnetic behavior.

Quantification of Fe in the nHs.

Iron concentration was determined using a standard colorimetric procedure. For the MNPs (1 mg/mL), an aliquot was digested with aqua regia for 15 min at 60°C and diluted with Milli-Q water. For the nHs, a digestion of the nHs was performed heating with HNO₃ (Panreac) and then with H₂O₂ (Panreac) (both steps at 90 °C and during 1 h each). A calibration curve was prepared by dilution of an iron standard solution of 1 mg/mL of Fe in 2% HNO₃ (Acros Organics, USA). The digested samples were incubated at room temperature for 15 min after the addition of KOH (4 N), 4,5dihydroxy-1,3-benzenedisulfonic acid disodium salt monohydrate (Tiron), and sodium phosphate buffer (0.2 M, pH 9.7). Finally, sample absorbance (480 nm) was

measured on an UV/vis spectrophotometer (Thermo Scientific Multiskan GO MA, USA) and compared to a calibration curve.

Analysis the Specific absorption rate (SAR).

The heating capabilities of MNPs under external AC magnetic field are quantified by the specific absorption rate (SAR) parameter (also referred to as specific loss power (SLP) to describe the same physical reality), which provides a measure of the rate at which energy is absorbed per unit mass of the magnetic nanoparticles.

$$\text{SAR [W/g]} = C \cdot (dT/dt) \cdot 1/m,$$

Where, 'C' is the specific heat capacity (eg. water 4185 W*s/l*K) (assuming 1 L=1 kg water), (dT/dt) is the heating rate in Kelvin per second, and 'm' is the concentration of the nanoparticles in g/L

Hyperthermia measurements were recorded with a magnetic heating system nB nanoscale Biomagnetics DM 100 series (nB nanoscale biomagnetics, Zaragoza, Spain). The samples, 1 mL of pure Fe₃O₄ MNPs suspensions at different concentrations, 0.5 and 1 mg/mL were placed in a vial, at the centre of an 8-turn coil, connected to the remote heat station of the device. With this setup, alternating magnetic fields with strength of 25.2 mT at a frequency of 829 kHz were generated. The temperature was measured using a fiber-optic probe, placed in the centre of the vial, connected to a computer, providing the temperature values each second and the data fitting for instant ZAR calculations was calculated using the in-built MaNiac Software.

Activation of the enzyme using hyperthermia.

To demonstrate the activation of the enzyme on application of a magnetic field we studied the increase in enzymatic activity using the colorimetric assay during a period of 20 min. Using nB nanoscale Biomagnetics DM 100 series (nB nanoscale biomagnetics, Zaragoza, Spain), a maximum frequency of 829 kHz and field of 25.2 mT for different time intervals of 2, 5, 10, 15 and 20 min was applied to a solution of nanohybrids with activity of (63.13 U/mg) containing the substrates 50 uL of ABTS and 100 uL of H₂O₂ with 850 μL of activity buffer potassium phosphate 0.1 M pH 5.0. Immediately following which the absorbance was measured spectrophotometrically at 420 nm and a linear graph of the absorbances was plotted. Similarly, controls were

analysed, using a thermoblock which was set to different temperatures of 30°C, 45°C and 55°C, with Eppendorf's containing the same enzymatic reaction assay. At the time aforementioned intervals, the Eppendorf tubes were removed, and the absorbance was measured. The data was analysed using GraphPad Prism 6.0 software and the increase in temperature was calculated and compared with the nHs exposed to hyperthermia.

Thermal stability of the enzyme using hyperthermia.

The stability of the enzyme was similar to the activation experiment wherein hyperthermia was measured using the equipment at its maximum field (25.2 mT) and frequency (829 kHz). The vial contained only 10 µL of the enzyme solution in 850 µL of the activity buffer and was exposed to the magnetic field for 5, 10 and 20 min without the substrates. The global temperature of the solution in the equipment was maintained below 30°C (~26-27°C). After exposure for the aforementioned time intervals the substrates (H₂O₂ and ABTS) were added, and the slope was measured spectrophotometrically with constant agitation for 10 min at 420 nm. Similar controls were incubated for 5, 10 and 20 min at 30°C, 45°C and 55°C and were measured spectrophotometrically at 420 nm for 10 min in constant agitation. The data was analysed using GraphPad Prism 6.0 software and the increase in temperature was calculated and compared with the nHs exposed to hyperthermia.

Biochemical characterization of the nHs

HPLC analysis of the conversion of 3-IAA by HRP.

Using a modification from Chui et al.¹³⁰ the oxidation of 3-indole acetic acid (3-IAA) by soluble and immobilized preparations (1 IU) was carried out in 100 mM sodium acetate buffer pH 5.0 containing 500 µM of 3-IAA at 25°C for 2 h. An aliquot of reaction mixture was injected into a reverse-phase HPLC on a C18 Columbus column at 25°C using an isocratic elution buffer of methanol/1 % acetic acid mixture (40:60, v/v) at a flow rate of 0.6 mL/min. The eluted products were monitored at absorbance of 250 nm using an Agilent 1100 series detector. The retention time for 3-IAA was 22 min and the reactive oxygen species were eluted from 3 min to 20 min.

Results and Discussion

Nanomaterials, which are similar to biological molecules in scale, can be used as diagnostic and therapeutic nanomedicines¹³¹. Many methods have been used for evaluating manufactured nanomaterials, including techniques in optical spectroscopy, electron microscopy, surface scanning, light scattering, circular dichroism, magnetic resonance, mass spectrometry, X-ray scattering and spectroscopy, and zeta-potential measurements, as well as methods in the categories of thermal techniques, centrifugation, chromatography, and electrophoresis¹³².

In the previous chapter we described the different pre and post strategies used to develop nHs that were active and provided a significant thermal, pH and operational stabilization of the HRP. Given the importance of physicochemical properties of nanodevices for biomedical applications, in this Chapter we focused on the investigation of the physicochemical characterization of the nHs using varied techniques. Although from previous studies we have learned that certain synthesis conditions favoured the activity and stability of the entrapped enzyme, characterization of the different nHs from the use of several PEI size were performed as could not anticipated which strategy could provide additional improved properties.

Analysis using Scanning Electron Microscopy (SEM) and Dynamic Light Scattering (DLS)

The analysis by SEM showed that when the entrapment of HRP using PEI MW 1300 was performed without chemical modification, biomimetic Si formed as preferentially disperse particles with a nanosized diameter range of ~ 300-550 nm with a sharp accumulation of ~400 nm diameter particles **Fig 6A and B**.

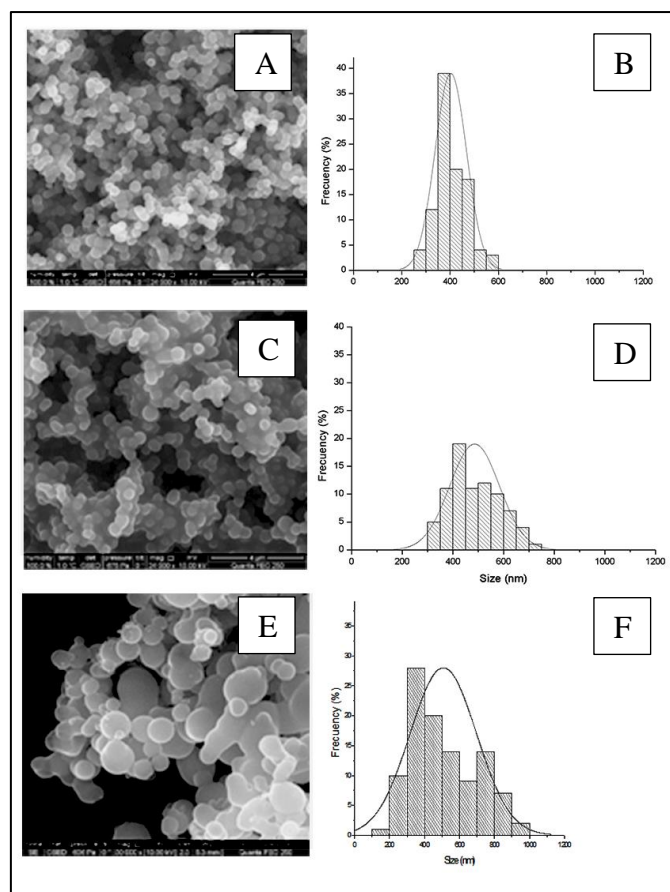


Figure 6. Analysis by scanning electron microscopy (SEM) of nanohybrids using PEI MW 1300 Da. A) BioSi@HRP, C) BioSi@HRPox E) BioSi@THRP_1300. B, D y F) correspond to histograms of frequency of particles versus their particle size in each case. Histogram was plotted using Origin Pro 8.0.

When oxidized HRP was entrapped and the resulting particles submitted to NaBH_4 reduction, biomimetic Si formed as interconnected randomly agglutinated particles of approximately ~300-800 nm **Fig 6C and D**. In this case, the Gaussian fitting of the nanoparticle size histogram showed a wider size distribution of the material, demonstrating an effect of the chemical modification of the enzyme on the synthesis of biomimetic silica. The oxidation of enzymatic sugar residues may have changed the ionization state of the enzyme at pH 8.0 which could alter the Si deposition process. Previous reports have already conferred a fundamental role of the interplay of attractive/repulsive electrostatic interactions during Si synthesis on the particle size and distribution of the material^{51,133}. The presence of trehalose during Si synthesis also affected the size distribution of the particles obtained with diameters ranging from 100 to 1000 nm. Moreover, trehalose significantly impacted the homogeneity of the sample **Fig 6E and F**. Given that the amount of protein used in all the entrapment experiments

was the same (1 mg/mL), size dispersion can be attributed solely to trehalose. These results corroborate with Rodriguez et al ¹³⁴ that found that the addition of carbohydrates to standard hydrostatic solutions altered the size of the spherical Si particles obtained from *in vitro* polycationic peptide-mediated biosilicification. Although their findings were obtained after Si precipitation without protein in the synthetic mixture, it became clear that sugar molecules imparted some degree of morphological control on the deposited silica.

Table 1 shows the results for DLS analysis of the different nanohybrids with and without MNPs. Addition of MNP in the synthesis mixture provided nanohybrids with smaller hydrodynamic sizes making the final diameter of the hybrid independent of the size of the PEI used (~500-600 nm). This correlates with the results obtained for an increase in %Y after addition of MNPs and the analysis by SEM of the samples that included MNPs **Fig 7**. The samples that included MNPs one again showed interconnected particles of a mean hydrodynamic radius of 400-450 nm **Fig 7**. The particle size distribution has a high dispersity that correlates with increased PDI results **Table 1** that did not impact on the activity of the nHs.

Table 1. Dynamic light scattering and net charge analysis of nanohybrids.

Hybrids	Hydrodynamic size (r.nm)		Poly dispersity index (PDI)		Zeta potential (mV)	
	MNP (-)	MNP (+)	MNP (-)	MNP (+)	MNP (-)	MNP (+)
BioSi@THRP_1300	630±26	684±8	0.199±0.136	0.311±0.03	6.79±0.791	23.4±4.68
BioSi@THRP_2000	815±52	589±28	0.104±0.067	0.321±0.04	6.87±0.701	21.5±4.24
BioSi@THRP_25000	535±23	491±26	0.129±0.063	0.402±0.08	8.31±0.701	11.6±5.46
BioSi@THRP_60000	1026±83	543±21	0.207±0.089	0.354±0.05	9.81±1.12	15.5±4.00

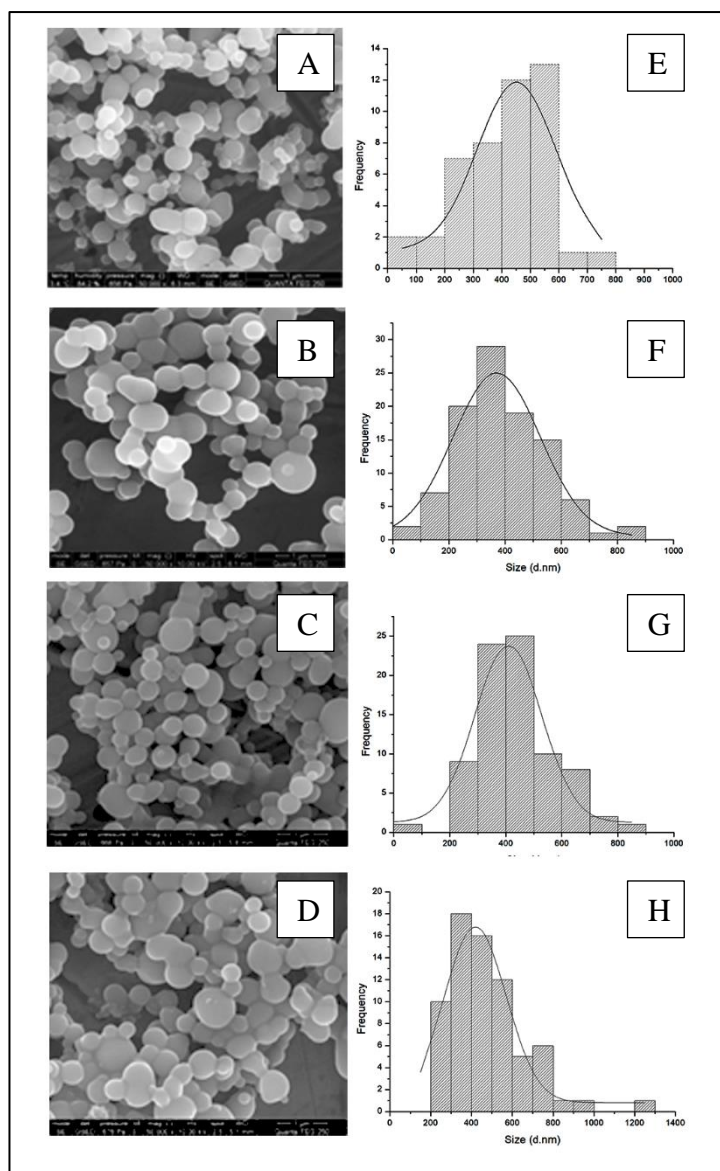


Figure 7. Analysis by SEM of nanohybrids with distinct PEIs A) BioSi@THRP_MNP_1300. B) BioSi@THRP_MNP_2000, C) BioSi@THRP_MNP_25000 and D) BioSi@THRP_MNP_60000. Similarly, E, F, G, H correspond to their histograms analysed using ImageJ and Origin 8 Pro.

Analysis using Transmission Electron Microscopy (TEM), Scanning Transmission Electron Microscopy (STEM) mode and EDX

From the TEM results we were able to determine the approximate localization of the MNPs within the matrix. The original commercial MNPs from Chemicell used for nHs synthesis are not isolated MNPs but clusters of MNPs embedded in a polyaspartic acid (PAA) matrix of 200 nm of mean diameter. The MNPs encapsulated within the nHs are easily identified (blue arrows) also as clusters but it is evident that the distribution is not uniform within the Si particles. From **Fig. 8** we can conclude that except for BioSi@T_HRP_MNP_60000 the rest of nHs showed a majority of MNPs located both deep inside the Si matrix as well as on the Si matrix surface but always linked to them (meaning that no isolated magnetic nanoparticles were found on the grid). Nevertheless, as it will showed below, the heterogeneous location of the nanoparticles does not seem to be an important factor to achieve the required local temperature during AMF for application for tuning HRP activity.

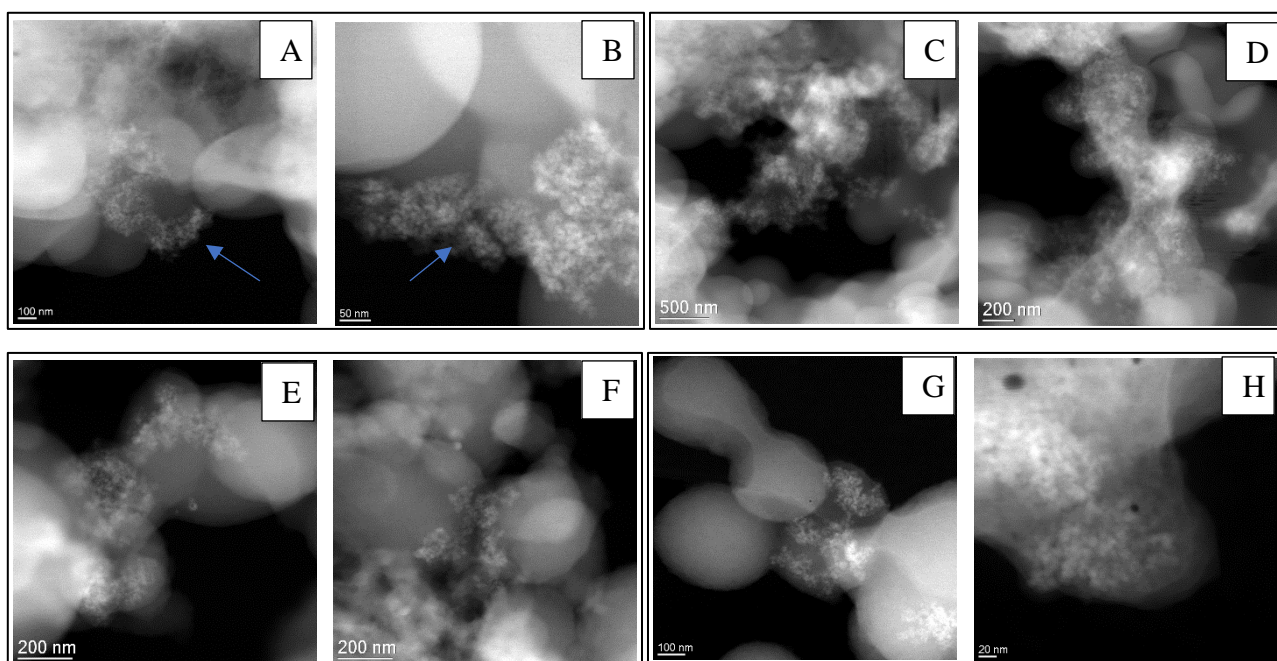


Figure 8. Transmission electron microscopy (TEM) images of the nanohybrids synthesised using different PEI. (A) and (B) BioSi@THRP_MNP_1300, (C) and (D) BioSi@THRP_MNP_2000, (E) and (F) BioSi@THRP_MNP_25000, (G) and (H) BioSi@THRP_MNP_60000.

Both the magnetic nanoparticles and the silica matrix can be easily distinguished from the STEM images, being the magnetic particles the smaller and brighter particles and the Silica matrix the bigger balls. Elemental mapping using EDX analysis showed Fe

content in all the nHs, proving a successful entrapment of the MNPs (blue boxes) (**Fig 9**). As the MW 1300 and 2000 are similar we analysed only the lowest, intermediate and highest MW PEI nHs. The composition of both parts has been confirmed by EDX, obtaining a clear signal from iron for the magnetic particles and for Si for the rest of the nanohybrid structure. The Cu signal observed in the image corresponds to the grid used for the sample preparation. (**Fig. 9**)

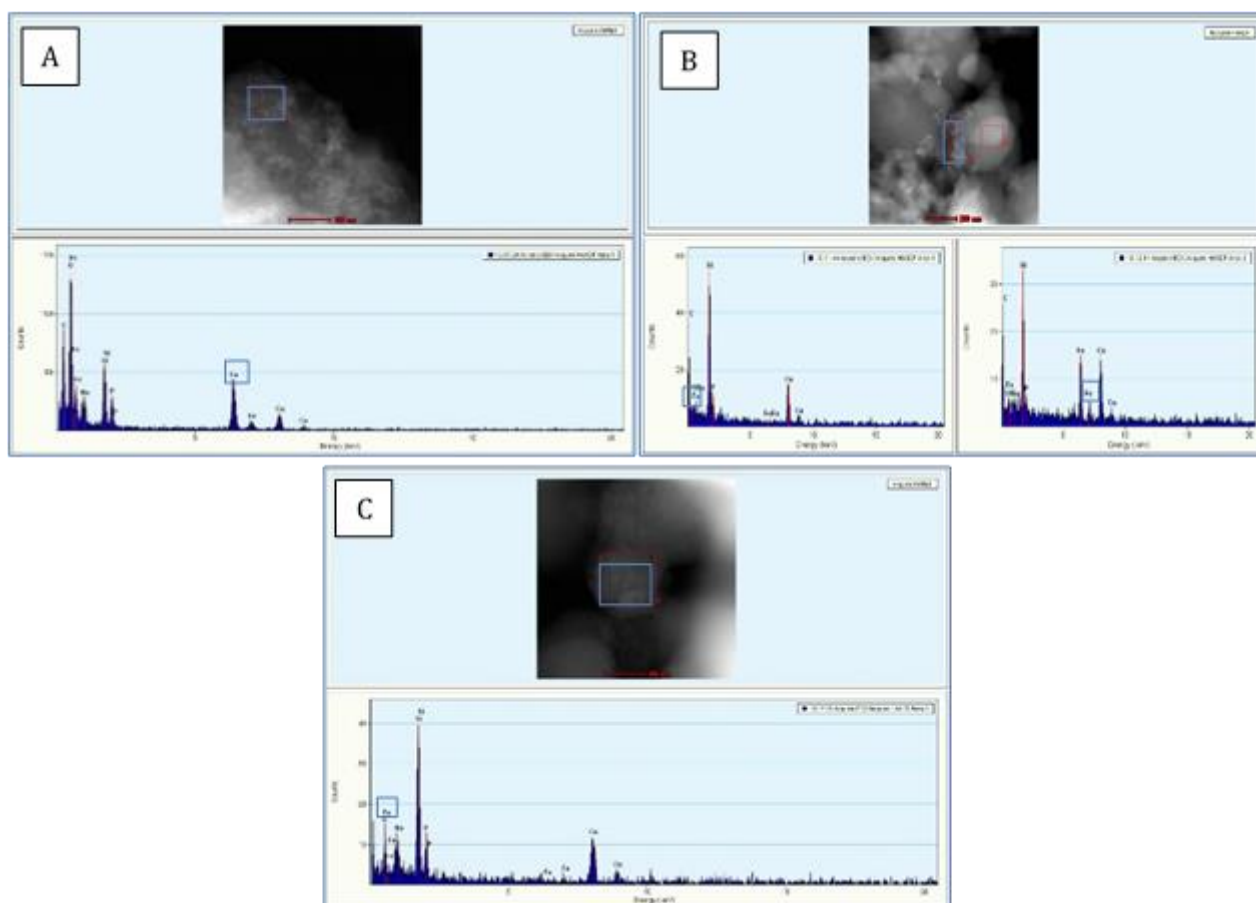


Figure 9. TEM EDX microanalysis showed the confirmed presence of iron (Fe) entrapped within the silica matrix using (A) BioSi@THRP_MNP_1300 and (B) BioSi@THRP_MNP_25000 (C) BioSi@THRP_MNP_60000.

Quantification of Fe in the nHs.

In order to quantify the concentration of Fe in nHs, a colorimetric assay described in Beola L et al.¹³⁵ was used by evaluation of initial Fe concentration in the synthetic mix and total Fe after digestion of the nHs. It was clear that all the MNPs offered were encapsulated as the concentration of Fe in the nHs were like that of the pure MNPs

(Table 2) offered in the synthesis. Initial concentration of MNPs offered in the synthesis was maintained the same.

Table 2. Concentration of Fe present in the various synthesis.

	Concentration of Iron (Fe) (mg/mL)
Pure MNPs offered to the synthesis	1.29 ± 0.02
Bio@THRPox_MNP_1300	1.39 ± 0.02*
Bio@THRPox_MNP_2000	1.22
Bio@THRPox_MNP_25000	1.15 ± 0.01
Bio@THRPox_MNP_60000	1.08

* The difference in the BioSi@THRP_MNP_1300 could be due to an error in manipulation of the sample.

BET surface analysis

Textural properties of the formed organo-silicas were determined by gas adsorption using nitrogen at 77 K as sensing probe. The formed nHs following the typical synthesis using PPEI MW of 1300, 2000 and 60000 present an apparent surface area of 21, 14 and 13 m²g⁻¹ respectively. These values are increased after the thermal removal of the organic molecules achieving up to 75 m²g⁻¹ for the PEI MW 1300, 45 m²g⁻¹ for the PEI MW of 2000 and 27 m²g⁻¹ when a larger molecule is used (60000) (**fig. 10**). Interestingly, a different trend is detected by using a branched molecule (PEI MW 25000). The textural properties of this kind of nHs present almost two times the apparent surface area (35 m²g⁻¹) of the linear molecules that form the nHs that is reduced to negligible values after the treatment. Their respective pore size distribution also present significant differences. When, PEI MW of 1300, 2000 and 60000 Da are used, the nHs present a main pore size distribution centred at ca. 2.2 nm meanwhile for those where PEI MW 25000 was used larger pores centered at 10 nm were obtained. The higher surface area in addition to the presence of larger and thus more accessible cavities using PEI MW 25000 Da did not relate to an increase in yield after HRP immobilization. However, it could provide certain differences in its behaviour under AMF compared to its counterparts.

Table 3. Pore size distribution from Surface BET analysis of the nHs

	Surface area (m ² /g)	Pore size distribution centered at (nm)
BioSi@THRP_MNP_1300	21.4046 ± 0.5035	2
BioSi@THRP_MNP_2000	13.9684 ± 0.1236	2
BioSi@THRP_MNP_25000	35.3540 ± 0.3742	10
BioSi@THRP_MNP_60000	13.8196 ± 0.1803	2

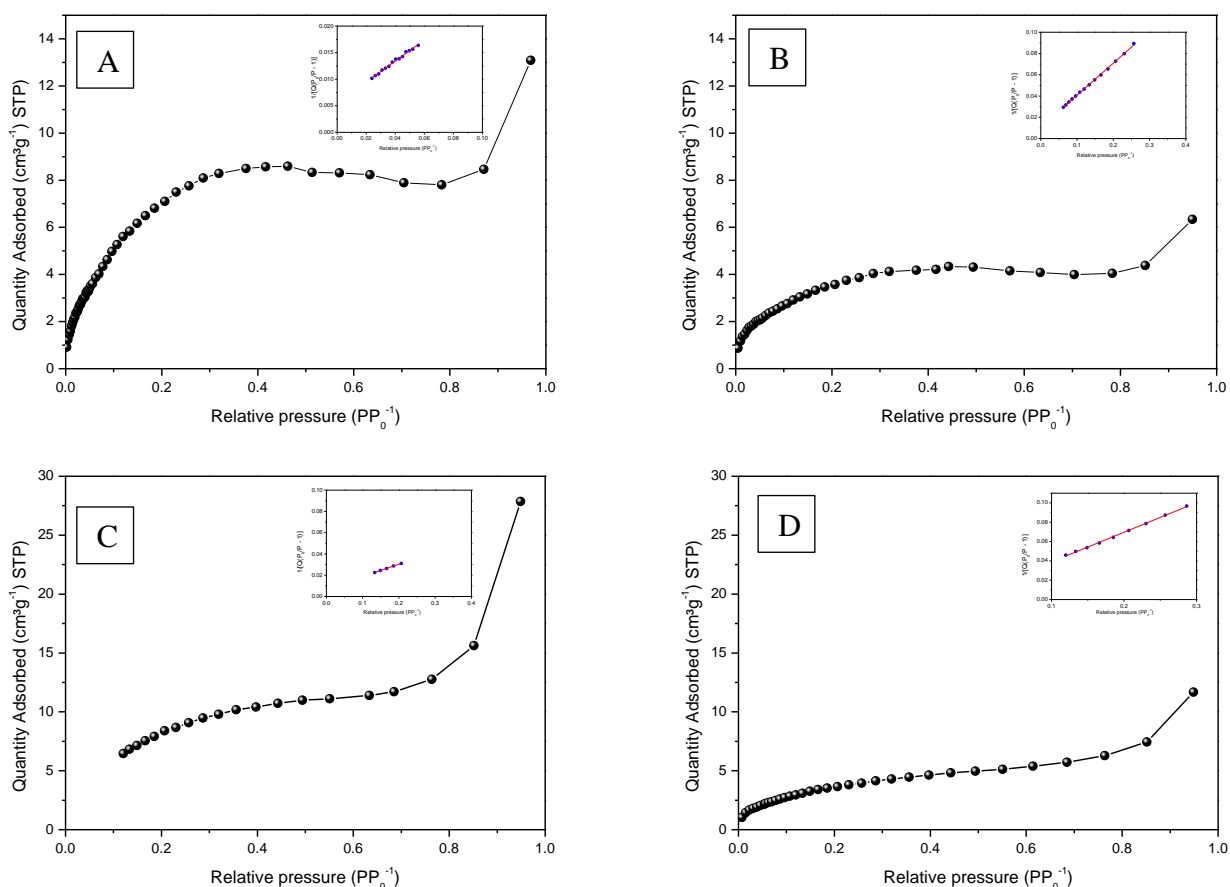


Figure 10. BET surface analysis of the nHs A) BioSi@THRP_MNP_1300 B) BioSi@THRP_MNP_2000 C) BioSi@THRP_MNP_25000 D) BioSi@THRP_MNP_60000

Inertisation of the surface with Glucose 1 M

Judging from SEM and dynamic light scattering analysis it was clear that there was aggregation among Si nanoparticles. This effect could be even more severe in the presence of biological fluids whose high ionic strengths and high content in biomacromolecules (proteins) usually affect NPs colloidal stability. A common strategy to achieve stable NPs dispersion is their surface modification using inert molecular

coatings. Therefore, considering the final objective of this work and given that the methodological approach required experiments in complex biological media we tried various inertisation agents such as dextran, bovine serum albumin (BSA) and glucose. These agents have previously proven to improve the overall colloidal stability of the⁵⁰ NPs.

Dextran is natural polymer, neutral, branched polysaccharide composed of glucose subunits with a high biocompatibility and due to its resistance to enzymatic degradation is sort after for biomedical use^{136,137}. It aids the coupling of other ligand groups and MNPs coated with dextran were showed to have a high MRI contrast and cellular uptake of these MNPs was reported to be 2-4 times higher than unmodified ones. The ability of proteins to generate a hydration shell *via* hydrogen bonds with water molecules prevents the adhesion of other proteins and therefore improves NPs stability¹³⁸. Moreover, functionalization of NPs with glycans not only ensures colloidal stability in protein-rich physiological media but also prevents phagocytosis by macrophages and exhibits excellent selectivity toward carbohydrate binding proteins.

BSA is also a largely used as stabilizing agent to avoid non-specific interactions and improve colloidal stability of NPs. Xia et al. showed that albumin coating of silica NPs enhanced their water-dispersibility and long-term stability under physiological conditions. Additionally, it reduced non-specific cellular uptake *in vitro* and prolonged blood circulation *in vivo* upon intravenous injection in mice¹³⁹.

Monosaccharides such as glucose could also act as stabilizing agent for NPs^{140,141}, indeed it present several advantages over other stabilizing agents such as that: i) it do not increase the global hydrodynamic size of the NP, ii) it is easy to work with, and iii) is inexpensive. Furthermore, its small size does not give rise to the shielding of other conjugated ligands, in contrast to what occurs within higher MW stabilizing agents. Lastly, monosaccharides could be used as passivation molecules but may also serve as targeting molecules, as carbohydrates present in the organism play a major role in many biological processes. In particular in the case of glucose it is well known that it could be used for active targeting of tumoral cells. As glucose is a major source of energy in mammalian cells, tumoral cells overexpressed glucose receptors¹⁴².

We therefore assayed and compared the inertisation of the nHs with Dextran, BSA and glucose (**Table 4**). From the results obtained we observed that the most promising agent

was glucose (1 M) which recovered almost all the enzymatic activity after inertisation. The increment in activity from the previously synthesised NPs could be due to the fact of a more homogenous dispersion of the NPs in the solution thus enabling the passage of substrate freely yielding a higher activity. The DLS results corroborated this with the decreased polydispersity index as compared to the control. In the case of dextran, the nHs lost all their activity, as dextran is a large polymer it could have blocked all the active sites of the enzyme or hindered the access of the substrate to the pores of the nHs (**Table 4**). Additionally, an increase in aggregation of nHs was observed in comparison with the control, which may be due to the large polymeric nature of dextran, composed of glucose chains that could cause the NPs to generate agglomerates. BSA showed an average yield (**Table 4**) in comparison to the control but was discarded as it did not improve the aggregation. (**Table 4**).

Table 4. Inertisation of the surface of the nHs.

Agent	Activity offered (IU)	Activity post-blocking (IU)	Hydrodynamic diameter (nm)	Polydispersity index (PDI)	Zeta Potential (mV)
BioSi@THRP_MNP_1300 w/o blocking	5.0	3.5*	684 ± 68	0.311 ± 0.03	23.4 ± 4.68
Dextran (0.1 g/ml)	5.5	0.32	5158 ± 93	1.09 ± 1.09	-
BSA (600 µg)	4.8	1.7	2237 ± 65	0.93 ± 2.06	-
Glucose (1 M)	5.0	4.9	574 ± 55	0.198 ± 0.09	5.36 ± 3.39

*Final yield after immobilization.

The aim of this experiment was to ensure the colloidal stability in various mediums with its final use in culture medium for the cytotoxicity assays. NP aggregation will significantly alter *in vitro* behaviour (dosimetry, NP uptake, cytotoxicity), as well as *in vivo* fate (pharmacokinetics, toxicity, biodistribution). Thus, understanding the factors driving NP colloidal stability and aggregation is paramount¹⁴³. Unlike regular salt solutions used for storage, culture medium, specifically DMEM (Dulbecco's Modified Eagle Medium), is more complex consisting of 6 salts and glucose, supplemented with

13 essential amino acids, and 8 vitamins developed to maintain and grow cell culture. Once stable NPs can become unstable by molecule/protein adsorption or loss of surface functionality, resulting in the formation of aggregates due to electrostatic interactions¹⁴³. It was observed that the surface inertisation with glucose 1 M added in diminishing the aforementioned effects with an overall ZP of 5.36 ± 3.39 . In the image below, the control in DMEM with 10% FBS (Fetal bovine serum) showed large clusters of aggregated nHs whereas after surface inertisation with glucose the aggregated were smaller in size and more dispersed in the media. For all further experiments, the nHs were modified with glucose.

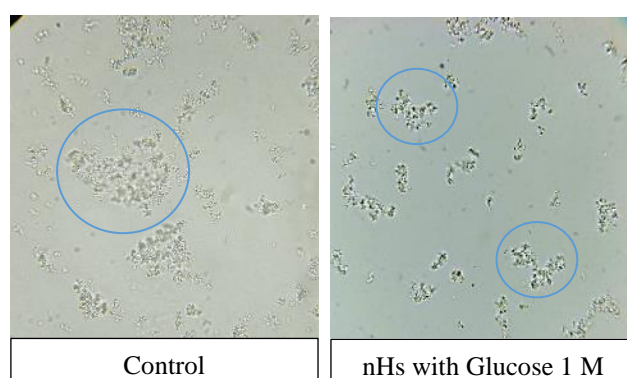


Figure 11. Aggregation in DMEM in an optic Microscope image.

Bioconversion of the pro-drug by nHs

In addition to colloidal stability and other feature that is necessary for the developed nHs for a potential use in DEPT is to show that they could indeed carry out the biotransformation of the prodrug indole-3-acetic acid (3IAA). Although we know that similar low molecular substrates molecules (such as ABTS) can be catalysed by the co-entrapped HRP, it is mandatory to show the activity of the nHs for this prodrug. This non-toxic plant hormone has been examined as a prodrug as upon transformation to its oxidized species, it induces cellular apoptosis in cancerous lines. HRP has been proposed as oxidizing enzyme of this compound for the so-called DEPT. The biocatalytic performance of the BioSi@THRP_MNP_1300 was tested in batch conversion of 3-IAA into its oxidized species. HPLC elution profiles showed that the nanohybrids catalysed the complete oxidation of a 500 mM prodrug solution within 30 min of reaction at the rate of 4 μ moles/min with the generation of at least five oxidized products **Fig. 12A and 12B**.

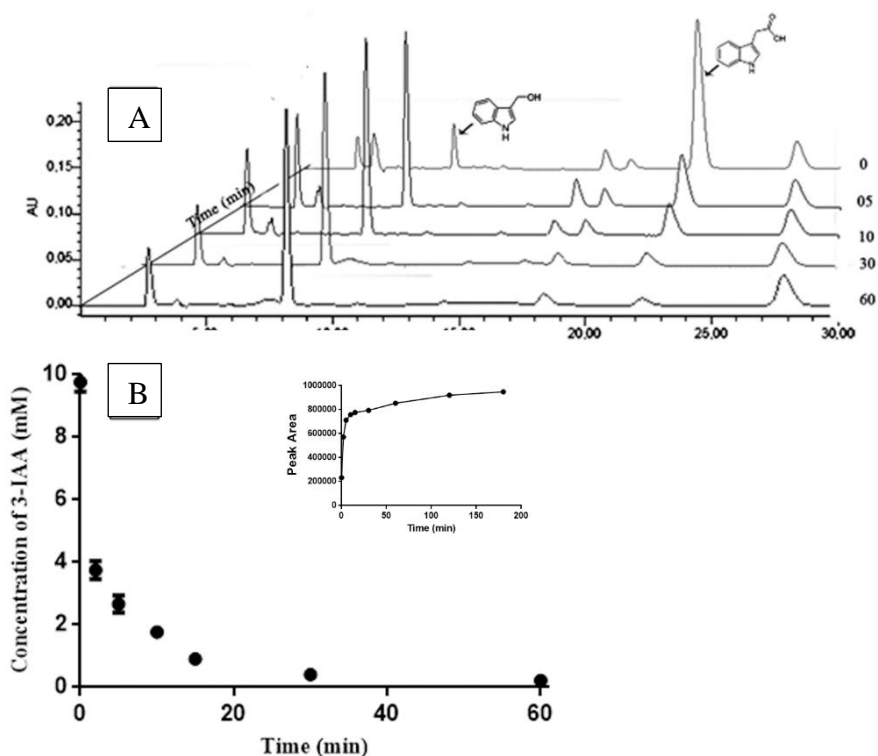


Figure 12. Oxidation of 3-IAA by the nanohybrids. A) Conversion of 3-IAA by nanohybrids BioSi@THRP_MNP_1300 at different intervals of time B) Conversion kinetic of 3-IAA by the nanohybrids. Reactions were carried at 25°C using 1 IU in a 100 mM sodium acetate buffer at pH 5.0 containing 500 mM of 3-IAA. Further details are described in Methods. **Inset-** Increment in the concentration (area) of the radical 3-ox-indol-carbinol.

The soluble enzyme however was 4 times faster (1 μ moles/min) and oxidised 3IAA within 15 min. This is because the enzyme is freely available to the substrate. The major product is expected to be oxindol-3-yl carbinol for its distinctive spectra and matching retention time from previous works using the same HPLC analysis condition¹⁴⁴.

SQUID analysis

As MNPs have the function to act as nanoheaters once entrapped within the biosilica shell, it is critical to study the magnetic properties of the obtained hybrids. The encapsulation of the MNPs could lead to their aggregation and this could alter their magnetic properties thus affecting their efficiency as nanoheaters. The magnetic characterization was performed in a Quantum Design (USA) MPMS-XL and MPMS-5S SQUID magnetometers equipped with an AC (Alternating current) magnetic

susceptibility option. From the hysteresis curves we evaluated the saturation magnetization of the samples (M_s), the coercive field (H_c) and the remanence (MR). At 300 K, all nHs samples display superparamagnetic behaviour with very small coercivity at 0 field, meaning that most of the nHs display a superparamagnetic behaviour at this temperature. The saturation magnetization of the different samples was determined at 5 T, after a correction of the diamagnetic contribution. At this field, nearly all magnetic moments are aligned in field direction and thus dipolar interactions between the particle's magnetic moments are negligible. Saturation magnetization is defined as the complete alignment of magnetic moment vector in the direction of magnetic field. Values obtained for these samples are along the reported for bulk magnetite or maghemite, confirming the ferrimagnetic behaviour of the material. **Fig. 13A** showed the magnetic hysteresis loop of MNPs of nHs prepared using linear 60000 Da PEI (BioSi@THRPox_MNP_60000 nHs), however similar results were obtained for all the developed nHs.

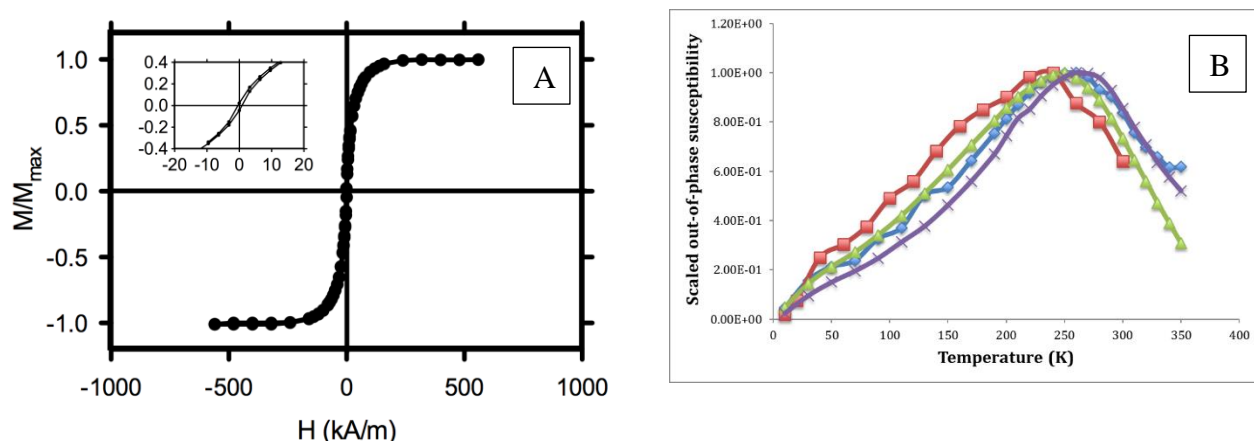


Figure 13. SQUID analysis **A)** Field dependent magnetization of sample BioSi@THRPox_MNP_60000 nHs showing almost negligible coercivity (see inset for more detail). **B)** Temperature dependence of the out-of-phase susceptibility for the four samples.

The AC susceptibility measurements were performed in the four samples of the different nHs prepared using different the PEIs to evaluate the impact that the different synthetic procedures could have on the magnetic properties of the nanohybrids. All materials present a similar behaviour, an out-of phase susceptibility maxima located between 240 and 260 K and an in-phase susceptibility maxima located at higher temperatures (around 340-350 K). This behaviour is the typical relation phenomenon displayed by assemblies of magnetic nanoparticles¹⁴⁵. AC susceptibility measurements

are interesting because different aggregation degrees of the particles affect the temperature location of the susceptibility maxima. For example, previous results for 9 nm magnetite nanoparticles prepared by thermal decomposition showed variation in the out-of-phase location in temperature from 30 to 100 K depending on the aggregation degree¹⁴⁶.

In the case of the all developed nanohybrids, no big differences are observed (**Fig. 13 B**) the temperature dependence of the out-of-phase susceptibility is shown for the four samples. Therefore, the differences observed in the SAR values by nHs with respect to the original MNPs used for the synthesis, will not be due to a variation of its magnetic properties but it will be most likely due to an isolation phenomenon caused by the silica matrix.

Analysis of Specific absorption rate (SAR).

Another key feature that is necessary to study in order to be able to achieve our final aim (tuning HRP activity against 3IAA by magnetic heating) is their efficiency of heating when AMF is applied.

A key characteristic of MNPs used for clinical hyperthermia is a high specific absorption rate (SAR), which depends on the MNPs' size, shape, composition, magnetic interaction, and concentration, as well as the applied magnetic field frequency and strength^{123,147}. The heating capacity of MNPs is a fundamental parameter in magnetic hyperthermia and is typically defined as the specific absorption rate (SAR), it can be found in the specialized literature also as specific loss power (SLP)¹⁴⁸. However, most existing MNPs require a high frequency or high AMF strength to deliver an adequate thermal dose to the tumour. For the use of our nHs in biomedicine in the treatment of cancer using hyperthermia it is important to study the superparamagnetic behaviour after entrapment as the entrapment procedure could cause loss in movement of the MNPs impeding the heating efficiency (Brown relaxation). Another factor is the size-dependent influence of concentration on SAR. The MNPs used in this work are commercial fluidMAG-PAA nanoparticles with a hydrodynamic diameter of 200 nm which have a multi-domain core and in-batch separability by an external magnetic field (magnetic separator) facilitating a fast and easy magnetic isolation. Upon exposure of MNPs to an AMF, the reorientation of the magnetic moments can produce energy in the form of heat by a variety of mechanisms. When MNPs are present in a suspension,

the movement of the whole particle can generate frictional losses with the environment, provided that the viscosity of the medium allows the MNPs to rotate freely (Brown relaxation). However, this could not occur in the same way once they are co-entrapped within nHs where the viscosity could be much higher. Besides, the silica shell could act as a heat insulator. This that could act negatively thinking on the use of nHs for traditional MHT applications should be beneficial for triggering magnetic heating of co-entrapped HRP molecules that are not linked directly to the surface of the MNPs. Firstly, we study the ability of the obtained nHs to raise the macroscopic temperature of an aqueous solution to study applying two different amplitudes of 25.2 and 30.0 mT with increasing field. All the samples had the same iron concentrations (**Table 2**). The pure MNPs at very low frequency did not show any heat generation on application of AMF. However, as the frequency increased at a constant amplitude of 25.2 mT the SAR increased exponentially. The heating efficiency was maximum at an amplitude of 25.2 mT and frequency of 829 kHz for a duration of 3 min.

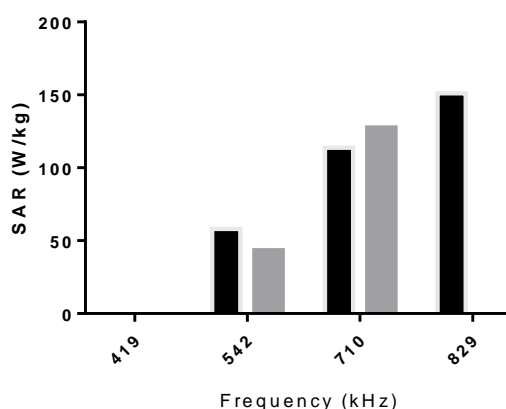


Figure 14. SAR (W/g) of commercial MNPs (1 mg/mL) at distinct amplitude (mT) 25.2 (■) and 30.0 (▒) and field 419, 542, 710 and 829 (kHz).

The heat performance of MNPs was measured at room temperature (24°C) with a maximum SAR of 151.15 W/g_{Fe} (**Fig. 14**) and an increase in global temperature from 24°C to 33°C after 3 min.

Similarly, we studied each of the nHs and observed that with an exception for the BioSi@THRPox_MNP_25000 all the other nHs showed a low heat generation performance when compared to the pure MNPs (**Table 5A**). BioSi@THRPox_MNP_25000 exhibited a higher heating efficiency and this could be corroborated to the results from TEM wherein we have a higher majority of MNPs

clusters outside the Si matrix and being a branched polymer could be that the MNPs have more freedom of movement in the matrix. At a maximum frequency of 829 kHz the temperature at increased from 24.4°C to 25.5°C a whole degree in comparison to the other nHs. For all the nHs the increase in frequency was directly proportional to the increase of SAR and the increase in MW of the PEI was inversely proportional to the SAR. From the SAR values obtained the difference between the MNPs solo and the nHs, it is evident that the Si cover does contribute to the overall heating efficiency at the global environment with a minimal increase in the temperature thus acting as a heating insulator. The lower SAR values can also be attributed to the fact that the MNPs entrapped with the matrix impede the free rotation (Brown relaxation) as well as the aggregation of the MNPs lowers the SAR. From literature it is known that the SAR values could shrink from 50-90% depending on surface they are absorbed to the location, whether, inside cells or tissues¹⁴⁹. Since SAR values are strongly dependent on the use of an AC field strength and frequency, the amplitude of 25.2 mT and frequency 829 kHz was selected for further studies which presented the best combination (**Table 5A and 5B**).

Table 5. A. Determination of SAR at a maximum field of 25.2 mT

Frequency (kHz)	Field (mT)	SAR (W/kg) _{Fe}			
		PEI MW 1300	PEI MW 2000	PEI MW 25000	PEI MW 60000
419	25.2	0.00	0.00	0.00	0.00
542		7.25	0.00	6.751	4.065
710		14.33	14.49	35.41	14.6
829		21.13	16.40	64.67	11.41

Table 5. B. Determination of SAR at a maximum field of 30.0 mT

Frequency (kHz)	Field (mT)	SAR (W/kg) _{Fe}			
		PEI MW 1300	PEI MW 2000	PEI MW 25000	PEI MW 60000
419	30.0	0.00	7.29	0.00	0.00
542		7.306	14.61	21.72	3.63
710		10.86	35.47	65.98	7.25

Activation of the enzyme using hyperthermia.

For the SAR measurement of the nHs, it is clearly observed that MNPs encapsulated decreased their efficiency to raise the macroscopic temperature of the aqueous solution in which they are suspended. But are they able to raise the temperature inside nHs and thus increased the activity of HRP molecules that are co-entrapped within the matrix. In order to determine this localized heating efficiency of the nHs we studied the increase in enzymatic activity after the application of an AMF cycle at maximum amplitude and frequency (25.2 mT and 829 kHz). Using a colorimetric substrate (ABTS), the increase in the slope of the activity of the enzyme when exposed to MHT was determined. The achieved activity was correlated with the activity obtained when incubating the nHs in a water bath at different temperatures. This allowed us to know the local heating that the entrapped HRP is sensing although the global temperature (24°C) of the solution did not showed an increase during AMF application. The plotted slope demonstrated that there was a direct relation between the increase in temperature and the activity of the enzyme. For the controls, it's a given, as we know that the enzyme is optimally active at 45°C when compared to 30°C. When HT was applied, we noticed an even bigger augment in the activity when compared to 30°C. (**Fig. 15**)

Table 6. Augment in activity (%) of the nHs after application of after application a maximum amplitude and frequency (25.2 mT and 829 kHz) at a global temperature of 24°C.

	Incubation with a water bath at		AMF application
	30°C	45°C	Global temperature= 24°C
BioSi@THRP_MNP_1300	100	103	174
BioSi@THRP_MNP_2000	100	85	173
BioSi@THRP_MNP_25000	100	101	209
BioSi@THRP_MNP_60000	100	64	145

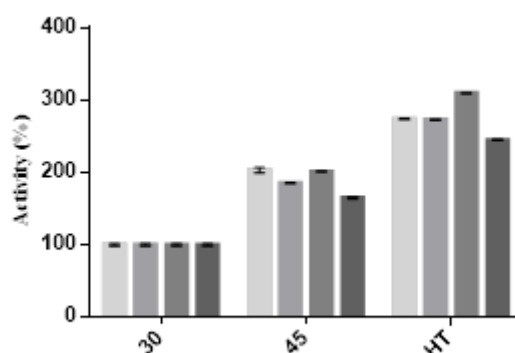


Figure 15. Augment in activity after application a maximum amplitude and frequency (25.2 mT and 829 kHz) at a global temperature of 24°C. BioSi@THRP_MNP_1300 (■), BioSi@THRP_MNP_2000 (■), BioSi@THRP_MNP_25000 (■), BioSi@THRP_MNP_60000 (■)

The activity obtained at 30°C incubation in a water bath was considered as nHs's 100% activity, and we compared the activity observed when incubated for 20 min at 45°C in water bath and when subjected for a cycle of AMF for 20 min. In the last case, there was an increase in the activity of 174% and 145% for the lowest and highest MW PEI, respectively, maintaining the global temperature at 24°C but with local environment temperatures inside the nHs exceeding 55°C (theoretically). A control of activity by incubation in a water-bath higher than 45°C was not possible as the substrate H₂O₂ undergoes thermal degradation and the results would not be reliable. Even in the case of the branched PEI (25000 Da) an increase of the enzymatic activity after MHT (**Table 6**) was observed. The results demonstrate that applying AMF it is possible to reach local temperatures greater than 45°C within the enzymes microenvironment without an increase in the overall temperature of the reaction medium. These results show that it

is possible to think about developing a novel "on/off" switch approach for the remote conversion of pro-drugs in cancer therapy by enzymes of thermal origin that show little or no activity at 37°C. This would allow a precise remote control of the therapy that solves a limitation of the current strategies that could not avoid its activation outside the target site.

Stability with HT

The marginal stability of biocatalysts in many types of reaction media often has prevented or delayed their implementation for biomedical applications. As the local temperatures reached within the nHs exceeds 55°C it is important to ensure the stability of the enzyme MHT post-activation and guarantee the efficacy of the conversion. In the previous chapter many measures have been taken in order to optimize the stability of the nHs.

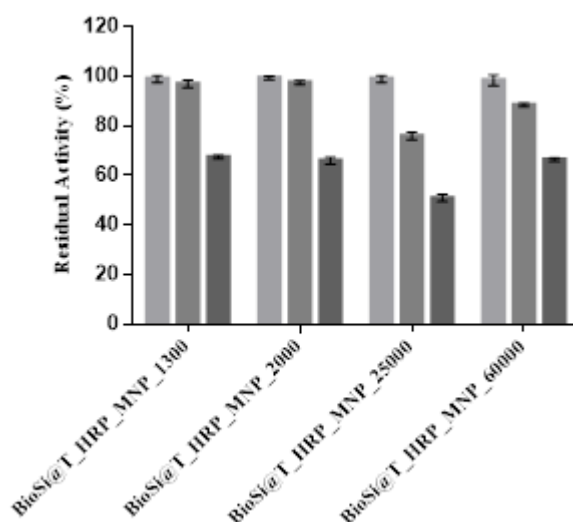


Figure 16. Stability of the nHs at after application after application a maximum amplitude and frequency (25.2 mT and 829 kHz) at a global temperature of 24°C. The global heating temperatures were maintained at 30°C (■) and 45°C (■) and local temperature was achieved after application of a maximum amplitude and frequency (25.2 mT and 829 kHz) (■) was applied.

All the nHs maintained above 60% of their initial activity except for the BioSi@THRP_MNP_25000 (**Fig. 16**) after applying AMF for 20 min. As observed from the activation that BioSi@THRP_MNP_25000 yielded a higher activity achieving a higher temperature at the microenvironment in turn denaturing the enzyme. Therefore, although in all cases an activation of the encapsulated enzyme triggered by MHT was

observed due to a lower stability after MHT treatment for further *in vitro* experiments BioSi@THRP_MNP_25000 were not used. Due to the similar behaviour observed among the nHs obtained with linear PEI, we decide to work only with BioSi@THRP_MNP_1300 and 60000, as examples of the lowest and highest MW sizes used.

Conclusions

In this chapter we have determined the physico-chemical properties of the optimized nHs. The diameter and polydispersity of the *in situ* prepared nanoparticles demonstrated a dependence on the size of the aminated polymer PEI used to deposit the siliceous material and the addition of the magnetic nanoparticles during synthesis. The different strategies used to determine the size were consistent showing a radius of approximately 600 nm for three of the PEI used. Incorporation of Fe in the nHs was demonstrated by different techniques and its ability to generate local heat after application of an AMF was demonstrated as HRP seems to sense a local temperature higher (around its optimum) than the macroscopic temperature of the solution in which the nHs is suspended. Our findings demonstrated that it was of paramount importance to functionalize the surface of the nHs with glucose to prevent aggregation in future studies under complex cell growth media. All in all the results in this chapter encourage us to continue with further studies of application of our designed nanodevice in *in vitro* cell studies.

Chapter 3

In Vitro Cytotoxicity Mediated By Magnetic Heating

Chapter Summary

In this chapter, we have evaluated the in vitro cytotoxicity of the optimized nHs with and without the effect of the AMF using a colon carcinoma cell line (HCT 116). First, surface engineered nanohybrids, for better colloidal stability in cell culture media were tested for cytotoxicity using different cell lines and in the absence of the prodrug. Cell viability was preserved up to concentrations of 20 ug/mL of nHs. Then we have studied the cytotoxicity effect generated by co-entrapped HRP due to bioconversion of 3-IAA in the presence or not of AMF. Although the global temperature of the cell culture was maintained at 37°C during the application of a 30 min cycle of AMF (829 kHz and 25.2 mT), an 80% decrease in cell viability in the presence of the nanobiocatalyst (2 UI, 10 mM IAA) was observed while only 30% cell death was detected when no AMF was applied.

TEM images of the HCT 116 cells after application of AMF in the presence of nHs and 3IAA demonstrated the presence of nHs inside the cells and a significant effect on the cellular integrity in the case of application of the AMF-cycle as compared to TEM images with and without 3IAA with no AMF application. Our results thus demonstrated that it is possible to locally increase the activity of the HRP co-entrapped with MNPs remotely via magnetic heating for a potential application of the nanobiocatalysts in DEPT anti-tumour therapy.

Introduction

Cancer and hyperthermia

Cancer is a major burden worldwide with an incidence among tens of millions of people and a mortality rate of more than half worldwide. Colorectal cancer (CRC) is a common and lethal disease and the risk of development is influenced by both environmental and genetic factors. According to GLOBOCAN 2018 there will be an estimate 18.1 million new cancer cases with an incidence of 6.1% and a mortality of 9.2% solely in colorectal cancer¹⁵⁰. Although there have been improvements in surgical treatment approximately 40% of patients still eventually die. This is due to metastasis to other organs, mainly the liver¹⁵¹. If detected at an early stage, CRC can be prevented by the removal of adenomatous polyps¹⁵². Although a variety of screening modalities, including fecal occult blood test¹⁵³, sigmoidoscopy¹⁵⁴, optical colonoscopy¹⁵⁵ and virtual colonography¹⁵⁶ have been developed; the miss rate of CRC is still considerable. For instance, the overall miss rate of colonoscopy is 24% and specially, potentially invasive flat and depressed lesions or adenomas smaller than 5 mm are easily missed¹⁵⁷. Thus, due to the relative sensitivity and specificity of conventional screening methods, almost 70% of CRC patients are diagnosed with metastatic disease. For the treatment of metastatic CRC, systemic injection of chemotherapeutics is considered a viable treatment option. However, this strategy has an insufficient therapeutic efficacy due to undesirable biodistribution of anticancer drugs that causes severe side effects and systemic toxicity. Thus, there is a real urgent clinical need for developing novel systems that enable targeted therapy to really affect survival for this disease.

Many therapies have been explored using targeted nanoparticles loaded with cytotoxic drugs or small interfering RNA (siRNA) aiming to induce cytotoxicity and anti-proliferative effects of cancerous cells without accumulation in normal organ tissues^{158,159}. In these examples the NPs acted only as vehicles that play an active role in improving biodistribution, bioaccumulation and internalization of the therapeutic agents. Other nanotherapy-based approach, relatively recently explored, benefit from locally injected or systemically administered nanoparticles that are activated by extrinsic energy sources (light or AMF) to generate heat, which in turn is coupled and transmitted to the tissues the nanoparticles reside within¹⁶⁰. Several factors can influence the extent of this heating (e.g. magnitude of the energy source, size and

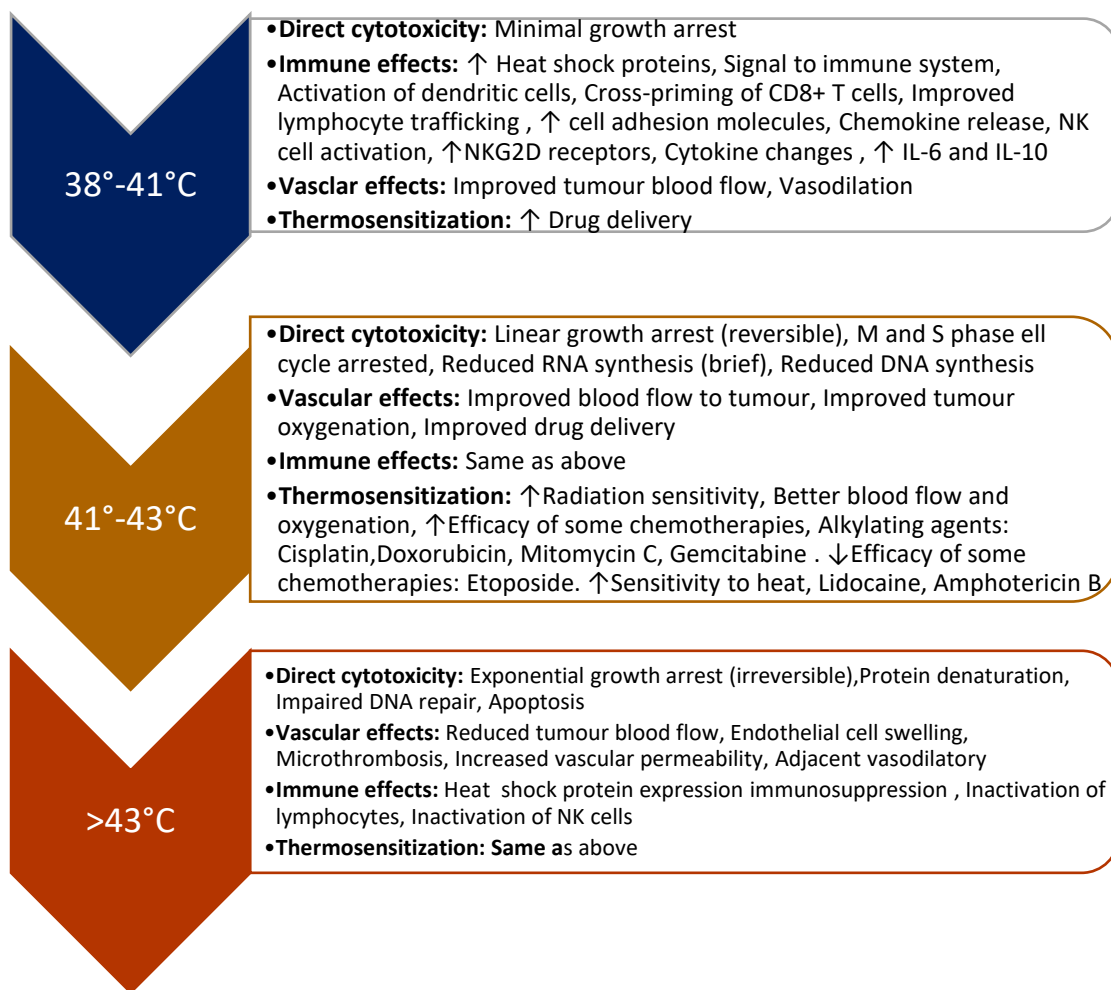
characteristic of the MNPs, concentration of MNPs in the tumour, the depth of the tumour within the body, etc). In this sense, it has been shown that triggering local heating through nanomaterials that act as heat mediators could directly induce cell death via necrosis and/or apoptosis and even ablation of cancer cells^{135,161}. In the last case, NPs induced destruction of protein and cell structure by heat which results in the shrinkage of the tumour size¹⁶².

In particular, in recent years, magnetic hyperthermia (MHT)¹⁶³, has emerged as a potential treatment for cancer¹⁶⁴. Indeed, the fact that magnetic nanoparticles (MNPs) have been approved by the Food and Drug Administration (FDA) of the USA as magnetic resonance imaging (MRI) contrast agents¹⁶⁵, and could be carefully designed to be nontoxic, nonimmunogenic, biocompatible, stable, and possibly biodegradable have boosted their application as nanoheaters for MHT¹⁶⁶.

Molecular mechanisms involved in cellular damage triggered by Hyperthermia

Conventional Hyperthermia (HT) has been defined as an antitumor treatment modality based essentially on the local global increase of tumours temperature through the heat transferred within cells from a heated environment. It is an already approved therapy for cancer^{167,168} aiming to achieve selective damage of the tumour tissue based on the fact that normal cells are less sensitive to heat and, therefore, their survival rate is higher when exposed to HT. The heating of biological tissue can be achieved by several physical mechanisms including microwave irradiation applied via radiofrequency antennas (dielectric heating), ohmic heating via electrode-applied high frequency currents, optical laser irradiation via fibres, water bath heating, etc¹⁶².

The molecular mechanisms involved in the cellular damage caused by conventional HT treatment are well known and the effect on cancer cells is multifactorial. Hyperthermia application can cause a wide range of changes at the cellular level which lead to loss of the cellular homeostasis¹⁶⁹. Indeed, the aim of achieving heating processes able to reach global temperatures $>43^{\circ}\text{C}$ is in order to trigger protein denaturation, heat shock protein production, specific immunomodulation, and DNA cross-linking, eventually leading to cell death by apoptosis/necrosis (**Scheme. 1**).



Scheme 1. Mechanisms of actions of hyperthermia. Adapted from Rampersaud *et al.*¹⁷⁰.

There are two phases of direct cytotoxicity associated with heat exposure a reversible (linear metabolic arrest); and an irreversible one (exponential phase). Irreversible cytotoxicity is easier to achieve with increasing temperatures and is directly related to the duration of exposure. **(Figure 1A & 1B)**. The transition from the linear to the exponential phase occurs at temperatures above 43°C and has a clear dose-response relationship between temperature and cell death¹⁷⁰. Although, the requisite thermal dose required for protein denaturation and cell membrane disruption occurs at a dose of 140 kcal/mol¹⁷⁰. Hildebrandt *et. al* demonstrated when exponentially growing cultured cells (e.g. Chinese hamster ovarian (CHO) cells were exposed to a defined temperature between 41 and 47°C, a dose-effect curve was defined by plotting the rate of cell death against the duration of hyperthermia¹⁷¹. The corresponding survival curves showed a

typical ‘shoulder’ that reflected the two-step process of cell ablation, as explained above. It’s marked by a linear growth arrest in the beginning of heat exposure (reflecting a reversible, non-lethal heat damage), which is followed by exponential cell death (**Fig. 1A**). One fundamental observation is, that the capability to induce cell death at lower temperatures <42–43 °C (below a certain ‘breakpoint’), was markedly lower than above 43°C. Similarly, Brüningk *et al* showed a similar tendency in the colorectal carcinoma cell line HCT 116 where survival curves were characterised by an exponentially linear descent following an initial shoulder region ¹⁷²(**Fig. 1B**).

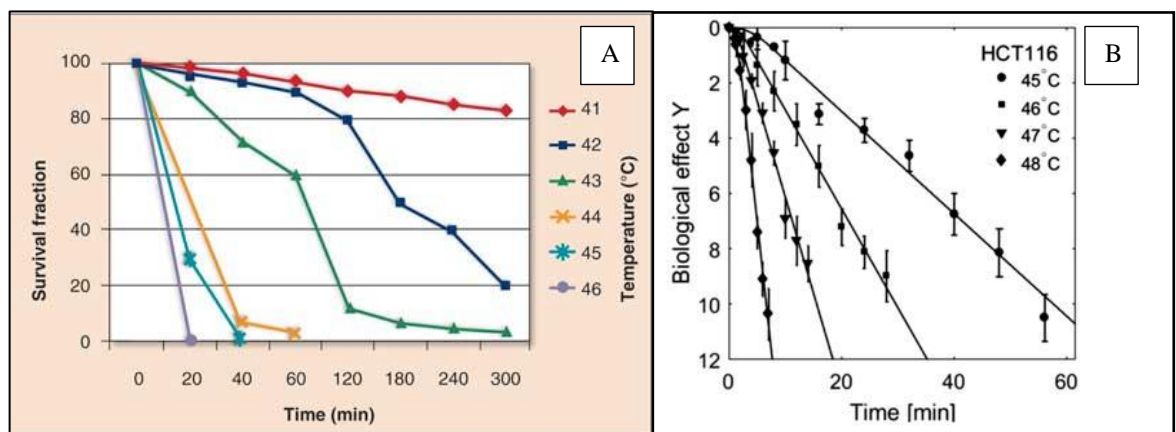
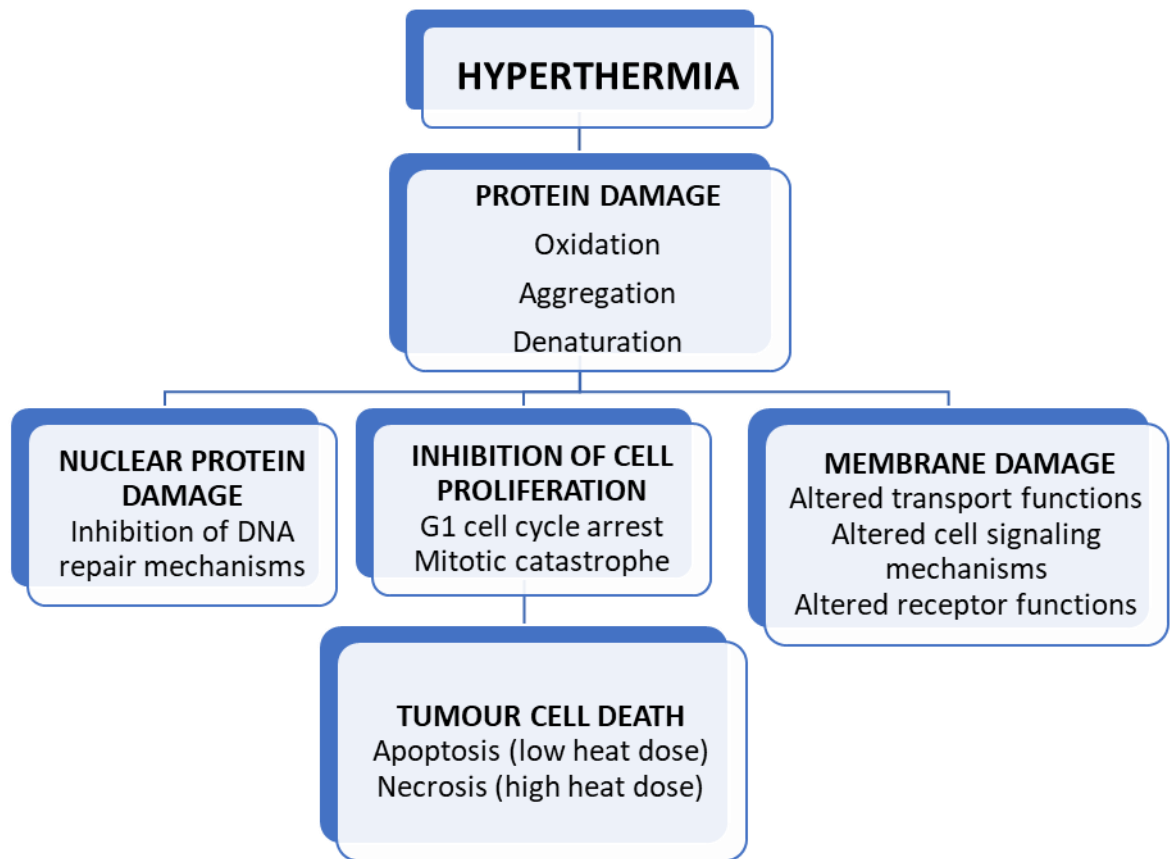


Figure 1. Hyperthermia-induced Cell Death of A) CHO cells Adapted from Rampersaud *et al.* ¹⁷⁰. and **B) HCT 116** exposed to different defined temperatures.

The heat application causes alterations in cellular membrane permeability and results in decreased levels of ATP¹⁷³. The most important events that occur upon heat application seem to relate to proteins. The proteins within the nucleus of cancerous cells appear to be particularly vulnerable to the effects of hyperthermia. In other words, the heat adds substantial stress to the cancerous cells and these metabolic changes that occur make them vulnerable on application of post therapies such as chemotherapy and radiation (**Scheme 2**). Fu *et. al* demonstrated through *in situ* cell tracking that sensor proteins of the DNA damage response (DDR) were the direct targets of HT. It was observed that HT could delay and decrease the formation of the DDR protein. Moreover, through the *in-situ* tracking of individual DDR protein, it was found that HT resulted in more unrepaired DDR protein over the period of observation compared with irradiation alone (**Scheme 2**)¹⁷³.



Scheme 2. Hyperthermia-induced cellular changes that could lead to tumour cell death. Adapted from Bettaieb *et. al*¹⁷⁴.

Apart from DNA damage, hyperthermia is associated with the increase of intracellular reactive oxygen species (ROS) and mitochondrial dysfunction. Hou *et. al* investigated the effect of hyperthermia in human OS (U-2 OS) cells after treatment at 43°C for 60 min which induced apoptosis in human OS cell lines. Furthermore, it was associated with increased ROS production and caspase-3 activation in U-2 OS cells. Mitochondrial dysfunction was followed by the release of cytochrome c from the mitochondria and was accompanied by decreased anti-apoptotic Bcl-2 and Bcl-xL, and increased pro-apoptotic proteins Bak and Bax¹⁷⁵. But the precise biochemical mechanisms involved till date remain unclear. Similarly, Ba *et. al* in a study demonstrated that colorectal cancer cells HCT 116 were sensitized with HT towards radiotherapy (RT) through ROS inducing autophagic cell death. The treatments promoted a statistically significant apoptosis of the HCT116 colorectal cancer cells when compared the mock group. It was demonstrated that a combination treatment of HT + RT brought about a significant down-regulation of protein light chain 3 (autophagosome formation marker) and Beclin1 (which participates in the early stages of autophagy by promoting nucleation of autophagic vesicles) or up-regulation mTOR (central regulator for cell growth) in

colorectal cancer cells when compared with RT or HT treatment alone. HT+RT eliminated the resistance of colorectal cancer cells HCT116 to RT through enhancement of their sensitivity via a mechanism involving ROS-modulated autophagic cell death. Thus, ROS inducing autophagic cell death play critical roles in the anti-cancer synergism between HT and RT¹⁷⁶.

It is important to highlight, that when discussing the mechanisms of cell death, it is very vital to consider the type of cell death that have been exposed to the HT treatment. Indeed several studies have previously reported that different cell lines express different sensitivities to heat, depending on tumour cell type¹⁷⁷. As an example of such difference, it has been shown that Glioblastoma U87MG and T98G expressed increased levels of Caspase 9 and heat shock protein 90 as markers of induced apoptosis compared to more thermo-tolerant A549 and H1299 lung carcinoma, U87MG breast adenocarcinoma, and PC8 prostate cancer cell lines after 3 days exposure to temperatures ranging from 33°C to 40°C¹⁷⁸.

In vitro and in vivo effects of Magnetic Hyperthermia

Although HT is an already approved treatment for cancer, it remains a challenge to control the spatial extent of heating in tissue using the traditional above-mentioned physical methods. In this sense, magnetic hyperthermia (MHT) improves the precision as the heating source (MNPs) are embedded into the tumour tissue and heating is triggered remotely using an external alternating magnetic field (AMF). Thus, it is much feasible to deliver heat to the tumour while preventing thermal injury to surrounding healthy tissues. Therefore, AMF allows gaining spatio-temporal control on HT. Indeed, MHT has shown success in the first clinical trials for prostate cancer and gliomas applying the MNPs by intratumorally¹⁷⁹.

Much current research focuses on developing advanced particles with excellent heating properties and the study of their effect on cell viability following hyperthermia^{180,181}. However, there is still very little understanding of the molecular mechanisms involved in the cellular damage triggered by MHT^{182,183}. This is because the heating source could be MNPs that are free to move in the interstitial fluid of the tumour tissue and/or that have been internalized by the tumoral cells. Not only the heating efficiency of the MNPs changes drastically whether they are free to move or fixed to the tumour tissue, but also the molecular mechanisms triggered by MNPs as heating sources could not be the

same¹⁶⁰. Thus, the attainable temperature in the particle-containing tissue is determined by the balance between heat generation in the particles and the depletion of heat into the tissue. The depletion process is mainly due to heat conduction, which depends if the cells are located in the cell cytoplasm and/or in the interstitial volume between tumour cells. It is important thus to highlight that MNPs act as nanoheaters a high temperature gradient is developed only on a very small distance from the MNPs. The generation of heat is completely different to the global heating of the bulk solution when using water-bath. The cells being in contact with the heated MNPs should experience a cytotoxic impact higher than when the heating is uniform. Besides, in the case of MNPs internalized by cells, the chances to get in contact with cell organelles are higher. All these facts ensure a high impact on cell viability even if the amount of MNPs on the tumour is not high enough to ensure a macroscopic temperature rise above 42°C (**Fig. 2**). In addition, there exist observations of ‘non-thermal’ damaging effects due to MNP oscillation under AMF that may induce mechanical damage in the cell interior¹⁸⁴. Indeed, the precise biophysical and molecular basis of all these effects deserves further investigation.

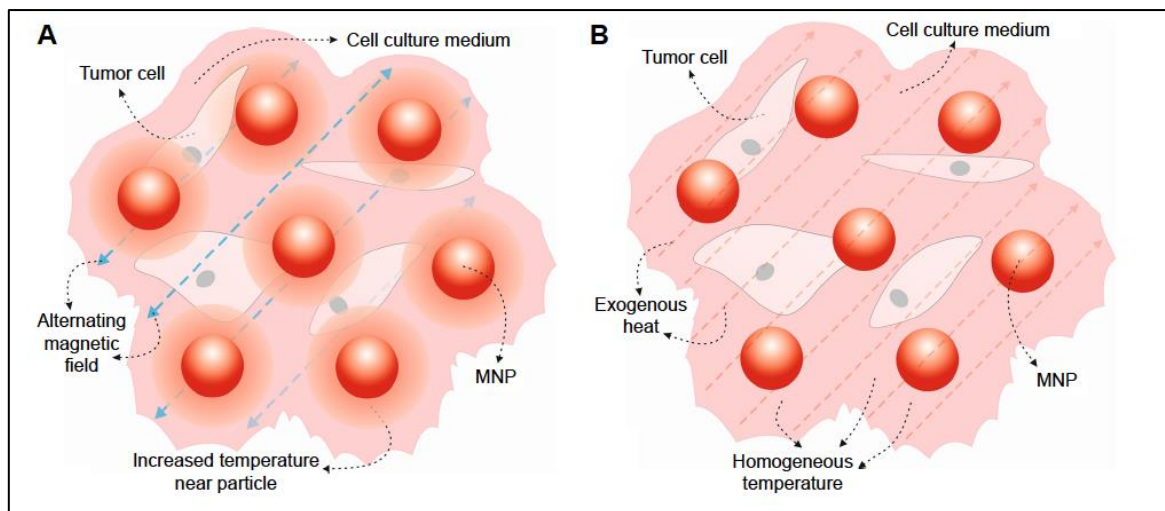


Figure 2. Comparative effects of magnetic and water-based hyperthermia treatments on human osteosarcoma cells **A)** Schematic representation of tumour cells heated by MNPs placed in AMF (MHT). Cells close to MNPs are subjected to higher treatment temperature due to high gradient temperature near MNPs. **B)** tumour cells and MNPs heated uniformly by exogenous heat (water-based hyperthermia). No temperature gradient near MNPs after equilibrium macroscopic temperature was established. Taken from Herea *et al*¹⁷⁷.

Therefore, when interpreting MHT biological effects, one should be aware that there is a superposition of different reaction paths of cell damage due to a superposition of effects of different physiological parameters. Thus, interpretations of MHT effects on cells have to be grounded essentially on the temperature gradient established around MNPs and on cell–MNP interaction at nano- and sub-micrometric scale, when MNPs are placed in AMF. In this respect, several papers focusing on evaluations of the temperature developed by the MNPs subjected to AMF revealed large differences between the inner temperatures around the MNPs surface and those of the liquid medium they are heating. Theoretical models showed that in order to increase the temperature of a tumour in a desired temperature range (42°C–46°C), the temperature generated on the MNPs surface has to be about twice higher¹⁸⁵. This was demonstrated experimentally, showing that after 5 minutes of heating in AMF, the inner temperature of the iron oxides nanocrystals was about twice that of the solution. Thus, for a temperature of 45°C of the cell culture medium, about 90°C are expected around MNPs. Besides, it was also shown an exponential decay of the gradient of temperature around MNPs at distances lower than 6 nm from the MNPs surface, as above this distance the temperature equals the macroscopic temperature of the bulk solution^{186,187}. Another important observation to highlight is that MNPs cooled down to the temperature of the

ambient fluid in seconds after the magnetic field is turned off¹⁸⁸. Therefore, the type of MNPs is critical for MHT therapy, as it has to have an optimal magnetic driven heating efficiency (SPR). Not only the type of MNP but also the concentration of MNP that reached the tumour site. Therefore, to date MHT therapy has showed positive results only when MNPs are injected intratumorally. Thus, although very promising, MHT in cancer therapy still faces many challenges until it can become a standard medical procedure. Among its pitfalls are: *i*) the need to improve MNPs capable of reaching and maintaining therapeutic temperatures inside tumour tissue; *ii*) the lack of knowledge of the molecular mechanisms involved in cellular damage; *iii*) the need to develop a safe, comfortable and reproducible application of MNPs to the tumour region, *iiii*) the inability to accurately perform thermal dosimetry and the dependence of heating efficiency on thermal dose rate; *iv*) the difficulty to achieve a uniform thermal profile within the tumour, the need of further study on the effects of temperature distribution on the cancer cells' viability as well as heat resistance of different tumour cell types; *v*) the reticence from the medical community and the difficulties to access the technical facilities needed for the treatment^{189, 162}.

Other Therapeutic Strategies based on the non-conventional use of Magnetic Heating.

Due to the challenges that still faces MHT, in the recent years it has been explored to use the energy released from MNPs when applying AMF to whether trigger the release or the activation of therapeutic agents¹⁸⁹. The main strategies that are being followed in the development of heat-responsive nanostructures to trigger the release of anti-tumoral agents are based whether on linking the drug via thermolabile bounds or the use of thermo-responsive organic shells (linked to the MNPs inorganic core) for drug encapsulation¹⁹⁰. In the case of the last strategy, several approaches have been used to trigger drug release including: *i*) the use of shells made by polymers with a conformational transition temperature above the body temperature. Thus, the heat released from the MNPs induce a reversible conformational change from a swollen hydrophilic state to a shrunken hydrophobic one, which results on the expelling of the aqueous content (and also the drug) from the polymer chains (*matrix transformation*); *ii*) the use of porous MNPs where the therapeutic agent is retained by pores blocked by the same type of thermo-responsive polymers that by polymers that act like heat-induced "switchable gates"; and *iii*) the use of thermo-sensitive polymers that undergo a

dissolution process at higher temperatures allowing the release of its cargo (*matrix degradation*) (**Fig. 3**).

Release of therapeutic molecules encapsulated in a thermo-responsive matrix

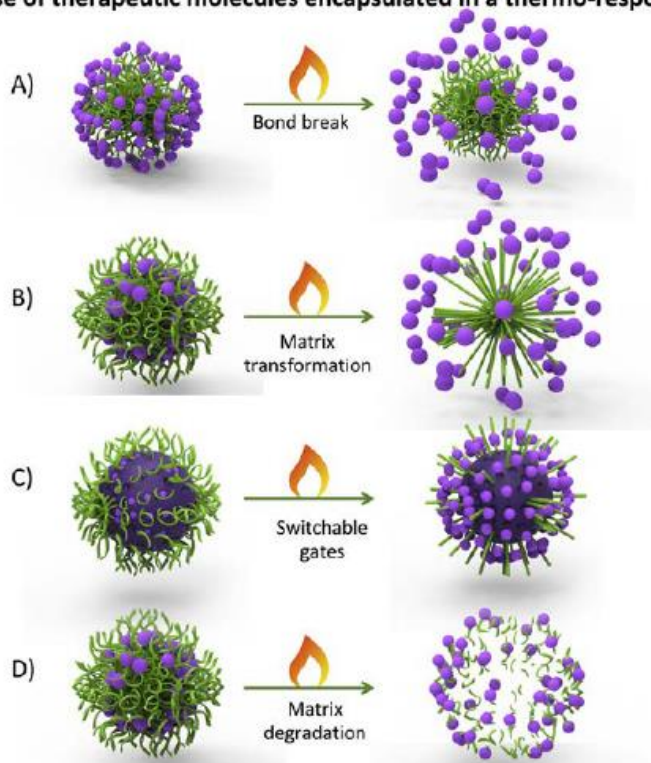


Figure 3. Strategies for the release of therapeutic molecules (purple spheres) linked to a thermo-responsive matrix (green). **A)** Breaking the bond between the drug and the particle, **B)** Transforming the matrix structure, **C)** Using the thermo-responsive matrix to open/close the pores from a mesoporous material and **D)** Degrading the matrix structure. Reproduced with the permission of Moros *et al.*¹⁸⁹

Instead of carrying a drug to be locally released, an alternative strategy is triggering *in situ* activation of therapeutic genes by MHT through the use of expression vectors containing heat-responsive promoters (**Fig. 4**). This elegant approach allows the *in situ* production of gene products that can directly kill the cells or act in a synergic way to increase the anti-tumoral effect of the hyperthermia with both spatial and temporal control^{191,192,193}.

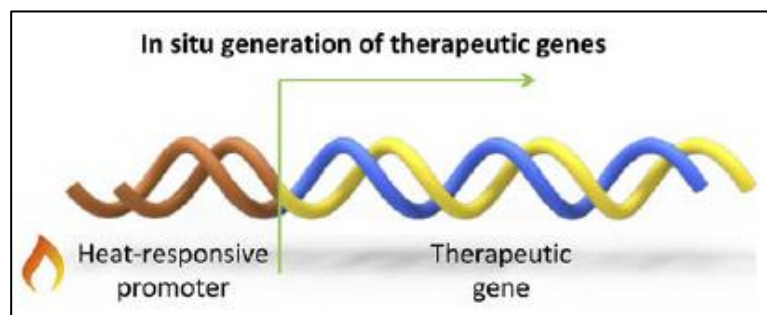


Figure 4. Schematic representation for the *in-situ* generation of therapeutic genes. A heat responsive promoter activates the expression of a therapeutic gene.

Gaining Spatio-Temporal over DEPT by Magnetic Heating.

As explained in **Chapter 1**, the final aim of this thesis is to explore a completely different strategy of using magnetic heating way for cancer therapy in a non-conventional way. In this sense we have focused on DEPT as therapy due to its interesting advantages and think on using the heat generated by MNPs under AMF to activate/significantly increase the activity of thermophilic therapeutic enzymes. We foresee that this would allow overcoming the great current challenge presented by this type of therapy: the lack of spatial control over the enzyme activation. In this sense, the use of alternating magnetic fields (AMF) as external *stimuli* to trigger enzyme activation presents a key advantage to achieve a breakthrough on DEPT: the possibility to have a careful control of the spatial distribution of the applied field gradients using AMF equipment's, which avoids problems related to side effects and systemic cytotoxicity.

Thus, being clearly demonstrated on **Chapter 2** that it is possible to tune by magnetic heating the activity of HRP co-entrapped with MNPs in silica NPs, **in this Chapter** we focused on proof the feasibility of this concept for triggering cell death in DEPT therapy *in vitro* with AMF-remote control.

Objective

To prove the feasibility of the concept of triggering *in vitro* cytotoxicity mediated through thermoactivation of therapeutic enzymes co-encapsulated on the previously developed nHs by magnetic heating.

Specific Objectives

Determine the cytotoxic effect of the nHs in HCT116 and HT29 in the absence of MHT and pro-drug.

Optimize conditions (amount of nHs, incubation times, AMF cycle application, etc) in order to trigger *in vitro* cytotoxicity in HCT116 remotely controlled by MHT

Evaluate in-depth the effect of the treatment: nHs internalization and cell structure by Transmission Electron Microscopy.

Materials and Methods

Materials

Horseshoe peroxidase Type VI (EC 1.11.1.7), polyethyleneimine (PEI) (MW 1300, 2000, 25000 and 60000), 2,2'-Azino-bis (3-ethylbenzothiazoline-6-sulfonic acid) diammonium salt (ABTS), indole-3-acetic acid (IAA), hydrogen peroxide and sodium cacodylate Buffer pH 6.5 were from Sigma Aldrich (St. Louis, MO). Tetramethyl orthosilicate (TMOS), trehalose and potassium phosphate monobasic were from MERCK (Whitehouse Station, NJ). Dibasic sodium phosphate and sodium acetate were from Biopack (Buenos Aires, Argentina). Gel filtration PD10-Columns were from GE Healthcare (Buckinghamshire, UK). Magnetic nanoparticles (MNPs) fluidMag-PAA (200 nm of aggregate size) were from Chemicell (Berlin, Germany). ((3-(4,5-Dimethylthiazol-2-yl)-2,5-Diphenyltetrazolium Bromide) MTT was from AppliChem, (Germany) acetic acid from Carlo Erba, (Italy). HaCaT (CVCL_0038 spontaneously transformed aneuploid immortal keratinocyte cell line from adult human skin), HT-29 (ATCC® HTB-38™ Human Colorectal Adenocarcinoma) cells were obtained from the cell bank of the Laboratorio de Biotecnología, Universidad ORT, Uruguay. HCT 116 (ATCC® CCL-247™) were obtained from Servicio de Animalario del Centro de Investigación Biomédica de Aragón CIBA, Zaragoza, Aragón. All other chemicals used were analytical grade reagents.

Methods

Cell viability studies of different concentrations of nHs using MTT in HaCat, HCT116 and HT29 cell lines

HaCaT cells were seeded at 2×10^4 cells/well in 96-well plates and incubated for 24 h at 37°C, 5% CO₂ in a humidified incubator. Then, media was renewed, and nanoparticles diluted in DMEM 10% FBS were added, ranging from 1.6 to 100 µg/mL. Triton X-100 0.5% was used as a death control. Interference controls (wells without cells) were also added: culture media and 100 µg/mL of nanoparticles. Cells were further incubated for 24 h. After incubation, cells were washed with PBS, and analysed using MTT ((3-(4,5-Dimethylthiazol-2-yl)-2,5-Diphenyltetrazolium Bromide) assay. After washing with PBS, 100 µL DMEM 10% FBS and 20 µL of 2.5 mg/mL MTT

(AppliChem, Germany) were added to each well. After 3 hours of incubation at 37°C, 50 µL/well of SDS 20% was added and incubated for 24 hours at 20°C. The absorption of the formazan solution was measured using a Multiskan™ FC Microplate Photometer at a wavelength of 570 nm.

Similarly, to study the effect of cell viability *in vitro*, HCT116 cells 50x10⁴ and HT29 50x10⁴ cells were incubated for 24 h in DMEM with 10% SFB supplemented with streptomycin-penicillin 1% for 24 h. The following day different concentrations of nHs BioSi@THRP_MNP_1300 (0.5 and 2 IU corresponding to 5 and 20 µg/mL).

HPLC analysis of the adsorption of IAA on BSA

To understand the effect of a complete medium on the concentrations of available 3-IAA in the assay, we incubated 10 mM of IAA with BSA (1 mg/mL) for 60 min. The sample was then centrifuged using a concentrator (MWCO 30 kDa) and the supernatant was filtered and injected in the HPLC. An aliquot of reaction mixture was injected into a reverse-phase HPLC on a C18 Columbus column at 25°C using an isocratic elution buffer of methanol/1 % acetic acid mixture (40:60, v/v) at a flow rate of 0.6 mL/min. The eluted products were monitored at absorbance of 250 nm using an Agilent 1100 series detector. The retention time for 3-IAA was 22 min and the reactive oxygen species were eluted from 3 min to 20 min.

nHs-mediated cell cytotoxicity using MTT assay

To study the effect of cell cytotoxicity *in vitro*, HCT116 cells 50x10⁴ cells were incubated for 24 h in DMEM with 10% SFB supplemented with streptomycin-penicillin 1% for 24 h. The following day different concentrations of nHs BioSi@THRP_MNP_1300 (0.5 and 2 IU corresponding to 5 and 20 µg/mL) and 1 and 2 mM of 3IAA were added and incubated for 6 h in PBS. After 6 h the cells were washed with PBS and 90 µL DMEM 10% FBS and 10 µL of 5 mg/mL MTT was added to each well. After 3 hours of incubation at 37°C, the formation of formazan crystals was observed. The plate was then taken out of the chamber and 100 µL of DMSO was added to measure the formazan solution Multiskan™ FC Microplate Photometer at a wavelength of 570 nm.

We then analysed the cytotoxic effect in the presence of DMEM supplemented with 10% SFB. HCT116 cells 50×10^4 cells were incubated for 24 h in DMEM with 10% SFB for 24 h. The following day different concentrations of nHs BioSi@THRP_MNP_1300 and BioSi@THRP_MNP_60000 0.5 and 2 IU corresponding to 5 and 20 $\mu\text{g}/\text{mL}$ with 10 mM of 3IAA were added and incubated for 24 h in DMEM with 10% SFB. After 24 h the cells were washed with PBS and 90 μL DMEM 10% FBS and 10 μL of 5 mg/mL MTT was added to each well. After 3 hours of incubation at 37°C, the formation of formazan crystals was observed. The plate was then taken out of the chamber and 100 μL of DMSO was added to measure the formazan solution Thermo Scientific Multiskan (GO MA, USA) at a wavelength of 570 nm.

Similarly, another human colon cancer cell line HT29 was used. HT29 50×10^4 cells were incubated for 24 h in DMEM with 10% SFB for 24 h. The following day different concentrations of nHs BioSi@THRP_MNP_1300 and BioSi@THRP_MNP_60000 0.5 and 2 IU corresponding to 5 and 20 $\mu\text{g}/\text{mL}$ and 10 mM of 3IAA were added and incubated for 24 h in DMEM with 10% SFB. After 24 h the cells were washed with PBS and 90 μL DMEM 10% FBS and 10 μL of 5 mg/mL MTT was added to each well. After 3 hours of incubation at 37°C, the formation of formazan crystals was observed. The plate was then taken out of the chamber and 100 μL of DMSO was added to measure the formazan solution at MultiScan Infinite® 200 PRO Tecan Life Sciences, (Männedorf, Zürich, Switzerland) a wavelength of 570 nm.

Hyperthermia-mediated cell cytotoxicity

To study the effect of hyperthermia *in vitro*, two experiments at distinct global temperatures were carried out. HCT-116 cells 1×10^6 cells were incubated for 24 h in a 24 multi-well plate with a coverglass placed in each well in a standard incubator. The following day in a sterile test tube containing DMEM supplemented with 10% SFB and streptomycin-penicillin 1%, 2 IU of HRP nHs (BioSi@THRP_MNP_1300 and BioSi@THRP_MNP_60000), 10 mM 3-IAA along with the Coverslip with the cells were placed on an in-house 3D printed support that was carefully lowered into a tube with a fibre-optic probe to control the global temperature reached over AMF application. The tube was placed in the AMF equipment (DMS100 series/DM1 applicator from nb Nanoscale Biomagnetics) and AMF was applied at the combination of maximum magnetic field intensity and frequency (25.2 mT and 829 kHz) for 30 min maintaining the global temperature at 24°C first and repeated then at 37°C to mimic the

corporal temperatures. A live control with and without MH application, cells with nHs and 3-IAA alone, as well as, a reaction mixture (2 IU with 10 mM 3IAA) without the application of AMF was also carried out. All the samples were treated in identically conditions to ensure a reproducible comparison among them. After the application of AMF, All the coverglasses were then returned to a new multi-well plate and incubated for 24 h at 37°C and 5% CO₂ in a humidified incubator. After 24 h, 0.5 mg/mL of MTT was added to each well. After 3 hours of incubation at 37°C, the formation of formazan crystals was observed. The supernatant was carefully discarded and 100 ul of DMSO was added and was measured spectrophotometrically at 570 nm in a Thermo Scientific Multiskan (GO MA, USA). For each Hyperthermia-mediated cell cytotoxicity experiment, triplicates were done for each assayed condition. Besides, each MHT experiment was also repeated 3 times. In addition to coverslips for MTT analysis, additional coverslips of each assayed condition were also kept for TEM analysis (see below).

Statistical analysis

All experiments were performed in triplicate. Statistical analysis was carried out using one-way ANOVA tests using GraphPad Prism v6.00 and expressed as mean \pm SD. P-values <0.05 were considered statistically significant. The confidence interval was 95%. Dunnett's post-test was used to determine which means differed from the total viability.

Fixation and Dehydration Protocol for TEM analysis

HCT-116 cells 1×10^6 cells were incubated on a coverslip for 24 h until they adhered. After being submitted to the treatment (AMF +/-, nHs +/-, 3IAA +/-) explained above. To the each well containing the coverslip, a medium containing 4% glutaraldehyde in sodium cacodilate buffer 0.2 M pH 7.2 (adjusted with HCl) for 2h at 4°C. The supernatant was then removed and add 2% glutaraldehyde in cacodilate buffer 0.1 M pH 7.2 was added it was left overnight at at 4°C. The following day the wells were washed twice with sodium cacodilate buffer 0.1 M pH 7.2 the dehydration was carried out at room temperature by incubation of the coverslip with 30% methanol (MeOH) for 5 min (2x), 50% MeOH for 5min (2x), 70% MeOH for 5 min (2x), 100% MeOH for 10 min (2x), and finally, anhydrous 100% MeOH for 5 min (2x). Once the samples were ready, there were stored at 4°C in anhydrous 100% MeOH until analysed by TEM.

Results and Discussion

Cell Cytotoxicity Studies at Different Concentrations Of nHs

Nanoparticles may cause by itself adverse health effects resulting from damage to membranes, changes in protein folding, DNA mutation, blood abnormalities and oxidative stress injuries^{194,195}. Knowledge on the toxicity of nanoparticles is of utmost importance at the start of any nanomaterial-based potential new therapeutic strategy. In this sense, measurements of cell viability and proliferation can provide an indication of the safety of nanomaterials. Thus, as our aim is to trigger cytotoxicity through prodrug conversion, we first study the intrinsic toxicity of the developed biohybrids using different cell lines and two different assays to assess cell viability: an indirect and a direct test.

Indirect tests to determine cell viability such as MTT (3-(4,5-dimethylthiazol-2-yl)-2,5-diphenyl tetrazolium bromide) use the ability of living cells to catalyse reactions, yielding measurable product whose quantity is proportional to the number of living cells. Direct methods include CVS (crystal violet staining), which measures the DNA mass of living cells. Although very popular, MTT has the limitation that could be significantly influenced if NPs to be analysed modify cell metabolism by increasing the NADPH level or the activity of LDH (lactate dehydrogenase). The CVS assay lacks the limitations undermining the accuracy of MTT and other assays based on enzymatic reactions. It is a simple, non-enzymatic assay for the quick analysis of the quantity of viable adherent cells based on the affinity between crystal violet and the external surface of the DNA double helix. Thus, the amount of dye absorbed depends on the total DNA content in the culture and permits the estimation of the number of the viable cells¹⁹⁶. Therefore, to avoid the risk of erroneous interpretation due the use of a single assay we used two assays to evaluate nHs cell cytotoxicity based on completely different biological mechanisms.

We therefore studied the cytotoxicity of the nHs BioSi@THRP_MNP_1300 and BioSi@THRP_MNP_60000 blocked with glucose 1M prepared in **Chapter 2**, as they are good candidates for the proposed therapy due to their good colloidal stability in cell culture media. Different concentrations of nHs were calculated using the dry weight of the immobilized pellet and were incubated in DMEM (Dulbecco's Modified Eagle Media) supplemented with 10% fetal bovine serum at 37°C, 5% CO₂ in a humidified

incubator for 24 h in 96 multi-well plates where different cell lines were previously adhered: *i*) HaCaT (CLS 300493), a spontaneously transformed aneuploid immortal keratinocyte cell line from adult human skin; *ii*) HCT 116 and HT29 cell lines of human colon carcinoma. As it could be observed we have selected healthy and colon cancerous cell lines to perform these cytotoxicity assays as resistance to cytotoxic materials could be different.

With HaCaT cells, results show that the nHs are well tolerated by HaCaT cells and no significant effect on cell viability is observed in a range of concentrations from 1.6 to 100 $\mu\text{g/mL}$ (**Fig. 5**). The complementary results with MTT confirmed a viability above ~75% in all tested concentrations. This indicates that synthesized nHs did not modify cell metabolism and this cell viability assay could be used without erroneous interpretation. However, the results with CVS demonstrated that the viability at higher concentrations was less than 75%. Considering the combined results and the drawbacks of CVS assay, we opted for the MTT assay for all future cytotoxicity studies and the favourable range considered was up to 25 $\mu\text{g/mL}$ as the higher concentrations could increase the chance of erroneous interpretation.

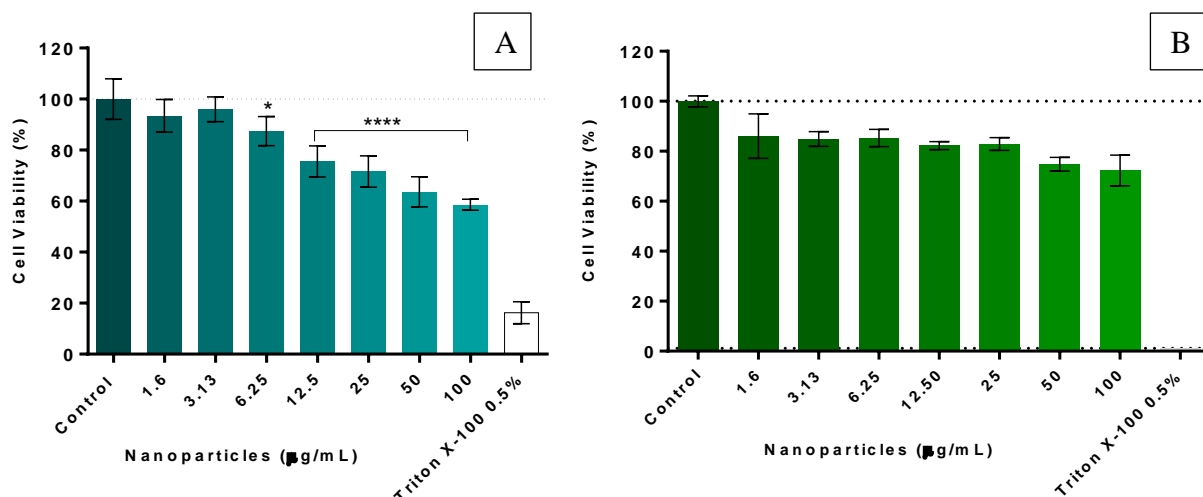


Figure 5. Cell viability studies with different concentrations of BioSi@THRP_MNP_1300 using HaCat cell line A) Crystal violet staining and B) MTT as cell viability assay. The data was normalized against the control (cells in DMEM, 10% FBS, considered 100%). A positive control of cell death was also included in the experimental design (Triton X-100 0.5% for 30 min at 37°C). Each condition was done in quintuplicates. Results from two independent experiments are shown as mean \pm SD. Statistical significance between the means with respect to the control total viable cells) was determined using a two-way ANOVA with Dunnett's multiple comparisons test (**** $p < 0.0001$; *** $p < 0.001$; ** $p < 0.01$; * $p \leq 0.05$; $p > 0.05$ no significance).

It is noteworthy that previous reports on cytotoxicity of silica aminated nanoparticles found an apoptotic effect of polyaminated polymers on the surface of the nanoparticles⁵⁰. This is not the case with our nHs, and this could be due to the surface charge neutralization achieved by blocking primary amine groups exposed on their surface by glucose. Other reason also could be their good colloidal stability and diminished interaction with proteins of the culture media, as positive NPs could strongly interact with them triggering their aggregation or the surface modification via the formation of a protein corona.

MTT cell viability assays were also performed with two different types of colorectal human cancer cell lines using the nHs BioSi@THRP_MNP_1300 and BioSi@THRP_MNP_60000 using 5 and 20 $\mu\text{g}/\text{mL}$. Similar results were achieved and non-significant effects on cell viability were observed with both types of nHs using concentrations of 5 and 20 $\mu\text{g}/\text{mL}$ (**Fig. 6 A & B**). Considering the data, obtained for the future cytotoxic assays in presence of the pro-drug, a concentration of 20 $\mu\text{g}/\text{mL}$ in each well was favoured.

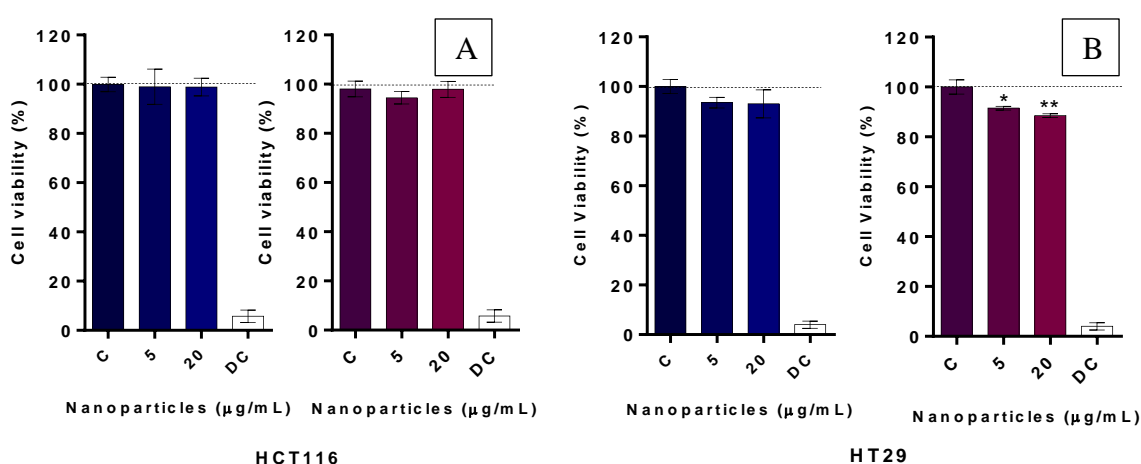


Figure 6. Cytotoxicity studies with different concentrations of BioSi@THRP_MNP_1300 (blue gradient) (5 and 20 $\mu\text{g}/\text{mL}$) and BioSi@THRP_MNP_60000 (fuchsia gradient) (5 and 20 $\mu\text{g}/\text{mL}$) using A) HCT116 cell line and B) HT29 using MTT as cell viability assay. The data was normalized against the control (cells in DMEM, 10% FBS, considered 100%). A positive control of cell death was also included in the experimental design (Triton X-100 0.5% for 30 min at 37°C, considered 0). Each condition was done in quintuplicates. Results from three independent experiments are shown as mean \pm SD. Statistical significance between the means with respect to the control (total viable cells) was determined using a two-way ANOVA with Dunnett's multiple comparisons test (**** $p < 0.0001$; *** $p < 0.001$; ** $p < 0.01$; * $p \leq 0.05$; $p > 0.05$ no significance).

Cytotoxicity in the presence of nHs and the prodrug

As a proof of its utility of the developed nHs in the proposed therapeutic application, the oxidation of 3IAA was conducted without AMF application, and the cytotoxicity triggered on HCT116 cell lines was analysed. As explained above, a concentration of nHs of 20 $\mu\text{g}/\text{mL}$ was used as we know that this concentration of nHs are not generating intrinsic cytotoxicity. In Chapter 2, we have previously demonstrated that both selected nHs (BioSi@THRP_MNP_1300 and BioSi@THRP_MNP_60000) were able to transform 3IAA into its oxidized species when incubated with the pro-drug in buffered

media. However, we need to show now that the amount oxidized species generated (concentration) is enough to induce cellular apoptosis in the cells incubated with hybrids in the presence of the prodrug, and that it also occurred in cell culture media.

Using MTT assay, the HCT116 cells were incubated for 6 h first in PBS with different concentrations of nanohybrids (corresponding to 0.5, 1 and 2 IU of HRP) and prodrug (1 mM and 2mM). All data was normalized against live control (LC) (cells with DMEM supplemented with 10% FBS, considered as 100%). Results were expressed as the mean +/- SD of triplicates of a representative experiment (**Fig. 7**).

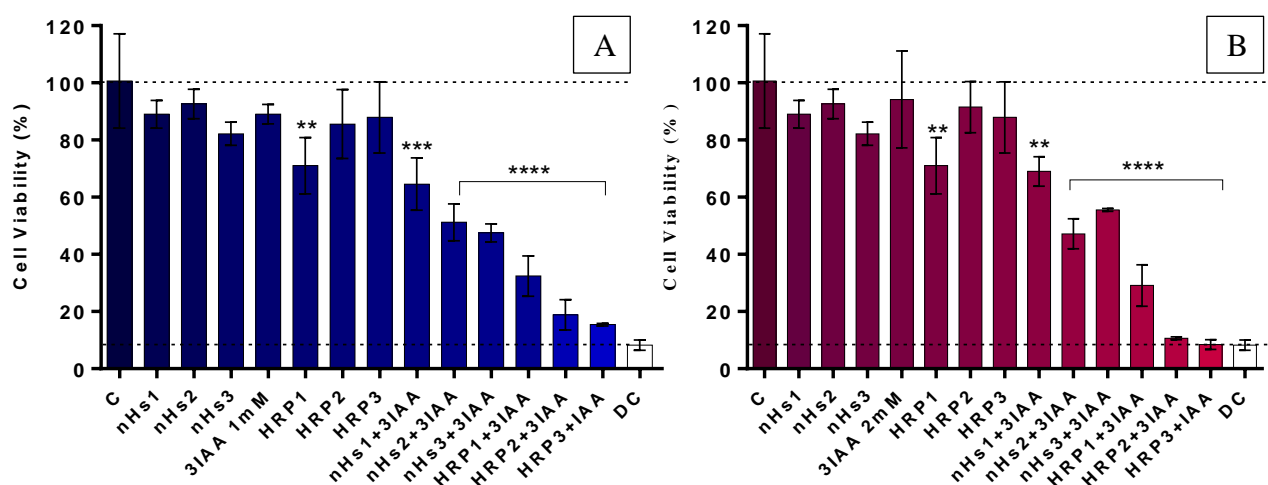


Figure 7. Cytotoxicity studies of nHs BioSi@THRP_MNP_1300 at different concentrations of 0.5, 1 and 2 IU. A) Using a concentration of 3IAA 1 mM B) Using a concentration of 3IAA 2 mM in HCT116 cell line in the presence of PBS for 6 h. The data was normalized against the control (cells in DMEM, 10% FBS, considered 100%). A positive control of cell death was also included in the experimental design (Triton X-100 0.5% for 30 min at 37°C). **C:** Control of live cells, **nH1/2/3:** control of nanohybrid at 5, 10, 20 µg/mL containing 0.5, 1 and 2 IU/mL respectively, **3IAA 1/2 mM:** Control of prodrug with concentrations of 1 and 2 mM, **HRP1/2/3:** control with soluble enzyme at 0.5, 1 and 2 IU/mL; **nHs1/2/3+3IAA:** nanohybrids and prodrug combinations; **HRP1/2/3+3IAA:** reaction mixture with soluble enzyme and prodrug combinations. **DC:** Death control. Results from three independent experiments are shown as mean ± SD. Results from three independent experiments are shown as mean ± SD. Statistical significance between the means with respect to the control total viable cells) was determined using a two-way ANOVA with Dunnett's multiple comparisons test (****p < 0.0001; ***p < 0.001; **p < 0.01; *p ≤ 0.05; p > 0.05 no significance).

The results show that after 6 hours in PBS, BioSi@THRP_MNP_PEI_1300 is well tolerated by the cells as not more than ~15% growth inhibition is observed in a range of concentrations of 5, 10 and 20 µg/mL which confirm the results shown in **Fig. 5**. Besides, when incubating the cells solely with the free enzyme or with the prodrug no significant cytotoxicity effect was observed. However, cell death was observed when

3-IAA and nanohybrids were co-incubated with the cells. Increasing amounts of enzyme units (0.5-2 IU/mL) in the assay was directly proportional to the decrease in cell viability demonstrating that the nanohybrid is efficient in the generation of toxic radicals.

It is worth noting that the soluble enzyme showed a greater cytotoxic effect in the presence of the prodrug in comparison to the co-entrapped one, as it is free and easily available for the oxidation of the prodrug. The HPLC analysis carried out in **Chapter 2** confirm these results as the soluble enzyme converted IAA (1 mM) 4 times faster as compared to the nHs in the same reaction. The rate of conversion is slower in the nanohybrids as the substrate had to traverse through the Si matrix to access the enzyme entrapped thus decreasing the rapid conversion of the prodrug. However, we already have demonstrated in Chapter 2 that integration of the enzyme in the composite material provided advantageous properties (higher thermal and operational stability) that counterbalance the decrease in the conversion rate of the prodrug 3-IAA. As the use of PBS does not mimic the corporal conditions in which the nHs are intended for, therefore, a similar experiment setup was carried out using DMEM supplemented with 10% FBS as incubation media.

From literature it is well known serum albumin has an affinity for indoles, such as tryptophan and IAA^{197,198}. The media for proliferation of cells is supplemented with 10% of fetal bovine serum (FBS) which is the most widely used serum-supplement for *in vitro* cell culture as it has very low levels of antibodies and contains more growth factors, allowing for versatility in many different cell culture applications. However, one of its major components is bovine serum albumin (BSA). Previous studies from, Bertuzzi *et. al* demonstrated that there was a clear binding of IAA to human serum albumin. The binding was enhanced at pH 5.0, whereas, the difference between binding at pH 7.4 and pH 8.5 was less evident¹⁹⁷. We analysed the effect adsorption of IAA (10 mM) on BSA (1 mg/mL) using an HPLC and observed that the concentration of available IAA in the assay was 10 less times than what was offered due to the adsorption on BSA (**Fig. 8**).

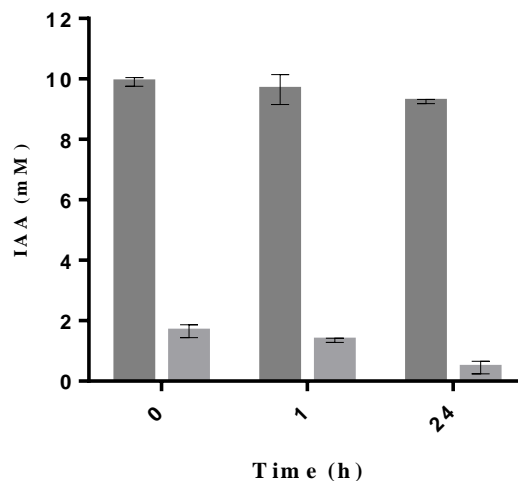


Figure 8. HPLC analysis of the adsorption of IAA (10 mM) onto BSA (1 mg/mL) where (■) control IAA (10 mM) and IAA+BSA (□).

Besides, the sequestration of free IAA by BSA is quite fast as even the HPLC analysis that was done immediately after mixing BSA and IAA showed a large decrease in the amount of free IAA. This will clearly hinder the production of radicals from IAA by nHs when incubated in complete cell culture media as a large part of IAA is not available for bioconversion as it is bound to the serum albumin. To counter this problem, we revised the concentrations of IAA offered up to 10 mM IAA wherein at least 2 mM would be free in solution and available for bioconversion by the enzyme. We had used HCT116 human colon cell line and using 10 mM of IAA we studied the cytotoxic effect of the nHs BioSi@THRP_MNP_1300 and BioSi@THRP_MNP_60000 blocked with 1 M glucose in DMEM with 10% FBS (Fig. 9).

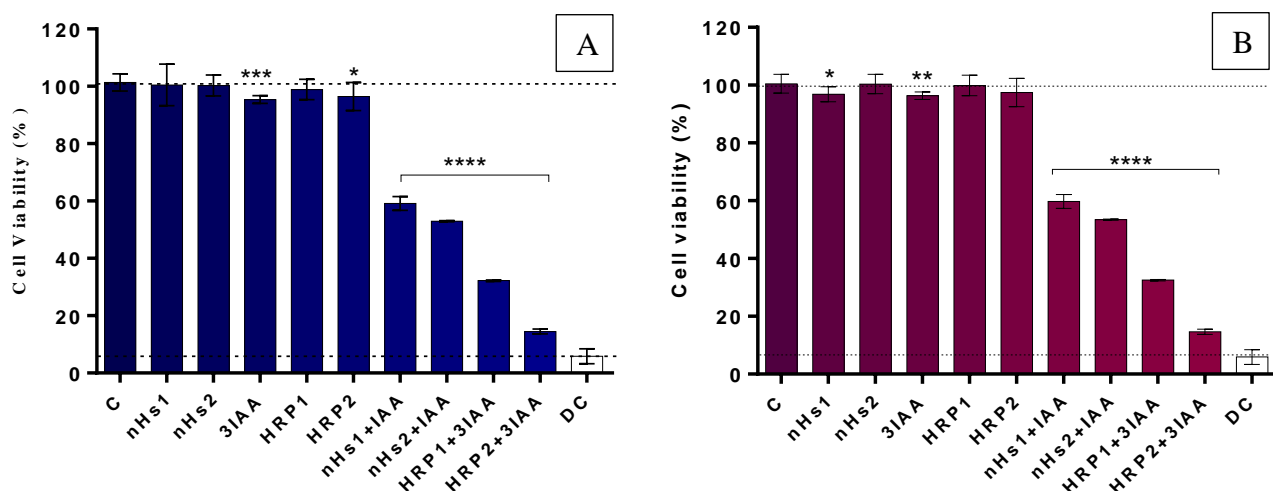


Figure 9. Effect of nanohybrids on the cell viability of HCT116. A) BioSi@T_HRP_PAA_1300 and B) BioSi@THRP_MNP_60000. HCT 116 cells were incubated for **24 h in DMEM with 10% FBS** with concentrations of nanohybrids (0.5, and 2 IU of enzyme) and just one concentration of **IAA of 10 mM**. The data was normalized as before against live control (cells with DMEM 10% FBS, considered as 100%). A positive death control was also included (Triton X-100 0.5% for 30 min at 37°C, considered 0). **C:** Control of live cells, **DC:** death control using Triton X-100 0.5% for 30 min at 37°C; **nH1/2:** control of nanohybrid at 5, 20 µg/mL containing 0.5 and 2 IU/mL respectively, **3IAA:** Control of prodrug with concentrations of 10 mM, **HRP1/2:** control with soluble enzyme at 0.5 and 2 IU/mL; **nHs1/2+3IAA:** nanohybrids and prodrug combinations; **HRP1/2+3IAA:** reaction mixture with soluble enzyme and prodrug combinations. Results from three independent experiments are shown as mean ± SD. Statistical significance between the means with respect to the control total viable cells) was determined using a two-way ANOVA with Dunnett's multiple comparisons test (****p < 0.0001; ***p < 0.001; **p < 0.01; *p ≤ 0.05; p > 0.05 no significance).

The results show that after 24 hours in DMEM, BioSi@THRP_MNP_PAA_1300 is well tolerated by the cells in a range of concentrations of 5 and 20 µg/mL (Fig. 9A). Besides, when incubating the cells solely with the free enzyme or with the prodrug no cytotoxicity effect was observed. However, cell death was observed when 3IAA and nHs were co-incubated with the cells. Increasing amounts of enzyme units (0.5 and 2 IU) in the assay showed a correlated decrease in cell viability to 60±2% and 52±1%, respectively, demonstrating that the optimized nanohybrid is efficient in the generation of toxic radicals. The soluble enzyme showed a greater cytotoxic effect (14±1%) in the presence of the prodrug in comparison to the immobilized one, as it is was previously discussed it is free and easily available for the oxidation of the prodrug. Similar results were observed with BioSi@THRP_MNP_60000 (Fig. 9B).

From literature, HCT116 are considered as a highly aggressive cell line with negligible capacity to differentiate, whereas, HT29 as an intermediate capacity to differentiate into enterocytes and mucin-expressing lineages¹⁹⁹. Makizumi et al. demonstrated that when HT29 and HCT116 when subjected to temperatures of 42° to 50°C for 15 min, in combination with 5-fluorouracil, oxaliplatin, or irinotecan at different sequences, HCT116 on pre-exposure to 45°C developed resistance to the three drugs. HCT116 have the wild type p53, is involved in the regulation of G1/S and G2/M arrest, whereas, HT29 has the mutant p53. This give HCT116 the advantage as p53 wild type delays cell cycle transition thus prolonged exposure can provide extra time for damage repair and reduce cytotoxicity of the drug. It also exhibited different expression profiles of several drug related genes making HCT116 a more robust cell line displaying a significant heterogeneity among the cell lines²⁰⁰.

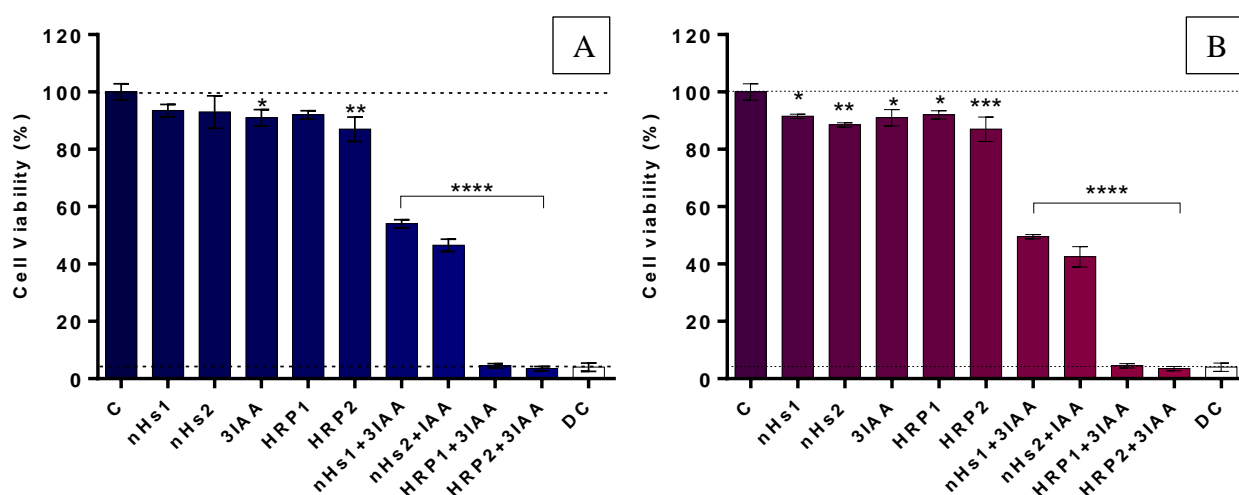


Figure 10. Effect of nano-hybrids on cell viability of HT29. A) BioSi@THRP_MNP_1300 B) BioSi@THRP_MNP_60000. Cytotoxicity studies using nHs at different concentrations (0.5 and 2 IU) with 10 mM of 3-IAA incubating with HT 29 Cell line for 24 h. The cells were incubated for 24 h in DMEM with 10% FBS with concentrations of nano-hybrids (0.5 and 2 IU of enzyme) and just one concentration of 3IAA of 10 mM. The data was normalized as before against live control (cells with DMEM 10% FBS, considered as 100%). A positive control of cell death was also included in the experimental design (Triton X-100 0.5% for 30 min at 37°C). **C**: Control of live cells, **DC**: death control. **nH_1/2**: control of nano-hybrid at 5, 20 µg/mL containing 0.5 and 2 IU/mL respectively, **3IAA**: Control of prodrug with concentrations of 10 mM, **HRP 1/2**: control with soluble enzyme at 0.5 and 10 IU/mL; **Reaction 1/2**: nano-hybrids and prodrug combinations; **HRP-R 1/2**: reaction mixture with soluble enzyme and prodrug combinations. Results from three independent experiments are shown as mean ± SD. Statistical significance between the means with respect to the control total viable cells) was determined using a two-way ANOVA with Dunnett’s multiple comparisons test (****p < 0.0001; ***p < 0.001; **p < 0.01; *p ≤ 0.05; p > 0.05 no significance).

In a similar experiment design, we analysed the effect of cytotoxicity also in another human colon cancer cell line (HT29) (**Fig. 10**). It was observed that after 24 hours in DMEM, BioSi@THRP_MNP_PEI_1300 is well tolerated by the cells as not more than ~10% growth inhibition is observed in a range of concentrations of 5 and 20 $\mu\text{g/mL}$. Besides, when incubating the cells solely with the free enzyme or with the prodrug alone no cytotoxicity effect was observed. However, cell death was observed when 3IAA and nanohybrids were co-incubated with the cells. Increasing the amounts of enzyme units (0.5 and 2 IU) in the assay did not show a correlated decrease in cell viability 53 ± 2 and $48\pm 2\%$, respectively, (**Fig. 10A**). The soluble enzyme showed a greater cytotoxic effect compared to the nHs as seen with the other cell line as well. Similar results were obtained with BioSi@THRP_MNP_60000 (**Fig. 10B**). The reproducibility of the cytotoxic effect in two cell lines showed the versatility of the developed surface engineered nHs *in vitro*. For the future experiments in hyperthermia we continued with the HCT116 cell line.

In order to show the importance of blocking the surface of nHs with glucose is a critical aspect for the success of 3IAA bioconversion, we have repeated the experimental design used with glucose-blocked nHs with nHs whose surface was not engineered. As it could be observed on **Fig. 11**, without glucose blocking the bioconversion of 3IAA by the hybrids did not occur. This could be explained but the extensive aggregation that suffer nHs without blocking in complete culture cell media.

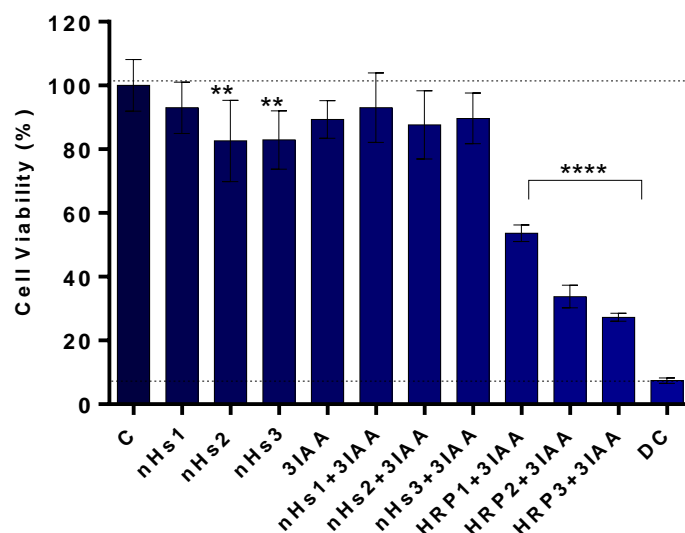


Figure 11. Effect of nano hybrids (BioSi@T_HRP_1300_MNP) without glucose 1 M on HT29 cell viability. Cytotoxicity studies using nHs at different concentrations (0.5, 1 and 2 IU) with 10 mM of 3-IAA incubating with HT 29 Cell line for 24 h. The cells were incubated for 24 h in DMEM with 10% FBS with concentrations of nano hybrids (0.5 and 2 IU of enzyme) and just one concentration of IAA of 10 mM. The data was normalized as before against live control (cells with DMEM 10% FBS, considered as 100%). **C**: Control of live cells, **DC**: death control using Triton X-100 0.5%. **nH_1/2**: control of nano hybrid at 5, 20 $\mu\text{g}/\text{mL}$ containing 0.5 and 2 IU/mL respectively, **3-IAA**: Control of prodrug with concentrations of 10 mM, **HRP 1/2**: control with soluble enzyme at 0.5 and 2 IU/mL; **Reaction 1/2**: nano hybrids and prodrug combinations; **HRP-R 1/2**: reaction mixture with soluble enzyme and prodrug combinations. Results from four independent experiments are shown as mean \pm SD. Statistical significance between the means with respect to the control total viable cells) was determined using a two-way ANOVA with Dunnett's multiple comparisons test (**** $p < 0.0001$; *** $p < 0.001$; ** $p < 0.01$; * $p \leq 0.05$; $p > 0.05$ no significance).

Cell cytotoxicity mediated by magnetic heating.

Our main aim is to be able to use the heat generated by MNPs under AMF to activate/significantly increase the activity of HRP in the conversion of the prodrug 3IAA. We have already proven that the developed nHs are thermally stable (**Chapter 1**), can that the co-entrapped cab be activated with the use of AMF using ABTS as substrate (**Chapter 2**). We have also shown above that the co-entrapped HRP is able to bioconvert IAA in complete cell culture media and it is able after 24 h of incubation to significantly reduce HCT116 cells viability. The next step is to demonstrate that we are able to increase the efficacy of the cytotoxicity of the nHs using the AMF by thermally activating the enzyme by the local generated by the co-entrapped MNPs. This should lead to a increase in the speed of 3IAA conversion and thus an increase on the

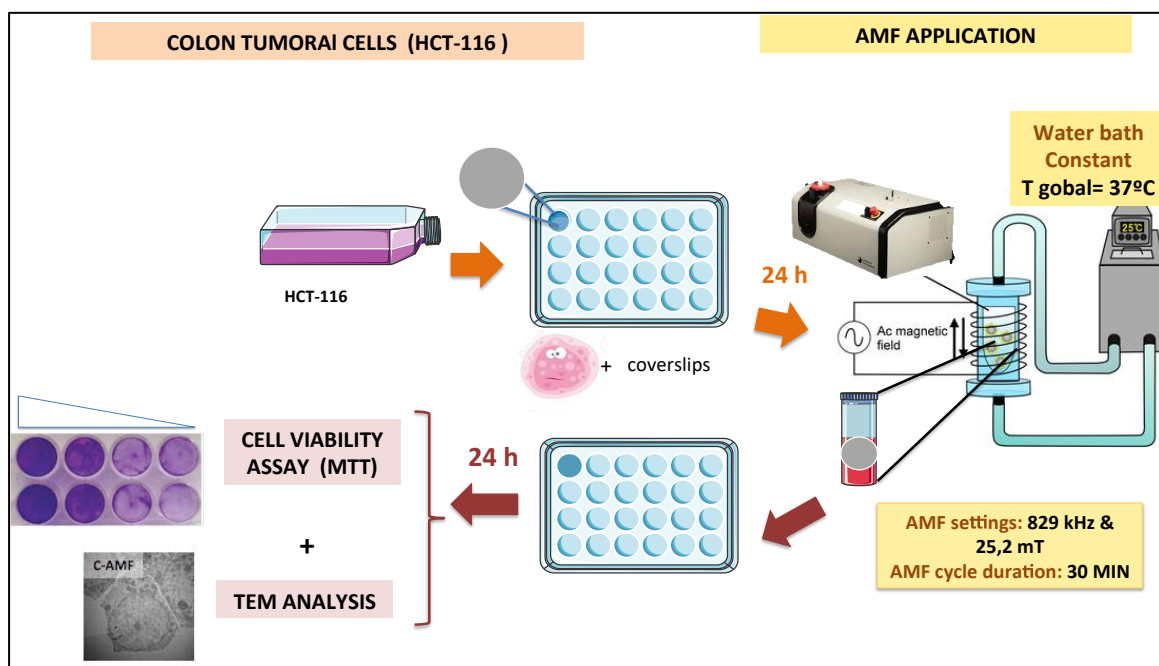
concentration of toxic radicals that should lead to an increase efficiency on decreasing cell viability when AMF are applied.

The increase of the HRP activity due to the AMF exposure was assessed through *in vitro* experiments where cells in the presence of nHs and 3IAA were exposed to AMF. The concentrations selected were 2 IU (20 µg/mL) for both types of nHs (BioSi@THRP_MNP_1300 and BioSi@THRP_MNP_60000), and 10mM for the 3IAA. Experiments were carried out at a global temperature of 37°C (controlled by a water bath), mimicking the *in vivo* application scenario. As multi well plates could not be introduced in the AMF applicator due to their size (DMS100 series/DM1 applicator, nb Nanoscale Biomagnetics), HCT116 cells were incubated first with coverslip to ensure their adhesion. Then the coverslip was carefully transferred to a vial where there were incubated for 30 min with the different conditions (**Table 1**).

NOMNECLATURE	INCUBATION CONDITIONS
C	HCT116 cells
C-AMF	HCT116 cells+ AMF cycle (829 kHz, 25.2 mT)
C-3IAA	HCT116+3IAA (10 mM)
nH-AMF	HCT116 cells+ nHs (2 IU 20 µg/mL)
nH+AMF	HCT116 cells+ nHs (2 IU, 20 µg/mL) +AMF cycle (829 kHz, 25.2 mT)
nHs+3IAA-AMF	HCT116 cells+ nHs (2 IU, 20 µg/mL)+ 3IAA (10 mM)
nHs+3IAA+AMF	HCT116 cells+ nHs(2 IU,20 µg/mL)+ 3IAA (10 mM)+ AMF cycle (829 kHz, 25.2 mT)

Table 1. Experimental set up of incubation conditions.

As sterility was maintained over the process, the different cell samples and the corresponding medium in which they were incubated where transferred to a new multi-well plate, and then were incubated for 24h in a standard cell incubator. Then cell viability was assessed by MTT, and TEM images were also carried out. **Scheme 1** showed the whole process.



Scheme 1. Description of the experimental design of the AMF application process using HTC116 cells attached to coverslip.

As it is explained in Methods Section, all the controls needed were included in the experimental design, and all the samples were treated in identically conditions for ensure a reproducible comparison among them. Results in **Fig. 12** show that both nHs do not present a cytotoxicity effect *per se*, the viability of cells incubated with the nHs was $89\pm 1\%$ and $82\pm 3\%$, for BioSi@THRP_MNP_1300 and BioSi@THRP_MNP_60000 respectively. Besides, when cells were incubated just with the 3IAA the viability was maintained always around $89\pm 2\%$. However, when cells were incubated in the presence of both the nHs and the prodrug, the death rate increased resulting in a cell viability of $63\pm 4\%$ for BioSi@THRP_MNP_1300, and $68\pm 3\%$ for BioSi@THRP_MNP_60000. This is due to the basal activity of the HRP at 37°C . All these results confirm that both nHs are not toxic and that the entrapped HRP molecules are able to transform the prodrug into toxic radicals, in agreement with our previous results⁹¹.

Besides, and worthy to stand out, when cells were exposed to an AMF (30 min, 829 kHz and 25.2 mT) in the presence of the nHs and 3IAA, the enhancement of the HRP activity due to the heat locally generated by the co-entrapped MNPs, led to a significantly decreased of cell viability. Indeed, cell viability was only of $19\pm 1\%$ for

cells incubated with BioSi@THRP_MNP_1300, and of $11\pm 2\%$ for BioSi@THRP_MNP_60000. To discard that the procedure of AMF application could affect the cell viability *per se*, a control sample consisting of cells exposed to the AMF was analyzed, finding that the cell viability remains always in $89\pm 2\%$. In addition, to confirm that the heat released by the MNPs when exposing them to the AMF was not the cause of the observed cell death, the viability of cells exposed to the AMF in the presence of just nHs was also analyzed giving good viability percentages for both types of nHs (around $78\pm 2\%$). Therefore, we could conclude that it is possible to tune by magnetic heating cell cytotoxicity induced by prodrug bioconversion. Besides, in assayed conditions, both nHs studied have similar efficiencies in increasing cell death with respect when AMF was not applied.

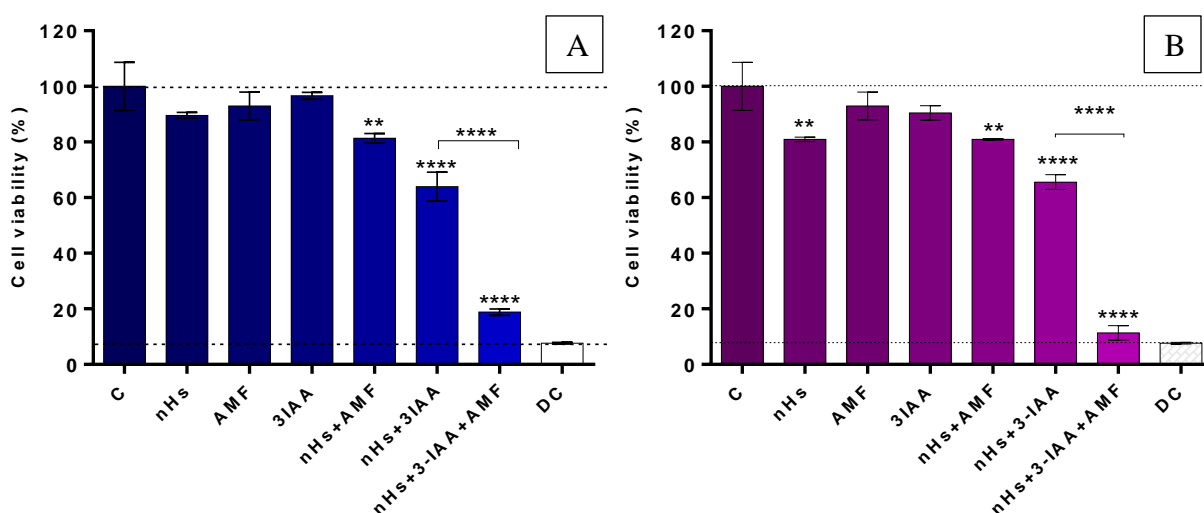


Figure 12. Cytotoxicity of 3IAA mediated by magnetic heating studied with MTT assay. A.) Cytotoxicity studies using the nHs with BioSi@THRP_1300_MNP and B.) Cytotoxicity studies using the nHs with BioSi@THRP_60000_MNP. The global temperature was maintained at 37°C during AMF application for 30 min at the maximum combination of frequency and field (829 kHz and 25.2 mT). See Scheme 4 for nomenclature and incubation conditions.

As we have established the efficacy of the nHs in hyperthermia mediated cytotoxicity, to evaluate in-depth the effect of the treatment, nHs internalization and the cell structure after different treatments were assessed by Transmission Electron Microscopy. These studies have been done only with cells incubated with BioSi@THRP_60000_MNP hybrid.

In contrast to the controls, the samples where cells were incubated with the nHs, (black particles) (~500-600 nm) were observed both outside and inside the cells, indicating the internalization of the nHs (**Fig. 13**). Three cases in which the cells were treated with the nHs were analyzed and compared with the controls and the observation of the cellular structures agree with the MTT results. First, when nHs were provided to the cells and submitted to an AMF exposure, a slight damage of the cells was observed. Although many cells still had a healthy aspect with a dense cytoplasm, others presented many vacuoles. Then, if nHs were provided to the cells together with 3IAA, a bigger cellular damage was observed in some of the cells. A large number of vacuoles within the cytoplasm were identified. In some cases, it was also possible to identify broken down of extracellular membranes (red arrow in **Fig. 13**). The typical structures of autophagosomes, with double layer membranes were also observed in some of these cells (green discontinued arrow in **Fig. 13**). Autophagosomes are double-membrane vesicles characteristic of macroautophagy, a degradative pathway for cytoplasmic material and organelles terminating in the lysosomal or vacuole compartment for mammals and yeast, respectively²⁰¹. Macroautophagy is induced by stress that could be clearly correlated with generation of toxic radicals by HRP. Finally, when the nHs were provided to the cells in combination with the administration of 3IAA and the exposure to the AMF, it was almost impossible to find a single complete cell. Only rest of discrete bodies, of similar size but different electron-density than the nHs, caused by the complete cell fragmentation were observed along most of the studied sample. The presence of autophagosomes was also observed in this case. This result agrees with the MTT data as there was only a $11\pm 2\%$ viability of the sample.

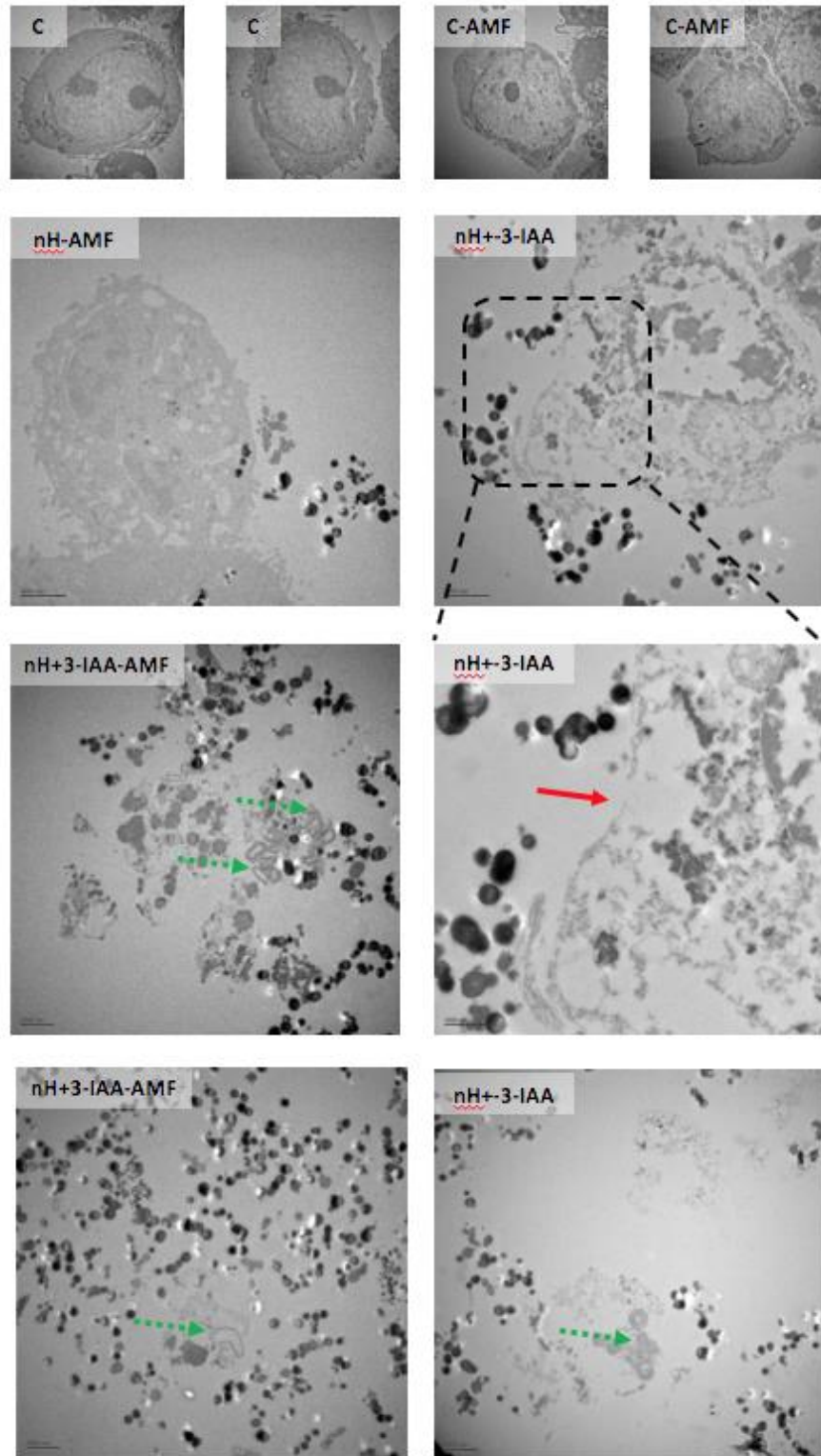


Figure 13. TEM images of the HCT 116 after application of AMF in the presence of nHs and IAA Where: C is the control HCT-116; C-AMF is the cell control with application of MH; nH -AMF is the control with the exposure to the AMF but without 3-IAA; nH+3IAA is the reaction without the application of MH; nH+3IAA-AMF is the reaction with the application of MH.

Conclusions

The use of nHs with two different MW of PEI (1300 and 60000 da) with horseradish peroxidase proved successful in DEPT. The novel nanohybrids consisting of MNPs were able to successfully oxidise indole-3-acetic acid into its peroxy radicals and were active against two colon cancer cell lines in cytotoxic studies. However, in the absence of the prodrug cytotoxicity using different cell lines was not observed, indicating that the cell cytotoxicity observed is a direct consequence of bioconversion of the prodrug by the co-entrapped HRP.

When an AMF was applied, bioconversion of the prodrug by the entrapped enzyme was clearly increased, and in this led to a large increase in the cell death efficiency by prodrug bioconversion with respect when AMF was not applied.

Altogether the obtained results show a great potentiality of the obtained biohybrids for DEPT anti-tumour therapy. The results showed that the surface engineered nanohybrids developed have a future prospect for use *in vivo* independently or in combination with other anti-tumoral therapies (radiotherapy, chemotherapy, etc).

Conclusions

In this thesis we have prepared a new nanosized hybrid material that combined MNPs, biomimetic silica and the enzyme HRP and demonstrated its utility for the remote activation of a therapeutic enzyme via magnetic heating. The diameter and polydispersity of the *in situ* prepared hybrid nanoparticles (nHs) demonstrated a dependence on the size of the aminated polymer PEI used to deposit the siliceous material and the addition of the magnetic nanoparticles (MNPs) during synthesis. Addition of the disaccharide trehalose during hybrid synthesis and a post immobilization chemical modification of the organic/inorganic material with glucose, provided exceptional thermal stability to the enzyme without compromising its activity towards a synthetic substrate. Evaluation of the activity of the immobilized preparation using 3IAA showed a 4-time decrease in the rate of conversion with respect to the soluble enzyme, probably due to partition effect of substrates and products.

The co-entrapped enzyme showed a significantly higher thermal stabilization factor compared with previous reports for HRP. Incorporation of the MNPs in the nHs was demonstrated by TEM, EDx and colorimetric measurements of Fe in disintegrated nHs compared to the Fe included in the synthesis. Although the distribution of the MNPs in the nHs was not homogeneous, the samples displayed superparamagnetic behaviour as demonstrated by SQUID analysis and the co-entrapment process does not induce an aggregation of the MNPs. The co-entrapped MNPs not only facilitated nHs separation in repeated batch transformations of a synthetic substrate but more importantly allowed to tune the activity of HRP under AMF. Indeed, under the application of a cycle of AMF, the heating capabilities of MNPs within the Si shell were quantified by determining the capacity of increasing the macroscopic temperature of the aqueous solution in which they are suspended (specific absorption rate, SAR). All the developed nHs showed lower SAR values than the pure MNPs used for the co-entrapment. As

neither magnetic properties nor aggregation of MNPs was observed by SQUID measurements after their encapsulation, the differences observed in the SAR values will be most likely due to an isolation phenomenon caused by the silica matrix. This thermal insulation effect seems to be a key feature to ensure the control of HRP activity by magnetic heating even if the enzyme is not attached to the MNP surface.

Indeed, MNPs ability to generate heat under AMF application was also demonstrated by a significant increase of the substrate rate of conversion of the encapsulated enzyme, which surpassed the rate shown at 45°C of a suspension of the nHs heated using a water-bath. This behaviour was observed while maintaining the overall (macroscopic) temperature of the reaction media at room temperature (25°C). This clearly implied that a local increase of temperature concentrated in the vicinity of the enzyme is the responsible of the increased-on enzyme activity, confirming a successful heat transfer within the nHs that reached the co-encapsulated HRP molecules.

Regarding *in vitro* cell studies, our findings demonstrate that the nHs are not cytotoxic up to concentrations of 20 ug/mL while they enabled a certain degree of cytotoxicity of cancerous cells in the same concentration upon transformation of the prodrug 3-IAA at 37 °C. Most importantly, there was a clear effect of AMF in the ability of the nHs to cause cell death in the presence of 3IAA. The effect of the AMF on the performance of the nHs was clearly showed by a significant decrease in the viability of the cells in cytotoxicity studies in comparison of cells incubated with nHs and the prodrug but without applying AMF. This difference in triggering a more effective decrease in cell viability was also confirmed by a complete cell fragmentation observed by transmission electron microscopy (TEM) only in cell samples incubated with nHs and prodrug to which an AMF cycle was applied. We believe these results clearly demonstrate our

hypothesis of a remote activation prodrug conversion by magnetic heating of the developed nHs.

In summary, the unprecedented approach for the preparation of a nanohybrid biocatalyst provided excellent properties that could be used in the development of alternative DEPT treatments with spatio-temporal control. The studies carried out with the nanohybrid prepared herein encourages additional experimentation for a better insight into its biomedical potential. Further experiments on the remote activation of the nHs *in vivo* would bring closer the application of this nanodevice for the treatment of cancer.

References

1. Dutz, S. & Hergt, R. Magnetic particle hyperthermia—a promising tumour therapy? *Nanotechnology* **25**, 452001 (2014).
2. Hervault, A. & Thanh, N. T. K. Magnetic nanoparticle-based therapeutic agents for thermo-chemotherapy treatment of cancer. *Nanoscale* **6**, 11553–11573 (2014).
3. International Agency for Research on Cancer, GLOBOCAN 2018 accessed via Global Cancer Observatory. Accessed September 2018.
4. Cagan, R. & Meyer, P. Rethinking cancer: Current challenges and opportunities in cancer research. *DMM Dis. Model. Mech.* **10**, 349–352 (2017).
5. Sharma, S. K. & Bagshawe, K. D. Antibody Directed Enzyme Prodrug Therapy (ADEPT): Trials and tribulations. *Adv. Drug Deliv. Rev.* **118**, 2–7 (2017).
6. Schellmann, N., Deckert, P. M., Bachran, D., Fuchs, H. & Bachran, C. Targeted enzyme prodrug therapies. *Mini Rev. Med. Chem.* **10**, 887–904 (2010).
7. Meffre, A. *et al.* Complex nano-objects displaying both magnetic and catalytic properties: A proof of concept for magnetically induced heterogeneous catalysis. *Nano Lett.* **15**, 3241–3248 (2015).
8. Solaro, R., Chiellini, F. & Battisti, A. Targeted Delivery of Protein Drugs by Nanocarriers. *Materials (Basel)*. **3**, 1928–1980 (2010).
9. Fang, J. *et al.* Augmentation of EPR Effect and Efficacy of Anticancer Nanomedicine by Carbon Monoxide Generating Agents. *Pharmaceutics* **11**, (2019).
10. Encapsulation Nanotechnologies. (2013). doi:10.1002/9781118729175
11. Prokop, A. & Davidson, J. M. Nanovehicular intracellular delivery systems. *J. Pharm. Sci.* **97**, 3518–90 (2008).

12. Rahoui, N., Jiang, B., Taloub, N. & Huang, Y. D. Spatio-temporal control strategy of drug delivery systems based nano structures. *J. Control. Release* **255**, 176–201 (2017).
13. Chang, D. *et al.* Biologically targeted magnetic hyperthermia: Potential and limitations. *Front. Pharmacol.* **9**, (2018).
14. Montazerabadi, A. *et al.* Folate-modified and curcumin-loaded dendritic magnetite nanocarriers for the targeted thermo-chemotherapy of cancer cells. *Artif. cells, nanomedicine, Biotechnol.* **47**, 330–340 (2019).
15. Knežević, N., Gadjanski, I. & Durand, J. O. Magnetic nanoarchitectures for cancer sensing, imaging and therapy. *J. Mater. Chem. B* **7**, 9–23 (2019).
16. Zakharchenko, A., Guz, N., Laradji, A. M., Katz, E. & Minko, S. Magnetic field remotely controlled selective biocatalysis. *Nat. Catal.* **1**, 73–81 (2018).
17. Bonifert, G., Folkes, L., Gmeiner, C., Dachs, G. & Spadiut, O. Recombinant horseradish peroxidase variants for targeted cancer treatment. *Cancer Med.* **5**, 1194–203 (2016).
18. Kazenwadel, F., Wagner, H., Rapp, B. E. & Franzreb, M. Optimization of enzyme immobilization on magnetic microparticles using 1-ethyl-3-(3-dimethylaminopropyl)carbodiimide (EDC) as a crosslinking agent. *Anal. Methods* **7**, 10291–10298 (2015).
19. Gröger, H. & Hummel, W. Combining the ‘two worlds’ of chemocatalysis and biocatalysis towards multi-step one-pot processes in aqueous media. *Curr. Opin. Chem. Biol.* **19**, 171–179 (2014).
20. Zheng, Z. . & Zhang, T. . Biocatalysis and Strategies for Enzyme Improvement. in *School of Environmental Sciences* (2012).
21. Homaei, A. A., Sariri, R., Vianello, F. & Stevanato, R. Enzyme immobilization: an update. *J. Chem. Biol.* **6**, 185–205 (2013).
22. Sipponen, M. H. *et al.* Spatially confined lignin nanospheres for biocatalytic ester synthesis in aqueous media. *Nat. Commun.* **9**, 2300 (2018).
23. Jackson, E., López-Gallego, F., Guisan, J. M. & Betancor, L. Enhanced

stability of l-lactate dehydrogenase through immobilization engineering. *Process Biochem.* (2016). doi:10.1016/j.procbio.2016.06.001

24. Romero-Fernández, M. *et al.* Designing continuous flow reaction of xylan hydrolysis for xylooligosaccharides production in packed-bed reactors using xylanase immobilized on methacrylic polymer-based supports. *Bioresour. Technol.* **266**, 249–258 (2018).
25. Pavlovic, M., Rouster, P., Somosi, Z. & Szilagyi, I. Horseradish peroxidase-nanoclay hybrid particles of high functional and colloidal stability. *J. Colloid Interface Sci.* **524**, 114–121 (2018).
26. Sulaiman, S., Mokhtar, M. N., Naim, M. N., Baharuddin, A. S. & Sulaiman, A. A Review: Potential Usage of Cellulose Nanofibers (CNF) for Enzyme Immobilization via Covalent Interactions. *Appl. Biochem. Biotechnol.* **175**, 1817–1842 (2014).
27. Mateo, C., Palomo, J. M., Fernandez-Lorente, G., Guisan, J. M. & Fernandez-Lafuente, R. Improvement of enzyme activity, stability and selectivity via immobilization techniques. *Enzyme Microb. Technol.* **40**, 1451–1463 (2007).
28. Misson, M., Zhang, H. & Jin, B. Nanobiocatalyst advancements and bioprocessing applications. (2015).
29. Jiang, Y. *et al.* Facile immobilization of enzyme on three dimensionally ordered macroporous silica via a biomimetic coating. *New J. Chem.* **39**, 978–984 (2015).
30. Gomes-Ruffi, C. R., Cunha, R. H. da, Almeida, E. L., Chang, Y. K. & Steel, C. J. Effect of the emulsifier sodium stearyl lactylate and of the enzyme maltogenic amylase on the quality of pan bread during storage. *LWT* **49**, 96–101 (2012).
31. Agostinelli, E. *et al.* Polyketone polymer: A new support for direct enzyme immobilization. *J. Biotechnol.* **127**, 670–678 (2007).
32. Bai, Y. *et al.* Identification of an acidic α -amylase from *Alicyclobacillus* sp. A4 and assessment of its application in the starch industry. *Food Chem.* **131**, 1473–1478 (2012).

33. Schückel, J., Matura, A. & van Pée, K.-H. One-copper laccase-related enzyme from *Marasmius* sp.: Purification, characterization and bleaching of textile dyes. *Enzyme Microb. Technol.* **48**, 278–284 (2011).
34. Hakala, T. K., Liitiä, T. & Suurnäkki, A. Enzyme-aided alkaline extraction of oligosaccharides and polymeric xylan from hardwood kraft pulp. *Carbohydr. Polym.* **93**, 102–108 (2013).
35. Jaros, D. & Rohm, H. Enzymes Exogenous to Milk in Dairy Technology | Transglutaminase. *Encyclopedia of Dairy Sciences* 297–300 (2011). doi:10.1016/b978-0-12-374407-4.00155-2
36. Ismail, B. & Nielsen, S. S. Invited review: Plasmin protease in milk: Current knowledge and relevance to dairy industry. *J. Dairy Sci.* **93**, 4999–5009 (2010).
37. Subba Rao, C., Sathish, T., Ravichandra, P. & Prakasham, R. S. Characterization of thermo- and detergent stable serine protease from isolated *Bacillus circulans* and evaluation of eco-friendly applications. *Process Biochem.* **44**, 262–268 (2009).
38. Soldatkin, O. O. *et al.* Novel conductometric biosensor based on three-enzyme system for selective determination of heavy metal ions. *Bioelectrochemistry* **83**, 25–30 (2012).
39. Apetrei, I. M., Rodriguez-Mendez, M. L., Apetrei, C. & de Saja, J. A. Enzyme sensor based on carbon nanotubes/cobalt(II) phthalocyanine and tyrosinase used in pharmaceutical analysis. *Sensors Actuators B Chem.* **177**, 138–144 (2013).
40. Chang, Q. & Tang, H. Immobilization of Horseradish Peroxidase on NH₂-Modified Magnetic Fe₃O₄/SiO₂ Particles and Its Application in Removal of 2,4-Dichlorophenol. *Molecules* **19**, 15768–15782 (2014).
41. Barbosa, O. *et al.* Glutaraldehyde in bio-catalysts design: a useful crosslinker and a versatile tool in enzyme immobilization. *RSC Adv.* **4**, 1583–1600 (2014).
42. Girelli, A. M. & Mattei, E. Application of immobilized enzyme reactor in on-line high performance liquid chromatography: A review. *J. Chromatogr. B* **819**, 3–16 (2005).

43. Mateo, C., Palomo, J. M., Fernandez-Lorente, G., Guisan, J. M. & Fernandez-Lafuente, R. Improvement of enzyme activity, stability and selectivity via immobilization techniques. *Enzyme Microb. Technol.* **40**, 1451–1463 (2007).
44. Betancor, L. & Luckarift, H. R. Bioinspired enzyme encapsulation for biocatalysis. *Trends Biotechnol.* **26**, 566–72 (2008).
45. Kreft, O., Prevot, M., Möhwald, H. & Sukhorukov, G. B. Shell-in-Shell Microcapsules: A Novel Tool for Integrated, Spatially Confined Enzymatic Reactions. *Angew. Chemie Int. Ed.* **46**, 5605–5608 (2007).
46. Cécile Berne, †,‡,§, Lorena Betancor, †,‡,§, Heather R. Luckarift, † and & Jim C. Spain*, ‡. Application of a Microfluidic Reactor for Screening Cancer Prodrug Activation Using Silica-Immobilized Nitrobenzene Nitroreductase. (2006). doi:10.1021/BM060166D
47. Nahalka, J., Liu, Z., Chen, X. & Wang, P. G. Superbeads: Immobilization in “Sweet” Chemistry. *Chem. - A Eur. J.* **9**, 372–377 (2003).
48. Salinas-Castillo, A., Pastor, I., Mallavia, R. & Mateo, C. R. Immobilization of a trienzymatic system in a sol–gel matrix: A new fluorescent biosensor for xanthine. *Biosens. Bioelectron.* **24**, 1053–1056 (2008).
49. Mohamad, N. R., Marzuki, N. H. C., Buang, N. A., Huyop, F. & Wahab, R. A. An overview of technologies for immobilization of enzymes and surface analysis techniques for immobilized enzymes. *Biotechnol. Biotechnol. Equip.* **29**, 205–220 (2015).
50. Jackson, E. *et al.* Protein-templated biomimetic silica nanoparticles. *Langmuir* **31**, 3687–3695 (2015).
51. Lechner, C. & Becker, C. Silaffins in Silica Biomineralization and Biomimetic Silica Precipitation. *Mar. Drugs* **13**, 5297–5333 (2015).
52. Liu, J., Yang, Q. & Li, C. Towards efficient chemical synthesis via engineering enzyme catalysis in biomimetic nanoreactors. *Chem. Commun.* **51**, 13731–13739 (2015).
53. Karthikeyan, S., Kurt, Z., Pandey, G. & Spain, J. C. Immobilized Biocatalyst for Detection and Destruction of the Insensitive Explosive, 2,4-Dinitroanisole

- (DNAN). *Environ. Sci. Technol.* **50**, 11193–11199 (2016).
54. Johnson, G. R. & Luckarift, H. R. *Enzyme stabilization via bio-templated silicification reactions. Methods in Molecular Biology* **1504**, (2017).
55. Betancor, L., Berne, C., Luckarift, H. R. & Spain, J. C. Coimmobilization of a redox enzyme and a cofactor regeneration system. *Chem. Commun. (Camb)*. 3640–3642 (2006). doi:10.1039/b604689d
56. Seo, J. H. *et al.* Liquid-phase biochemical sensing with disk-type resonant microsensor. in *TRANSDUCERS and EUROSENSORS '07 - 4th International Conference on Solid-State Sensors, Actuators and Microsystems* (2007). doi:10.1109/SENSOR.2007.4300488
57. Cazaban, D., Wilson, L. & Betancor, L. Lipase Immobilization on Siliceous Supports : Application to Synthetic Reactions. *Curr. Org. Chem.* **21**, 85–92 (2017).
58. Heck, T., Faccio, G., Richter, M. & Thöny-Meyer, L. Enzyme-catalyzed protein crosslinking. *Appl. Microbiol. Biotechnol.* **97**, 461–75 (2013).
59. Migneault, I., Dartiguenave, C., Bertrand, M. J. & Waldron, K. C. Glutaraldehyde: behavior in aqueous solution, reaction with proteins, and application to enzyme crosslinking. *Biotechniques* **37**, 790–802 (2004).
60. Veitch, N. C. Horseradish peroxidase: a modern view of a classic enzyme. *Phytochemistry* **65**, 249–259 (2004).
61. Gazaryan, I. G., Lagrimini, L. M., Ashby, G. A. & Thorneley, R. N. Mechanism of indole-3-acetic acid oxidation by plant peroxidases: anaerobic stopped-flow spectrophotometric studies on horseradish and tobacco peroxidases. *Biochem. J.* **313** (Pt 3), 841–7 (1996).
62. Warinowski, T. *et al.* Peroxidases Bound to the Growing Lignin Polymer Produce Natural Like Extracellular Lignin in a Cell Culture of Norway Spruce. *Front. Plant Sci.* **7**, 1523 (2016).
63. Kukavica, B. M., Veljovic-Jovanovic, S. D., Menckhoff, L. & Lüthje, S. Cell wall-bound cationic and anionic class III isoperoxidases of pea root: biochemical characterization and function in root growth. *J. Exp. Bot.* **63**,

- 4631–45 (2012).
64. Welinder, K. G. COVALENT STRUCTURE OF THE GLYCOPROTEIN HORSERADISH In the present communication the complete amino acid sequence of a plant peroxidase is presented for the first time . The amino acid sequence of the dominating cathodic horseradish peroxidase isoenzyme. *FEBS Lett.* **72**, 19–23 (1976).
 65. Maehly, A. C. [143] Plant peroxidase. *Methods in Enzymology* 801–813 (1955). doi:10.1016/s0076-6879(55)02307-0
 66. Gajhede, M., Schuller, D. J., Henriksen, A., Smith, A. T. & Poulos, T. L. Crystal structure of horseradish peroxidase C at 2.15 Å resolution. *Nat. Struct. Biol.* **4**, 1032–1038 (1997).
 67. Mao, L., Luo, S., Huang, Q. & Lu, J. Horseradish Peroxidase Inactivation: Heme Destruction and Influence of Polyethylene Glycol. *Sci. Rep.* **3**, 3126 (2013).
 68. Krainer, F. W. & Glieder, A. An updated view on horseradish peroxidases: recombinant production and biotechnological applications. *Appl. Microbiol. Biotechnol.* **99**, 1611–1625 (2015).
 69. Azevedo, A. M. *et al.* Horseradish peroxidase: a valuable tool in biotechnology. *Biotechnol. Annu. Rev.* **9**, 199–247 (2003).
 70. Herna, J. *et al.* Catalase-like activity of horseradish peroxidase : relationship to enzyme inactivation by H₂O₂. *Biochem. J* **354**, (2001).
 71. Schulte-Ladbeck, R., Kolla, P. & Karst, U. A field test for the detection of peroxide-based explosives. *Analyst* **127**, 1152–1154 (2002).
 72. Degradation of Hormones Using Recombinant HRP Isoenzymes. (2013).
 73. Dalal, S. & Gupta, M. N. Treatment of phenolic wastewater by horseradish peroxidase immobilized by bioaffinity layering. *Chemosphere* **67**, 741–747 (2007).
 74. Hiner, A. N. P. *et al.* A Comparative Study of the Inactivation of Wild-Type, Recombinant and Two Mutant Horseradish Peroxidase Isoenzymes C by

- Hydrogen Peroxide and m-chloroperoxybenzoic Acid. *Eur. J. Biochem.* **234**, 506–512 (1995).
75. O'Brien, A. M., O'Fágáin, C., Nielsen, P. F. & Welinder, K. G. Location of crosslinks in chemically stabilized horseradish peroxidase: implications for design of crosslinks. *Biotechnol. Bioeng.* **76**, 277–84 (2001).
76. Ryan, B. J. & Ó'Fágáin, C. Arginine-to-lysine substitutions influence recombinant horseradish peroxidase stability and immobilisation effectiveness. *BMC Biotechnol.* **7**, 86 (2007).
77. *on the definition of nanomaterial (Text with EEA relevance).*
78. Marchesan, S. & Prato, M. Nanomaterials for (Nano)medicine. *ACS Med. Chem. Lett.* **4**, 147–9 (2013).
79. Litsardakis, G. et al. Magnetic nanoparticles : developments and applications. (2012).
80. Wang, W.-W. & Yao, J.-L. Synthesis and magnetic property of silica/iron oxides nanorods. (2010). doi:10.1016/j.matlet.2010.01.034
81. Clemons, T. D., Kerr, R. H. & Joos, A. Multifunctional Magnetic Nanoparticles: Design, Synthesis, and Biomedical Applications. *Comprehensive Nanoscience and Nanotechnology* 193–210 (2019). doi:10.1016/b978-0-12-803581-8.10462-x
82. Wu, W., He, Q. & Jiang, C. Magnetic Iron Oxide Nanoparticles: Synthesis and Surface Functionalization Strategies. *Nanoscale Res. Lett.* **3**, 397–415 (2008).
83. Kouassi, G. K., Irudayaraj, J. & McCarty, G. Activity of glucose oxidase functionalized onto magnetic nanoparticles. *Biomagn. Res. Technol.* **3**, 1 (2005).
84. Zdarta, J., Meyer, A., Jesionowski, T. & Pinelo, M. A General Overview of Support Materials for Enzyme Immobilization: Characteristics, Properties, Practical Utility. *Catalysts* **8**, 92 (2018).
85. Ribeiro, L. M. O. et al. Immobilization of the enzyme invertase in SBA-15 with surfaces functionalized by different organic compounds. *J. Porous Mater.*

(2018). doi:10.1007/s10934-018-0615-2

86. Cao, S.-L., Li, X.-H., Lou, W.-Y. & Zong, M.-H. Preparation of a novel magnetic cellulose nanocrystal and its efficient use for enzyme immobilization. *J. Mater. Chem. B* **2**, 5522–5530 (2014).
87. Pavlovic, M., Rouster, P., Somosi, Z. & Szilagyi, I. Horseradish peroxidase-nanoclay hybrid particles of high functional and colloidal stability. *J. Colloid Interface Sci.* **524**, 114–121 (2018).
88. Ritter, D. W., Roberts, J. R. & McShane, M. J. Glycosylation site-targeted PEGylation of glucose oxidase retains native enzymatic activity. *Enzyme Microb. Technol.* **52**, 279–285 (2013).
89. Henley, J. P. & Sadana, A. Categorization of enzyme deactivations using a series-type mechanism. *Enzyme Microb. Technol.* **7**, 50–60 (1985).
90. Betancor, L. & Luckarift, H. Co-immobilized coupled enzyme systems in biotechnology. *Biotechnol. Genet. Eng. Rev.* **27**, 95–114 (2010).
91. Correa, S. *et al.* Design of stable magnetic hybrid nanoparticles of Si-entrapped HRP. (2019). doi:10.1371/journal.pone.0214004
92. Sadasivuni, K. K., Ponnamma, D., Rajan, M., Ahm Basheer & Al-Maadeed, M. A. S. A. *Polymer nanocomposites in biomedical engineering.*
93. Zakharova, G. S., Uporov, I. V. & Tishkov, V. I. Horseradish peroxidase: Modulation of properties by chemical modification of protein and heme. *Biochem.* **76**, 1391–1401 (2011).
94. Ramírez Tapias, Y. A., Rivero, C. W., Gallego, F. L., Guisán, J. M. & Trelles, J. A. Stabilization by multipoint covalent attachment of a biocatalyst with polygalacturonase activity used for juice clarification. *Food Chem.* **208**, 252–257 (2016).
95. Jain, N. K. & Roy, I. Effect of trehalose on protein structure. *Protein Sci.* **18**, 24–36 (2009).
96. Neville, F., Broderick, M. J. F., Gibson, T. & Millner, P. A. Fabrication and Activity of Silicate Nanoparticles and Nanosilicate-Entrapped Enzymes Using

- Polyethyleneimine As a Biomimetic Polymer. *Langmuir* **27**, 279–285 (2011).
97. Kazenwadel, F., Wagner, H., Rapp, B. E. & Franzreb, M. Optimization of enzyme immobilization on magnetic microparticles using 1-ethyl-3-(3-dimethylaminopropyl)carbodiimide (EDC) as a crosslinking agent. *Anal. Methods* **7**, 10291–10298 (2015).
 98. Curtis, K. A. *et al.* Unusual Salt and pH Induced Changes in Polyethylenimine Solutions. *PLoS One* **11**, e0158147 (2016).
 99. Sahare, P., Ayala, M., Vazquez-Duhalt, R. & Agrawal, V. Immobilization of peroxidase enzyme onto the porous silicon structure for enhancing its activity and stability. *Nanoscale Res. Lett.* **9**, 409 (2014).
 100. Wu, C., Böttcher, C. & Haag, R. Enzymatically crosslinked dendritic polyglycerol nanogels for encapsulation of catalytically active proteins. *Soft Matter* **11**, 972–80 (2015).
 101. Kannoujia, D. K., Ali, S. & Nahar, P. Pressure-induced covalent immobilization of enzymes onto solid surface. *Biochem. Eng. J.* **48**, 136–140 (2009).
 102. Sahare, P., Ayala, M., Vazquez-Duhalt, R. & Agrawal, V. Immobilization of peroxidase enzyme onto the porous silicon structure for enhancing its activity and stability. *Nanoscale Res. Lett.* **9**, 1–9 (2014).
 103. Wu, C., Böttcher, C. & Haag, R. Enzymatically crosslinked dendritic polyglycerol nanogels for encapsulation of catalytically active proteins. *Soft Matter* **11**, 972–980 (2015).
 104. McNamara, K. & Tofail, S. A. M. Nanosystems: the use of nanoalloys, metallic, bimetallic, and magnetic nanoparticles in biomedical applications. *Phys. Chem. Chem. Phys.* **17**, 27981–27995 (2015).
 105. Grillone, A. & Ciofani, G. Magnetic Nanotransducers in Biomedicine. *Chem. - A Eur. J.* **23**, 16109–16114 (2017).
 106. Ding, C. & Li, Z. A review of drug release mechanisms from nanocarrier systems. *Mater. Sci. Eng. C* **76**, 1440–1453 (2017).

107. Rai, M. & Kon, K. V. *Nanotechnology in diagnosis, treatment and prophylaxis of infectious diseases*.
108. Alivisatos, A. P. Perspectives on the Physical Chemistry of Semiconductor Nanocrystals. (1996). doi:10.1021/JP9535506
109. Arruebo, M., Fernández-Pacheco, R., Ibarra, M. R. & Santamaría, J. Magnetic nanoparticles for drug delivery. *Nano Today* **2**, 22–32 (2007).
110. Khan, H. A., Sakharkar, M. K., Nayak, A., Kishore, U. & Khan, A. Nanoparticles for biomedical applications: An overview. *Nanobiomaterials* 357–384 (2018). doi:10.1016/B978-0-08-100716-7.00014-3
111. Ruiz, A. *et al.* Biodistribution and pharmacokinetics of uniform magnetite nanoparticles chemically modified with polyethylene glycol. *Nanoscale* **5**, 11400 (2013).
112. Jun, Y., Seo, J. & Cheon, J. Nanoscaling Laws of Magnetic Nanoparticles and Their Applicabilities in Biomedical Sciences. *Acc. Chem. Res.* **41**, 179–189 (2008).
113. Fahmy, S. A., Alawak, M., Brüßler, J., Bakowsky, U. & El Sayed, M. M. H. Nanoenabled Bioseparations: Current Developments and Future Prospects. *Biomed Res. Int.* **2019**, 1–15 (2019).
114. Tapeinos, C. *Magnetic Nanoparticles and Their Bioapplications. Smart Nanoparticles for Biomedicine* (Elsevier Inc., 2018). doi:10.1016/b978-0-12-814156-4.00009-4
115. Akbarzadeh, A., Samiei, M. & Davaran, S. Magnetic nanoparticles: preparation, physical properties, and applications in biomedicine. *Nanoscale Res. Lett.* **7**, 144 (2012).
116. Kolhatkar, A. G., Jamison, A. C., Litvinov, D., Willson, R. C. & Lee, T. R. *Tuning the magnetic properties of nanoparticles. International journal of molecular sciences* **14**, (2013).
117. Ansari, S. A. M. K. *et al.* Magnetic Iron Oxide Nanoparticles: Synthesis, Characterization and Functionalization for Biomedical Applications in the Central Nervous System. *Mater. (Basel, Switzerland)* **12**, (2019).

118. Benz, M. Superparamagnetism : Theory and Applications. *Superparamagnetism Theory Appl.* 1–27 (2012).
119. Behrouzkia, Z., Joveini, Z., Keshavarzi, B., Eyvazzadeh, N. & Aghdam, R. Z. Hyperthermia: How Can It Be Used? *Oman Med. J.* **31**, 89–97 (2016).
120. Liu, J. *et al.* Local hyperthermia for esophageal cancer in a rabbit tumor model: Magnetic stent hyperthermia versus magnetic fluid hyperthermia. *Oncol. Lett.* **6**, 1550–1558 (2013).
121. Colombo, M. *et al.* Biological applications of magnetic nanoparticles. *Chem. Soc. Rev.* **41**, 4306 (2012).
122. Shubitidze, F., Kekalo, K., Stigliano, R. & Baker, I. Magnetic nanoparticles with high specific absorption rate of electromagnetic energy at low field strength for hyperthermia therapy. *J. Appl. Phys.* **117**, 094302 (2015).
123. Hergt, R., Dutz, S. & Röder, M. Effects of size distribution on hysteresis losses of magnetic nanoparticles for hyperthermia. *J. Phys. Condens. Matter* **20**, 385214 (2008).
124. Piñeiro-Redondo, Y. *et al.* The influence of colloidal parameters on the specific power absorption of PAA-coated magnetite nanoparticles. *Nanoscale Res. Lett.* **6**, 383 (2011).
125. DeNardo, S. J. *et al.* Development of Tumor Targeting Bioprobes (111In-Chimeric L6 Monoclonal Antibody Nanoparticles) for Alternating Magnetic Field Cancer Therapy. *Clin. Cancer Res.* **11**, 7087s-7092s (2005).
126. Munir, T. *et al.* Treatment of breast cancer with capped magnetic-NPs induced hyperthermia therapy. *J. Mol. Struct.* **1196**, 88–95 (2019).
127. Dalmazzo, L. F. F. *et al.* Antibody-targeted horseradish peroxidase associated with indole-3-acetic acid induces apoptosis in vitro in hematological malignancies. *Leuk. Res.* **35**, 657–62 (2011).
128. Folkes, L. K. & Wardman, P. Oxidative activation of indole-3-acetic acids to cytotoxic species- a potential new role for plant auxins in cancer therapy. *Biochem. Pharmacol.* **61**, 129–36 (2001).

129. Lisa K. Folkes*, P. W. Oxidative activation of indole-3-acetic acids to cytotoxic species— a potential new role for plant auxins in cancer therapy. *Biochem. Pharmacol.* **61**, 129–136 (2001).
130. Chiu, Y.-R., Ho, W.-J., Chao, J.-S. & Yuan, C.-J. Enzyme-encapsulated silica nanoparticle for cancer chemotherapy. *J. Nanoparticle Res.* **14**, 829 (2012).
131. Hachani, R., Lowdell, M., Birchall, M. & Thanh, N. T. K. Tracking stem cells in tissue-engineered organs using magnetic nanoparticles. *Nanoscale* **5**, 11362 (2013).
132. Lin, P.-C., Lin, S., Wang, P. C. & Sridhar, R. Techniques for physicochemical characterization of nanomaterials. *Biotechnol. Adv.* **32**, 711–26 (2014).
133. Lungu, C. N., Diudea, M. V, Putz, M. V & Grudziński, I. P. Linear and Branched PEIs (Polyethylenimines) and Their Property Space. *Int. J. Mol. Sci.* **17**, 555 (2016).
134. Rodríguez, F., Glawe, D. D., Naik, R. R., Hallinan, K. P. & Stone, M. O. Study of the chemical and physical influences upon in vitro peptide-mediated silica formation. *Biomacromolecules* **5**, 261–265 (2004).
135. Beola, L. *et al.* Dual Role of Magnetic Nanoparticles as Intracellular Hotspots and Extracellular Matrix Disruptors Triggered by Magnetic Hyperthermia in 3D Cell Culture Models. *ACS Appl. Mater. Interfaces* **10**, 44301–44313 (2018).
136. Bagwe, R. P., Hilliard, L. R. & Tan, W. Surface Modification of Silica Nanoparticles to Reduce Aggregation and Nonspecific Binding. *Langmuir* **22**, 4357–4362 (2006).
137. Umut, E. Surface Modification of Nanoparticles Used in Biomedical Applications. in *Modern Surface Engineering Treatments* (InTech, 2013). doi:10.5772/55746
138. Guerrini, L., Alvarez-Puebla, R. & Pazos-Perez, N. Surface Modifications of Nanoparticles for Stability in Biological Fluids. *Materials (Basel)*. **11**, 1154 (2018).
139. Xia, B., Zhang, W., Shi, J. & Xiao, S. Engineered Stealth Porous Silicon Nanoparticles via Surface Encapsulation of Bovine Serum Albumin for

- Prolonging Blood Circulation in Vivo. *ACS Appl. Mater. Interfaces* **5**, 11718–11724 (2013).
140. Moros, M. *et al.* Engineering biofunctional magnetic nanoparticles for biotechnological applications. *Nanoscale* **2**, 1746 (2010).
 141. Moros, M. *et al.* Monosaccharides versus PEG-Functionalized NPs: Influence in the Cellular Uptake. *ACS Nano* **6**, 1565–1577 (2012).
 142. Adekola, K., Rosen, S. T. & Shanmugam, M. Glucose transporters in cancer metabolism. *Curr. Opin. Oncol.* **24**, 650–654 (2012).
 143. Moore, T. L. *et al.* Nanoparticle colloidal stability in cell culture media and impact on cellular interactions. *Chem. Soc. Rev.* **44**, 6287–6305 (2015).
 144. Chiu, Y. R., Ho, W. J., Chao, J. S. & Yuan, C. J. Enzyme-encapsulated silica nanoparticle for cancer chemotherapy. *J. Nanoparticle Res.* **14**, 1–10 (2012).
 145. López, A., Gutiérrez, L. & Lázaro, F. J. The role of dipolar interaction in the quantitative determination of particulate magnetic carriers in biological tissues. *Phys. Med. Biol.* **52**, 5043–5056 (2007).
 146. Gutiérrez, L. *et al.* Ac magnetic susceptibility study of *in vivo* nanoparticle biodistribution. *J. Phys. D. Appl. Phys.* **44**, 255002 (2011).
 147. Hergt, R., Dutz, S. & Zeisberger, M. Validity limits of the Néel relaxation model of magnetic nanoparticles for hyperthermia. *Nanotechnology* **21**, 015706 (2010).
 148. Fratila, R. M. & de la Fuente, J. M. Introduction to Hyperthermia. *Nanomater. Magn. Opt. Hyperth. Appl.* 1–10 (2019). doi:10.1016/B978-0-12-813928-8.09997-X
 149. Fratila, R. M. & Jesús Martínez De La Fuente. *Nanomaterials for magnetic and optical hyperthermia applications.*
 150. Freddie Bray, BSc, MSc, PhD1; Jacques Ferlay, ME2; Isabelle Soerjomataram, MD, MSc, PhD3; Rebecca L. Siegel, MPH4; Lindsey A. Torre, MSPH5; Ahmedin Jemal, PhD, D. Global Cancer Statistics 2018: GLOBOCAN. *Chem. List.* **107**, 843–847 (2013).

151. Zhao, R. Perspectives on the treatment of colorectal carcinoma. *World J. Gastrointest. Oncol.* **2**, 229 (2010).
152. Winawer, S. J. *et al.* Prevention of Colorectal Cancer by Colonoscopic Polypectomy. *N. Engl. J. Med.* **329**, 1977–1981 (1993).
153. Hardcastle, J. & Hardcastle, P. T. gamma-Aminobutyric acid and intestinal secretion. *Gastroenterology* **111**, 1163–1164 (1996).
154. Nemani, K. V., Ennis, R. C., Griswold, K. E. & Gimi, B. Magnetic nanoparticle hyperthermia induced cytosine deaminase expression in microencapsulated *E. coli* for enzyme–prodrug therapy. *J. Biotechnol.* **203**, 32–40 (2015).
155. Rex, D. K. *et al.* Colonoscopic miss rates of adenomas determined by back-to-back colonoscopies. *Gastroenterology* **112**, 24–28 (1997).
156. Ramos, A. P., Cruz, M. A. E., Tovani, C. B. & Ciancaglini, P. Biomedical applications of nanotechnology. *Biophys. Rev.* **9**, 79–89 (2017).
157. Rembacken, B. J. *et al.* Flat and depressed colonic neoplasms: a prospective study of 1000 colonoscopies in the UK. *Lancet* **355**, 1211–1214 (2000).
158. Li, Y., Humphries, B., Yang, C. & Wang, Z. Nanoparticle-Mediated Therapeutic Agent Delivery for Treating Metastatic Breast Cancer-Challenges and Opportunities. *Nanomater. (Basel, Switzerland)* **8**, (2018).
159. Choi, H. S. & Frangioni, J. V. Nanoparticles for biomedical imaging: fundamentals of clinical translation. *Mol. Imaging* **9**, 291–310 (2010).
160. Kaur, P., Aliru, M. L., Chadha, A. S., Asea, A. & Krishnan, S. Hyperthermia using nanoparticles – Promises and pitfalls. *Int. J. Hyperth.* **32**, 76–88 (2016).
161. Fratila, R. M. & Jesús Martínez De La Fuente. *Nanomaterials for magnetic and optical hyperthermia applications.*
162. Dutz, S. & Hergt, R. Magnetic nanoparticle heating and heat transfer on a microscale: Basic principles, realities and physical limitations of hyperthermia for tumour therapy. *Int. J. Hyperth.* **29**, 790–800 (2013).
163. Revia, R. A. & Zhang, M. Magnetite nanoparticles for cancer diagnosis,

- treatment, and treatment monitoring: recent advances. *Biochem. Pharmacol.* **19**, 157–168 (2016).
164. Abenojar, E. C., Wickramasinghe, S., Bas-Concepcion, J. & Samia, A. C. S. Structural effects on the magnetic hyperthermia properties of iron oxide nanoparticles. *Prog. Nat. Sci. Mater. Int.* **26**, 440–448 (2016).
 165. Gobbo, O. L., Sjaastad, K., Radomski, M. W., Volkov, Y. & Prina-Mello, A. Magnetic Nanoparticles in Cancer Theranostics. *Theranostics* **5**, 1249–63 (2015).
 166. Ai, J. *et al.* Nanotoxicology and nanoparticle safety in biomedical designs. *Int. J. Nanomedicine* **6**, 1117–27 (2011).
 167. Falk, M. H. & Issels, R. D. Hyperthermia in oncology. *Int. J. Hyperthermia* **17**, 1–18
 168. Wust, P. *et al.* Hyperthermia in combined treatment of cancer. *Lancet Oncol.* **3**, 487–497 (2002).
 169. Moise, S., Byrne, J. M., El Haj, A. J. & Telling, N. D. The potential of magnetic hyperthermia for triggering the differentiation of cancer cells. *Nanoscale* **10**, 20519–20525 (2018).
 170. Edward N. Rampersaud, M. Z. V. M. P. B. A. I. M. Hyperthermia as a Treatment for Bladder Cancer. (2010).
 171. Hildebrandt, B. *et al.* *The cellular and molecular basis of hyperthermia. Critical Reviews in Oncology/Hematology* **43**, (2002).
 172. Brüningk, S. C. *et al.* A comprehensive model for heat-induced radiosensitisation. *Int. J. Hyperthermia* **34**, 392–402 (2018).
 173. Hayat, H. & Friedberg, I. Heat-induced alterations in cell membrane permeability and cell inactivation of transformed mouse fibroblasts. *Int. J. Hyperthermia* **2**, 369–78
 174. Bettaieb, A. & Averill-Bates, D. A. Thermotolerance induced at a mild temperature of 40°C alleviates heat shock-induced ER stress and apoptosis in HeLa cells. *Biochim. Biophys. Acta - Mol. Cell Res.* **1853**, 52–62 (2015).

175. Hou, C.-H., Lin, F.-L., Hou, S.-M. & Liu, J.-F. Hyperthermia Induces Apoptosis through Endoplasmic Reticulum and Reactive Oxygen Species in Human Osteosarcoma Cells. *Int. J. Mol. Sci.* **15**, 17380 (2014).
176. Ba, M.-C. *et al.* Hyperthermia enhances radiosensitivity of colorectal cancer cells through ROS inducing autophagic cell death. *J. Cell. Biochem.* **119**, 3763–3774 (2018).
177. Herea, D.-D. *et al.* Comparative effects of magnetic and water-based hyperthermia treatments on human osteosarcoma cells. *Int. J. Nanomedicine* **Volume 13**, 5743–5751 (2018).
178. Kalamida, D. *et al.* Fever-Range Hyperthermia vs. Hypothermia Effect on Cancer Cell Viability, Proliferation and HSP90 Expression. *PLoS One* **10**, e0116021 (2015).
179. Ortega, D. & Pankhurst, Q. A. Magnetic hyperthermia. *Nanoscience* 60–88 doi:10.1039/9781849734844-00060
180. Lima-Tenório, M. K., Gómez Pineda, E. A., Ahmad, N. M., Fessi, H. & Elaissari, A. Magnetic nanoparticles: In vivo cancer diagnosis and therapy. *Int. J. Pharm.* **493**, 313–327 (2015).
181. Espinosa, A. *et al.* Magnetic (Hyper)Thermia or Photothermia? Progressive Comparison of Iron Oxide and Gold Nanoparticles Heating in Water, in Cells, and In Vivo. *Adv. Funct. Mater.* **28**, 1803660 (2018).
182. Moroz, P., Jones, S. K. & Gray, B. N. Magnetically mediated hyperthermia: current status and future directions. *Int. J. Hyperth.* **18**, 267–284 (2002).
183. Dewhirst, M. W., Viglianti, B. L., Lora-Michiels, M., Hanson, M. & Hoopes, P. J. Basic principles of thermal dosimetry and thermal thresholds for tissue damage from hyperthermia. *Int. J. Hyperth.* **19**, 267–294 (2003).
184. Kim, D.-H. *et al.* Biofunctionalized magnetic-vortex microdiscs for targeted cancer-cell destruction. *Nat. Mater.* **9**, 165–171 (2009).
185. Ebrahimi, M. On the temperature control in self-controlling hyperthermia therapy. *J. Magn. Magn. Mater.* **416**, 134–140 (2016).

186. Riedinger, A. *et al.* Subnanometer Local Temperature Probing and Remotely Controlled Drug Release Based on Azo-Functionalized Iron Oxide Nanoparticles. *Nano Lett.* **13**, 2399–2406 (2013).
187. Dias, J. T. *et al.* DNA as a Molecular Local Thermal Probe for the Analysis of Magnetic Hyperthermia ** *Angewandte*. 1–5 (2013).
doi:10.1002/anie.201305835
188. Dong, J. & Zink, J. I. Taking the Temperature of the Interiors of Magnetically Heated Nanoparticles. *ACS Nano* **8**, 5199–5207 (2014).
189. Moros, M. *et al.* Triggering antitumoural drug release and gene expression by magnetic hyperthermia. *Adv. Drug Deliv. Rev.* **138**, 326–343 (2019).
190. Hervault, A. *et al.* Doxorubicin loaded dual pH- and thermo-responsive magnetic nanocarrier for combined magnetic hyperthermia and targeted controlled drug delivery applications. *Nanoscale* **8**, 12152–12161 (2016).
191. Ortner, V. *et al.* Magnetic field-controlled gene expression in encapsulated cells. *J. Control. Release* **158**, 424–32 (2012).
192. de Sousa, M. E. *et al.* Stress-Induced Gene Expression Sensing Intracellular Heating Triggered by Magnetic Hyperthermia. *J. Phys. Chem. C* **120**, 7339–7348 (2016).
193. Ito, A., Shinkai, M., Honda, H. & Kobayashi, T. Heat-inducible TNF- α gene therapy combined with hyperthermia using magnetic nanoparticles as a novel tumor-targeted therapy. *Cancer Gene Ther.* **8**, 649–654 (2001).
194. Hao, N., Li, L. & Tang, F. Shape-mediated biological effects of mesoporous silica nanoparticles. *J. Biomed. Nanotechnol.* **10**, 2508–2538 (2014).
195. Chinen, A. B. *et al.* Nanoparticle Probes for the Detection of Cancer Biomarkers, Cells, and Tissues by Fluorescence. *Chem. Rev.* **115**, 10530–10574 (2015).
196. Śliwka, L. *et al.* The Comparison of MTT and CVS Assays for the Assessment of Anticancer Agent Interactions. *PLoS One* **11**, e0155772 (2016).
197. Bertuzzi, A. *et al.* Binding of indole-3-acetic acid to human serum albumin and

- competition with L-tryptophan. *Clin. Chim. Acta.* **265**, 183–92 (1997).
198. Kim, Y. S., Min, J. K., Kim, D. & Jung, J. A soluble auxin-binding protein, ABP57. Purification with anti-bovine serum albumin antibody and characterization of its mechanistic role in the auxin effect on plant plasma membrane H⁺-ATPase. *J. Biol. Chem.* **276**, 10730–6 (2001).
199. Yeung, T. M., Gandhi, S. C., Wilding, J. L., Muschel, R. & Bodmer, W. F. Cancer stem cells from colorectal cancer-derived cell lines. *Proc. Natl. Acad. Sci. U. S. A.* **107**, 3722–7 (2010).
200. Makizumi, R., Yang, W.-L., Owen, R. P., Sharma, R. R. & Ravikumar, T. S. Alteration of Drug Sensitivity in Human Colon Cancer Cells after Exposure to Heat: Implications for Liver Metastasis Therapy using RFA and Chemotherapy. *Int. J. Clin. Exp. Med.* **1**, 117–29 (2008).
201. Jin, M. & Klionsky, D. J. Regulation of autophagy: Modulation of the size and number of autophagosomes. *FEBS Lett.* **588**, 2457–2463 (2014).

Acknowledgments

Chapter 1

I would like to acknowledge and thank the Laboratorio de Biotecnología, Universidad ORT for the use of the all the laboratory equipment and materials and reagents.

PEDECIBA for the funding of the materials and chemical reagents.

Chapter 2

I would like to acknowledge and thank the Laboratorio de Microscopias Avanzadas at Instituto de Nanociencia de Aragon - Universidad de Zaragoza (LMA-INA), Servicio General de Apoyo a la Investigación-SAI, Universidad de Zaragoza for offering access to their instruments and expertise that allowed the physicochemical characterization of the developed nHs.

Instituto de Ciencia de Materiales de Aragón (ICMA - Universidad de Zaragoza) for the use of the nB nanoscale Biomagnetics DM 100 series (nB nanoscale biomagnetics, Zaragoza, Spain) for the hyperthermia experiments.

NanoImmunotech for the use of the Malvern ZS nano instrument for the DLS and Zeta Potential analysis.

Sara Puertas from NanoImmunotech for the analysis and optimization of the preliminary DLS experiments.

Lucía Gutiérrez for her help in the SQUID analysis and interpretation of the samples.

Laboratorio de Biotecnología, Universidad ORT for the use of their HPLC equipment.

Chapter 3

I would like to acknowledge and thank Laboratorio de Biotecnología, Universidad ORT and Servicio de Animalario del Centro de Investigación Biomédica de Aragón CIBA, Zaragoza, Aragon for use the cell lines.

Inés Tiscornia, Laboratorio de Biotecnología, for her help in the design and execution of the preliminary cellular studies with the HaCat Cell line and for assisting in the technical know-how of cell culture.

Karen Perelmuter, Department of Cell Biology, Instituto Pasteur de Montevideo for her help in the preliminary studies with the HT29 cell line. Mariela Bollati, Head of the Cell Biology Department, Instituto Pasteur de Montevideo, for her contribution towards the design of the experiments

Laura Asín, Instituto de Nanotecnología Aragon, for her expertise and help in all the hyperthermia-mediated cytotoxicity studies that were carried out

Annexe

Theoretical basis of Techniques

Dynamic Light Scattering

This technique has been used to determine the hydrodynamic size of the NPs in solution and to obtain information about the stability of the NPs suspended in a buffer solution. The measurements have been performed on Malvern ZS nano instrument at NanoImmunoTech (NIT) S.L., Zaragoza, Spain.

Dynamic Light Scattering (DLS) also referred to as Photon Correlation Spectroscopy (PCS) or Quasi-Elastic Light Scattering (QELS) is a well-established technique for measuring the size of molecules and particles under the micron region size. It is typically used for measuring the size distribution of particles like proteins, nanoparticles and micelles. When an electromagnetic radiation strikes a sample containing NPs randomly suspended in a solution, it is dispersed. If the NPs are moving, the intensity of the light scattering will change over time. That is, the intensity of the measured scattered light fluctuates over time as a result of the Brownian motion (translation diffusion) that NPs have when dissolved in a solution. The function that describes the fluctuations of the intensity dispersed over time is the autocorrelation function. Using mathematical algorithms, this correlation function can be related to the hydrodynamic size of the NPs, since the Brownian movement is different depending on their size. To find the hydrodynamic size influence parameters such as temperature and solvent viscosity. The hydrodynamic size therefore depends on both the nucleus of the NP and the surrounding layer, as well as the interaction with the buffer molecules.

The instrument is composed of a monochromatic laser that uses a light source at a fixed wavelength, which reaches the sample (Figure 1). The light is scattered by the NPs at all angles, and a detector located at 90° detects the one that has been scattered in that direction. Fluctuations in the intensity of the scattered light are converted into electrical pulses and directed to a digital correlator that generates the autocorrelation function. The diameter that is measured in DLS is called hydrodynamic diameter and refers as how a particle diffuses into a liquid and corresponds with the diameter of a sphere that has the same diffusion coefficient as the particle we are measuring.

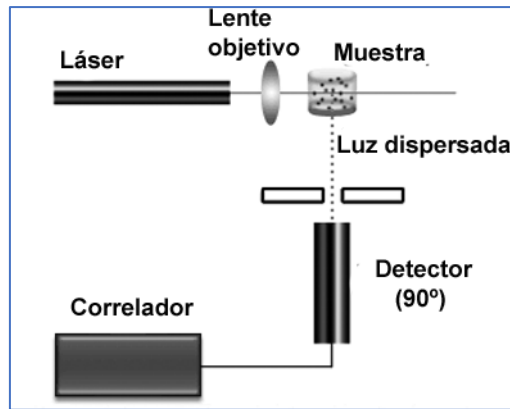


Figure 1. Schematic diagram of the DLS device used to measure the diameter of the NPs.

However, the diffusion coefficient depends not only in the core dimension but on any molecule, which is in the surface. That is why diameters obtained with this technique are frequently bigger than the values obtained by TEM.

We can choose to obtain three different distributions based on the intensity, volume or number. A very simple way of describing the differences between volume, intensity and number distribution is to consider two populations of spherical particles of diameters of 5 and 50 nm presented in equal numbers (Figure 2).

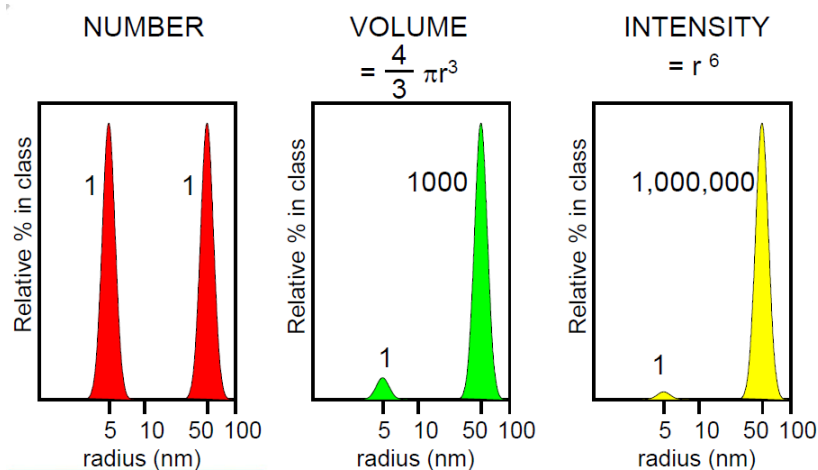


Figure 2: Number, volume and intensity distribution of a mixture of particles with diameter of 5 and 50 nm present in equal numbers.

A simple way to describe the differences between the distribution in terms of intensity, volume and number is to consider two populations of spherical particles with the same proportion of NPs of 5 and 50 nm (Figure 4). The representation in terms of intensity of this distribution gives rise to two peaks positioned at 5 and 50 nm with a ratio of 1:

1,000,000. The approximation in volume will give rise to two peaks with a 1: 1000 ratio, due to the fact that the volume is proportional to r^3 instead of r^6 as in the case of intensity (from Rayleighs approximation).

In this work the samples were prepared by diluting the NPs in Type I filtered water. Ten measurements of each sample were made at 25°C and the results were analysed in terms of intensity using the software ZetaSizer. It must be borne in mind that for the measures to be reproducible, the NPs must be stable over time.

Zeta Potential

This technique has been used to determine the surface charge of NPs in solution, which gives an idea of the electrostatic stability of NPs in a solution at a given pH. The measurements were performed on a Malvern ZS nano instrument at NanoImmunoTech (NIT) S.L., Zaragoza, Spain. The measurements of the surface charge at different pHs allow us to find the isoelectric point of the NPs, that is, the pH at which the net charge of the NP is zero (Figure 3a). The more negative or positive charge the NPs have at a given pH, the more stable they will be by electrostatic repulsion.

The measurement of the potential Z is done by applying an electric field to the dispersion where the NPs are located. The NPs will migrate to the opposite load pole with a velocity proportional to the magnitude of the potential Z (Figure 3b). This migration rate will depend on the dielectric constant of the medium and its viscosity. Once the electrophoretic mobility of the NP is known, the sample is irradiated and the variations in light scattering at an angle of 17° that are directly proportional to the speed of the NPs are analysed we can obtain the Z potential by applying

Henry's equation: the potential (ζ) can be calculated from electrophoretic mobility:

$$U_e = \frac{2\varepsilon\zeta f(ka)}{3\eta}$$

U_e being the electrophoretic mobility, ϵ the dielectric constant of the medium, ζ the zeta potential, η the viscosity of the medium and $f(\kappa a)$ is the function of Henry whose value can be equal to 1.5 for 200 nm particles dispersed in media with ionic strength greater than 10^{-3} M (Smoluchowski approximation) or equal to 1 when it comes to smaller particles (Hückel approximation) .

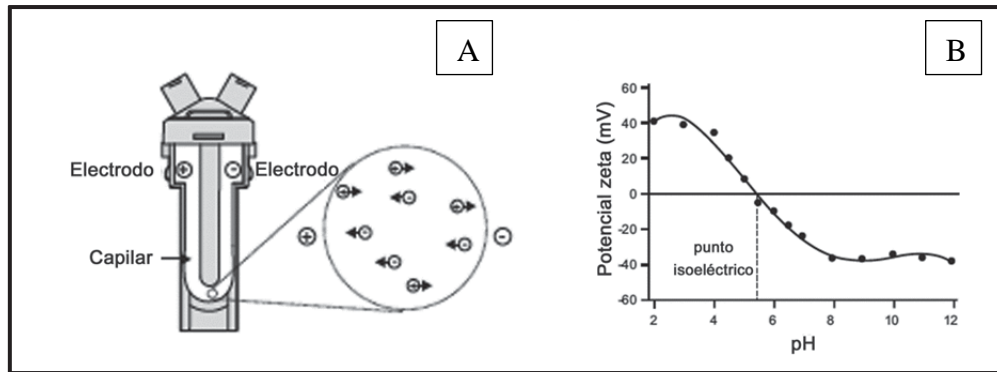


Figure 3. A) Zeta potential measurement cell; B) Calculation of the isoelectric point of a sample by determination of the potential at different pHs.

To measure the electrophoretic mobility of the NPs once the potential difference has been applied, a Doppler laser is used. The measurement is carried out by analysing the light that the particles disperse at a certain angle, which is proportional to the migration speed of the NPs. For the measurement of potential Z, NPs solutions were prepared at an approximate concentration of 0.001 mg / mL in Type I filtered water. The measurements were analysed after performing 10 repetitions of each.

SEM

The Scanning Electron Microscope (SEM) uses a focus beam of high-energy electrons rather than light to obtain a variety of signals from the surface of a solid material. The signals obtained from sample-electrons interaction reveal information of the sample, such as morphology, chemical composition and crystalline structure.

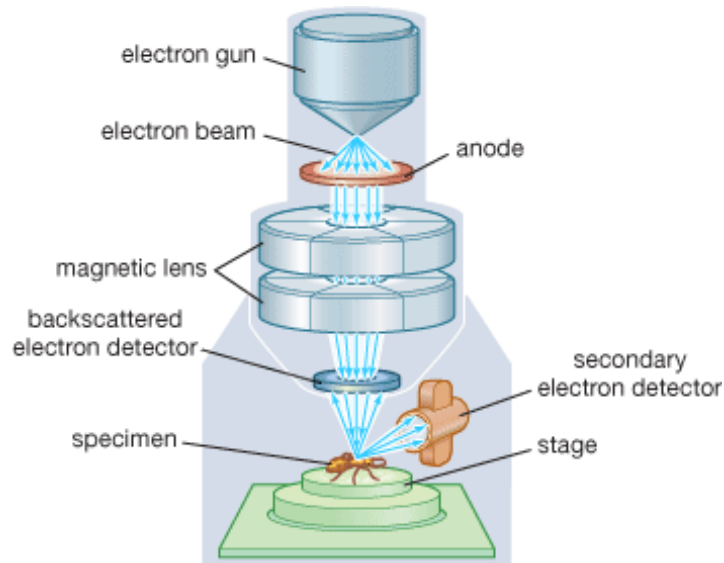


Figure 4: Scanning Electron Microscope scheme. Image taken from the Online Encyclopaedia Britannica.

An electron source at the top of the microscope, which may be a tungsten filament or a Lanthanum hexaboride source, emits the electrons that travel through vacuum in the column, and instead of glass lenses for focusing the light in light microscope SEM uses electromagnetic lenses to focus the electrons into a very thin beam. Accelerated electrons in a SEM carry significant amount of kinetic energy, which dissipate when the interaction with the sample takes place. The signals that are produced include secondary electrons (SE), backscattered electrons (BSE), diffracted backscattered electrons (DBSE), photons (X-Ray), visible light and heat (Figure 5). Secondary electrons and backscattered electrons are commonly used for imaging samples, the former are more used to obtain data about the morphology and come from the incident electrons, and the latter are more valuable to reveal contrast in composition between light and heavy metals as they come from the sample. X-Ray generation is produced by inelastic interaction between the incident electrons and electrons of the sample, and when the excited electron returns to the lowest energy state, they yield X-Ray that are of a fixed wavelength (corresponding to the difference between the energy in the two states). Thus, characteristic X-Ray are produced in different elements when their electrons are excited by the electron beam in the SEM. They are a useful tool to analyse the materials by SEM.

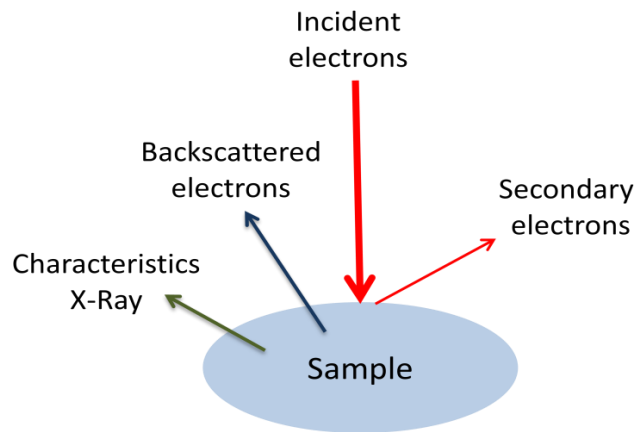


Figure 5: Electron-sample interaction signals

TEM

As in SEM microscope, TEM uses electrons as “light” source and their much lower wavelength makes it possible to get a resolution a thousand times better than with a light microscope. The electron source and the electromagnetic lenses are similar as the ones in SEM microscope. Typically, a TEM consists of three stages of lensing, which are the condenser lenses, the objective lenses and the projector lenses. The condenser lenses are responsible for primary electron beam formation, the objective lenses focus the beam that comes through the sample and the projector lenses are used to expand the beam onto the fluorescent screen.

The electron beam travel in vacuum conditions through the sample we want to study and depending on the density and the composition of the material some of the electrons are scattered and disappear from the incident beam. At the bottom of the microscope the unscattered electrons hit a fluorescent screen forming the image of the sample. Image can be recorded using a CCD camera. A schematic illustration of a typical TEM is represented in the **Fig. 6**.

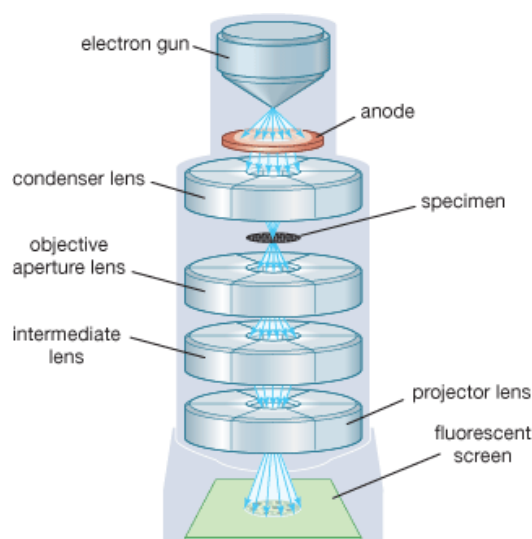


Figure 6: Transmission Electron Microscope scheme. Image taken from the Online Encyclopaedia Britannica.

The shape, size and distribution of the NPs were analysed with a TEM, acquiring the images with a Tecnai T20 microscope (FEI), equipped with a thermionic cannon and accelerator voltage of up to 200 kV. Exceptionally some high-resolution images were taken using a Tecnai F30 microscope (FEI). Both microscopes are located in the Advanced Microscopy Laboratory (LMA) of the University of Zaragoza.

Superconducting QUantum Interference Devices (SQUIDS)

The magnetic characterization of the NPs was carried out using a commercial quantum interference device SQUID (Superconducting quantum interference device) type MPMS-XL-5 T, located at the Institute of Nanoscience of Aragon (Figure 7). This magnetometer allows to characterize the magnetic properties of a material with a high sensitivity (10^{-7} emu) and basically consists of the following components: a high precision temperature control system, a superconducting coil to apply a maximum stable external magnetic field of 5T and a detection system consisting of coils of superconducting wire, which integrates a SQUID type sensor.

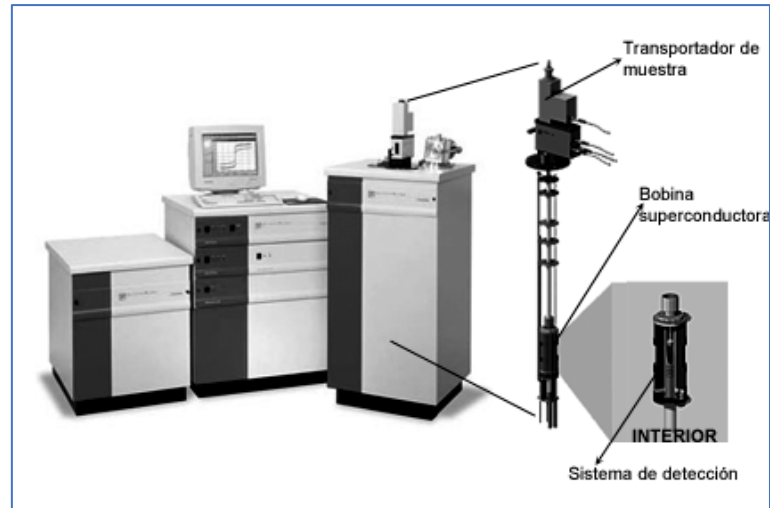


Figure 7. Image of the SQUID MPMS-XL. On the right, the sample conveyor system together with the superconducting coil is shown expanded, and within it the detection system.

The Quantum Design MPMS XL-5 SQUID Magnetometer is a very sensitive tool to measure the magnetization of materials, as function of temperature and magnetic field. The magnetic signal of the sample is obtained via a superconducting *pick-up coil* with 4 windings (Figure. 8 B). This coil is, together with a SQUID antenna (red in Figure. 8 A), part of a whole superconducting circuit transferring the magnetic flux from the sample to a RF-SQUID device which is located away from the sample in the liquid helium bath. This device acts as a magnetic flux-to-voltage converter (blue in Figure. 8 A). This voltage is then amplified and read out by the magnetometer's electronics (green in Figure. 8 a).

When the sample is moved up and down it produces an alternating magnetic flux in the pick-up coil which leads to an alternating output voltage of the SQUID device. By locking the frequency of the readout to the frequency of the movement (RSO, reciprocating sample oscillation), the magnetometer system can achieve the extremely high sensitivity for ultra-small magnetic signals as described above.

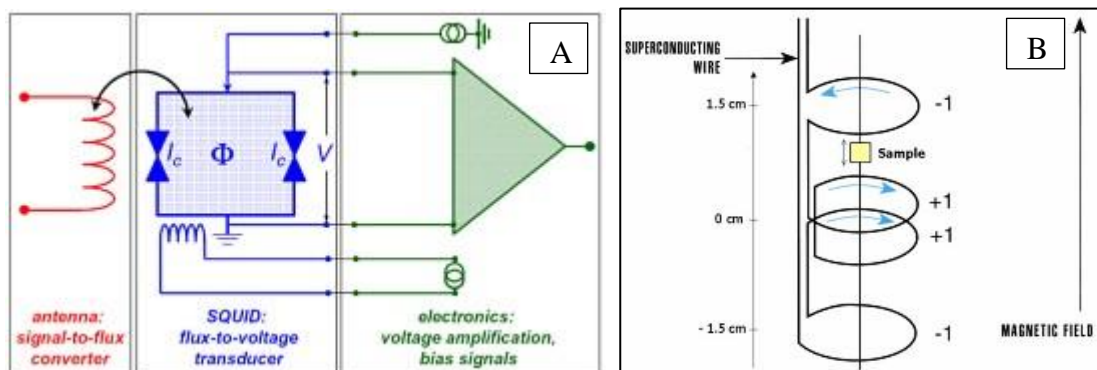


Figure 8 A). SQUID: flux-to-voltage converter B). Pick-up coil

To determine 100 μl of each sample were placed inside a polycarbonate capsule and sealed with vacuum grease for their magnetic characterization. The magnetic characterization was performed in a Quantum Design (USA) MPMS-XL and MPMS-5S SQUID magnetometers equipped with an AC (Alternating current) magnetic susceptibility option. Field dependent magnetization was recorded at 300 K under decreasing field starting from 5 T, and at 10 K in the field range between -5 T and 5 T.

Specific Power Absorption

Hyperthermia is one of the many clinical protocols used as co-adjuvant therapy for cancer treatment. It has demonstrated a clear synergistic effect when combined with radiotherapy, as well as enhancing effects with numerous cytotoxic drugs. Magnetic Hyperthermia (MHT) uses a combination of alternating magnetic fields (AMF) and magnetic nanoparticles (MNPs) as heating agents. The goal is to heat specifically and exclusively a local tumour region by means of the magnetic losses of magnetic nanoparticles in an external, alternating magnetic field, doing it without damaging the surrounding healthy tissue.



Figure 9. Magnetic hyperthermia nB bioscale biomagnetics DM 100. Image taken from the nB nanoScale Biomagnetics online product directory.

The basis of hyperthermia is the release of heat by the sample measured through the increase in colloidal temperature. The usual method for heat (Q) measurements is to use thermally insulated system, and apply the thermodynamic relation:

$$Q = C_s m_{ff} \Delta T \quad (1)$$

Where C_s is the specific heat of the fluid in (J/K g), m_{ff} is the mass of the fluid (g) and ΔT is the temperature increase (K). As this amount of heat is an extensive property, which means that it depends on the amount of sample we want to measure, it is more accurate to use the specific power absorption (SPA), defined as the amount of energy converted into heat per time unit and per material mass unit. From the expression (1), Power (P) absorbed and converted into heat can be expressed as:

$$P = \frac{Q}{\Delta t} = C_s m_{ff} \frac{\Delta T}{\Delta t} \quad (2)$$

The Power, P , is given in Watts. Specific power (i.e. the absorbed power per material gram) is called the Specific Power Absorption (SPA), and is experimentally obtained

using expression (2) and measuring temperature increase $\Delta T = T_f - T_i$ of a magnetic fluid in a time range $\Delta t = t_f - t_i$

$$SPA = \frac{P}{m_{NP}} = \frac{m_{LIQ} c_{LIQ} + m_{NP} c_{NP}}{m_{NP}} \left(\frac{\Delta T}{\Delta t} \right) \quad (3)$$

Where m_{NP} is the mass of the NPs which are diluted in a mass m_{LIQ} of liquid (colloid), and c_{LIQ} and c_{NP} are the specific heat from the solvent and the NPs, respectively. If the NPs concentration is small, we can approximate $m_{LIQ} c_{LIQ} + m_{NP} c_{NP} \approx m_{LIQ} c_{LIQ}$ and the equation will be:

$$SPA = \frac{c_{LIQ} \delta_{LIQ}}{\phi} \left(\frac{\Delta T}{\Delta t} \right) = \frac{m_{LIQ} c_{LIQ}}{m_{NP}} \left(\frac{\Delta T}{\Delta t} \right) \quad (4)$$

Where ρ_{LIQ} and $\phi = m_{LIQ}/V_{LIQ}$ are the liquid density and the concentration in terms of weight of the NPs in the colloid, respectively.

The SPA value is an indicator of how good a magnetic colloid is to produce an increase of temperature, and this is an important property of the MNPs to be selected for MFH.

Hyperthermia measurements were recorded with a magnetic heating system nB nanoscale Biomagnetics DM 100 series (nB nanoscale biomagnetics, Zaragoza, Spain). The samples, 1 mL of pure Fe₃O₄ MNPs suspensions at different concentrations, 0.5 and 1 mg/mL were placed in a vial, at the centre of an 8-turn coil, connected to the remote heat station of the device. With this setup, alternating magnetic fields with strength of 25.2 mT at a frequency of 829 kHz were generated. The temperature was measured using a fiber-optic probe, placed in the centre of the vial, connected to a computer, providing the temperature values each second using and data fitting for instant ZAR calculations using the in-built MaNiac Software.

Publications

Book Chapters

Cellulose-Based Nanosupports for Enzyme Immobilization

Erienne Jackson, Sonali Correa, and Lorena Betancor

***In situ* immobilization of enzymes in biomimetic silica**

Erienne Jackson, Sonali Correa and Lorena Betancor.

Paper

Design of stable magnetic hybrid nanoparticles of Si-entrapped HRP

Sonali Correa, Sara Puertas, Lucía Gutiérrez, Laura Asín, Jesús Martínez de la Fuente, Valeria Grazú, Lorena Betancor

Published: April 1, 2019 DOI: <https://doi.org/10.1371/journal.pone.0214004>

Journal: PLOS One

RESEARCH ARTICLE

Design of stable magnetic hybrid nanoparticles of Si-entrapped HRP

Sonali Correa¹, Sara Puertas², Lucía Gutiérrez^{3,4,5}, Laura Asín⁵, Jesús Martínez de la Fuente^{4,5}, Valeria Grazú^{4,5*}, Lorena Betancor^{1*}

1 Laboratorio de Biotecnología, Universidad ORT Uruguay, Montevideo, Uruguay, **2** Nanoimmunotech S.L., Zaragoza, Spain, **3** Instituto de Nanociencia de Aragón, Universidad de Zaragoza, Campus Río Ebro, Edificio I+D, Zaragoza, Spain, **4** Instituto de Ciencia de Materiales de Aragón (ICMA), Consejo Superior de Investigaciones Científica, Zaragoza, Spain, **5** Centro de Investigación Biomédica en Red de Bioingeniería, Biomateriales y Nanomedicina (CIBER-BBN), Madrid, Spain

* betancor@ort.edu.uy (LB); vgrazu@unizar.es (VG)



Abstract

Hybrid and composite nanoparticles represent an attractive material for enzyme integration due to possible synergic advantages of the structural builders in the properties of the nanobiocatalyst. In this study, we report the synthesis of a new stable hybrid nanobiocatalyst formed by biomimetic silica (Si) nanoparticles entrapping both Horseradish Peroxidase (HRP) (EC 1.11.1.7) and magnetic nanoparticles (MNPs). We have demonstrated that tailoring of the synthetic reagents and post immobilization treatments greatly impacted physical and biocatalytic properties such as an unprecedented ~280 times increase in the half-life time in thermal stability experiments. The optimized nanohybrid biocatalyst that showed superparamagnetic behaviour, was effective in the batch conversion of indole-3-acetic acid, a prodrug used in Direct Enzyme Prodrug Therapy (DEPT). Our system, that was not cytotoxic *per se*, showed enhanced cytotoxic activity in the presence of the prodrug towards HCT-116, a colorectal cancer cell line. The strategy developed proved to be effective in obtaining a stabilized nanobiocatalyst combining three different organic/inorganic materials with potential in DEPT and other biotechnological applications.

OPEN ACCESS

Citation: Correa S, Puertas S, Gutiérrez L, Asín L, Martínez de la Fuente J, Grazú V, et al. (2019) Design of stable magnetic hybrid nanoparticles of Si-entrapped HRP. PLoS ONE 14(4): e0214004. <https://doi.org/10.1371/journal.pone.0214004>

Editor: Andrew C. Marr, Queen's University Belfast, UNITED KINGDOM

Received: November 16, 2018

Accepted: March 5, 2019

Published: April 1, 2019

Copyright: © 2019 Correa et al. This is an open access article distributed under the terms of the [Creative Commons Attribution License](https://creativecommons.org/licenses/by/4.0/), which permits unrestricted use, distribution, and reproduction in any medium, provided the original author and source are credited.

Data Availability Statement: All relevant data are within the manuscript and its Supporting Information files.

Funding: SC is funded by ANII (POS_NAC_2015_1_109910).

Competing interests: The authors have declared that no competing interests exist.

Introduction

The possibilities for practical applications of immobilized enzymes are continuously growing and a steady number of immobilization methods have been recently developed to preserve the activity of biotechnologically important enzymes in unnatural environments [1–4]. Apart from industrial large-scale applications, immobilization techniques on nanoscale supports have enabled and amplified the integration of enzymes in biosensors [5–7], nano/microreactors [8,9] or in the generation of hybrid nanostructures for biomedical applications [8,10,11]. Design of tailored strategies for enzyme immobilization has proved essential to achieve better specific activities, robustness and reusability of the material integrated enzymes, addressing the major problems that restrain industrial or therapeutic implementation of enzymatic reactions [12–14].

Selection of the support material for enzyme immobilization is a critical aspect due to its major impact on the properties of the biocatalyst. Its shape and textural characteristics of, hydrophilicity/hydrophobicity properties, biocompatibility, toxicity or physicochemical stability can directly influence the performance and utility of the immobilized enzyme [15–17]. Consequently, the discovery and use of new support materials with desired properties has become extremely important in the design of immobilized biocatalysts.

In this regard, scientific attention has been directed towards hybrid and composite materials, which combine properties of both composite precursor and maximize their advantages [4,18]. Upon integration of the different materials, it is desired that the intrinsic characteristics of each individual component are preserved, exhibiting new additional properties due to the synergetic effect between the structural builders. When immobilizing an enzyme in composite supports, scientists aim for a combined benefit of the materials on the properties of the biocatalyst.

Biomimetic silica (Si) has been used in the past to generate hybrid inorganic/organic nanocomposites for a range of applications. It can be synthesized as a nanostructured material with divergent morphologies within minutes under mild and green conditions [19,20]. Any material contained in the synthetic mixture may become entrapped within the biomimetic Si nanoparticles [17,21–23]. The mild synthetic approach (room temperature, neutral pH, free of organic solvents) is compatible with a range of enzymes for which the strategy has also resulted in stabilization [24–26]. Moreover, for biomedical applications such as enzyme replacement therapies or direct enzyme prodrug activation, encapsulation of enzymes in a Si nanocarrier could reduce the immunogenicity of the enzyme. However, synthetic strategies for biomimetic Si nanobiocatalysts are not universal as they provide distinct properties to different enzymes and may be tailored to improve a desired attribute [13].

HRP is a heme-containing enzyme that uses hydrogen peroxide as electron acceptor. Its importance in biotechnology is long established as it is involved in a variety of biological processes, it is able to amplify weak signals, it is stable towards external factors (e.g. peroxide species, temperature) and has a high turnover number [27]. In the past decade, HRP related investigations have regained interest following the discovery of new natural isoenzymes with different biochemical properties and the development of an efficient recombinant expression system that facilitated its production. New HRP properties might enable the effective use of this enzyme in polymer synthetic reactions in the presence of organic solvents or as a therapeutic agent in cancer therapy [28,29]. In the light of these new applications, we believe it is timely to propose novel immobilization strategies for HRP on tailored materials that augment its practical possibilities.

In this study, we demonstrate a new approach to integrate and stabilize HRP in biohybrid magnetic nanoparticles (biomimetic Si + magnetic nanoparticles (MNPs)). The hybrid immobilization system provided ease of separation in biocatalytic applications or accumulation of HRP nanobiocatalyst where desired. Each material included in the nano-hybrid contributed to the improvement of the properties of the nanohybrid which enabled its use in the conversion of indole-3-acetic acid (3-IAA), a prodrug used in cancer therapy.

Materials and methods

Horseshoe peroxidase Type VI (EC 1.11.1.7), polyethylenimine (PEI) (MW 1300, 2000, 25000 and 60000), 2,2'-Azino-bis (3-ethylbenzothiazoline-6-sulfonic acid) diammonium salt (ABTS) and hydrogen peroxide were from Sigma Aldrich (St. Louis, MO). Tetramethyl orthosilicate (TMOS), trehalose and potassium phosphate monobasic were from MERCK (Whitehouse Station, NJ). Dibasic sodium phosphate and sodium acetate were from Biopack (Buenos

Aires, Argentina). Gel filtration PD10-Columns were from GE Healthcare (Buckinghamshire, UK). Magnetic nanoparticles (MNPs) fluidMag-PAA (200 nm of aggregate size) were from Chemicell (Berlin, Germany). All other chemicals used were analytical grade reagents.

Determination of HRP activity

The activity of the free and entrapped enzyme preparations was measured by a colorimetric assay using 9.1 mM ABTS, ($\epsilon_M = 36.8 \text{ mM}^{-1}\text{cm}^{-1}$), as a substrate. The final assay contained 1.7 mL of 0.1 M potassium phosphate, pH 5.0 at 25°C, 0.1 mL of 9.1 mM ABTS, 0.2 mL 0.3% (w/w) hydrogen peroxide solution (H_2O_2) in deionized water and 10 μL of the soluble and nanohybrid preparations. The oxidation of ABTS was measured in a spectrophotometer at a wavelength of 405 nm for 2 min (Unico SQ-2800 UV-Vis). One enzyme unit (IU) was defined as the amount of HRP able to oxidize 1 μmol of ABTS in the above-mentioned conditions.

Entrapment of HRP in biomimetic Si nanoparticles. Aliquots of 0.4 mL of horseradish peroxidase Type VI solutions (protein concentration varied from 0.5 to 20 mg/mL) in potassium phosphate buffer (0.1 M, pH 8.0) were mixed with 0.1 mL of 10% polyethyleneimine (PEI) adjusted to pH 8.0 with HCl and 0.1 mL of a hydrolyzed TMOS solution prepared by diluting TMOS in hydrochloric acid (1 mM) to a final concentration of 1 M. The enzyme, buffer and PEI were mixed and gently agitated in an end-over-end roller for 15 min at 25°C. Then, the hydrolysed TMOS was added and this mixture was incubated for 5 min at 25°C. The resultant entrapped HRP preparation was then centrifuged (13500 rpm) for 5 min, washed five times by centrifugation and resuspension with sodium phosphate buffer 0.1 M pH 8.0 at 25°C and sonicated in an ultrasonic cleaner at 130 W and 20 kHz, (SONICS & MATERIALS, INC.) for 5 min. The immobilized nanobiocatalysts entrapped in Si are noted as [BioSi@HRP](#).

Immobilization percentage was defined as:

$$\%I = \frac{(\text{Initial activity} - \text{Activity in supernatant}) * 100}{\text{Initial activity}}$$

Immobilization yield was defined as:

$$\%Y = \frac{(\text{Activity in immobilized preparation}) * 100}{\text{Initial activity} - \text{Activity in supernatant}}$$

Oxidation of HRP. HRP was oxidized using a modification of Zalipsky's PEGylation protocol with the aim of generating aldehyde groups in its sugar moieties [30]. Peroxidase (3 mg) was dissolved in 1.8 mL of 10 mM sodium phosphate containing 154 mM sodium chloride, pH 7.2. Simultaneously, 8.6 mg of sodium periodate were dissolved in 200 μL of distilled water and protected from light. The sodium periodate solution was immediately added to the enzyme solution, and the sample was gently agitated. The 2 mL mixture was incubated in the dark for 1 h at 25°C with constant agitation. The reaction was then quenched by the addition of 2.5 μL of glycerol (99.5%) and the oxidized enzyme was then purified by using a desalting PD10 column equilibrated with 100 mM sodium phosphate pH 6.0 containing 154 mM sodium chloride. Oxidized HRP was concentrated to 1 mg/mL using Vivaspinn 500 with a 30 KDa cut off membrane. The oxidised enzyme is noted as HRPox.

Covalent three-dimensional immobilization of the entrapped HRP. HRPox (1 mg/mL) was entrapped in Si nanoparticles using the above-mentioned protocol. The entrapped enzyme was then incubated in 25 mM sodium bicarbonate, pH 10.0 (R 1:10) overnight at 4°C to facilitate the formation of Schiff's bases between the aldehyde groups generated in the enzyme and unreacted amino group from the support. The Schiff's bases were finally reduced using sodium

borohydride (1 mg/ml, 1:10) during 30 min at 25°C. The nanoparticles were then washed by centrifugation and resuspension in 0.1 M sodium phosphate buffer pH 8.0 three times.

Co-entrapment with magnetic nanoparticles. 10 μ L of a 25 mg/mL solution of MNPs (chemicell FluidMAG-PAA, 200 nm) were brought to a magnetic separation rack during 5 min. The supernatant was removed and resuspended in the same volume of 0.1 M sodium phosphate buffer, pH 8.0. The co-entrapment procedure was the same as the one described above for the entrapment of HRP but adding the washed 10 μ L suspension before the TMOS addition.

Aliquots of 0.4 mL of oxidized horseradish peroxidase solutions (protein concentration 1 mg/mL) in potassium phosphate buffer (0.1 M, pH 8.0) were mixed with 0.1 mL of 10% polyethyleneimine (PEI) adjusted to pH 8.0 with HCl and 10 μ L suspension of the washed magnetic nanoparticles. The mixture was incubated for 10 min under gentle agitation at 25°C after which 0.1 mL of a hydrolyzed TMOS solution prepared by diluting TMOS in hydrochloric acid (1 mM) to a final concentration of 1 M, were added.

The resultant entrapped HRP preparation containing MNPs (BioSi@HRP_MNP) was then centrifuged (13500 rpm) for 5 min and washed five times by centrifugation and resuspension in 0.6 mL of sodium phosphate buffer 0.1 M pH 8.0. The nanoparticles suspension was sonicated in an ultrasonic cleaner at 130 W and 20 kHz (SONICS & MATERIALS, INC.) for 5 min and finally reduced using the above-mentioned protocol for a three-dimensional covalent immobilization.

General procedures for nanoparticles characterization. The morphology and particle size distribution of the resulting nanoparticles (NPs) were characterized by Environmental Scanning Electron Microscopy (ESEM) images were obtained using a QUANTA-FEG 250 microscope in “wet-mode” using a Peltier stage and a gaseous secondary electron detector (GSED). The secondary electron images were taken at a voltage range between 10–15 keV, low temperature (1°C), high chamber relative humidity (100%) and high Pressure (659 Pa) to maintain the wet sample hydrated avoiding the sample damage during the observation. The sample was prepared in milliQ water in a dilution of (1:10000) and sonicated prior to measurements for 3 min to improve the dispersity.

Dynamic light scattering (DLS) and Z-potential measurements were performed on a Malvern ZS nano instrument at 25°C. Each sample was prepared by diluting the sample (1:100000) with milliQ water of which 1 mL was added to a quartz cuvette. They were measured 10 times, with a combination of 3 runs per measurement. The data was analysed using Zetasizer software. Similarly, the z-potential was measured using the same sample in a Folded Capillary Zeta Cell and the sample was measured 10 times and analysed using the aforementioned software.

Magnetic characterization was performed as follows: 50 μ L of the liquid sample were placed inside a polycarbonate capsule and sealed with vacuum grease for their magnetic characterization. The magnetic characterization was performed in a Quantum Design (USA) MPMS-XL SQUID magnetometer. Field dependent magnetization was recorded at 300 K under decreasing field starting from 2 T, in the field range between -2 T and 2 T.

Reuse of nanohybrid by magnetic separation. The reusability of the immobilized enzyme nanohybrids was studied by repeated usage for 10 enzymatic cycles. Enzymatic reactions using 9.1 mM of ABTS and 0.3% hydrogen peroxide as substrates were performed in a 2 mL reaction volume containing potassium phosphate buffer pH 5.0, and a fixed amount of immobilized enzyme (20 U). Between each cycle, the nanohybrids were carefully separated using a magnetic separator (Chemicell- MagnetoPURE BIG SIZE) and then resuspended in the reaction mixture. The reactions were measured spectrophotometrically at 405 nm for 2 min. The activity determined during the first cycle was considered 100% for the calculation of remaining percentage activity after each use.

Determination of reducing sugars by DNS method. To analyse the concentration of trehalose by DNS, serial dilutions of trehalose from 0.07 g/L to 10 g/L were made. To 2 mL of these solutions 1 mL of dilute hydrochloric acid was added and boiled for 1 min following which was cooled and the acid was neutralized with sodium hydrogen carbonate. Similarly, the supernatant of an immobilized preparation (stored for 1 month), for which we intended to observe trehalose leakage, was hydrolysed to convert the non-reducing sugar into a reducing sugar.

To the hydrolysed preparations 250 µl of DNS reagent was added. The mixture was heated at 90°C for 15 min to develop the range of colours which formed the standard to analyse our sample. Finally, distilled water was added to bring the final volume to 1 mL which were cooled to room temperature and the absorbance was recorded at 570 nm in a spectrophotometer.

Temperature profile of the nanoabiocatalysts. To study the optimum temperature, the reactants were heated in a water bath to a range of temperatures (20°C to 60°C). Upon reaching the desired temperature 10 µL enzyme was added to the reactant mixture and measured spectrophotometrically at 405 nm for 2 min.

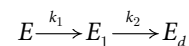
To analyse the range of thermal stability, the enzyme preparations were incubated in 0.1 M sodium phosphate pH 8.0 for 1 h at the aforementioned temperatures (20 to 60°C) after which the activity was measured spectrophotometrically at 405 nm for 2 min.

pH stability analysis of the nanoabiocatalysts. HRP preparations were incubated in 0.1 M sodium phosphate buffer pH 7.0 and 8.0, 25 mM sodium acetate pH 3.0, 4.0, and 5.0, and 25 mM sodium bicarbonate pH 10.0. Aliquots of soluble and entrapped suspensions were withdrawn, and their residual activity was measured as previously described after 1 h of incubation.

Thermal stability of the nanoabiocatalysts. The thermal stability was carried out at 50°C, wherein, aliquots of soluble and entrapped suspensions were withdrawn at different time intervals and their residual activity was measured as previously described. Residual activity was defined as:

$$Residual\ Activity = \frac{a}{a_0} \tag{1}$$

Where a are the IU at a time point and a_0 is the initial activity in IU. Biocatalysts inactivation was modeled based on the deactivation theory proposed by Henley and Sadana[31] using Graph Pad Prism. Inactivation parameters were determined from the best-fit model of the experimental data which was the one based on two-stage series inactivation mechanism without residual activity, as represented in the following scheme:



where k_1 and k_2 are first-order transition rates constants. E , E_1 and E_d are the corresponding enzyme species of progressively less specific activity, being the last one completely inactive. The mathematical model that represents this mechanism is:

$$\frac{a}{a_0} = \left(1 + \alpha \left(\frac{k_1}{k_2 - k_1} \right) \right) e^{-k_1 \times t} - \left(\alpha \left(\frac{k_1}{k_2 - k_1} \right) \right) e^{-k_2 \times t} \tag{2}$$

where α is the enzyme specific activity. Inactivation parameters were determined from the best-fit model of the experimental data. Half-life (time at which the residual enzyme activity is half of its initial value; $t_{1/2}$) was used to compare the stability of the different biocatalysts, being determined by interpolation from the respective model described by Eq 2. The stability factor (SF) was the parameter used for a quantitative comparison of the stability of the biocatalysts

and was found by

$$\text{Stabilization factor} = \frac{t_{1/2}}{t_{1/2_0}}. \quad (3)$$

Where $t_{1/2}$ is the half life time of the more stable sample and $t_{1/2_0}$ is the half life time of the less stable sample.

Oxidation of 3-IAA by enzymatic preparations. The oxidation of 3-indole acetic acid (3-IAA) by soluble and immobilized preparations (1 UI) was carried out as in [28], in 100 mM sodium acetate buffer pH 5.0 containing 500 mM of 3-IAA at 25°C for 2 h. An aliquot of reaction mixture was injected into a reverse-phase HPLC on a C18 Columbus column at 25°C using an isocratic elution buffer of methanol/1% acetic acid mixture (40:60, v/v) at a flow rate of 0.6 mL/min. The eluted products were monitored at absorbance of 250 nm using an Agilent 1100 series detector. The retention time for 3-IAA was 22 min and the reactive oxygen species were eluted from 3 min to 20 min.

Cytotoxicity and cell viability 3-(4,5-Dimethylthiazol-2-Yl)-2,5-Diphenyltetrazolium Bromide (MTT) assay. The experiments were carried out with human colorectal cancer (HCT 116) cell line. HCT116 shows less internalization compared to other cell lines and withstand higher temperatures[32] which suits future in vitro experiments related to the application of the nanobiocatalysts in direct enzyme prodrug activation. Additionally, it has been optimized for future 3D model experiments and genetically modified to constitutively express luciferase, which allows better biomedical imaging of tumour growth in in vivo experiments. To study the cytotoxic effect of the nanohybrids with 3-IAA we plated 15×10^3 cells HCT 116 per well in a 96-well plate and incubated in DMEM with 10% FBS, 1% glutamine (Invitrogen) and 1% penicillin/streptomycin (Invitrogen) for 24 hours in an incubator at 37°C and in presence of 5% CO₂. We then removed the medium and washed the cells with PBS. Following which we added varied nanohybrids with varied enzymatic activity resulting in 0.5 IU, 1 IU or 2 IU along with the prodrug with final concentration in the well of 1 mM or 2 mM of 3-IAA. The medium selected for this incubation was PBS. The cells when then incubated for 6 h at 37°C. Different controls were prepared to analyse the cytotoxicity effect of every single component; nanohybrids and the prodrug. Besides, samples with the enzyme in suspension alone and in combination with the prodrug were prepared to be able to compare the efficiency of the nanohybrids. The supernatant was then removed and 100 μ l of complete medium and 10 μ l of MTT (5mg/ml) was added per well and was incubated for 2 h 37°C, until intracellular purple formazan crystals are visible under microscope. The plate was centrifuged at 1200 rpm for 25 min at RT. Following the removal of the supernatant and addition of 100 μ l of DMSO per well to solubilize the formazan crystals, the absorbance was measured at 570 nm. Every sample was prepared in triplicates.

Results and discussion

Sol-gel and functionalized mesoporous Si have been previously used for enzyme immobilization. These methods have some inherent limitations such as harsh synthetic conditions or poor retention of the immobilized enzyme different from biomimetic Si synthesis [19,33]. The immobilization approach follows a one-pot procedure, wherein, Si synthesis and enzyme entrapment occur simultaneously. Biomimetic reactions for Si deposition and HRP entrapment has been utilized in the past with modest results in terms of stabilization [28,34]. However, in previous reports we and others have demonstrated that this type of immobilization technique necessitates tailoring to the particular enzyme and bioconversion for optimal properties of the biocatalyst [13,35]. In order to maximize the stability and enzymatic performance

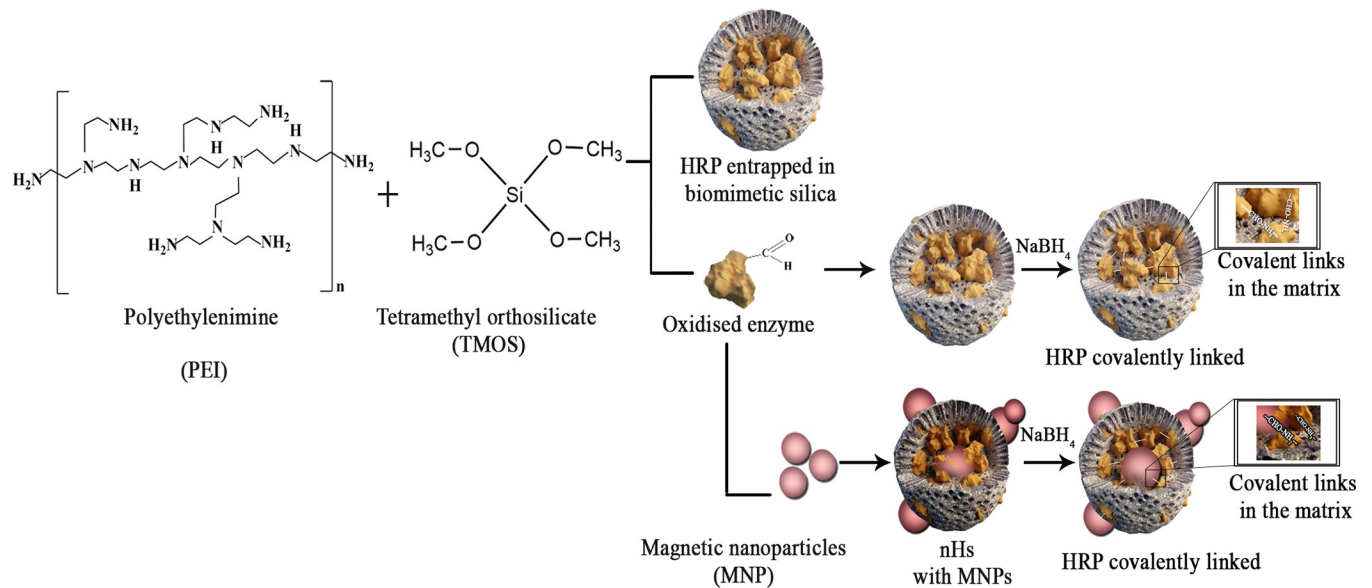


Fig 1. Schematic representation of different synthesis of silica and the co-entrapment of the enzyme with magnetic nanoparticles.

<https://doi.org/10.1371/journal.pone.0214004.g001>

of HRP immobilized preparations, we studied three different configurations of the immobilized enzyme [Fig 1](#).

We first studied the entrapment process of HRP solely in biomimetic Si and the properties of the obtained immobilized preparation. A range of HRP concentrations were used to evaluate the immobilization parameters in silica entrapment and select a minimal amount of enzyme that allowed the preparation of a high specific activity biocatalyst [S1 Table](#). In the light of the results obtained we chose 1 mg/mL HRP concentration for further experiments using different MW polyethylenimine (PEI) as a catalyst for the Si deposition. PEIs with MW of ~ 1300, 2000, 25000 and 60000 were used to study the role of the amine rich catalyst in the nanoparticle synthesis and HRP stabilization. PEI is a polymer containing primary, secondary and tertiary amino groups, having a strong anion exchange capacity under a broad range of conditions, and the capability to chemically react with different chemical groups on either an enzyme or a support. Difference in PEI sizes could not only affect biological aspects of the biocatalyst but also its physicochemical properties [8,36]. Additionally, post immobilization chemical strategies have often improved otherwise unstable immobilized enzyme preparations [37,38]. We therefore attempted to crosslink the enzyme once entrapped within the Si matrix via chemical connection of aldehyde groups of the enzyme to unreacted amino groups of the PEI [Fig 1](#). To the extent of our knowledge, there is no previous report on this approach for HRP immobilization in biomimetic Si nanoparticles (NPs). Considering the degree of glycosylation of this enzyme [39], we performed a standard mild oxidation via NaIO_4 of the enzyme. This treatment generates aldehyde groups on HRP sugar residues that could form Schiff's bases with amino groups of the PEI used as a catalyst for the Si deposition. Similar to the chemistry used to immobilize proteins on glyoxyl activated supports [40], a further reducing step via Na_2BH_4 , would transform the first reversible interaction between the enzyme and the matrix into a three dimensional multiple covalent attachment of HRP within the Si particles [Fig 1](#). The strategy was followed in the presence of trehalose, a common additive used to gain protein stability [12]. A direct correlation between the surface tension of trehalose solutions and the thermal stability of various proteins has been established and it is also known that

trehalose significantly increases the half-life of HRP [5]. No impact was observed in the immobilization percentage (%I) and immobilization yield (%Y) of the preparations after including the trehalose and the reduction step in the preparation of the nanobiocatalyst S2 Table.

Regarding the effect of the different PEI MW, except for the BioSi@T_HRP_PEI_60000, the immobilization percentage (%I) and immobilization yield (%Y) of the different HRP were above 60%. Protein immobilization yield was between 78±2% and 83±4% for all the preparations. The nanohybrid obtained with PEI MW 1300 displayed the higher results for %I and %Y Table 1. This preparation contained 1.33 mg HRP/g of wet support and 1.05 IU/g of wet support.

None of the immobilized preparations obtained showed enzyme leakage as measured in the supernatant of a suspension incubated at 4 °C for 1 month.

When adding MNPs to the synthetic mixture, we observed that for the nanohybrids with PEI MW 60000 there was an increase in the %Y from 33±5% to 57±5%. Probably, at higher PEI MWs a denser cover of Si could affect the partition of substrate/product through the solution thus yielding lower expressed activity of HRP after immobilization. The presence of MNPs could direct a Si deposition in a more compact polymeric shell, reducing mass transfer limitations.

Analysis by SEM showed that when entrapment of HRP using PEI MW 1300 was performed without chemical modification, biomimetic Si formed as preferentially disperse particles with a nanosized diameter range of ~ 300–550 nm with a sharp accumulation of ~ 400 nm diameter particles Fig 2A and 2B. When oxidized HRP was entrapped and the resulting particles submitted to NaBH₄ reduction, biomimetic Si formed as interconnected randomly agglutinated particles of approximately ~ 300–800 nm Fig 2C and 2D. In this case, the Gaussian fitting of the nanoparticle size histogram showed a wider size distribution of the material, demonstrating an effect of the chemical modification of the enzyme on the synthesis of biomimetic silica. The oxidation of enzymatic sugar residues may change the ionization state of the enzyme at pH 8.0 which could alter the Si deposition process. Previous reports have already conferred a fundamental role of the interplay of attractive/repulsive electrostatic interactions during Si synthesis on the particle size and distribution of the material [22,41]. The presence of trehalose during Si synthesis also affected the size distribution of the particles obtained with diameters ranging from 100 to 1000 nm. Moreover, trehalose significantly impacted the homogeneity of the sample Fig 2E and 2F. Given that the amount of protein used in all the entrapment experiments was the same (1 mg/mL), size dispersion can be attributed solely to trehalose. These results corroborate with Rodriguez et al [42] that found that the addition of carbohydrates to standard hydrostatic solutions altered the size of the spherical Si particles obtained from *in vitro* polycationic peptide-mediated biosilicification. Although their findings were obtained after Si precipitation without protein in the synthetic mixture, it became clear that sugar molecules imparted some degree of morphological control on the deposited silica.

Table 1. Immobilization parameters of nanohybrids with different sizes of PEI.

Entrapment	Immobilization (%)	Immobilization yield (%)	Protein immobilization yield (%)
BioSi@T_HRP_1300	60 ± 4	78 ± 1	82±1
BioSi@T_HRP_2000	61 ± 3	77 ± 2	80±2
BioSi@T_HRP_25000	64 ± 2	70 ± 5	77±1
BioSi@T_HRP_60000	70 ± 2	33 ± 5	77±4
BioSi@T_HRP_MNP_1300	83 ± 5	71 ± 2	78±1
BioSi@T_HRP_MNP_2000	76 ± 2	69 ± 4	78±3
BioSi@T_HRP_MNP_25000	77 ± 2	70 ± 5	83±4
BioSi@T_HRP_MNP_60000	69 ± 2	57 ± 5	78±2

<https://doi.org/10.1371/journal.pone.0214004.t001>

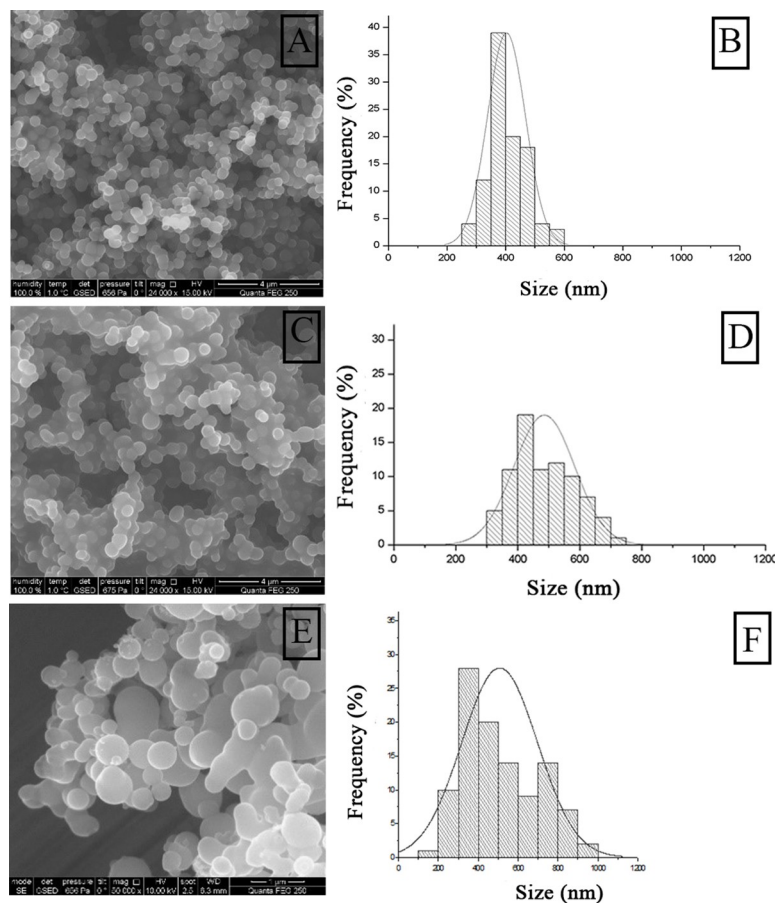


Fig 2. Analysis by scanning electron microscopy (SEM) of nanohybrids using PEI MW 1300. A) BioSi@HRP, C) BioSi@HRPox E) BioSi@T_HRP_1300. B, D y F) correspond to histograms of frequency of particles versus their particle size in each case.

<https://doi.org/10.1371/journal.pone.0214004.g002>

Table 2 shows the results for DLS analysis of the different nanohybrids with and without MNPs. Addition of MNP in the synthetic mixture provided nanohybrids with smaller hydrodynamic sizes making the final diameter of the hybrid independent of the size of the PEI used (~500–600 nm). This correlates with the results obtained for an increase in %Y after addition of MNPs and the analysis by SEM of the samples that included MNPs Fig 3. The samples that included MNPs showed again interconnected particles of a mean diameter of 400–450 nm Fig 3. The particle size distribution has a high dispersity that correlates with increased PDI results Table 2 that did not impact on the activity of the nanobiocatalysts.

Table 2. Dynamic light scattering and net charge analysis of nanohybrids.

Hybrids	Hydrodynamic size (nm)		Poly dispersity index (PDI)		Zeta potential (mV)	
	MNP (-)	MNP (+)	MNP (-)	MNP (+)	MNP (-)	MNP (+)
BioSi@THRP_1300	630 ± 26	684 ± 68	0.199 ± 0.136	0.311 ± 0.03	6.79 ± 0.791	23.4 ± 4.68
BioSi@THRP_2000	815 ± 52	589 ± 28	0.104 ± 0.067	0.321 ± 0.044	6.87 ± 0.701	21.5 ± 4.24
BioSi@THRP_25000	535 ± 23	491 ± 26	0.129 ± 0.063	0.402 ± 0.080	8.31 ± 0.701	11.6 ± 5.46
BioSi@T_HRP_60000	1026 ± 83	543 ± 21	0.207 ± 0.089	0.354 ± 0.059	9.81 ± 1.12	15.5 ± 4.00

<https://doi.org/10.1371/journal.pone.0214004.t002>

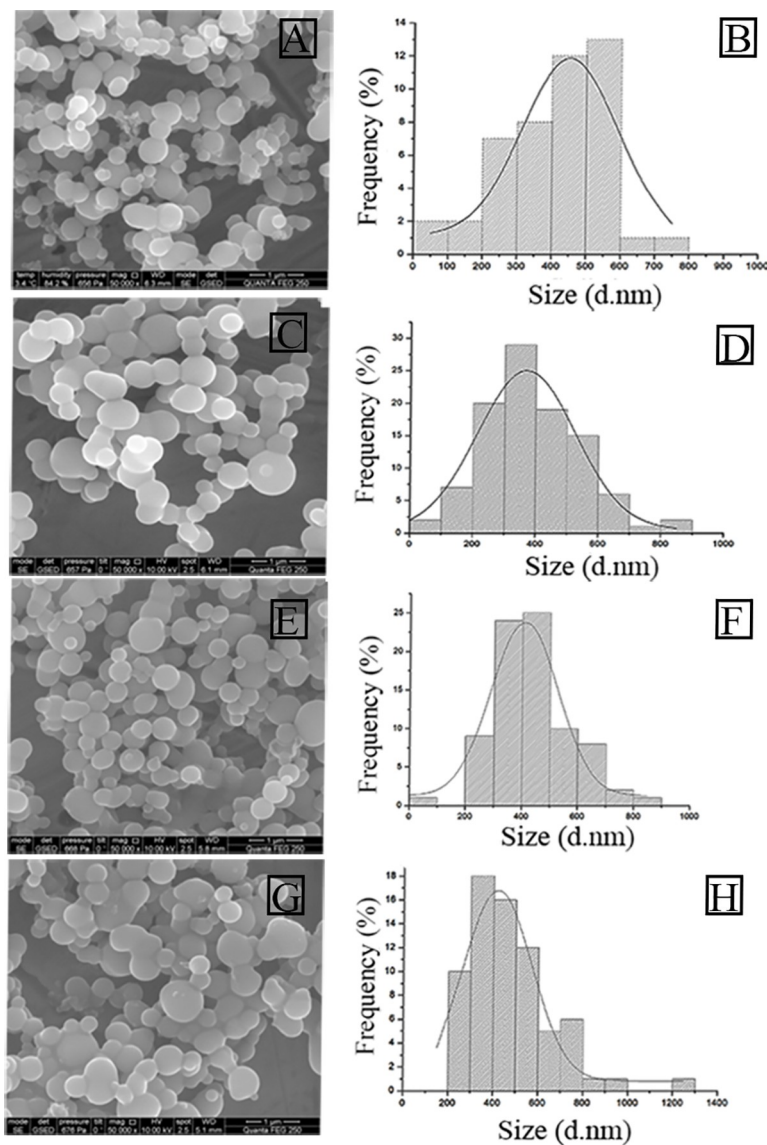


Fig 3. Analysis by SEM of nanohybrids with distinct PEIS. A) BioSi@T_HRP_MNP_1300. C) BioSi@T_HRP_MNP_2000, E) BioSi@T_HRP_MNP_25000 and G) BioSi@T_HRP_MNP_60000. Similarly, B, D, F, H correspond to their histograms analyzed using ImageJ and Origin 8 Pro.

<https://doi.org/10.1371/journal.pone.0214004.g003>

Stabilization of enzymes is a key factor to determine their full potential as biocatalysts. Our studies on thermal stability of the entrapped enzyme demonstrated that, after fitting the experimental data to the exponential model from Henley and Sadana [43], the physically entrapped HRP (BioSi@HRP) had a half-life time of 65.4 min at 50 °C compared to the soluble enzyme that reached 50% of its initial activity after only 2.4 min Fig 4. Thermal stabilization improved considerably after chemical modification of the nanobiocatalysts Fig 4B. When using PEI MW 1300, modified nanoparticles showed a half-life time of 150 min compared to 65.4 min of the unmodified entrapped HRP. The effect of trehalose and the chemical crosslinking on the thermal stability of the immobilized HRP was additive, as the preparation had a stabilization factor (SF) of 176 compared to the soluble HRP Fig 4B. Since the Si NP is a porous material, we excluded the possibility of trehalose leakage by incubating an immobilized preparation in

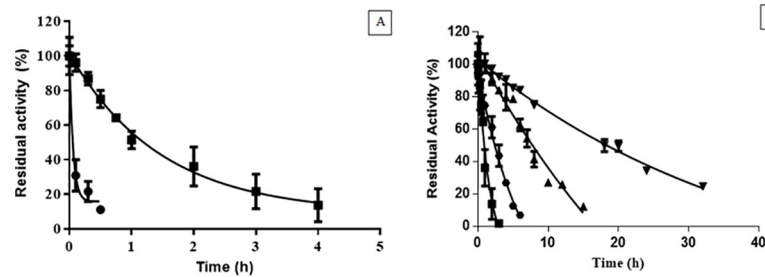


Fig 4. Thermal stability at 50°C of different HRP preparations. A) Soluble enzyme (HRP) (●), BioSi@HRP (■). Aliquots were taken at mentioned time intervals and measured spectrophotometrically at 405nm. The half-lives were determined as 0.04 h and 1.09 h for the soluble and immobilized preparations, respectively. B) Thermal stability of the BioSi@HRP (■), BioSi@HRPox (●), BioSi@T_HRP_1300(▲) and BioSi@T_HRP_MNP_1300 (▼) showing half-lives 1.09 h, 2.5 h, 7.02 h, 21.3 h.

<https://doi.org/10.1371/journal.pone.0214004.g004>

suspension at 4°C for 1 month and determination of reducing sugars in the supernatant. On measurement of the supernatant, no trehalose was detected under these conditions [S3 Table](#). Moreover, a suspension of BioSi@T_HRP_MNP_1300 containing 12.5 IU/mL in sodium phosphate buffer 0.1 M pH 8.0, retained 84%±3 (10.5±0.4 IU/mL) of its initial activity after 6 months of shelf storage at 4°C.

We believe these results demonstrate that a three-dimensional rigidification of the enzyme structure is a determinant factor to a drastic improvement in its stability. Some indications of this effect had been previously obtained by immobilization of enzymes on matrixes modified with polymeric molecules in which it was believed that regions of the biomolecules were embedded within the support, improving their stability [38]. However, an entrapment process assures that most of the enzymatic molecules lay within the matrix which is fundamental to reinforce our three-dimensional stabilization hypothesis.

When stability of nanohybrids including MNPs was studied at 50°C, we observed a 532 SF of the enzyme entrapped in Si with MNPs (BioSi@THRP_MNP_1300) compared to the soluble enzyme [Fig 4B](#).

Considering that the MNPs contain primary amino groups that could further react with the aldehyde generated upon mild oxidation in the HRP, we believe the presence of the MNPs provided an additional source of functional groups for multi-point covalent interaction. Moreover, the MNPs offer a more rigid surface to the enzyme to the flexible Si network formed as a shell of the nanohybrid. This may restrain enzyme distortion and contribute to a greater stabilization.

The nanohybrids with distinct PEIs showed an increase in the half-life similar to nanohybrids with PEI MW 1300 respect to the soluble with an exception of PEI MW 25000 which showed a SF of 20 with respect to the soluble enzyme [Fig 5](#). The branched nature of this PEI amplifies the loading enzyme but could leave the enzyme more exposed to degradation caused by temperature increase [44].

Reports for immobilization and stabilization of HRP are ubiquitous. The majority of these reports include inhouse fabricated supports and conditions for stability evaluation vary extensively. For instance, using commercially available biogenic porous silica, Sahare et al found a SF of 23[45] with an immobilized preparation with similar specific activity to the one used in our work. HRP immobilized onto PVA-PAAM nanofibers was found to retain 64% of its initial activity at 4°C after 55 days which represents a lower storage stability compared to the nanohybrid prepared herein[46]. For each of these examples it is important to highlight that the nature of the support used and the chemistry of HRP immobilization is different for that developed in this work. The different immobilization strategies might better suit precise applications, which eventually will make the stability results relevant.

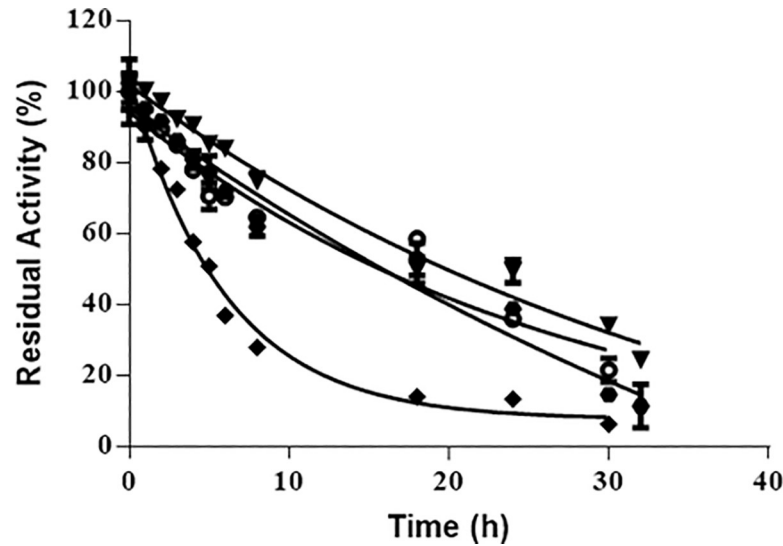


Fig 5. Thermal stability of the enzyme preparations with distinct polyethyleneimines (PEI). (BioSi@T_HRP_MNP_1300 (▼), BioSi@T_HRP_MNP_2000 (●), BioSi@T_HRP_MNP_25 000 (◆), BioSi@T_HRP_MNP_60 000 (○) entrapped in silica with a magnetic core. The half-lives were determined as 21 h, 20 h, 8 h, 22 h, respectively.

<https://doi.org/10.1371/journal.pone.0214004.g005>

We have selected BioSi@THRP_MNP_PEI_1300 for further experiments, under the premise that it was the most thermostable preparation obtained in our work with higher %Y and % I. We have studied the remaining activities of HRP preparations after 1 hour of incubation in several pHs [S1 Fig](#). pH stability often restrains the applicability of enzymatic preparations as it may have a profound impact on the loss of structural integrity of many proteins. Our results demonstrate that the nanohybrids were more stable under acidic pH. There was no observed effect of the MNPS on the pH stability. Additionally, no loss of integrity of the NPs was observed after 1 hour of incubation at the different pHs.

Optimal pH and optimal temperature of HRP did not change upon integration of the enzyme in the nanohybrids [S2A and S2B Fig](#).

It was important to demonstrate that after the Si modification, the nanohybrids maintained their superparamagnetic properties. [Fig 6](#) shows the field dependent magnetization of the BioSi@THRP_MNP_1300 at 300 K. The sample displayed superparamagnetic behaviour with negligible coercivity at zero field.

Operational stability of the BioSi@THRP_MNP_1300 was also assessed after several enzymatic cycles using the chromogenic substrate ABTS and hydrogen peroxide. In all studied cycles, the immobilized enzyme was magnetically separated and was assessed for its remnant catalytic activity. After 5 reuses the nanohybrids maintained 30% of its initial activity [Fig 7](#).

As a proof of its utility in a biotechnological relevant biotransformation, we studied the oxidation of 3-IAA. This non-toxic plant hormone has been examined as a prodrug candidate as, upon transformation to its oxidized species, it induces cellular apoptosis in cancerous lines. HRP has been proposed as oxidizing enzyme of this compound for the so-called direct enzyme prodrug therapy. The biocatalytic performance of the BioSi@THRP_MNP_1300 was tested in batch conversion of 3-IAA into its oxidized species. HPLC elution profiles showed that the nanohybrids catalysed the complete oxidation of a 500 mM prodrug solution within 30 min of reaction with the generation of at least five oxidized products [Fig 8A and 8B](#).

The major product is expected to be oxindol-3-yl carbinol for its distinctive spectra and matching retention time from previous works using the same HPLC analysis conditions. This

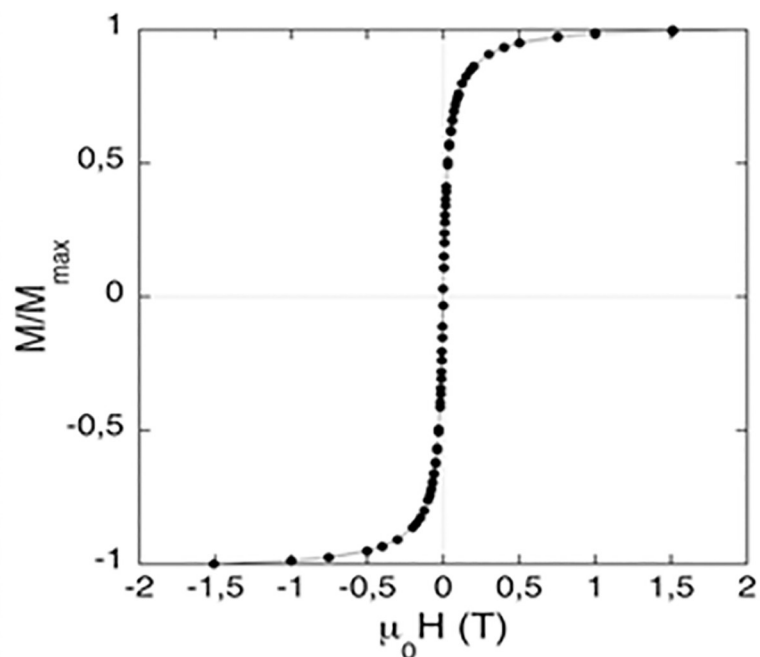


Fig 6. Field dependent magnetization of BioSi@T_HRP_MNP_1300. The measurements are shown at 300 K after diamagnetic correction.

<https://doi.org/10.1371/journal.pone.0214004.g006>

type of immobilized biocatalyst could be potentially applied to biotransformations such as *in situ* clean-up of contaminated environments [47,48], lignin polymerization for hydrophobicity enhancement of fibres [49] or other polymerization reactions applied in pharmaceuticals [50].

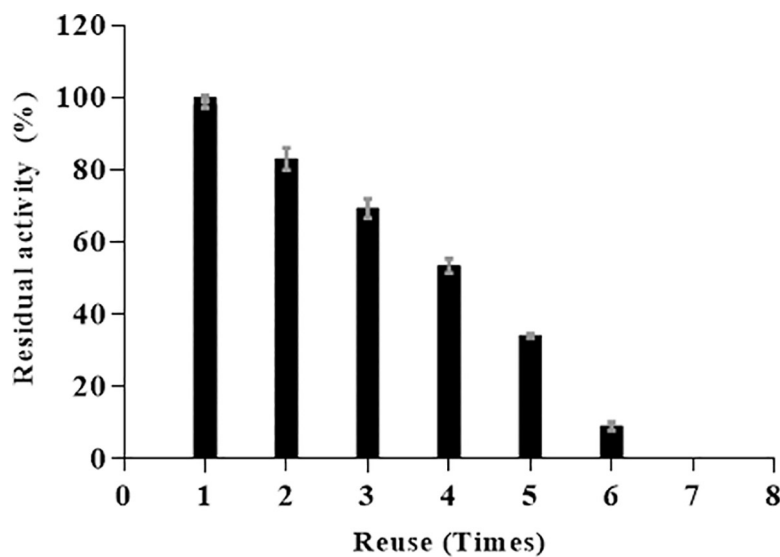


Fig 7. Operational stability of BioSi@T_HRP_MNP_1300. Residual enzyme activity after 6 reuses with substrates (ABTS and H_2O_2) and separation using a magnetic separator.

<https://doi.org/10.1371/journal.pone.0214004.g007>

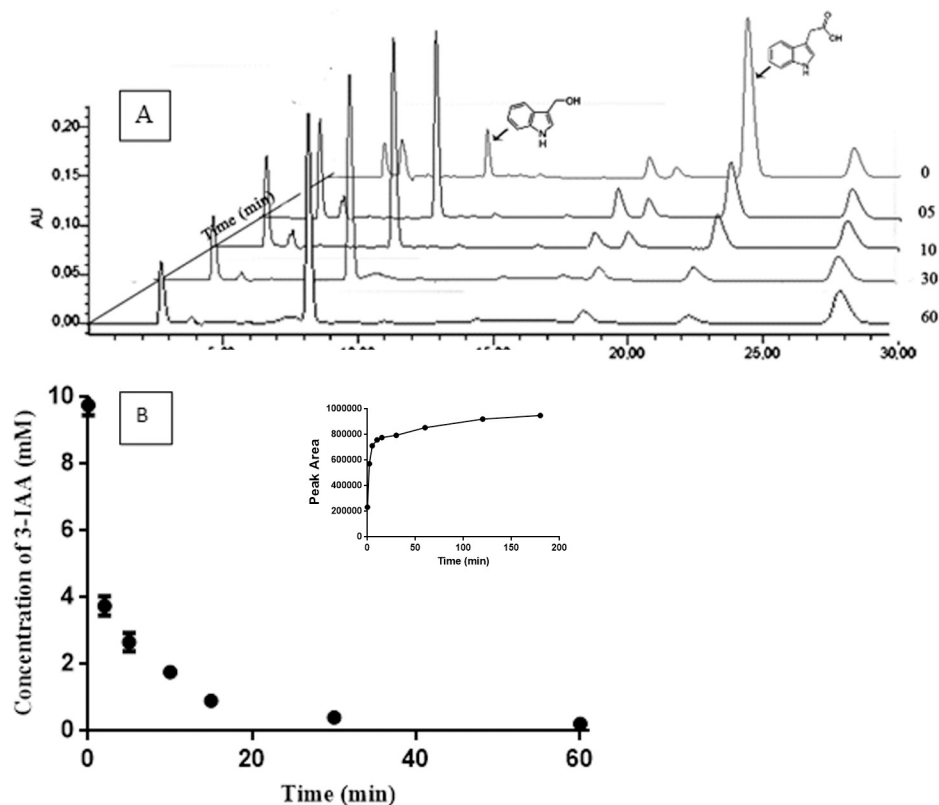


Fig 8. Oxidation of 3-IAA by the nanohybrids. A) Conversion of 3-IAA by nanohybrids BioSi@T_HRP_MNP_1300 at different intervals of time B) Conversion kinetic of 3-IAA by the nanohybrids. Reactions were carried at 25°C using 1 UI in a 100 mM sodium acetate buffer at pH 5.0 containing 500 mM of 3-IAA. Further details are described in Methods. Inset- Increment in the concentration (area) of the radical 3-ox-indol-carbinol.

<https://doi.org/10.1371/journal.pone.0214004.g008>

Anticipating a possible biomedical application of the HRP entrapped nanomaterial produced herein, we further investigated its cytotoxicity towards the model colorectal cancer cell line HCT 116 (ATCC) (Fig 9A and 9B). NPs may cause adverse health effects resulting from damage to membranes, changes in protein folding, DNA mutation, blood abnormalities and oxidative stress injuries. Measurements of cell viability and proliferation can provide an indication of the safety of nanomaterials.

The results show that after 6 hours in PBS, BioSi@THRP_MNP_PEI_1300 is well tolerated by the cells as not more than ~15% growth inhibition is observed in a range of concentrations of 5, 10 and 20 µg/mL. Besides, when incubating the cells solely with the free enzyme or with the prodrug no cytotoxicity effect was observed. However, cell death was observed when 3-IAA and nanohybrids were co-incubated with the cells. Increasing amounts of enzyme units (0.5–2 IU/mL) in the assay showed a correlated decrease in cell viability demonstrating that the optimized nanohybrid is efficient in the generation of toxic radicals. We can also see in the results that the two prodrug concentrations selected resulted in very similar cell viability values.

It is worth noting that the soluble enzyme showed a greater cytotoxic effect in the presence of the prodrug in comparison to the immobilized one, as it is free and easily available for the oxidation of the prodrug. The rate of conversion is slower in the nanohybrids as the substrate had to traverse through the Si matrix to access the enzyme entrapped thus decreasing the rapid conversion of the radicals in the assay. However, we have demonstrated that integration of the

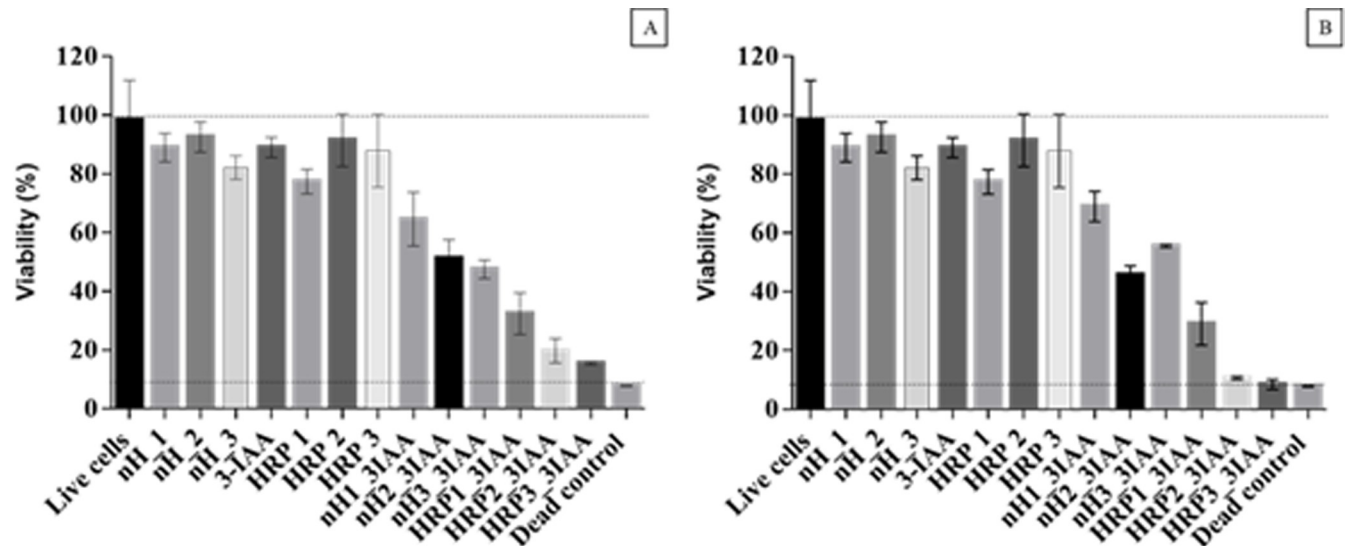


Fig 9. Effect of nano hybrids (BioSi@T_HRP_1300_MNP) on HCT 116 (ATCC) cell viability. Cytotoxicity studies using MTT were assayed. Cells were incubated for 6 h in PBS with concentrations of nano hybrids (0.5, 1 and 2 IU of Enzyme) and concentrations of prodrug 1 mM and 2mM. A) Corresponds to the data normalized against live control (cells with DMEM 10% FBS, considered as 100%) for an assay using 1 mM of 3-IAA. B) Corresponds to the data normalized against live control (cells with DMEM 10% FBS, considered as 100%) for an assay using 2 mM of 3-IAA. Results were expressed as the mean \pm SD of triplicates of a representative experiment. Live cells: Control of live cells, nH_{1/2/3}: control of nano hybrid at 5, 10, 20 μ g/mL containing 0.5, 1 and 2 IU/mL respectively, 3-IAA: Control of prodrug with concentrations of 1 and 2 mM, HRP_{1/2/3} ctrl: control with soluble enzyme at 0.5, 1 and 2 IU/mL; nH_{1/2/3}_3IAA: nano hybrids and prodrug combinations; HRP 1/2/3_3IAA: reaction mixture with soluble enzyme and prodrug combinations.

<https://doi.org/10.1371/journal.pone.0214004.g009>

enzyme in the composite material provided advantageous properties that counterbalance any decrease in the conversion rate of the prodrug 3-IAA.

Although extensive analysis is necessary to fully understand nanomaterials toxic effects, the results of MTT in this work confirmed the utility of BioSi@THRP_MNP_PEI_1300 in directed enzyme prodrug therapy (DEPT), which encourages further investigations into *in vitro* and *in vivo* effects of the material.

Conclusions

In this work we have prepared a new nanosized hybrid material that combined MNPs, biometric silica and the enzyme HRP. The diameter and polydispersity of the *in situ* prepared nanoparticles demonstrated a dependence on the size of the aminated polymer PEI used to deposit the siliceous material and the addition of the magnetic nanoparticles during synthesis. Addition of the disaccharide trehalose and a post immobilization chemical modification of the organic/inorganic material provided exceptional stability to the enzyme without compromising its activity. In fact, the immobilized enzyme showed a significantly higher thermal stabilization factor compared with previous reports for HRP [51,52]. The superparamagnetic properties of the nano hybrid facilitated its separation in repeated batch transformations of a synthetic substrate. Our findings demonstrate that the material is not cytotoxic while it enabled the cytotoxicity of cancerous cells upon transformation of the prodrug 3-IAA. In summary, the unprecedented approach for the preparation of a nano hybrid biocatalyst provided excellent properties that could enable a range of potential applications. Further experiments on conversion of alternate substrates of immobilized HRP will broaden the range of applications of the system. Moreover, the cytotoxic studies carried out with the nano hybrid prepared herein encourages additional experimentation for a better insight into its biomedical potential.

Supporting information

S1 Table. Entrapment of different concentrations of soluble HRP in biomimetic silica nanoparticles.

(DOCX)

S2 Table. Immobilization parameters of nHs with different immobilization strategies.

(DOCX)

S3 Table. Determination of Trehalose via DNS assay.

(DOCX)

S1 Fig. pH stability of different HRP preparations. pH stability of the enzyme preparations: soluble enzyme (black), BioSi@HRPox (gray), BioSi@T_HRP_MNP_1300 (white).

(TIF)

S2 Fig. Temperature profile of different HRP preparations. A) Optimal temperature of the enzyme preparations: soluble enzyme (black), BioSi@HRPox (gray), BioSi@T_HRP_MNP_1300 (white). B) Thermal stability of the enzyme preparations: soluble enzyme (black), BioSi@HRPox (gray), BioSi@T_HRP_MNP_1300 (white).

(TIF)

Acknowledgments

LB and SC acknowledge PEDECIBA Química, ANII and Universidad ORT Uruguay. We thank TD for helpful insight in the discussion of the results and Rodrigo Mila for help with the graphical abstract. The authors would like to acknowledge the use of Servicio General de Apoyo a la Investigación-SAI, Universidad de Zaragoza.

Author Contributions

Conceptualization: Valeria Grazú, Lorena Betancor.

Formal analysis: Sonali Correa, Laura Asín, Jesús Martínez de la Fuente.

Funding acquisition: Jesús Martínez de la Fuente, Valeria Grazú, Lorena Betancor.

Investigation: Sonali Correa, Sara Puertas, Lucía Gutiérrez, Laura Asín.

Methodology: Lorena Betancor.

Resources: Jesús Martínez de la Fuente.

Supervision: Lorena Betancor.

Validation: Sonali Correa, Sara Puertas, Lucía Gutiérrez.

Visualization: Sonali Correa.

Writing – original draft: Lorena Betancor.

Writing – review & editing: Valeria Grazú.

References

1. Sipponen MH, Farooq M, Koivisto J, Pellis A, Seitsonen J, Österberg M. Spatially confined lignin nanoparticles for biocatalytic ester synthesis in aqueous media. *Nat Commun*. Springer US;: 1–7. <https://doi.org/10.1038/s41467-018-04715-6> PMID: 29895870
2. Jackson E, Lopez FG, Guisan JM, Betancor L. Enhanced stability of l-lactate dehydrogenase through immobilization engineering. *Process Biochem*. 2016; <https://doi.org/10.1016/j.procbio.2016.03.002>

3. Romero-Fernández M, Moreno-Perez S, H. Orrego A, Martins de Oliveira S, I. Santamaría R, Díaz M, et al. Designing continuous flow reaction of xylan hydrolysis for xylooligosaccharides production in packed-bed reactors using xylanase immobilized on methacrylic polymer-based supports. *Bioresour Technol*. Elsevier; 2018; 266: 249–258. <https://doi.org/10.1016/j.biortech.2018.06.070> PMID: 29982045
4. Pavlovic M, Rouster P, Somosi Z, Szilagyi I. Horseradish peroxidase-nanoclay hybrid particles of high functional and colloidal stability. *J Colloid Interface Sci*. Elsevier Inc.; 2018; 524: 114–121. <https://doi.org/10.1016/j.jcis.2018.04.007> PMID: 29635084
5. Sharma SK, Leblanc RM. Biosensors based on β -galactosidase enzyme: Recent advances and perspectives. *Anal Biochem*. Elsevier Inc.; 2017; 535: 1–11. <https://doi.org/10.1016/j.ab.2017.07.019> PMID: 28735682
6. Rakhi RB, Nayuk P, Xia C, Alshareef HN. Novel amperometric glucose biosensor based on MXene nanocomposite. *Sci Rep*. Nature Publishing Group; 2016; 6: 1–10. <https://doi.org/10.1038/s41598-016-0001-8>
7. Consolati T, Bolivar JM, Petrasek Z, Berenguer J, Hidalgo A, Guisán JM, et al. Biobased, Internally pH-Sensitive Materials: Immobilized Yellow Fluorescent Protein as an Optical Sensor for Spatiotemporal Mapping of pH Inside Porous Matrices. *ACS Appl Mater Interfaces*. 2018; 10: 6858–6868. <https://doi.org/10.1021/acsami.7b16639> PMID: 29384355
8. Berne C, Betancor L, Luckarift HR, Spain JC. Application of a microfluidic reactor for screening cancer prodrug activation using silica-immobilized nitrobenzene nitroreductase. *Biomacromolecules*. 2006; 7: 2631–2636. <https://doi.org/10.1021/bm060166d> PMID: 16961327
9. Bolivar JM, Nidetzky B. Multiphase biotransformations in microstructured reactors: opportunities for biocatalytic process intensification and smart flow processing. *Green Process Synth*. 2013; 2. <https://doi.org/10.1515/gps-2013-0091>
10. Maximov V, Reukov V, Vertegel AA. Targeted delivery of therapeutic enzymes. *J Drug Deliv Sci Technol*. Elsevier Masson SAS; 2009; 19: 311–320. [https://doi.org/10.1016/S1773-2247\(09\)50066-4](https://doi.org/10.1016/S1773-2247(09)50066-4)
11. Fejerskov B, Jarlstad Olesen MT, Zelikin AN. Substrate mediated enzyme prodrug therapy. *Adv Drug Deliv Rev*. Elsevier B.V.; 2017; 118: 24–34. <https://doi.org/10.1016/j.addr.2017.04.013> PMID: 28457884
12. Jackson E, López-Gallego F, Guisán JM, Betancor L. Enhanced stability of l-lactate dehydrogenase through immobilization engineering. *Process Biochem*. 2016; <https://doi.org/10.1016/j.procbio.2016.03.002>
13. Cazaban D, Wilson L, Betancor L. Lipase Immobilization on Siliceous Supports: Application to Synthetic Reactions. *Curr Org Chem*. 2017; 21: 85–92. <https://doi.org/10.2174/1385272821666161108103>
14. Guisán JM. New opportunities for immobilization of enzymes. *Methods Mol Biol*. 2013; 1051: 1–13. https://doi.org/10.1007/978-1-62703-550-7_1 PMID: 23934794
15. Zdarta J, Meyer A, Jesionowski T, Pinelo M. A General Overview of Support Materials for Enzyme Immobilization: Characteristics, Properties, Practical Utility. *Catalysts*. 2018; 8: 92. <https://doi.org/10.3390/catal8020092>
16. Ribeiro LMO, Falleiros LNSS, de Resende MM, Ribeiro EJ, Almeida RMRG, da Silva AOS. Immobilization of the enzyme invertase in SBA-15 with surfaces functionalized by different organic compounds. *J Porous Mater*. Springer US; 2018; <https://doi.org/10.1007/s10934-018-0615-2>
17. Karthikeyan S, Kurt Z, Pandey G, Spain JC. Immobilized Biocatalyst for Detection and Destruction of the Insensitive Explosive, 2,4-Dinitroanisole (DNAN). *Environ Sci Technol*. 2016; 50: 11193–11199. <https://doi.org/10.1021/acs.est.6b03044> PMID: 27617621
18. Cao S-L, Li X-H, Lou W-Y, Zong M-H. Preparation of a novel magnetic cellulose nanocrystal and its efficient use for enzyme immobilization. *J Mater Chem B*. 2014; 2: 5522–5530. <https://doi.org/10.1039/C4TB00584H>
19. Betancor L, Luckarift HR. Bioinspired enzyme encapsulation for biocatalysis. *Trends Biotechnol*. Elsevier; 2008; 26: 566–72. Available: <http://www.cell.com/article/S016779908001972/fulltext> <https://doi.org/10.1016/j.tibtech.2008.06.009> PMID: 18757108
20. Johnson GR, Luckarift HR. Enzyme stabilization via bio-templated silicification reactions. *Methods in Molecular Biology*. 2017. https://doi.org/10.1007/978-1-4939-6499-4_6
21. Jackson E, Ferrari M, Cuestas-Ayllon C, Fernández-Pacheco R, Perez-Carvajal J, De La Fuente JM, et al. Protein-templated biomimetic silica nanoparticles. *Langmuir*. 2015; 31: 3687–3695. <https://doi.org/10.1021/la504978r> PMID: 25741589
22. Lechner C, Becker C. Silaffins in Silica Biomineralization and Biomimetic Silica Precipitation. *Mar Drugs*. 2015; 13: 5297–5333. <https://doi.org/10.3390/md13085297> PMID: 26295401

23. Liu J, Yang Q, Li C. Towards efficient chemical synthesis via engineering enzyme catalysis in biometric nanoreactors. *Chem Commun*. 2015; 51: 13731–13739. <https://doi.org/10.1039/C5CC04590H> PMID: 26208044
24. Johnson GR, Luckariff HR. Enzyme stabilization via bio-templated silicification reactions. *Methods in Molecular Biology*. 2017. https://doi.org/10.1007/978-1-4939-6499-4_6 PMID: 27770414
25. Betancor L, Berne C, Luckariff HR, Spain JC. Coimmobilization of a redox enzyme and a cofactor regeneration system. *Chem Commun (Camb)*. 2006; 3640–3642. <https://doi.org/10.1039/b604689d> PMID: 17047791
26. Seo JH, Betancor L, Demirci KS, Byun A, Spain J, Brand O. Liquid-phase biochemical sensing with disk-type resonant microsensors. *TRANSDUCERS and EUROSensors '07 - 4th International Conference on Solid-State Sensors, Actuators and Microsystems*. 2007. <https://doi.org/10.1109/SENSOR.2007.4300488>
27. Krainer FW, Glieder A. An updated view on horseradish peroxidases: recombinant production and biotechnological applications. *Appl Microbiol Biotechnol*. 2015; 99: 1611–1625. <https://doi.org/10.1007/s00253-014-6346-7> PMID: 25575885
28. Chiu YR, Ho WJ, Chao JS, Yuan CJ. Enzyme-encapsulated silica nanoparticle for cancer chemotherapy. *J Nanoparticle Res*. 2012; 14: 1–10. <https://doi.org/10.1007/s11051-012-0829-1>
29. Nanayakkara S, Zhao Z, Patti AF, He L, Saito K. Immobilized horseradish peroxidase (I-HRP) as biocatalyst for oxidative polymerization of 2,6-dimethylphenol. *ACS Sustain Chem Eng*. 2014; 2: 1947–1950. <https://doi.org/10.1021/sc500392k>
30. Ritter DW, Roberts JR, McShane MJ. Glycosylation site-targeted PEGylation of glucose oxidase retains native enzymatic activity. *Enzyme Microb Technol*. Elsevier Inc.; 2013; 52: 279–285. <https://doi.org/10.1016/j.enzmictec.2013.01.004> PMID: 23540931
31. Henley JP, Sadana A. Categorization of enzyme deactivations using a series-type mechanism. *Enzyme Microb Technol*. 1985; 7: 50–60. Available: <http://www.sciencedirect.com/science/article/pii/S0141022985900134>
32. Makizumi R, Yang WL, Owen RP, Sharma RR, Ravikumar TS. Alteration of Drug Sensitivity in Human Colon Cancer Cells after Exposure to Heat: Implications for Liver Metastasis Therapy using RFA and Chemotherapy. *Int J Clin Exp Med*. 2008; 1: 117–129. PMID: 19079666
33. Betancor L, Luckariff H. Co-immobilized coupled enzyme systems in biotechnology. *Biotechnol Genet Eng Rev*. 2010; 27: 95–114. PMID: 21415894
34. Zamora P, Narváez A, Domínguez E. Enzyme-modified nanoparticles using biomimetically synthesized silica. *Bioelectrochemistry*. Elsevier B.V.; 2009; 76: 100–106. <https://doi.org/10.1016/j.bioelechem.2009.05.006> PMID: 19540173
35. Cui J, Liang L, Han C, Lin Liu R. Stabilization of Phenylalanine Ammonia Lyase from *Rhodotorula glutinis* by Encapsulation in Polyethyleneimine-Mediated Biomimetic Silica. *Appl Biochem Biotechnol*. 2015; 176: 999–1011. <https://doi.org/10.1007/s12010-015-1624-0> PMID: 25906687
36. Bahulekar R, Ayyangar NR, Ponrathnam S. Polyethyleneimine in immobilization of biocatalysts. *Enzyme Microb Technol*. 1991; 13: 858–868. [https://doi.org/10.1016/0141-0229\(91\)90101-F](https://doi.org/10.1016/0141-0229(91)90101-F) PMID: 1367996
37. Palomo JM, Filice M, Romero O, Guisan JM. Improving lipase activity by immobilization and post-immobilization strategies. *Humana Press Inc.*; 2013; 1051: 255–273. https://doi.org/10.1007/978-1-62703-550-7_17 PMID: 23934810
38. Lopez-Gallego F, Betancor L, Hidalgo A, Dellamora-Ortiz G, Mateo C, Fernández-Lafuente R, et al. Stabilization of different alcohol oxidases via immobilization and post immobilization techniques. 2007; 40: 278–284. <https://doi.org/10.1016/j.enzmictec.2006.04.021>
39. Zakharova GS, Uporov I V., Tishkov VI. Horseradish peroxidase: Modulation of properties by chemical modification of protein and heme. *Biochem*. 2011; 76: 1391–1401. <https://doi.org/10.1134/S0006297911130037> PMID: 22339595
40. Ramírez Tapias YA, Rivero CW, Gallego FL, Guisán JM, Trelles JA. Stabilization by multipoint covalent attachment of a biocatalyst with polygalacturonase activity used for juice clarification. *Food Chem*. 2016; 208: 252–257. <https://doi.org/10.1016/j.foodchem.2016.03.086> PMID: 27132847
41. Hyde EDER, Seyfaee A, Neville F, Moreno-Atanasio R. Colloidal Silica Particle Synthesis and Future Industrial Manufacturing Pathways: A Review. *Ind Eng Chem Res*. 2016; 55: 8891–8913. <https://doi.org/10.1021/acs.iecr.6b01839>
42. Rodríguez F, Glawe DD, Naik RR, Hallinan KP, Stone MO. Study of the chemical and physical influences upon in vitro peptide-mediated silica formation. *Biomacromolecules*. 2004; 5: 261–265. <https://doi.org/10.1021/bm034232c> PMID: 15002982

43. Henley JP, Sadana A. Categorization of enzyme deactivations using a series-type mechanism. *Enzyme Microb Technol.* 1985; 7: 50–60.
44. Lungu CN, Diudea M V, Putz M V, Grudziński IP. Linear and Branched PEIs (Polyethylenimines) and Their Property Space. *Int J Mol Sci. Multidisciplinary Digital Publishing Institute (MDPI)*; 2016; 17: 555. <https://doi.org/10.3390/ijms17040555> PMID: 27089324
45. Sahare P, Ayala M, Vazquez-Duhalt R, Pal U, Loni A, Canham LT, et al. Enhancement of Peroxidase Stability Against Oxidative Self-Inactivation by Co-immobilization with a Redox-Active Protein in Mesoporous Silicon and Silica Microparticles. *Nanoscale Res Lett.* 2016; 11. <https://doi.org/10.1186/s11671-016-1605-4> PMID: 27650291
46. Temoçin Z, İnal M, Gökğöz M, Yiğitoğlu M. Immobilization of horseradish peroxidase on electrospun poly(vinyl alcohol)–polyacrylamide blend nanofiber membrane and its use in the conversion of phenol. *Polym Bull.* 2018; 75: 1843–1865. <https://doi.org/10.1007/s00289-017-2129-5>
47. Jiang Y, Tang W, Gao J, Zhou L, He Y. Immobilization of horseradish peroxidase in phospholipid-templated titania and its applications in phenolic compounds and dye removal. *Enzyme Microb Technol.* Elsevier Inc.; 2014; 55: 1–6. <https://doi.org/10.1016/j.enzmictec.2013.11.005> PMID: 24411438
48. Wang M, Abad D, Kickhoefer VA, Rome LH, Mahendra S. Vault Nanoparticles Packaged with Enzymes as an Efficient Pollutant Biodegradation Technology. *ACS Nano.* 2015; 9: 10931–10940. <https://doi.org/10.1021/acsnano.5b04073> PMID: 26493711
49. Liu R, Dong A, Fan X, Yu Y, Yuan J, Wang P, et al. Enzymatic Hydrophobic Modification of Jute Fibers via Grafting to Reinforce Composites. *Appl Biochem Biotechnol.* 2016; 178: 1612–1629. <https://doi.org/10.1007/s12010-015-1971-x> PMID: 26754422
50. Lončar N, Fraaije MW. Catalases as biocatalysts in technical applications: current state and perspectives. *Appl Microbiol Biotechnol.* 2015; 99: 3351–3357. <https://doi.org/10.1007/s00253-015-6512-6> PMID: 25761626
51. Sahare P, Ayala M, Vazquez-Duhalt R, Agrawal V. Immobilization of peroxidase enzyme onto the porous silicon structure for enhancing its activity and stability. *Nanoscale Res Lett.* 2014; 9: 1–9. <https://doi.org/10.1186/1556-276X-9-1>
52. Wu C, Böttcher C, Haag R. Enzymatically crosslinked dendritic polyglycerol nanogels for encapsulation of catalytically active proteins. *Soft Matter.* 2015; 11: 972–980. <https://doi.org/10.1039/c4sm01746c> PMID: 25519490



Cellulose-Based Nanosupports for Enzyme Immobilization

41

Erienne Jackson, Sonali Correa, and Lorena Betancor

Contents

1	Introduction	1236
2	Cellulose Architectures for Enzyme Immobilization	1237
2.1	Natural Cellulose Supports for Enzyme Immobilization	1237
2.2	Microfibrillated Cellulose	1238
2.3	Cellulose Nanocrystals	1238
2.4	Bacterial Cellulose Nanosupports	1239
2.5	Electrospun Cellulose	1239
2.6	Synthetic Supports	1241
3	Strategies for the Immobilization of Enzymes in Cellulose-Based Nanocarriers	1241
3.1	Immobilization by Cross-Linking	1241
3.2	Immobilization by Physical Adsorption	1243
3.3	Covalent Immobilization	1244
3.4	Combined Strategies	1245
3.5	Immobilization by Entrapment	1247
4	Cellulose-Based Nanobiocatalysts at Work	1247
4.1	Biomedical Applications	1247
4.2	Food Applications	1249
4.3	Environmental Applications	1249
5	Conclusion	1250
	References	1250

Abstract

Integration of biocatalysts and nanoscale materials offer multiple advantages over micro-scaled heterogeneous biocatalysts. Apart from providing reusability and sustainability of the enzyme, the use of nanosupports is aimed at increasing

E. Jackson · S. Correa · L. Betancor (✉)
Laboratorio de Biotecnología, Facultad de Ingeniería, Universidad ORT Uruguay,
Montevideo, Uruguay
e-mail: betancor@ort.edu.uy

© Springer Nature Switzerland AG 2019
Md. I. H. Mondal (ed.), *Cellulose-Based Superabsorbent Hydrogels*,
Polymers and Polymeric Composites: A Reference Series,
https://doi.org/10.1007/978-3-319-77830-3_42

1235

the surface area available for biocatalyst immobilization and improving the yields in bioconversions through better biocatalyst mobility and less diffusional problems. Among many nanomaterials for enzyme immobilization, cellulose stands out as biocompatible, biodegradable, and environmentally-friendly regarding its biological source. In this chapter, we discuss the steady advancement in utilizing different nanostructured cellulosic materials for enzyme immobilization. We address the use of hybrid materials that include cellulose and improve the properties of the heterogeneous biocatalyst. The methodologies for functionalization and integration of enzymes on nanocellulose hydrogels are discussed including covalent linkage through chemical modification, entrapment, and cross-linking. We consider its applications to biomedicine, food industry, and environmental science with a special emphasis on the impact of the enzymatic properties caused after immobilization on cellulosic supports.

Keywords

Enzyme immobilization · Cellulose · Nanosupports · Biocatalysis · Nanobiotechnology

1 Introduction

Nanobiocatalysis is a new frontier of emerging nanosized material supports in enzyme immobilization application. Enzymes are remarkable biocatalysts and have been used in biotechnology for many years because of their interesting characteristics such as substrate and product specificity, ease of preparation, and ability to function under mild conditions with no toxic by-products for more environmentally-friendly conversions.

Enzyme association to insoluble materials, commonly known as enzyme immobilization, provides a number of advantages to the applied use of enzymes: immobilized enzymes can be reused, minimizes costs and time of analysis, facilitates the continuous use of the biocatalyst, and may improve enzyme properties such as operational or thermal stability [1, 2]. A wide variety of techniques are now available for the preparation of immobilized enzymes that may include chemical or physical mechanisms, addition of aiding agents during immobilization, or combination of different strategies to obtain more active and stable preparations. Moreover, investigations on material science have contributed with a plethora of new supports compatible with enzyme activity and better physical and mechanical properties. Such is the case of nanosupports, rapidly adopted for enzyme immobilization, as they reduce diffusion limitations and maximize the functional surface area to increase enzyme loading. Active immobilized enzymes in nanomaterials, also known as nanobiocatalysts, have been studied for a wide variety of applications [3].

Cellulose, as a natural polymer resource is abundant, renewable, and biocompatible and has gained interest due to its optical, mechanical, chemical, and rheological properties that make it suitable for materials applications, actuators/sensors, drug delivery systems, biomedical science, and biotransformations [4]. As it is produced

from plants and bacteria, the nature of its structure varies and offers numerous possibilities for the attachment of enzymatic molecules and functionalization with non-natural reactive groups which further expands the possibility of associating biocatalysts to its structure. It was only in the last 10 years that researchers were able to develop and study strategies for the preparation of cellulose-based nanostructures. These studies have rampaged from a mere 4 articles in 2006 and 2007 related to “nanocellulose” to 365 articles published in 2016 (source Scopus). The recent interest on these materials is not fortuitous but the result of a slow unveiling of the opportunities that this material has on biotechnological applications. It is therefore timely to revise the piled evidence of nanocellulose materials that have been used in the immobilization of enzymes, the different methodological approaches to obtain them and their suitability for biocatalytic applications with a view of the future impact of these composites in biocatalysis.

2 Cellulose Architectures for Enzyme Immobilization

There are a number of cellulose nanostructures able to support enzyme immobilization: cellulose nanofibers (CNF), which can be electrospun, microfibrillated cellulose (MFC), nanocrystalline cellulose (CNC), or bacterial nanocellulose (BC). CNF can be produced from both cellulose I source, such as wood fibers, cotton, and agricultural crops, and cellulose II source, such as lyocell fibers using various techniques such as grinding, high-pressure homogenization, and sonication. There are four different polymorphs of cellulose: cellulose I, II, III, and IV. Cellulose I, native cellulose, is the form found in nature, and it occurs in two allomorphs, I α and I β . Cellulose II, or regenerated cellulose, the most stable crystalline form, emerges after recrystallization or mercerization with aqueous sodium hydroxide. The major distinction between these two forms of cellulose lies in the layout of their atoms: cellulose II has antiparallel packing, whereas the chains in cellulose I run in a parallel direction. Finally, cellulose III $_I$ and III $_{II}$ are obtained by ammonia treatment of cellulose I and II, respectively, and with the modification of cellulose III with glycerol, cellulose IV is finally produced [5].

The isolation of cellulose from its sources can be carried out by top-down or bottom-up method. The bottom-up approach is used to process material from small molecules into complex structures [6]. The top-down method usually involves various mechanical, chemical, and biological treatments, or a combination of two or more methods which is used for the removal of plant constituents apart from cellulose.

2.1 Natural Cellulose Supports for Enzyme Immobilization

Natural sources of cellulose could be generalized as rigid and partially crystalline. Cellulose is the main constituent in the most abundant organic compound on earth, especially within wood and natural fibers (kenaf, palm, cotton, hemp, flax, etc.). Almost 65–70% of cellulose compound is contained in plant fibers and comprised C,

H, and O elements [1, 7, 8]. Kenaf (*Hibiscus cannabinus* L.) is a lignocellulosic fiber having a high cellulose content, low specific gravity, and good mechanical properties along with good chemical characteristics, large surface area, and low coefficient thermal expansion. The isolation process of kenaf raw bast fiber has been done by using combinations of chemical and physical treatments which can remove matrix substances such as lignin and hemicellulose, and disintegrate the micron-sized cellulose fiber into nanofiber [9]. This process results in changes in the appearance of the material from micron-sized to nanosized fibers. It is organized as web-like network structure with long entangled cellulosic filaments with an average diameter ranged as less than 100 nm right up to less than 10 nm depending on the ultrasonication output power. Thus, ultrasonication disintegration plays an important role in the determination of the diameter of the fiber. The nanofibril has been successfully observed as an individual wire-like fiber [10], arranged in longitudinal direction as aggregated fibers with high specific surface area and strong association due to interfiber hydrogen bonding between hydroxyl groups of adjacent fibers.

2.2 Microfibrillated Cellulose

Microfibrillated cellulose (MFC) is a material derived by disintegrating digested cellulose through a homogenizing process in a reciprocating motion producing a high pressure drop. The strategy results in shearing and impact forces that in turn expose microfibrils regardless of the starting material [11]. The production of MFC by fibrillation of cellulose fibers involves intensive mechanical treatment. Additionally, it could involve prior chemical treatments to purify the cellulose depending on the raw material. MFC consists of aggregates of cellulose microfibrils. Its diameter is in the range 20–60 nm and it has a length of several micrometers. If we consider that the microfibrils have a 2–10 nm-thick fibrous cellulose structure and a length of several tens of microns, then MFC is composed of 10–50 microfibrils [5]. The raw materials and fibrillation techniques dictate the cellulose degree of polymerization, morphology, and nanofiber aspect ratio. MFC can further be subclassified depending on the treatment it undergoes. On transverse cleavage of the microfibrils along the amorphous regions and subsequent sonication, they form rod-like structures called “cellulose whiskers” with a typical diameter of 2–20 nm and wide length distribution of 100–600 nm. Their almost perfect crystalline arrangement makes them a potential reinforcing material [12].

2.3 Cellulose Nanocrystals

Cellulose nanocrystals (CNCs) are rod-like cellulose nanomaterials that can be economically prepared from various cellulosic materials by the elimination of amorphous regions of cellulose. This material is interesting as a nanofiller due to its nanoscale dimensions, high specific area, and highly rigid crystalline structure [11, 13]. Generally, CNCs are formed upon the elimination of disordered or amorphous regions of cellulose through several strategies, including acid hydrolysis,

microfluidization, and TEMPO-mediated oxidation. BC and cotton linter cellulose long fiber (CLC) can also produce cellulose nanocrystals (CNC) [14]. Reports from Roman et al. have shown that CNCs are much safer than other nanomaterials in use in biomedicine as targeted drug delivery systems. They have been used to immobilize various enzymes such as lysozyme, papain, and glucose oxidase [4, 13, 15]. The CNC-CLC and CNC-BC showed higher loading capacity of the protein, enhanced stability and activity, and overall a potential support for application in biomedicine, bioelectronic, and biocatalytic fields.

2.4 Bacterial Cellulose Nanosupports

Cellulose synthesized by bacteria is called bacterial cellulose (BC) or sometimes microbial cellulose and is obtained as a gel-like three-dimensional mat formed by entangled nanofibrils of cellulose [16]. Different from cellulose from wood pulp, BC is devoid of other contaminating polysaccharides which provide high crystallinity and purity to the material and its isolation and purification are relatively simple, not requiring energy- or chemical-intensive processes. The ability to naturally synthesize BC is restricted to a few genre of bacteria being the most common bacteria associated with the synthesis of cellulose *Gluconacetobacter xylinus* as it is the only one able to produce it at the industrial level [17]. After polymerization of glucose residues occurring in the cytoplasm, an extracellular secretion of the glucan chains occurs in a hierarchically linear arrangement favored by van der Waals forces and hydrogen bridges. Intra- and interfiber hydrogen bonding favor crystalline packing of the fiber for amorphous and crystalline regions [18]. The resulting microfibrils aggregate to produce a typical ribbon assembly with a lateral width of 40–60 nm. This structuration provides a specific density, tensile strength, and hydrophilicity that suit the material for functionalization and application to cosmetic industry, paper industry, food processing and packaging, and tissue engineering. Furthermore, the unique fibrillar nanostructure of BC (Fig. 1) determines its distinguished physical and mechanical properties such as high porosity, large surface area, excellent mechanical strength, and good biocompatibility [19]. BC-forming microorganisms can be cultivated in mannitol-based medium with alternative source of carbons and the supernatant freeze-dried to form a BC sponge after purification. Acid hydrolysis of BC form bacterial cellulose nanocrystals (BCNs) that have a higher hydrophilicity due to increased number of hydroxyl groups while being able to establish hydrophobic interactions due to its highly ordered crystalline organization (Fig. 1). This amphiphilic capacities can be applied to stabilize surfactant-free emulsions [20].

2.5 Electrospun Cellulose

Electrospinning is a simple, cost-effective, and scalable technique that utilizes electrical charge to form fine fibers from a polymer solution or polymer melt. In the past decades, electrospinning has emerged as a facile, economical, and scalable

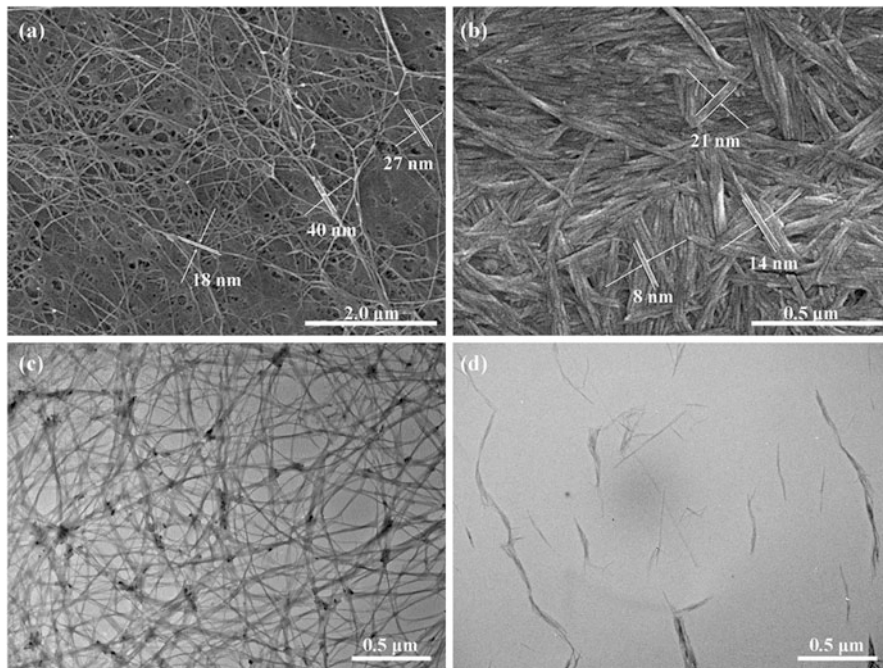


Fig. 1 An example of bacterial cellulose from *Acetobacter xylinum*. SEM images of (a) BC and (b) BCNs; TEM images of (c) BC and (d) BCNs. (Reproduced with permission from [20])

technique to produce polymeric fibers with a diameter ranging from micro- to nanometer scale. The biggest advantages of electrospun nanofibers are the high specific surface area, high porosity, and interconnectivity [21]. In biocatalysis, electrospun nanofibers could be used as the support for enzyme immobilization, and the immobilized enzyme could be reused and simultaneous biocatalytic reaction and enzyme-product separation is possible.

Substrates of this technique can be salts of cellulose such as cellulose acetate. The properties of the final material obtained can vary depending on the concentration and electrical conductivity of the starting solution, applied electrical potential, fiber collection distance and time, flow rate, and inner diameter of the reservoir during the process [6].

Electrospun cellulose has been used in a layer-by-layer self-assembled (LBL) configurations based on the electrostatic interactions of additional materials sequentially added to cellulose mats. This material was prepared by alternate adsorption of highly positively charged enzyme Naringinase (NA) and negatively charged alginate (ALG) from dilute solutions on the surface of negatively charged cellulose acetate nanofibrous mats via electrostatic attraction. The self-assembly of NA and ALG gave the reversal of the surface charge, demonstrating the successful polyelectrolyte multilayer deposited onto electrospun cellulose acetate nanofibers [21].

2.6 Synthetic Supports

In the recent years, the preparation of lignocellulose-based materials and biomimetic synthetic wood composites containing cellulose, hemicellulose, and lignin by using ionic liquids (ILs) as well as cellulose/starch/lignin film, lignocellulose aerogel, and all-wood composites have been reported [8, 22]. The major components of wood have been reported to be dissolved in ILs and successfully reconstituted as hydrogels, thin films, and electrospun materials. Fabrication of homogeneous composites from cellulose/hemicellulose/lignin has been achieved via an uncomplicated process by using in 1-ethyl-3-methylimidazolium acetate resulting in hydrogel beads composites with controllable properties [8]. The material shows a regular spherical shape and it is noted that the surface could be controlled by altering the ratio of cellulose, xylan, and lignin. When all three components were present, it was referred to as a wood mimetic composite which was a viable support for the entrapment of lipase and stabilization of its activity.

3 Strategies for the Immobilization of Enzymes in Cellulose-Based Nanocarriers

There are many enzyme immobilization approaches in cellulose-based nanocarriers already available and many more are being developed. Most of these approaches share the goals of finding a biocompatible support for enzyme immobilization, provide a higher surface area to increase the enzyme loading, and achieve high stability and reusability of the biocatalyst with a simple and mild methodology. In this regard, cellulose materials have been studied due to its low cost and biocompatibility [23, 24]. Cellulose materials have been proven to be environmentally friendly and are able to work under mild conditions [23, 25].

Among many strategies for enzyme immobilization, cellulose-based nanobiocatalysts have been developed mainly using four different approaches to retain the enzyme in the cellulosic support: entrapment, cross-linking, adsorption, and covalent immobilization.

In this chapter, we describe these four immobilization strategies in cellulosic-based nanosupports and examine the impact of the immobilization process on the biocatalyst activity and stability through several examples.

3.1 Immobilization by Cross-Linking

Chemical modification of enzymes after immobilization such as chemical cross-linking is a widely used strategy in the preparation of insoluble biocatalysts [26]. The enzyme is generally adsorbed to the nanosupport and then cross-linked with a bifunctional agent such as glutaraldehyde (Fig. 2). This approach can improve the enzyme stability as well as reduce enzyme leakage, a common problem in

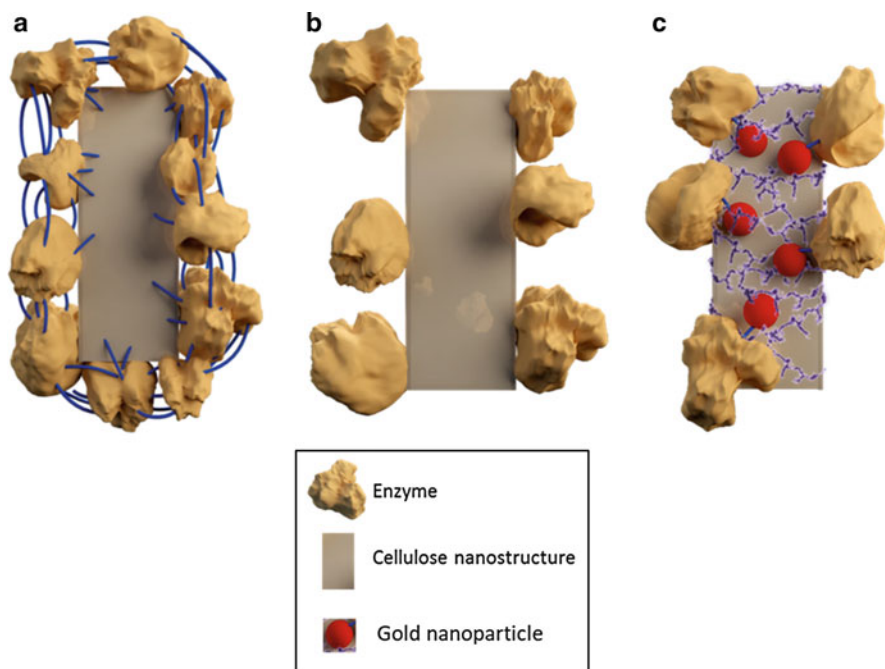


Fig. 2 Schematic representation of an enzyme immobilized on cellulose nanosupport via (a) adsorption and cross-linking, (b) physical adsorption, and (c) covalent immobilization to gold nanoparticles (AuNPs) attached to the support

noncovalently attached enzymes to supports. An alternative approach to a previous adsorption of the enzyme on a support is its precipitation and further cross-linking. Further advantages could be obtained if additives or other material are present during the precipitation. For instance, magnetic nanoparticles can be added to the mixture to form a hybrid nanobiocatalyst to ease its separation from reaction media.

Magnetic cellulose nanocrystals (MCNCs) have been used as a support for enzyme immobilization [13, 27]. The enzyme can be mixed with an aqueous suspension of MCNC and be deposited on its surface in the presence of a precipitant such as ethanol. Upon precipitation, addition of a cross-linking agent such as glutaraldehyde generates a chemical attachment between the immobilized molecules [23].

Immobilization on MCNCs via the described precipitation-cross-linking process was successfully accomplished with different types of enzymes [13, 27]. For instance, following this strategy, a nanobiocatalyst papain/MCNC has been prepared with high enzyme-loading capacity (333 mg protein/g MCNCs). The highest enzyme activity recovery was 80.1% at a mass ratio of 1:3 papain to MCNC. This could be attributable to the abundant active $-OH$ groups of the cellulose nanocrystals that contribute to the cross-linking of the enzymes on the MCNC. When comparing the nanobiocatalyst with the free enzyme, the optimal pH value increased from 6.5 to 7.0 and the temperature for the highest activity was 75 °C, 5 degrees higher

than that of the free enzyme. The change in optimal temperature was attributed to an increase in the enzyme conformational rigidity (seen in a secondary structure study). When comparing the kinetic behavior of free and immobilized papain, a higher V_{\max} (2.07×10^{-2} compared to 1.19×10^{-2} $\mu\text{mol/ml}\cdot\text{min}$) and lower K_M (0.85–1.27 mM) were found, thus demonstrating the increase in enzyme-substrate apparent affinity. This phenomenon could be attributable to the fact that the enzyme was anchored on the surface of MCNC, making the substrate accessible to the enzyme and in turn increasing the apparent affinity, or that the immobilization of papain onto the MCNC may have resulted in the conformational changes, helping the enzyme to suitably orient its active site toward the substrate. The immobilized enzyme was also proved to be more thermally stable. When comparing at the same temperature, the immobilized enzyme exhibited higher activity recovery than its free counterpart, 30% after 7 h incubation at 80 °C, while the free enzyme was inactivated after only 3 h. Moreover, the nanobiocatalyst showed no significant loss of activity when stored at 4 °C for 30 days. Finally, the reusability of the immobilized preparation was successful in maintaining 52.4% of its initial activity after 6 cycles.

3.2 Immobilization by Physical Adsorption

Physical adsorption of the enzymes on insoluble cellulose-based nanosupports has been reported elsewhere for the production of stable immobilized preparations that avoided leakage provided a strong enzyme-support interaction was established [28]. This immobilization approach has a major advantage considering the simplicity of the steps required, although functionalization of bare cellulose with ionizable/hydrophobic groups is sometimes necessary to achieve strong enzymatic adsorption of enzymes.

Physical adsorption of enzymes is feasible onto cellulose nanocrystals (CNCs) by incubating both the support and the enzyme under shaking at room temperature [13]. At neutral pH, a high fraction of sulfonate groups on the CNCs are ionized and the cationic sites or amino groups of the enzyme may have ionic interaction with anionic groups of CNCs (Fig. 2). The adsorption level of enzymes onto cellulose increases by the oxidation of cellulose primary hydroxyl groups to carboxyl groups; this strategy has been tested with cellulose fibers and could be translated to nanostructures [29].

When immobilizing a lipase from a *C. rugose* with this approach, an immobilization yield was low (51%) [13]. The decrease of lipase activity after immobilization may be due to the changes in spatial conformation of lipase and lower accessibility of substrate to the active site. However, the thermal stability can be enhanced by this approach. In the case of lipases, an immobilized enzyme to CNCs maintained over 50% of the residual activity when incubated at 60 °C for 1 h. Under the same conditions, the residual activity of the free lipase was only 11%. When comparing the half-lives, the immobilized enzyme was 27 times higher than of the free lipase. This increase in thermal stability may be associated to the enhanced ionic

interactions between anionic sulfonate groups of CNCs and the lipase, and the increased interactions caused by the higher surface area of the nanomaterial [13]. With this strategy, the pH profiles of free and immobilized lipase were similar, pH 8 being the optimal for both. A difference was found at pH 5, where the relative activity of immobilized lipase was 3.7 times higher than that of free lipase, and at pH 10, where free lipase showed no activity while the relative activity of immobilized lipase was 27.8%. The pH profiles for the stability of free and immobilized lipase were also very similar after a 5h incubation. The residual activities of immobilized lipase in buffers from pH 3 to pH 8 were approximately 140% higher than those of the free lipase. At alkaline pH, the stability of the lipase was significantly enhanced by immobilization on CNC (8.8 times higher at pH 10). Increased activity and stability in alkaline pH may be caused by increased ionic interaction between anionic groups of CNCs and the lipase since the anionic form of the sulfate half-ester in CNC is dominant at an alkaline pH.

Physical adsorption of lipase not always results in a more stable preparation. In a study where the adsorption of a *Candida rugosa* lipase was performed on a cellulose nanofiber membrane, the preparation demonstrated a low enzyme loading and poor enzyme stability [30]. These types of examples still prove the necessity of protocol optimization in order to tailor the immobilization strategy to a particular support or a desired enzyme.

Functionalization of nanocellulose-based supports for adsorption of enzymes has also been achieved via coverage of the cellulose surface with ionic polymers. Efficient immobilization of papain was achieved using CNCs associated to polyethyleneimine (PEI) modified Fe_3O_4 nanoparticles [16]. Magnetic nanoparticles embedded on CNCs facilitated the separation of the particles from a reaction mixture, simplifying the reuse of the biocatalysts. This support was successfully used for the immobilization and separation of papain from the reaction mixture which under optimal conditions resulted in a preparation with an enzyme activity of 227 $\mu\text{g}/\text{min.g}$. When studying the kinetic parameters of this preparation, the immobilized papain required higher substrate concentration compared to the free papain which could be explained by the increased steric hindrance and diffusion impediments. However, compared with free papain, the immobilized papain still demonstrated high catalytic efficiency.

Also, the immobilized papain exhibited higher relative activity in both acidic and alkaline pH ranges when compared to its free form. The immobilized enzyme retained over 90% of its original activity after incubation for 1 h at 40 °C, almost twice the activity measured for the free enzyme [16].

3.3 Covalent Immobilization

Covalent immobilization of enzymes is often chosen over adsorption strategies because it overcomes the primary disadvantage of adsorption which is enzyme dissociation (leakage) [28]. A number of functionalization strategies have been developed for cellulose nanomaterials for the covalent bonding of enzymes

[13, 31, 32]. One of this approaches involved functionalization of cellulose nanocrystals (CNCs) with cyanogen bromide, a functional group that is able to react with amino-terminal groups of enzymes under neutral pH [31]. Peroxidase has been immobilized in CNCs following this approach resulting in a highly active preparation (594 IU/g) with a higher catalytic efficiency when compared to the free enzyme.

Modification of CNCs can be also obtained via esterification with amino acids such as glycine through the abundant hydroxyl groups on the CNC surface. Lysozyme, for example, can be covalently immobilized via amide linkage of its glutamate and aspartate residues to the surfaces of amino-modified materials. In this case, lysozyme-amino-glycine-CNC conjugates were created using a carbodiimide-activated coupling reaction. The prepared nanobiocatalyst showed a high enzyme loading (604 mg/g CNCs) and high antimicrobial activity (1500 IU/mg biocatalyst) against *Micrococcus lysodeikticus* [32].

An alternative strategy for covalent immobilization can involve the addition of another material to the system. An approach described by Boluk et al. [33] involved the immobilization of a glucose oxidase (GOx) through the formation of covalent bonds between the enzyme and gold nanoparticles (AuNPs) attached to rod-like cellulose nanocrystals (Fig. 2). The AuNPs must be previously functionalized with thiol linkers and later activated, offering a multipoint attachment of GOx molecules to the nanocomposite surface. In this approach, the CNCs have been incubated with cationic PEI which covers the nanocrystals by ionic interactions; then negatively charged AuNPs were deposited on the CNC/PEI electrostatically resulting in a CNC/PEI/AuNPs nanocomposite. The enzyme (GOx) was covalently attached to the thiol-functionalized nanocomposite by activation of the $-\text{COOH}$ group using 1-ethyl-3-(3-dimethylaminopropyl) carbodiimide hydrochloride (EDC) and N-hydroxysuccinimide (NHS). The best case resulted in a 25.2 mg of GOx loaded per gram of support. Interestingly, the amount of GOx immobilized on this support increased with decreasing thiol-linker length. The difference could be attributed to their ability to access the AuNPs, as these particles are densely packed.

3.4 Combined Strategies

A new trend in the preparation of immobilized nanobiocatalysts is the combination of different strategies previous to, during, and/or after the immobilization process. The different strategies may have a synergistic effect on the desired properties of the final enzymatic preparation. To improve both loading and stability of enzymes, a three-step approach of enzyme precipitate coating (EPC), consisting of covalent enzyme attachment, enzyme precipitation, and crosslinking, has been successful in achieving both high enzyme loading and stability of enzymes on cellulose nanofibers (CNFs) (Fig. 3a) [34]. Such is the case of immobilization of α -chymotrypsin (CT) on CNFs by the EPC approach. In this approach, magnetic nanoparticles can be added to the enzyme mixture during the precipitation and cross-linking steps to produce

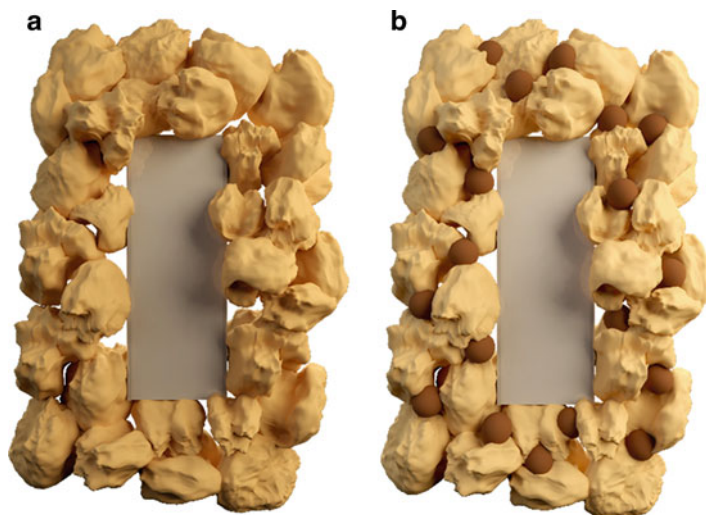


Fig. 3 Schematic representation of enzymes immobilized to cellulose nanofibers by (a) enzyme precipitate coating (EPC) and (b) magnetically separable EPC (Mag-EPC)

magnetically separable EPC (Mag-EPC) allowing for facile nanobiocatalyst separation (Fig. 3b).

As previously mentioned, this immobilization process consists of three steps. First, carboxyl groups of CNFs can be modified by EDC/NHS reaction for the covalent attachment between enzymes and CNFs, second, enzyme precipitation by ammonium sulfate, and third, enzyme cross-linking with glutaraldehyde treatment. The amine-functionalized magnetic nanoparticles can be added to enzyme solution in the step of enzyme precipitation (Fig. 3b).

The enzyme loadings with (Mag-EPC) and without (EPC) magnetic nanoparticles were estimated to be 3.5 and 3.0 mg CT/mg CNF, respectively. Interestingly, Mag-EPC showed two times higher activity than EPC. The efficiency of cross-linking between enzymes and magnetic nanoparticles was improved possibly due to a higher amount of amine groups on the surface of magnetic nanoparticles, resulting in an increased enzyme loading of Mag-EPC than EPC, as reflected in the activity data (0.43 and 0.74 IU/mg CT for EPC and Mag-EPC, respectively). After incubation under rigorous shaking for 30 days, EPC and Mag-EPC maintained 77% and 50% of their initial activities, respectively, while the free enzyme showed only 0.2%. High stability of EPC can be explained by ammonium sulfate precipitation and cross-linking of CTs. Enzyme precipitation by ammonium sulfate allows enzyme molecules to be closely packed based on “salting out” effect. Interestingly, the Mag-EPC residual activity was lower than that of EPC; this could be caused by the release of large aggregates of CTs and magnetic nanoparticles which would make the enzyme more vulnerable to denaturation under rigorous shaking [34].

3.5 Immobilization by Entrapment

Immobilization by entrapment involves the physical confinement of one or more enzymes in an insoluble matrix. In this strategy, the matrix is usually formed during the immobilization process. The bibliography related to immobilization by entrapment in cellulose nanosupports is scarce. The main drawback for this approach could be related to the very low solubility of cellulose in an aqueous solution since is highly crystalline. Nonetheless, there are successful cases using micro-sized supports. For example, a lipase from *C. rugose* was entrapped in a hydroxypropylmethyl-cellulose and chitosan matrix. Although this strategy involved many steps and over 48 h of synthesis, the result was a highly active and stable preparation [35].

Also, the rapid development of more and greener ionic liquids, which can dissolve cellulose, opens a new window of opportunities in this field. Again, successful examples can be found with cellulose-based micro-supports. Lipase from a *C. rugose* was entrapped into a cellulose–biopolymer using a biocompatible ionic liquid, 1-ethyl-3-methylimidazolium. This strategy also resulted in a preparation with good residual activity [36].

The technological approach employed on these successful cases could be applied for the development of similar strategies involving nanocellulose.

4 Cellulose-Based Nanobiocatalysts at Work

Application of immobilized enzymes on cellulose spans a wide variety of fields. The biodegradability of cellulosic materials has recently drawn the attention of researchers which boosted investigation of its potential in sensitive biotechnological areas such as biomedicine or environmental sciences. In this section, a few recent examples of cellulose-based nanobiocatalysts will be described to provide the reader with a sense of the applicability of these materials.

4.1 Biomedical Applications

Reactive oxygen species are implicated in cellular injuries, the initiation and progression of the aging process, and a vast variety of clinical abnormalities. In order to reduce the damage generated by these compounds, a nanofibrous cellulose mat containing attached catalase was prepared and tested in vitro on human umbilical vascular endothelial cells (HUVECs). The immobilized preparation based on electrospun nanofibers proved to have a protective effect on cells previously exposed to H₂O₂ which in turn pointed to a potential strategy to prevent cell damage by reactive oxygen species. The work also showed that the number of coating bilayers in the catalase-modified nanofibrous mats acted as important factor affecting their cytotoxicity and biocompatibility. This was an explorative work with potential to overcome H₂O₂-induced adverse effects at the cellular levels [37].

The antibacterial properties of lysozyme, a hydrolytic enzyme that catalyzes the breakdown of peptidoglycan polymers found in the bacterial cell wall, has been exploited and tested while using immobilized preparations on cellulosic materials. In comparison to many other antibacterial nanoparticles in use, lysozyme immobilized on cellulose possesses low toxicity, high biocompatibility, and selectivity. Researching its potential in a biomedical wound dressing, lysozyme was immobilized via different approaches to cellulose nanofibers aerogels (CNFs) [38]. The performance of the nanobiocatalysts was evaluated against nonimmobilized enzyme and silver nanoparticles. The antimicrobial activity of the preparations was tested against *Escherichia coli* and *Staphylococcus aureus* demonstrating the feasibility of using lysozyme-modified CNFs for this application. The preparation containing lysozyme was not only inhibitory of bacterial growth but was also more stable than the soluble enzyme, which amplifies the possibilities of its application considering the importance of shelf life of biological based products.

A work from Abouhmad et al. [39] also investigated the antibacterial properties of a lysozyme immobilized on CNC. Following different approaches for the integration of hen egg white- and T4 lysozyme, the work demonstrated that the surface modification and the mode of immobilization are critical for the retention of the enzymatic (lytic and hydrolytic) and antibacterial activity as well as stability of the immobilized enzymes. The positive charge on the nanocrystals and lysozyme activity improved the enzymatic action and broadened the scope to Gram-negative bacteria that are normally more challenging to inactivate.

Biosensors offer simple, portable, and disposable analytical devices applicable in clinical diagnosis, food quality control, and environmental monitoring. They depend on a biological recognition capable of being translated on a signal proportional to a target analyte. Particularly, paper-based sensors that offer affordability and ease of preparation although protein immobilization could be challenging to achieve an even distribution of oriented enzyme molecules that could increase the sensibility of the sensing device. A recent work on the development of a lactate biosensor has tackled this problem by using a recombinant lactate dehydrogenase fused with a cellulose-binding domain (CBD) which in nature promotes arbohydrate binding functionality for cellulases. The tag allowed a highly specific binding affinity on filter paper. Moreover, it enhanced enzyme binding capacity and stability, leading to much improved sensor sensitivity and lifetime. The one-step binding procedure using enzyme crude extract aimed at an efficient sensor fabrication strategy for production of high-performance paper sensors that could be extended to nanocellulosic materials for increased sensibility [40].

In another biosensing approach, glutamate dehydrogenase was immobilized on bacterial cellulosic nanofiber with a view on its application in artificial kidney machines and their dialysate liquid regeneration systems as a glutamate-sensing device. The study showed the success of cross-linked immobilization of glutamate dehydrogenase on 30–70 nm bacterial cellulosic nanofiber from *Gluconacetobacter xylinum*. The enzyme was cross-linked to the nanofibers using glutaraldehyde. The study provided an inexpensive, simple, efficient, and reliable technique for

immobilization of glutamate dehydrogenase on bacterial nanofiber which may contribute to find alternative for glutamate determination in solution [41].

4.2 Food Applications

Stem bromelain is a cysteine protease obtained from stems of pineapples (*Ananas comosus*). Although it finds some applications in medicine, this protease is widely used in food industries such as beer clarification, meat tenderization, and baking industries. Using casein as a model substrate, Talingtaisong et al. demonstrated that when the enzyme was immobilized on gauze-reinforced regenerated cellulose (RC) fibers, it became more heat resistant [42]. The enzyme was attached to the RC fibers through covalent immobilization via aldehyde groups introduced by activation with glutaraldehyde and was able to resist up to nine reuses in casein hydrolysis with 40% loss in activity. The results provide an opportunity for bromelain to be reused and used in other processing conditions.

Another interesting application of a cellulose-immobilized biocatalyst is that of naringinase. Naringin and limonin are two of the major compounds that contribute to a bitter taste in citrus juices. Enzymatic and physicochemical treatments have been applied to reduce bitterness, naringinase being one of the enzymes applied as it is able to break down naringin in flavorless products. Naringinase was immobilized within a hybrid layer-by-layer self-assembled material containing alginate and electrospun cellulose acetate nanofibers [21]. As expected, the activity of immobilized naringinase increased with multilayer increasing. The immobilized preparation was applied to remove the bitterness in the grapefruit juice. About 22.72% naringin and 60.71% limonin were removed from the grapefruit juice by adsorption and hydrolysis. The results demonstrated that naringinase-immobilized electrospun cellulose acetate nanofibrous mat are potential materials to remove bitterness for fruit juice.

4.3 Environmental Applications

Biobased treatments of contaminant compounds have received a great deal of interest due to their minimal impact on the ecosystem, their higher efficiency, and their cost effectiveness. Application of immobilized decontaminant biocatalysts is one of the approaches followed to treat, sense, or remove contaminant wastes from water and soil. Although the literature on cellulose-immobilized enzymes on decontamination is not abundant, a few recent examples have demonstrated the potential of cellulosic-supported enzymes for this application. For example, laccase, a well-known phenol/polyphenol decontaminant biocatalyst, was immobilized on cellulose nanofiber and utilized for reactive dyes and simulated dye effluent (SDE) decoloration [43]. After covalent immobilization on electrospun nanofibers, the immobilized preparation was able to decolorate solutions of six different reactive dyes. Optimization of the conversion was performed after statistical analysis revealing that both the concentration of immobilized enzyme and type of

mediator for the catalysis were determinant in the result of the decontamination reactions. The immobilized preparations could be recycled more than 10 times while maintaining more than 50% of its initial activity.

Another example that represents a promising application of immobilized enzymes in cellulosic materials is the utilization of an ether hydrolase enzyme for the decontamination of 2,4-dinitroanisole (DNAN) [44]. This compound is nowadays preferred to 2,4,6-trinitrotoluene (TNT) given that it is less heat and shock sensitive. Strategies to decontaminate firing ranges and wastes from manufacturing sites should comply with biosafety and environmental regulations and therefore there is a constant search for new strategies to remediate explosive components. Additionally, analytical devices for the evaluation of contamination levels are also needed. The work described by the group of Prof. J C Spain used a DNAN demethylase entrapped in biomimetic silica which was further attached to cellulose discs. The immobilized enzyme became more stable and was able to detect 15–500 μM DNAN concentration.

5 Conclusion

Ideal supports for enzyme immobilization should be biocompatible, easy to functionalize, inexpensive, and biodegradable. Additionally, immobilization strategies should provide advantages for enzyme applications over the use of soluble enzymes to counterbalance any additional cost in the preparation of the biocatalyst (i.e., stabilization, increased activity, possibility of reuse). We believe this chapter compiles evidence that proves the benefits of nanocellulosic materials as supports for enzyme immobilization. Moreover, the methodologies for enzyme immobilization on cellulose-based nanocarriers presented suggest that cellulose can be a viable and dynamic material for stable and efficient enzyme immobilization via different approaches. Finally, the variety of applications, which are now in a continuous growth phase, only serve to foretell a promising future for the development of technological solutions involving cellulose-immobilized nanobiocatalysts.

Acknowledgments The authors acknowledge ANII, PEDECIBA, and Universidad ORT Uruguay for providing financial support.

References

1. Sulaiman S, Mokhtar MN, Naim MN, Baharuddin AS, Sulaiman A (2014) A review: potential usage of cellulose nanofibers (CNF) for enzyme immobilization via covalent interactions. *Appl Biochem Biotechnol* 175:1817–1842. <https://doi.org/10.1007/s12010-014-1417-x>
2. Mateo C, Palomo JM, Fernandez-Lorente G, Guisan JM, Fernandez-Lafuente R (2007) Improvement of enzyme activity, stability and selectivity via immobilization techniques. *Enzym Microb Technol* 40:1451–1463. <https://doi.org/10.1016/j.enzmictec.2007.01.018>
3. Misson M, Zhang H, Jin B (2015) Nanobiocatalyst advancements and bioprocessing applications. *J R Soc Interf* 12:20140891

4. Esmaili C, Abdi MM, Mathew AP, Jonoobi M, Oksman K, Rezayi M (2015) Synergy effect of nanocrystalline cellulose for the biosensing detection of glucose. *Sensors (Switzerland)* 15:24681–24697. <https://doi.org/10.3390/s151024681>
5. Lavoine N, Desloges I, Dufresne A, Bras J (2012) Microfibrillated cellulose – its barrier properties and applications in cellulosic materials: a review. *Carbohydr Polym* 90:735–764. <https://doi.org/10.1016/j.carbpol.2012.05.026>
6. Panatadasirisuk W, Vongsetskul T, Sucharitakul J, Chaiyen P, Tangboriboonrat P (2015) Functionalized electrospun regenerated cellulose fibers for immobilizing pyranose 2-oxidase. *React Funct Polym* 86:47–51. <https://doi.org/10.1016/j.reactfunctpolym.2014.11.008>
7. Sulaiman S, Mokhtar MN, Naim MN, Baharuddin AS, Salleh MAM, Sulaiman A (2015) Study on the preparation of cellulose nanofibre (CNF) from Kenaf Bast fibre for enzyme immobilization application. *Sains Malaysiana* 44:1541–1550
8. Park S, Kim SH, Won K, Choi JW, Kim YH, Kim HJ, Yang YH, Lee SH (2015) Wood mimetic hydrogel beads for enzyme immobilization. *Carbohydr Polym* 115:223–229. <https://doi.org/10.1016/j.carbpol.2014.08.096>
9. Karimi S, Tahir PM, Karimi A, Dufresne A, Abdulkhani A (2014) Kenaf bast cellulosic fibers hierarchy: a comprehensive approach from micro to nano. *Carbohydr Polym* 101:878–885. <https://doi.org/10.1016/j.carbpol.2013.09.106>
10. Sulaiman S, Cieh NL, Mokhtar MN, Naim MN, Kamal SMM (2017) Covalent immobilization of cyclodextrin glucanotransferase on kenaf cellulose nanofiber and its application in ultrafiltration membrane system. *Process Biochem* 55:85–95. <https://doi.org/10.1016/j.procbio.2017.01.025>
11. Pandey JK, Takagi H, Nakagaito AN, Kim HJ (2015) Handbook of polymer nanocomposites. Processing, performance and application: volume C: polymer nanocomposites of cellulose nanoparticles. In: *Handb Polym Nanocomposites process perform Appl Vol C Polym nanocomposites Cellul nanoparticles C: 1–511*. <https://doi.org/10.1007/978-3-642-45232-1>
12. Shahrousvand M, Tabar FA, Shahrousvand E, Babaei A, Hasani-Sadrabadi MM, Sadeghi GMM, Jafari H, Salimi A (2017) High aspect ratio phospho-calcified rock candy-like cellulose nanowhiskers of wastepaper applicable in osteogenic differentiation of hMSCs. *Carbohydr Polym* 175:293–302. <https://doi.org/10.1016/j.carbpol.2017.08.001>
13. Kim HJ, Park S, Kim SH, Kim JH, Yu H, Kim HJ, Yang YH, Kan E, Kim YH, Lee SH (2015) Biocompatible cellulose nanocrystals as supports to immobilize lipase. *J Mol Catal B Enzym* 122:170–178. <https://doi.org/10.1016/j.molcatb.2015.09.007>
14. Uth C, Zielonka S, Hörner S, Rasche N, Plog A, Orelma H, Avrutina O, Zhang K, Kolmar H (2014) A Chemoenzymatic approach to protein immobilization onto crystalline cellulose Nanoscaffolds. *Angew Chemie Int Edgl* 53(46):12618–12623. <https://doi.org/10.1002/anie.201404616>
15. Mahmoud KA, Lam E, Hrapovic S, Luong JHT (2013) Preparation of well-dispersed gold/magnetite nanoparticles embedded on cellulose nanocrystals for efficient immobilization of papain enzyme. *ACS Appl Mater Interf* 5:4978–4985. <https://doi.org/10.1021/am4007534>
16. Pacheco G, Nogueira CR, Meneguín AB, Trovatti E, Silva MCC, Machado RTA, Ribeiro SJL, da Silva Filho EC, da S, Barud H (2017) Development and characterization of bacterial cellulose produced by cashew tree residues as alternative carbon source. *Ind Crop Prod* 107:13–19. <https://doi.org/10.1016/j.indcrop.2017.05.026>
17. Keshk SM (2014) Bacterial cellulose production and its industrial applications. *J Bioprocess Biotech* 4:150–160. <https://doi.org/10.4172/2155-9821.1000150>
18. Iris SL, Calvar L, Liu JMCJ, Cheng ADK (2013) Biosynthesis, production and applications of bacterial cellulose. *Cellulose* 20:2191–2219. <https://doi.org/10.1007/s10570-013-9994-3>
19. Sampaio LMP, Padrão J, Faria J, Silva JP, Silva CJ, Dourado F, Zille A (2016) Laccase immobilization on bacterial nanocellulose membranes: antimicrobial, kinetic and stability properties. *Carbohydr Polym* 145:1–12. <https://doi.org/10.1016/j.carbpol.2016.03.009>
20. Yan H, Chen X, Song H, Li J, Feng Y, Shi Z, Wang X, Lin Q (2017) Food hydrocolloids synthesis of bacterial cellulose and bacterial cellulose nanocrystals for their applications in

- the stabilization of olive oil Pickering emulsion. *Food Hydrocoll* 72:127–135. <https://doi.org/10.1016/j.foodhyd.2017.05.044>
21. Huang W, Zhan Y, Shi X, Chen J, Deng H, Du Y (2017) Controllable immobilization of naringinase on electrospun cellulose acetate nanofibers and their application to juice debittering. *Int J Biol Macromol* 98:630–636. <https://doi.org/10.1016/j.ijbiomac.2017.02.018>
 22. Kang Y, Ahn Y, Lee SH, Hong JH, Ku MK, Kim H (2013) Lignocellulosic nanofiber prepared by alkali treatment and electrospinning using ionic liquid. *Fibers Polym* 14:530–536. <https://doi.org/10.1007/s12221-013-0530-8>
 23. Cao S, Xu P, Ma Y, Yao X, Yao Y, Zong M, Li X, Lou W (2016) Recent advances in immobilized enzymes on nanocarriers. *Cuihua Xuebao/Chinese J Catal* 37:1814–1823. [https://doi.org/10.1016/S1872-2067\(16\)62528-7](https://doi.org/10.1016/S1872-2067(16)62528-7)
 24. Sulaiman S, Mokhtar MN, Naim MN, Baharuddin AS, Sulaiman A (2015) A review: potential usage of cellulose nanofibers (CNF) for enzyme immobilization via covalent interactions. *Appl Biochem Biotechnol* 175:1817–1842. <https://doi.org/10.1007/s12010-014-1417-x>
 25. Ayissi Eyebe G, Bideau B, Boubekour N, Loranger É, Domingue F (2017) Environmentally-friendly cellulose nanofibre sheets for humidity sensing in microwave frequencies. *Sensors Actuators B Chem* 245:484–492. <https://doi.org/10.1016/j.snb.2017.01.130>
 26. Barbosa O, Ortiz C, Berenguer-Murcia Á, Torres R, Rodrigues RC, Fernandez-Lafuente R (2014) Glutaraldehyde in bio-catalysts design: a useful crosslinker and a versatile tool in enzyme immobilization. *RSC Adv* 4:1583–1600. <https://doi.org/10.1039/c3ra45991h>
 27. Cao SL, Xu H, Li XH, Lou WY, Zong MH (2015) Papain@magnetic Nanocrystalline cellulose Nanobiocatalyst: a highly efficient biocatalyst for dipeptide biosynthesis in deep eutectic solvents. *ACS Sustain Chem Eng* 3:1589–1599. <https://doi.org/10.1021/acssuschemeng.5b00290>
 28. Liu Y, Chen JY (2016) Enzyme immobilization on cellulose matrixes. *J Bioact Compat Polym* 31:553–567. <https://doi.org/10.1177/0883911516637377>
 29. Karra-Chaabouni M, Bouaziz I, Boufi S, Botelho Do Rego AM, Gargouri Y (2008) Physical immobilization of *Rhizopus oryzae* lipase onto cellulose substrate: activity and stability studies. *Colloids Surfaces B Biointerfaces* 66:168–177. <https://doi.org/10.1016/j.colsurfb.2008.06.010>
 30. Huang X-J, Chen P-C, Huang F, Ou Y, Chen M-R, Xu Z-K (2011) Immobilization of *Candida rugosa* lipase on electrospun cellulose nanofiber membrane. *J Mol Catal B Enzym* 70:95–100. <https://doi.org/10.1016/j.molcatb.2011.02.010>
 31. Yang R, Tan H, Wei F, Wang S (2008) Peroxidase conjugate of cellulose nanocrystals for the removal of chlorinated phenolic compounds in aqueous solution. *Biotechnology* 7:233–241. <https://doi.org/10.3923/biotech.2008.233.241>
 32. Edwards JV, Prevost NT, Condon B, French A, Wu Q (2012) Immobilization of lysozyme-cellulose amide-linked conjugates on cellulose I and II cotton nanocrystalline preparations. *Cellulose* 19:495–506. <https://doi.org/10.1007/s10570-011-9637-5>
 33. Incani V, Danumah C, Boluk Y (2013) Nanocomposites of nanocrystalline cellulose for enzyme immobilization. *Cellulose* 20:191–200. <https://doi.org/10.1007/s10570-012-9805-2>
 34. Je HH, Noh S, Hong SG, Ju Y, Kim J, Hwang DS (2017) Cellulose nanofibers for magnetically-separable and highly loaded enzyme immobilization. *Chem Eng J* 323:425–433. <https://doi.org/10.1016/j.cej.2017.04.110>
 35. Badgujar KC, Bhanage BM (2015) Carbohydrate base co-polymers as an efficient immobilization matrix to enhance lipase activity for potential biocatalytic applications. *Carbohydr Polym* 134:709–717. <https://doi.org/10.1016/j.carbpol.2015.08.036>
 36. Kim MH, An S, Won K, Kim HJ, Lee SH (2012) Entrapment of enzymes into cellulose-biopolymer composite hydrogel beads using biocompatible ionic liquid. *J Mol Catal B Enzym* 75:68–72. <https://doi.org/10.1016/j.molcatb.2011.11.011>
 37. Huang R, Deng H, Cai T, Zhan Y, Wang X, Chen X, Ji A, Li X (2014) Layer-by-layer immobilized catalase on electrospun Nanofibrous Mats protects against oxidative stress induced by hydrogen peroxide. *J Biomed Nanotechnol* 10:1346–1358. <https://doi.org/10.1166/jbn.2014.1802>

38. Uddin KMA, Orelma H, Mohammadi P, Borghei M, Laine J, Linder M, Rojas OJ (2017) Retention of lysozyme activity by physical immobilization in nanocellulose aerogels and antibacterial effects. *Cellulose* 24:2837–2848. <https://doi.org/10.1007/s10570-017-1311-0>
39. Abouhmad A, Dishisha T, Amin MA, Hatti-Kaul R (2017) Immobilization to positively charged cellulose nanocrystals enhances the antibacterial activity and stability of hen egg white and T4 lysozyme. *Biomacromolecules* 18:1600–1608. <https://doi.org/10.1021/acs.biomac.7b00219>
40. Dai G, Hu J, Zhao X, Wang P (2017) Sensors and actuators B : chemical a colorimetric paper sensor for lactate assay using a cellulose-binding recombinant enzyme. *Sensors Actuators B Chem* 238:138–144. <https://doi.org/10.1016/j.snb.2016.07.008>
41. Pesaran M, Amoabediny G (2017) Study on the stability and reusability of glutamate dehydrogenase immobilized on bacterial cellulose nanofiber. *Fibers Polym* 18:240–245. <https://doi.org/10.1007/s12221-017-6864-x>
42. Talingtaisong S, Vongsetskul T (2017) Gauze-reinforced electrospun regenerated cellulose ultrafine fibers for immobilizing bromelain. *Cellulose* 24:2967–2975. <https://doi.org/10.1007/s10570-017-1307-9>
43. Sathishkumar P, Kamala-Kannan S, Cho M, Kim JS, Hadibarata T, Salim MR, Oh BT (2014) Laccase immobilization on cellulose nanofiber: the catalytic efficiency and recyclic application for simulated dye effluent treatment. *J Mol Catal B Enzym* 100:111–120. <https://doi.org/10.1016/j.molcatb.2013.12.008>
44. Karthikeyan S, Kurt Z, Pandey G, Spain JC (2016) Immobilized biocatalyst for detection and destruction of the insensitive explosive, 2,4-Dinitroanisole (DNAN). *Environ Sci Technol* 50:11193–11199. <https://doi.org/10.1021/acs.est.6b03044>

Metadata of the chapter that will be visualized online

Chapter Title	In Situ Immobilization of Enzymes in Biomimetic Silica
Copyright Year	2020
Copyright Holder	Springer Science+Business Media, LLC, part of Springer Nature
Author	Family Name Jackson Particle Given Name Erienne Suffix Division Laboratorio de Biotecnología, Facultad de Ingeniería Organization Universidad ORT Uruguay Address Montevideo, Uruguay
Author	Family Name Correa Particle Given Name Sonali Suffix Division Laboratorio de Biotecnología, Facultad de Ingeniería Organization Universidad ORT Uruguay Address Montevideo, Uruguay
Corresponding Author	Family Name Betancor Particle Given Name Lorena Suffix Division Laboratorio de Biotecnología, Facultad de Ingeniería Organization Universidad ORT Uruguay Address Montevideo, Uruguay Email betancor@ort.edu.uy
Abstract	In this chapter we describe different strategies for enzyme immobilization in biomimetic silica nanoparticles. Synthesis of this type of support is performed under mild and biocompatible conditions and has been proven suitable for the immobilization and stabilization of a range of enzymes and enzymatic systems in nanostructured particles. Immobilization occurs by entrapment while the silica matrix is formed via catalysis of a polyamine molecule and the presence of silicic acid. Parameters such as enzyme, polyamine molecule, or source of Si concentration have been tailored in order to maximize enzymatic loads, stabilities, and specific activities of the catalysts. We provide different approaches for the immobilization and co-immobilization of enzymes that could be potentially extensible to other biocatalysts.
Keywords (separated by '-')	Biomimetic silica - Enzyme immobilization - Entrapment

In Situ Immobilization of Enzymes in Biomimetic Silica

Erienne Jackson, Sonali Correa, and Lorena Betancor

Abstract

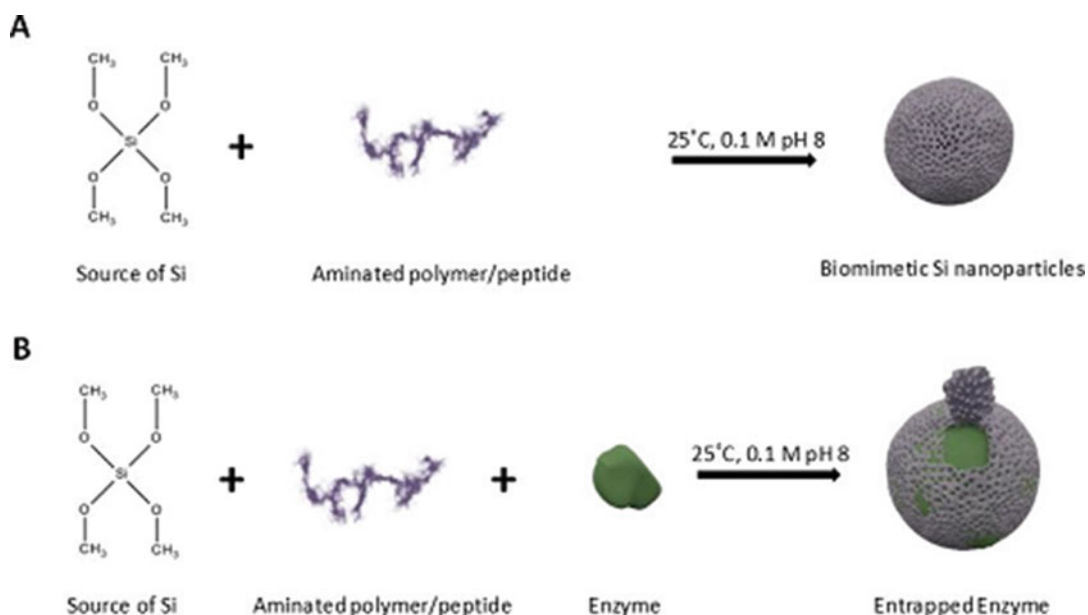
In this chapter we describe different strategies for enzyme immobilization in biomimetic silica nanoparticles. Synthesis of this type of support is performed under mild and biocompatible conditions and has been proven suitable for the immobilization and stabilization of a range of enzymes and enzymatic systems in nanostructured particles. Immobilization occurs by entrapment while the silica matrix is formed via catalysis of a polyamine molecule and the presence of silicic acid. Parameters such as enzyme, polyamine molecule, or source of Si concentration have been tailored in order to maximize enzymatic loads, stabilities, and specific activities of the catalysts. We provide different approaches for the immobilization and co-immobilization of enzymes that could be potentially extensible to other biocatalysts.

Key words Biomimetic silica, Enzyme immobilization, Entrapment

1 Introduction

Enzyme encapsulation or entrapment refers to a non-covalent immobilization strategy where polymers self-assemble in the presence of soluble enzymes. Various matrices can be used for entrapment, such as chitosan, collagen, cellulose triacetate, polyacrylamide, agar, silicon rubber, and polyvinyl alcohol [1–3]. In any approach to immobilize enzymes, the goal is to achieve a high specific activity without compromising any other advantages of immobilization such as higher stability. In recent years, several methods that achieve higher volumetric activities have been reported. Silica sol–gel encapsulation of enzymes is an example of such methods and has been widely used for the immobilization of biocatalysts [4, 5] One of the primary limitations of the sol–gel technique, however, is poor loading efficiency and enzyme leakage. Additionally, these methods often include harsh sol–gel processing conditions that result in the loss of enzyme activity. Inspired from silaffin proteins used by unicellular diatoms [6], the utilization of the so-called biomimetic approaches in the production of organic–inorganic nanostructures is of great interest to the scientific and

AU1



Scheme 1 General procedure for the preparation of (a) biomimetic Si nanoparticles and (b) in situ immobilized enzymes in biomimetic Si nanoparticles

industrial community due to the relatively moderate physicochemical conditions needed for its synthesis [7]. Biomimetic silica can be synthesized within minutes under mild and green conditions as nanostructured silica with divergent morphologies [8]. The synthesis necessitates a source of Si and an organic aminated small molecule or polymer in order to catalyze the precipitation of the nanoparticles in phosphate buffer at pH 8 (Scheme 1). Any material contained in the synthetic mixture may become entrapped within the biomimetic silica nanoparticles and therefore this strategy has been commonly used for enzyme immobilization [9–12].

A fundamental attribute of this immobilization methodology is its versatility which allows it to be widely applicable to a range of biomolecules. Since a primordial work from Luckarift et al. [13] and due to its biocompatibility and facile and quick synthesis, this entrapment strategy has been used to immobilize oxidases, hydrolases, and coupled enzyme systems.

Co-immobilization of enzymes using in situ immobilization approaches benefits from the close proximity of the different biocatalysts which translate into higher catalytic efficiencies of the overall reaction. Biomimetic silica encapsulation has been used in the past for the co-entrapment of a variety of multienzyme configurations as well as the preparation of combi robust biocatalysts for bioconversions of biosensing applications [14, 15].

However, the synthetic strategy for biomimetic silica nanobio-catalysts can provide distinct properties to different enzymes and

33
34
35
36
37
38
39
40
41
42
43
44
45
46
47
48
49
50
51
52
53
54
55
56
57

may be tailored to improve a desired attribute [13]. For instance, optimization of immobilized conditions to achieve active and stable nanobiocatalysts has included in the past studies of the synthetic precursor ratios, alternate aminated molecules, or inclusion of organic solvents during synthesis. Addition of enzyme stabilization molecules for the in situ entrapment or post immobilization strategies such as cross-linking could further improve the stability of the biocatalysts.

Results on the biomimetic silica entrapment of different enzymes seem to indicate a dependence of the physical and textural properties of the Si nanoparticles with properties such as size, shape, or chemistry of the surface of the enzymatic molecule [16]. As in any other immobilization strategy, parameters such as loading capacity of the nanobiocatalysts or specific activity are also directly influenced by the properties of the enzyme to be immobilized. However, in in situ immobilization strategies they also play a fundamental role in the synthesis of the material support to the extent of preventing its formation under certain unbalanced ratios of the synthetic precursors and enzyme concentration [10].

In this chapter, we describe strategies for the in situ immobilization and co-immobilization of enzymes in biomimetic Si nanoparticles selecting a few examples that highlight the potential of the technique and providing insight into the main parameters that should be considered when extending the strategy to other biomolecules.

2 Materials

1. Solution 1: 1 mg/mL of Horseradish peroxidase (HRP), Type IV in deionized water.
2. Solution 2: 85 mM potassium phosphate, pH 5.0, 0.45 mM 2,2'-azino-bis(3-ethylbenzothiazoline-6-sulphonic acid) (ABTS), 0.03% (w/w) hydrogen peroxide solution (H_2O_2) previously prepared in deionized water.
3. Solution 3: 0.8 mM of pyruvate, 0.2 mM of NADH in 25 mM sodium phosphate buffer at pH 7.0.
4. Solution 4: 0.015 mg/mL of LDH in 25 mM sodium phosphate buffer at pH 7.0.
5. Solution 5: 0.1 mM ribostamycin, 0.5 mM γ -Glu-AHBA-SNAC, and 0.2 mM de DTNB in buffer HEPES 50 mM pH 7.0.
6. Solution 6: 20 mM oNPG and 1 mM $MgCl_2$ in potassium phosphate buffer.
7. Solution 7: 60 mM sodium phosphate buffer pH 6.0, 0.3 M glucose, 0.06 mg/mL ABTS in distilled water.

8. Solution 8: 1.6 mg/mL of HRP, 154 mM sodium chloride in 10 mM sodium phosphate, pH 7.2.
9. Solution 9: 43 mg/mL sodium periodate in distilled water (*see Note 1*).
10. Solution 10: 10% of polyethylenimine (PEI) or 12 mg/mL of spermidine (SP) in deionized water.
11. Solution 11: 157 μL of tetramethyl orthosilicate (TMOS, 1 M) in 1 mL of 1 mM hydrochloric acid (*see Note 2*).
12. Solution 12: Sodium phosphate buffer 0.025 M, pH 7.0, 0.5 M NaCl (*see Note 3*).

3 Methods

3.1 Enzyme Activity

1. Horseradish peroxidase activity assay contained 2 mL of assay solution 2 at 25 °C and 10 μL of solution 1. The oxidation of ABTS ($\epsilon_M = 36.8 \text{ mM}^{-1} \text{ cm}^{-1}$) was measured in a spectrophotometer at a wavelength of 405 nm for 2 min.
2. Lipase from *Rhizomucor miehei* (RML) activity was performed by continuously measuring the increase in the absorbance at 348 nm produced by the released *p*-nitrophenol in the hydrolysis of 0.4 mM pNPP in 25 mM sodium phosphate buffer at pH 7.0 at 30 °C.
3. L-Lactate dehydrogenase (LDH) activity was measured in 2.5 mL of solution 3 at 25 °C. The reaction was started by addition of 20 μL of solution 4 and followed during 120 s at 340 nm ($\epsilon_{\text{MNADH}} = 6220 \text{ M}^{-1} \text{ cm}^{-1}$).
4. The activity of the acyltransferase BtrH was measured in 108 μL of solution 5 at 25 °C. The reaction was started by addition of 0.2 mg of BtrH, and the SNAC release was followed during 10 min at 412 nm ($\epsilon_M = 14,150 \text{ M}^{-1} \text{ cm}^{-1}$).
5. β -Galactosidase (Grade VIII) activity was determined spectrophotometrically by following the increase in absorbance at 405 nm caused by the hydrolysis of *o*-nitrophenyl- β -D-galactopyranoside (oNPG) in solution 6, 2 min at 25 °C.
6. Glucose oxidase activity was determined spectrophotometrically by the increase in absorbance at 414 nm resulting from the oxidation of 2,2'-azino-bis(3-ethylbenz-tiazoline-6-sulfonic acid) (ABTS) by a coupled peroxidase-catalyzed reaction. The reaction mixture consisted of 1 mL of solution 7 and 0.1 mL of solution 1.

One enzyme unit (IU) was defined as the amount of enzyme that catalyzes the formation of 1 μmol of product per minute under the specified conditions.

3.2 Oxidation of HRP	1. Add 1.8 mL of solution 8 to 200 μ L of solution 9.	143
	2. Keep sample in gentle agitation in the dark for 1 h at 25 °C. To stop the reaction, add 2.5 μ L of glycerol and purify the oxidized enzyme using a desalting PD10 column equilibrated with 100 mM sodium phosphate pH 7.0 containing 154 mM sodium chloride.	144 145 146 147 148
	3. Evaluate the activity of the enzyme to consider any activity loss after chemical modification.	149 150 151
3.3 In Situ Enzyme Immobilization by Entrapment in Biomimetic Silica	The following is a general procedure with ratios of the component of the synthetic mixture (TMOS, aminated molecule, enzymatic solution) that usually provides good immobilization yields for a range of enzymes. However, the ratios may be varied to optimize the performance for a specific enzyme [10].	152 153 154 155 156
	1. Prepare a 10 mL enzymatic solution with a desired concentration in 0.1 M sodium phosphate dibasic buffer pH 8.0, add 2.5 mL of solution 10, and mix.	157 158 159
	2. Add 2.5 mL of solution 11, mix by inverting the tube several times, and keep in agitation for 5 min at room temperature (<i>see Note 4</i>).	160 161 162
	3. Centrifuge for 10 min at $4600 \times g$ and wash once in solution 12 and twice with sodium phosphate buffer 0.025 M, pH 7.0.	163 164
	4. Sonicate for 5 min to improve monodispersity.	165
	5. Evaluate the activity of the enzymatic mixture prior to immobilization and in the immobilized suspension.	166 167 168
3.4 Cross-Linking of Entrapped HRP	1. HRP immobilization by entrapment is performed as previously described, using the oxidized enzyme.	169 170
	2. Incubate 1 g of immobilized HRP in silica nanoparticles in 10 mL of sodium bicarbonate 25 mM at pH 10.0, 16 h at 4 °C.	171 172
	3. Finally, reduce the preparation by adding sodium borohydride (1 mg/mL) to the mixture under gentle agitation for 30 min (<i>see Note 5</i>). Centrifuge and resuspend in 0.025 M sodium phosphate buffer pH 7.0 for activity measurement.	173 174 175 176
	4. Evaluate the activity of the immobilized cross-linking suspension.	177 178 179

4 Results 180

4.1 In Situ Immobilization of Enzymes in Biomimetic Silica Nanoparticles	1. Prepare solutions of enzyme of varying concentrations in 0.1 M sodium phosphate buffer pH 8.	181 182
	2. Measure the activity of the different enzymatic preparations.	183
	3. Perform the in situ immobilization described in Subheading 3.3 of the different enzymatic preparations using PEI 10% or	184 185

t.1 **Table 1**
 t.2 **Examples of the results obtained for different enzymes immobilized by in situ entrapment in biomimetic silica**

t.2	Enzyme	Immobilization (%)	Y_A (%)	Source
t.3	Peroxidase from Horseradish	82 ± 4	49 ± 6	This work
t.4	Lipase from <i>Rizomucor miehei</i>	90 ± 1	24 ± 1	This work
t.5	Acyltransferase from <i>Bacillus circulans</i>	90 ± 2	20 ± 4	This work
t.6	Lipase from <i>Trametes versicolor</i>	82 ± 7	71 ± 1	[10]
t.7	β -galactosidase from <i>E. coli</i>	76 ± 7	42 ± 8	This work
t.8	Glucose oxidase from <i>Aspergillus niger</i>	50 ± 5	71 ± 2	This work
t.9	Enoate reductase recombinant from <i>E. coli</i>	34	92	[18]
t.10	Papain from <i>Carica papaya</i>	83	83	[17] ^a
t.11	Nitroreductase from <i>Pseudomonas pseudoalcaligenes</i>	80 ± 5	60 ± 5	[19]

t.12 ^aNo aminated molecule was needed for Si precipitation

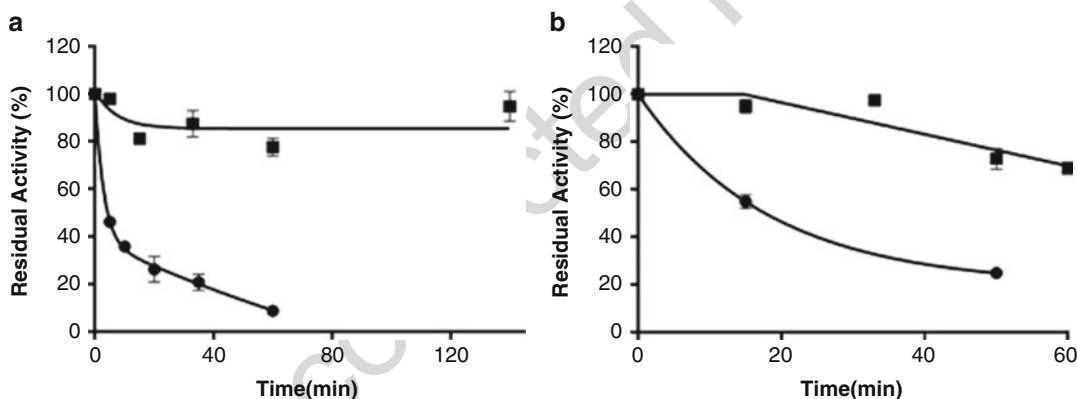


Fig. 1 Thermal stability of soluble and in situ entrapped enzymes in biomimetic silica. **(a)** β -galactosidase preparations at 54 °C, **(b)** glucose oxidase preparations at 50 °C. In both graphs solid circles: PEI; open diamonds: soluble

Spermidine 12 mg/mL keeping the supernatant of the immo- 186
 bilization after the first centrifugation. It is worth mentioning 187
 that a number of additional aminated molecules have been used 188
 for Si deposition. In fact, proteins with high amounts of Lys on 189
 their surface are able to auto catalyze their own Si 190
 entrapment [17]. 191

4. Measure the activity of the supernatant after silica precipitation. 192
5. Measure the activity after resuspension of the biocatalysts in 193
 working buffer solution of the enzyme. 194
6. Weight the amount of biocatalyst formed after immobilization. 195

7. Evaluate the amount of enzyme immobilized by difference of activity in the starting enzymatic preparation and the supernatant after immobilization (Immobilization %). Measure the immobilization yield either in terms of protein (Υ_P) and/or activity (Υ_A) according to Eqs. (1) and (2), respectively:

$$\Upsilon_P(\%) = \frac{P}{P_0} \times 100 \quad (1)$$

$$\Upsilon_A(\%) = \frac{A}{A_0} \times 100 \quad (2)$$

where P_0 represents the amount of offered protein, P the amount of loaded protein in the biocatalyst, A_0 the offered enzyme activity, and A the activity expressed in the biocatalyst.

8. Υ_P and Υ_A as well as the amount of Si nanoparticles of the biocatalysts obtained, and specific activity depend on multiple factors related to physicochemical and biochemical nature of the enzyme to be immobilized. Table 1 shows the results obtained for the enzymes analyzed in this chapter and examples of previous works using PEI 10% for the Si deposition. It is worth noting that these results have been obtained under similar conditions from those described above.
9. Regarding stabilization, there are multiple examples of stabilized in situ entrapped enzymes. Figure 1 shows thermos stabilization achieved for β -galactosidase and glucose oxidase after immobilization using this approach.

4.2 Stabilization of HRP Through 3D Cross-Linking in Biomimetic Silica Nanoparticles

1. Perform a mild oxidation via NaIO_4 as previously described (see Subheading 3.2). This treatment generates aldehyde groups on the sugar moieties of this highly glycosylated enzyme. Any glycosylated protein could be cross-linked after in situ entrapment in biomimetic silica. Additionally, any other chemical modification of the enzyme surface protein to introduce aldehyde groups could also allow for a 3D multipoint covalent immobilization of the encapsulated enzyme.
2. Assay the catalytic activity of the preparation after gel filtration in a PD-10 column into phosphate buffer 0.1 M pH 8.0.
3. Entrap the oxidized enzyme in silica nanoparticles as described in Subheading 3.3 using PEI 10%.
4. Incubate the immobilized preparation at pH 10 as described in Subheading 3.4. This incubation promotes the formation of Schiff's bases between the aldehyde groups of the enzyme (obtained by its oxidation) and unreacted amino groups of the PEI near the entrapped enzymatic structure. The reducing step via Na_2BH_4 transform the first reversible interaction between the enzyme and the matrix, into a three-dimensional multiple covalent attachment of HRP within the silica particles.

t.1 **Table 2**
 Results obtained after in situ immobilization of HRP in biomimetic silica nanoparticles

t.2	HRP (mg/mL)	Immobilization (%)	Y_A (%)	UI (UI/mg)
t.3	0.5	94 ± 3	50 ± 2	1.042 ± 4 × 10 ⁻³
t.4	1	85 ± 2	59 ± 2	1.025 ± 2 × 10 ⁻³
t.5	3	83 ± 2	53 ± 3	1.286 ± 4 × 10 ⁻³
t.6	5	82 ± 4	49 ± 6	1.700 ± 7 × 10 ⁻³
t.7	7.5	63 ± 4	42 ± 2	2.125 ± 5 × 10 ⁻³
t.8	10	54 ± 3	12 ± 3	1.887 ± 8 × 10 ⁻³
t.9	20	34 ± 5	10 ± 5	1.900 ± 7 × 10 ⁻³

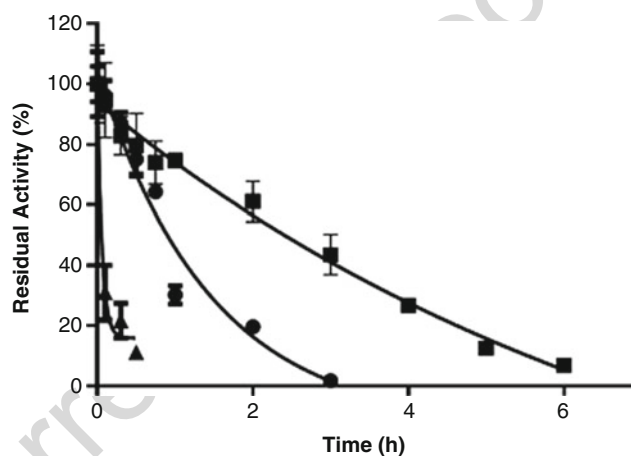


Fig. 2 Graphical representation of the thermal stability at 50 °C of the soluble (▲), entrapped enzyme (●) and the cross-linked entrapped enzyme (■). The half-life increased from 2.5 min to 53 min and 156 min, respectively. The experimental data was fitted to the exponential model from Henley and Sadana [20]

5. After reduction, wash twice with phosphate buffer by centrifugation for 10 min at $4500 \times g$ and resuspend in 25 mM phosphate buffer pH 7.0. Optimal results in terms of specific activity are obtained when using 5–7.5 mg/mL as starting HRP concentration (Table 2). 238
239
240
241
242
6. The studies on thermal stability demonstrated that the entrapped and cross-linked enzyme preparation presented a half-life time of 156 min, significantly higher compared to the solely entrapped enzyme or the non-immobilized HRP (53 and 2.4 min for their half-life time respectively) (Fig. 2). 243
244
245
246
247
248

**4.3 Use of Alternate
Aminated Catalysts for
In Situ Entrapment of
Lipase from
Ryzomucor miehei
(RML)**

1. Perform a gel filtration of the commercial enzyme in a PD-10 column using sodium phosphate buffer 0.1 M pH 8.0. Measure the activity of the preparation. 249
Use of spermidine for in situ entrapment: 250
251
2. Prepare a 12 mg/mL solution of spermidine in sodium phosphate buffer 0.1 M pH 8.0 and a solution of silicic acid as described in the Subheading 3.3. 253
254
255
3. Mix 1 mL of gel-filtrated RML with 0.5 mL spermidine solution. 256
257
4. Add 0.5 mL of silicic acid solution. 258
5. Centrifuge for 10 min at $4600 \times g$ and wash once in sodium phosphate buffer 0.025 M, pH 7.0, 0.5 M NaCl, and twice with sodium phosphate buffer 0.025 M, pH 7.0. 259
260
261
6. Measure the activity in the suspension. 262
Use of PEI for in situ entrapment: 263
7. Prepare a 10% PEI solution in sodium phosphate buffer 0.1 M pH 8.0 and a solution of silicic acid as described in Subheading 3.3. 264
265
266
8. Mix 1 mL of gel-filtrated RML with 0.1 mL of PEI solution. 267
9. Add 0.5 mL of silicic acid solution. 268
10. Centrifuge for 10 min at $4600 \times g$ and wash once in sodium phosphate buffer 0.025 M, pH 7.0, 0.5 M NaCl, and twice with sodium phosphate buffer 0.025 M, pH 7.0. 269
270
271
11. Measure the activity in the suspension. 272
12. Both immobilized preparations were significantly more stable than the soluble RML (Fig. 3). 273
274
275

4.4 Co-Immobilization of the Coupled Enzyme System BtrH and BtrG

The acyltransferase (BtrH) and γ -glutamyl cyclotransferase (BtrG) are two of the eight enzymes involved in the natural production of Butirosin B [21], a glycosidic antibiotic of relevance used to treat resistant infections. Previous works demonstrated the concerted action of these enzymes starting from synthetic precursors such as *N*-acetylcysteamine (SNAC) derivatives [22]. The following example involves the co-entrapment of both enzymes as a model of immobilized enzymatic system. 276
277
278
279
280
281
282
283

1. Prepare 1 mL solution of 0.2 mg of BtrH and 0.4 mg of BtrG in sodium phosphate buffer 0.1 M pH 8 and measure BtrH activity. 284
285
286
2. Add 0.25 mL of PEI 10% and mix. 287
3. Rapidly add 0.25 mL of previously hydrolyzed TMOS (silicic acid solution). 288
289
4. Mix the solution by inverting the tube three times. 290

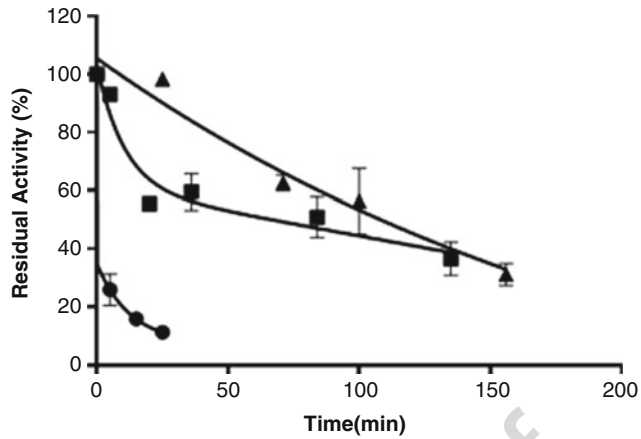


Fig. 3 Thermal stability at 60 °C of different RML preparations. Soluble enzyme (RML) (●), in situ entrapped enzyme using PEI (■), and in situ entrapped enzyme using spermidine (▲). The preparations were incubated in 25 mM sodium phosphate buffer pH 7

t.1 **Table 3**
 Results obtained for the entrapment and co-entrapment of BtrH and BtrG

Encapsulated enzymes	Immobilization (%)	Y_A (%)
BtrG	96.8 ± 1.1^a	ND
BtrH	89.7 ± 2.2	13.5 ± 2.01
BtrG and BtrH	75.2 ± 1.1	20 ± 3.5

t.6 ^aDetermined using protein concentration

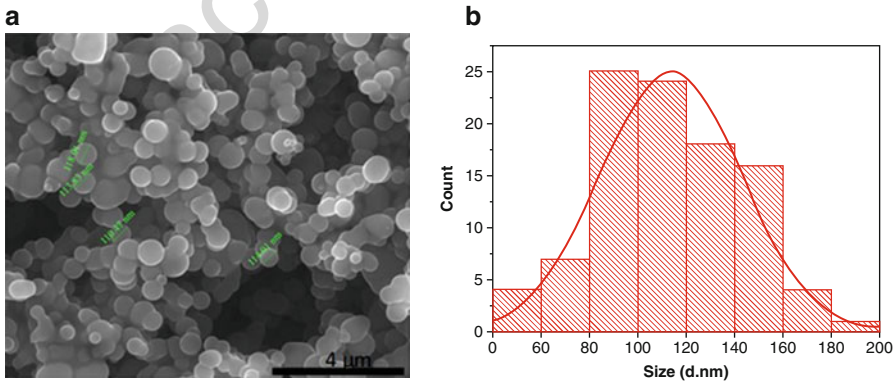


Fig. 4 (a) SEM analysis of in situ co-immobilized preparations of BtrH and BtrG. **(b)** Histogram representation of nanoparticle diameters using ImageJ

5. Centrifuge for 10 min at $4600 \times g$ and wash once in sodium phosphate buffer 0.1 M, pH 8.0, 0.5 M NaCl, and twice with sodium phosphate buffer 0.1 M, pH 8.0. 291
292
293
6. Measure BtrH activity in the suspension to evaluate any possible loss in activity during immobilization. 294
295
7. In situ immobilization for the co-entrapment of BtrG and BtrH did not affect significantly the %I (Table 3). 296
297
8. Although the Υ_A obtained for BtrH, the only activity that was possible to measure uncoupled with a chromogenic substrate was low (Table 3), analysis by LC-MS using γ -Glu-AHBA-SNAC and ribostamycin as substrate showed the presence of butirosin B. This compound is the expected product of the concerted action of both enzymes which proved that BtrH was active in the nano-co-entrapped biocatalysts. 298
299
300
301
302
303
304
9. Characterization by scanning electron microscopy of the in situ co-entrapped preparation showed dispersed as well as interconnected nanoparticles of a mean diameter of ~ 110 nm (Fig. 4). The shape and polydispersity obtained is similar for previously entrapped isolated proteins. However, the mean size obtained for the nanobiocatalyst is significantly smaller than reported entrapped proteins [16, 17]. 305
306
307
308
309
310
311
312

5 Notes

1. Sodium periodate solution should be prepared fresh and keep protected from light. 314
315
2. Vortex until solution is clear. This solution should be freshly prepared. 316
317
3. NaCl is sometimes necessary to remove non-entrapped ionically adsorbed enzymatic molecules to the surface of the nanoparticles. 318
319
320
4. Solutions should be added in the specified order. 321
5. Keep the vessel open as small amounts of H_2 are formed during reduction. 322
323

324 **References**

- 326 1. Krasňan V, Stloukal R, Rosenberg M, Rebroš
327 M (2016) Immobilization of cells and enzymes
328 to LentiKats[®]. *Appl Microbiol Biotechnol*
329 100:2535–2553
- 330 2. Monier M, Youssef I, Abdel-Latif DA (2018)
331 Synthesis of photo-responsive chitosan-cinna-
332 mate for efficient entrapment of β -galactosidase
333 enzyme. *React Funct Polym* 124:129–138
- 334 3. Zdarta J, Meyer A, Jesionowski T, Pinelo M
335 (2018) A general overview of support materials
336 for enzyme immobilization: characteristics,
337 properties, practical utility. *Catalysts* 8:92–119
- 338 4. Cazaban D, Wilson L, Betancor L (2017)
339 Lipase immobilization on siliceous supports:
340 application to synthetic reactions. *Curr Org*
341 *Chem* 21:96–103
- 342 5. Ronda L, Bruno S, Campanini B, Mozzarelli A,
343 Abbruzzetti S, Cupane A, Levantino M, Bettati
344 S (2015) Immobilization of proteins in silica
345 gel: biochemical and biophysical properties.
346 *Curr Org Chem* 19:1653–1668
- 347 6. Kröger N, Poulsen N (2008) Diatoms—from
348 cell wall biogenesis to nanotechnology. *Annu*
349 *Rev Genet* 42:83–107
- 350 7. Lechner C, Becker C (2015) Silaffins in silica
351 biomineralization and biomimetic silica precip-
352 itation. *Mar Drugs* 13:5297–5333
- 353 8. Yang SH (2013) Biomimetic silica nanostruc-
354 tures on the surface, controlled by polyvalent
355 counteranions. *Solid State Sci* 23:1–7
- 356 9. Betancor L, Luckarift HR (2008) Bioinspired
357 enzyme encapsulation for biocatalysis. *Trends*
358 *Biotechnol* 26:566–572
- 359 10. Cazaban D, Illanes A, Wilson L, Betancor L
360 (2018) Bio-inspired silica lipase nanobiocata-
361 lysts for the synthesis of fatty acid methyl esters.
362 *Process Biochem* 74:86–93
- 363 11. Patel SKS, Otari SV, Chan Kang Y, Lee J-K
364 (2017) Protein–inorganic hybrid system for
365 efficient his-tagged enzymes immobilization
366 and its application in xylulose production.
367 *RSC Adv* 7:3488–3494
- 368 12. Johnson GR, Luckarift HR (2017) Enzyme
369 stabilization via bio-templated silicification
370 reactions. *Methods Mol Biol* 1504:61–73
13. Luckarift HR, Spain JC, Naik RR, Stone MO 371
(2004) Enzyme immobilization in a biomi- 372
metic silica support. *Nat Biotechnol* 373
22:211–213 374
14. López-Gallego F, Jackson E, Betancor L 375
(2017) Heterogeneous systems biocatalysis: 376
the path to the fabrication of self-sufficient arti- 377
ficial metabolic cells. *Chem Eur J* 378
19:17841–17849 379
15. Betancor L, Johnson GR, Luckarift HR (2013) 380
Stabilized laccases as heterogeneous bioelec- 381
trocatalysts. *ChemCatChem* 5:46–60 382
16. Jackson E, Ferrari M, Cuestas-Ayllon C, Fer- 383
nández-Pacheco R, Perez-Carvajal J, De La 384
Fuente JM, Grazú V, Betancor L (2015) 385
Protein-templated biomimetic silica nanoparti- 386
cles. *Langmuir* 31:3687–3695 387
17. Zhou L, Wang C, Jiang Y, Gao J (2013) 388
Immobilization of papain in biosilica matrix 389
and its catalytic property. *Chinese J Chem* 390
Eng 21:670–675 391
18. Li H, Xiao W, Xie P, Zheng L (2018) 392
Co-immobilization of enoate reductase with a 393
cofactor-recycling partner enzyme. *Enzym* 394
Microb Technol 109:66–73 395
19. Berne C, Betancor L, Luckarift HR, Spain JC 396
(2006) Application of a microfluidic reactor for 397
screening cancer prodrug activation using 398
silica-immobilized nitrobenzene nitroreduc- 399
tase. *Biomacromolecules* 7:2631–2636 400
20. Henley JP, Sadana A (1985) Categorization of 401
enzyme deactivations using a series-type mech- 402
anism. *Enzym Microb Technol* 7:50–60 403
21. Li Y, Llewellyn NM, Giri R, Huang F, Spencer 404
JB (2005) Biosynthesis of the unique amino 405
acid side chain of butirosin: possible 406
protective-group chemistry in an acyl carrier 407
protein-mediated pathway. *Chem Biol* 408
12:665–675 409
22. Llewellyn NM, Spencer JB (2008) Chemoen- 410
zymatic acylation of aminoglycoside antibio- 411
tics. *Chem Commun* 3786–3788 412

Author Queries

Chapter No.: 17 459802_4_En

Query Refs.	Details Required	Author's response
AU1	Please check the hierarchy of the section headings and confirm if correct.	

Uncorrected Proof

RESEARCH ARTICLE

Design of stable magnetic hybrid nanoparticles of Si-entrapped HRP

Sonali Correa¹, Sara Puertas², Lucía Gutiérrez^{3,4,5}, Laura Asín⁵, Jesús Martínez de la Fuente^{4,5}, Valeria Grazú^{4,5*}, Lorena Betancor^{1*}

1 Laboratorio de Biotecnología, Universidad ORT Uruguay, Montevideo, Uruguay, **2** Nanoimmunotech S.L., Zaragoza, Spain, **3** Instituto de Nanociencia de Aragón, Universidad de Zaragoza, Campus Río Ebro, Edificio I+D, Zaragoza, Spain, **4** Instituto de Ciencia de Materiales de Aragón (ICMA), Consejo Superior de Investigaciones Científica, Zaragoza, Spain, **5** Centro de Investigación Biomédica en Red de Bioingeniería, Biomateriales y Nanomedicina (CIBER-BBN), Madrid, Spain

* betancor@ort.edu.uy (LB); vgrazu@unizar.es (VG)



Abstract

Hybrid and composite nanoparticles represent an attractive material for enzyme integration due to possible synergic advantages of the structural builders in the properties of the nanobiocatalyst. In this study, we report the synthesis of a new stable hybrid nanobiocatalyst formed by biomimetic silica (Si) nanoparticles entrapping both Horseradish Peroxidase (HRP) (EC 1.11.1.7) and magnetic nanoparticles (MNPs). We have demonstrated that tailoring of the synthetic reagents and post immobilization treatments greatly impacted physical and biocatalytic properties such as an unprecedented ~280 times increase in the half-life time in thermal stability experiments. The optimized nanohybrid biocatalyst that showed superparamagnetic behaviour, was effective in the batch conversion of indole-3-acetic acid, a prodrug used in Direct Enzyme Prodrug Therapy (DEPT). Our system, that was not cytotoxic *per se*, showed enhanced cytotoxic activity in the presence of the prodrug towards HCT-116, a colorectal cancer cell line. The strategy developed proved to be effective in obtaining a stabilized nanobiocatalyst combining three different organic/inorganic materials with potential in DEPT and other biotechnological applications.

OPEN ACCESS

Citation: Correa S, Puertas S, Gutiérrez L, Asín L, Martínez de la Fuente J, Grazú V, et al. (2019) Design of stable magnetic hybrid nanoparticles of Si-entrapped HRP. PLoS ONE 14(4): e0214004. <https://doi.org/10.1371/journal.pone.0214004>

Editor: Andrew C. Marr, Queen's University Belfast, UNITED KINGDOM

Received: November 16, 2018

Accepted: March 5, 2019

Published: April 1, 2019

Copyright: © 2019 Correa et al. This is an open access article distributed under the terms of the [Creative Commons Attribution License](https://creativecommons.org/licenses/by/4.0/), which permits unrestricted use, distribution, and reproduction in any medium, provided the original author and source are credited.

Data Availability Statement: All relevant data are within the manuscript and its Supporting Information files.

Funding: SC is funded by ANII (POS_NAC_2015_1_109910).

Competing interests: The authors have declared that no competing interests exist.

Introduction

The possibilities for practical applications of immobilized enzymes are continuously growing and a steady number of immobilization methods have been recently developed to preserve the activity of biotechnologically important enzymes in unnatural environments [1–4]. Apart from industrial large-scale applications, immobilization techniques on nanoscale supports have enabled and amplified the integration of enzymes in biosensors [5–7], nano/microreactors [8,9] or in the generation of hybrid nanostructures for biomedical applications [8,10,11]. Design of tailored strategies for enzyme immobilization has proved essential to achieve better specific activities, robustness and reusability of the material integrated enzymes, addressing the major problems that restrain industrial or therapeutic implementation of enzymatic reactions [12–14].

Selection of the support material for enzyme immobilization is a critical aspect due to its major impact on the properties of the biocatalyst. Its shape and textural characteristics of, hydrophilicity/hydrophobicity properties, biocompatibility, toxicity or physicochemical stability can directly influence the performance and utility of the immobilized enzyme [15–17]. Consequently, the discovery and use of new support materials with desired properties has become extremely important in the design of immobilized biocatalysts.

In this regard, scientific attention has been directed towards hybrid and composite materials, which combine properties of both composite precursor and maximize their advantages [4,18]. Upon integration of the different materials, it is desired that the intrinsic characteristics of each individual component are preserved, exhibiting new additional properties due to the synergetic effect between the structural builders. When immobilizing an enzyme in composite supports, scientists aim for a combined benefit of the materials on the properties of the biocatalyst.

Biomimetic silica (Si) has been used in the past to generate hybrid inorganic/organic nanocomposites for a range of applications. It can be synthesized as a nanostructured material with divergent morphologies within minutes under mild and green conditions [19,20]. Any material contained in the synthetic mixture may become entrapped within the biomimetic Si nanoparticles [17,21–23]. The mild synthetic approach (room temperature, neutral pH, free of organic solvents) is compatible with a range of enzymes for which the strategy has also resulted in stabilization [24–26]. Moreover, for biomedical applications such as enzyme replacement therapies or direct enzyme prodrug activation, encapsulation of enzymes in a Si nanocarrier could reduce the immunogenicity of the enzyme. However, synthetic strategies for biomimetic Si nanobiocatalysts are not universal as they provide distinct properties to different enzymes and may be tailored to improve a desired attribute [13].

HRP is a heme-containing enzyme that uses hydrogen peroxide as electron acceptor. Its importance in biotechnology is long established as it is involved in a variety of biological processes, it is able to amplify weak signals, it is stable towards external factors (e.g. peroxide species, temperature) and has a high turnover number [27]. In the past decade, HRP related investigations have regained interest following the discovery of new natural isoenzymes with different biochemical properties and the development of an efficient recombinant expression system that facilitated its production. New HRP properties might enable the effective use of this enzyme in polymer synthetic reactions in the presence of organic solvents or as a therapeutic agent in cancer therapy [28,29]. In the light of these new applications, we believe it is timely to propose novel immobilization strategies for HRP on tailored materials that augment its practical possibilities.

In this study, we demonstrate a new approach to integrate and stabilize HRP in biohybrid magnetic nanoparticles (biomimetic Si + magnetic nanoparticles (MNPs)). The hybrid immobilization system provided ease of separation in biocatalytic applications or accumulation of HRP nanobiocatalyst where desired. Each material included in the nano-hybrid contributed to the improvement of the properties of the nanohybrid which enabled its use in the conversion of indole-3-acetic acid (3-IAA), a prodrug used in cancer therapy.

Materials and methods

Horseshoe peroxidase Type VI (EC 1.11.1.7), polyethylenimine (PEI) (MW 1300, 2000, 25000 and 60000), 2,2'-Azino-bis (3-ethylbenzothiazoline-6-sulfonic acid) diammonium salt (ABTS) and hydrogen peroxide were from Sigma Aldrich (St. Louis, MO). Tetramethyl orthosilicate (TMOS), trehalose and potassium phosphate monobasic were from MERCK (Whitehouse Station, NJ). Dibasic sodium phosphate and sodium acetate were from Biopack (Buenos

Aires, Argentina). Gel filtration PD10-Columns were from GE Healthcare (Buckinghamshire, UK). Magnetic nanoparticles (MNPs) fluidMag-PAA (200 nm of aggregate size) were from Chemicell (Berlin, Germany). All other chemicals used were analytical grade reagents.

Determination of HRP activity

The activity of the free and entrapped enzyme preparations was measured by a colorimetric assay using 9.1 mM ABTS, ($\epsilon_M = 36.8 \text{ mM}^{-1}\text{cm}^{-1}$), as a substrate. The final assay contained 1.7 mL of 0.1 M potassium phosphate, pH 5.0 at 25°C, 0.1 mL of 9.1 mM ABTS, 0.2 mL 0.3% (w/w) hydrogen peroxide solution (H_2O_2) in deionized water and 10 μL of the soluble and nanohybrid preparations. The oxidation of ABTS was measured in a spectrophotometer at a wavelength of 405 nm for 2 min (Unico SQ-2800 UV-Vis). One enzyme unit (IU) was defined as the amount of HRP able to oxidize 1 μmol of ABTS in the above-mentioned conditions.

Entrapment of HRP in biomimetic Si nanoparticles. Aliquots of 0.4 mL of horseradish peroxidase Type VI solutions (protein concentration varied from 0.5 to 20 mg/mL) in potassium phosphate buffer (0.1 M, pH 8.0) were mixed with 0.1 mL of 10% polyethyleneimine (PEI) adjusted to pH 8.0 with HCl and 0.1 mL of a hydrolyzed TMOS solution prepared by diluting TMOS in hydrochloric acid (1 mM) to a final concentration of 1 M. The enzyme, buffer and PEI were mixed and gently agitated in an end-over-end roller for 15 min at 25°C. Then, the hydrolysed TMOS was added and this mixture was incubated for 5 min at 25°C. The resultant entrapped HRP preparation was then centrifuged (13500 rpm) for 5 min, washed five times by centrifugation and resuspension with sodium phosphate buffer 0.1 M pH 8.0 at 25°C and sonicated in an ultrasonic cleaner at 130 W and 20 kHz, (SONICS & MATERIALS, INC.) for 5 min. The immobilized nanobiocatalysts entrapped in Si are noted as [BioSi@HRP](#).

Immobilization percentage was defined as:

$$\%I = \frac{(\text{Initial activity} - \text{Activity in supernatant}) * 100}{\text{Initial activity}}$$

Immobilization yield was defined as:

$$\%Y = \frac{(\text{Activity in immobilized preparation}) * 100}{\text{Initial activity} - \text{Activity in supernatant}}$$

Oxidation of HRP. HRP was oxidized using a modification of Zalipsky's PEGylation protocol with the aim of generating aldehyde groups in its sugar moieties [30]. Peroxidase (3 mg) was dissolved in 1.8 mL of 10 mM sodium phosphate containing 154 mM sodium chloride, pH 7.2. Simultaneously, 8.6 mg of sodium periodate were dissolved in 200 μL of distilled water and protected from light. The sodium periodate solution was immediately added to the enzyme solution, and the sample was gently agitated. The 2 mL mixture was incubated in the dark for 1 h at 25°C with constant agitation. The reaction was then quenched by the addition of 2.5 μL of glycerol (99.5%) and the oxidized enzyme was then purified by using a desalting PD10 column equilibrated with 100 mM sodium phosphate pH 6.0 containing 154 mM sodium chloride. Oxidized HRP was concentrated to 1 mg/mL using Vivaspinn 500 with a 30 KDa cut off membrane. The oxidised enzyme is noted as HRPox.

Covalent three-dimensional immobilization of the entrapped HRP. HRPox (1 mg/mL) was entrapped in Si nanoparticles using the above-mentioned protocol. The entrapped enzyme was then incubated in 25 mM sodium bicarbonate, pH 10.0 (R 1:10) overnight at 4°C to facilitate the formation of Schiff's bases between the aldehyde groups generated in the enzyme and unreacted amino group from the support. The Schiff's bases were finally reduced using sodium

borohydride (1 mg/ml, 1:10) during 30 min at 25°C. The nanoparticles were then washed by centrifugation and resuspension in 0.1 M sodium phosphate buffer pH 8.0 three times.

Co-entrapment with magnetic nanoparticles. 10 µL of a 25 mg/mL solution of MNPs (chemicell FluidMAG-PAA, 200 nm) were brought to a magnetic separation rack during 5 min. The supernatant was removed and resuspended in the same volume of 0.1 M sodium phosphate buffer, pH 8.0. The co-entrapment procedure was the same as the one described above for the entrapment of HRP but adding the washed 10 µL suspension before the TMOS addition.

Aliquots of 0.4 mL of oxidized horseradish peroxidase solutions (protein concentration 1 mg/mL) in potassium phosphate buffer (0.1 M, pH 8.0) were mixed with 0.1 mL of 10% polyethyleneimine (PEI) adjusted to pH 8.0 with HCl and 10 µL suspension of the washed magnetic nanoparticles. The mixture was incubated for 10 min under gentle agitation at 25°C after which 0.1 mL of a hydrolyzed TMOS solution prepared by diluting TMOS in hydrochloric acid (1 mM) to a final concentration of 1 M, were added.

The resultant entrapped HRP preparation containing MNPs (BioSi@HRP_MNP) was then centrifuged (13500 rpm) for 5 min and washed five times by centrifugation and resuspension in 0.6 mL of sodium phosphate buffer 0.1 M pH 8.0. The nanoparticles suspension was sonicated in an ultrasonic cleaner at 130 W and 20 kHz (SONICS & MATERIALS, INC.) for 5 min and finally reduced using the above-mentioned protocol for a three-dimensional covalent immobilization.

General procedures for nanoparticles characterization. The morphology and particle size distribution of the resulting nanoparticles (NPs) were characterized by Environmental Scanning Electron Microscopy (ESEM) images were obtained using a QUANTA-FEG 250 microscope in “wet-mode” using a Peltier stage and a gaseous secondary electron detector (GSED). The secondary electron images were taken at a voltage range between 10–15 keV, low temperature (1°C), high chamber relative humidity (100%) and high Pressure (659 Pa) to maintain the wet sample hydrated avoiding the sample damage during the observation. The sample was prepared in milliQ water in a dilution of (1:10000) and sonicated prior to measurements for 3 min to improve the dispersity.

Dynamic light scattering (DLS) and Z-potential measurements were performed on a Malvern ZS nano instrument at 25°C. Each sample was prepared by diluting the sample (1:100000) with milliQ water of which 1 mL was added to a quartz cuvette. They were measured 10 times, with a combination of 3 runs per measurement. The data was analysed using Zetasizer software. Similarly, the z-potential was measured using the same sample in a Folded Capillary Zeta Cell and the sample was measured 10 times and analysed using the aforementioned software.

Magnetic characterization was performed as follows: 50 µl of the liquid sample were placed inside a polycarbonate capsule and sealed with vacuum grease for their magnetic characterization. The magnetic characterization was performed in a Quantum Design (USA) MPMS-XL SQUID magnetometer. Field dependent magnetization was recorded at 300 K under decreasing field starting from 2 T, in the field range between -2 T and 2 T.

Reuse of nanohybrid by magnetic separation. The reusability of the immobilized enzyme nanohybrids was studied by repeated usage for 10 enzymatic cycles. Enzymatic reactions using 9.1 mM of ABTS and 0.3% hydrogen peroxide as substrates were performed in a 2 mL reaction volume containing potassium phosphate buffer pH 5.0, and a fixed amount of immobilized enzyme (20 U). Between each cycle, the nanohybrids were carefully separated using a magnetic separator (Chemicell- MagnetoPURE BIG SIZE) and then resuspended in the reaction mixture. The reactions were measured spectrophotometrically at 405 nm for 2 min. The activity determined during the first cycle was considered 100% for the calculation of remaining percentage activity after each use.

Determination of reducing sugars by DNS method. To analyse the concentration of trehalose by DNS, serial dilutions of trehalose from 0.07 g/L to 10 g/L were made. To 2 mL of these solutions 1 mL of dilute hydrochloric acid was added and boiled for 1 min following which was cooled and the acid was neutralized with sodium hydrogen carbonate. Similarly, the supernatant of an immobilized preparation (stored for 1 month), for which we intended to observe trehalose leakage, was hydrolysed to convert the non-reducing sugar into a reducing sugar.

To the hydrolysed preparations 250 µl of DNS reagent was added. The mixture was heated at 90°C for 15 min to develop the range of colours which formed the standard to analyse our sample. Finally, distilled water was added to bring the final volume to 1 mL which were cooled to room temperature and the absorbance was recorded at 570 nm in a spectrophotometer.

Temperature profile of the nanoabiocatalysts. To study the optimum temperature, the reactants were heated in a water bath to a range of temperatures (20°C to 60°C). Upon reaching the desired temperature 10 µL enzyme was added to the reactant mixture and measured spectrophotometrically at 405 nm for 2 min.

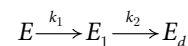
To analyse the range of thermal stability, the enzyme preparations were incubated in 0.1 M sodium phosphate pH 8.0 for 1 h at the aforementioned temperatures (20 to 60°C) after which the activity was measured spectrophotometrically at 405 nm for 2 min.

pH stability analysis of the nanoabiocatalysts. HRP preparations were incubated in 0.1 M sodium phosphate buffer pH 7.0 and 8.0, 25 mM sodium acetate pH 3.0, 4.0, and 5.0, and 25 mM sodium bicarbonate pH 10.0. Aliquots of soluble and entrapped suspensions were withdrawn, and their residual activity was measured as previously described after 1 h of incubation.

Thermal stability of the nanoabiocatalysts. The thermal stability was carried out at 50°C, wherein, aliquots of soluble and entrapped suspensions were withdrawn at different time intervals and their residual activity was measured as previously described. Residual activity was defined as:

$$\text{Residual Activity} = \frac{a}{a_0} \tag{1}$$

Where a are the IU at a time point and a_0 is the initial activity in IU. Biocatalysts inactivation was modeled based on the deactivation theory proposed by Henley and Sadana[31] using Graph Pad Prism. Inactivation parameters were determined from the best-fit model of the experimental data which was the one based on two-stage series inactivation mechanism without residual activity, as represented in the following scheme:



where k_1 and k_2 are first-order transition rates constants. E , E_1 and E_d are the corresponding enzyme species of progressively less specific activity, being the last one completely inactive. The mathematical model that represents this mechanism is:

$$\frac{a}{a_0} = \left(1 + \alpha \left(\frac{k_1}{k_2 - k_1} \right) \right) e^{-k_1 \times t} - \left(\alpha \left(\frac{k_1}{k_2 - k_1} \right) \right) e^{-k_2 \times t} \tag{2}$$

where α is the enzyme specific activity. Inactivation parameters were determined from the best-fit model of the experimental data. Half-life (time at which the residual enzyme activity is half of its initial value; $t_{1/2}$) was used to compare the stability of the different biocatalysts, being determined by interpolation from the respective model described by Eq 2. The stability factor (SF) was the parameter used for a quantitative comparison of the stability of the biocatalysts

and was found by

$$\text{Stabilization factor} = \frac{t_{1/2}}{t_{1/2_0}}. \quad (3)$$

Where $t_{1/2}$ is the half life time of the more stable sample and $t_{1/2_0}$ is the half life time of the less stable sample.

Oxidation of 3-IAA by enzymatic preparations. The oxidation of 3-indole acetic acid (3-IAA) by soluble and immobilized preparations (1 UI) was carried out as in [28], in 100 mM sodium acetate buffer pH 5.0 containing 500 mM of 3-IAA at 25°C for 2 h. An aliquot of reaction mixture was injected into a reverse-phase HPLC on a C18 Columbus column at 25°C using an isocratic elution buffer of methanol/1% acetic acid mixture (40:60, v/v) at a flow rate of 0.6 mL/min. The eluted products were monitored at absorbance of 250 nm using an Agilent 1100 series detector. The retention time for 3-IAA was 22 min and the reactive oxygen species were eluted from 3 min to 20 min.

Cytotoxicity and cell viability 3-(4,5-Dimethylthiazol-2-Yl)-2,5-Diphenyltetrazolium Bromide (MTT) assay. The experiments were carried out with human colorectal cancer (HCT 116) cell line. HCT116 shows less internalization compared to other cell lines and withstand higher temperatures[32] which suits future in vitro experiments related to the application of the nanobiocatalysts in direct enzyme prodrug activation. Additionally, it has been optimized for future 3D model experiments and genetically modified to constitutively express luciferase, which allows better biomedical imaging of tumour growth in in vivo experiments. To study the cytotoxic effect of the nanohybrids with 3-IAA we plated 15×10^3 cells HCT 116 per well in a 96-well plate and incubated in DMEM with 10% FBS, 1% glutamine (Invitrogen) and 1% penicillin/streptomycin (Invitrogen) for 24 hours in an incubator at 37°C and in presence of 5% CO₂. We then removed the medium and washed the cells with PBS. Following which we added varied nanohybrids with varied enzymatic activity resulting in 0.5 IU, 1 IU or 2 IU along with the prodrug with final concentration in the well of 1 mM or 2 mM of 3-IAA. The medium selected for this incubation was PBS. The cells when then incubated for 6 h at 37°C. Different controls were prepared to analyse the cytotoxicity effect of every single component; nanohybrids and the prodrug. Besides, samples with the enzyme in suspension alone and in combination with the prodrug were prepared to be able to compare the efficiency of the nanohybrids. The supernatant was then removed and 100 μ l of complete medium and 10 μ l of MTT (5mg/ml) was added per well and was incubated for 2 h 37°C, until intracellular purple formazan crystals are visible under microscope. The plate was centrifuged at 1200 rpm for 25 min at RT. Following the removal of the supernatant and addition of 100 μ l of DMSO per well to solubilize the formazan crystals, the absorbance was measured at 570 nm. Every sample was prepared in triplicates.

Results and discussion

Sol-gel and functionalized mesoporous Si have been previously used for enzyme immobilization. These methods have some inherent limitations such as harsh synthetic conditions or poor retention of the immobilized enzyme different from biomimetic Si synthesis [19,33]. The immobilization approach follows a one-pot procedure, wherein, Si synthesis and enzyme entrapment occur simultaneously. Biomimetic reactions for Si deposition and HRP entrapment has been utilized in the past with modest results in terms of stabilization [28,34]. However, in previous reports we and others have demonstrated that this type of immobilization technique necessitates tailoring to the particular enzyme and bioconversion for optimal properties of the biocatalyst [13,35]. In order to maximize the stability and enzymatic performance

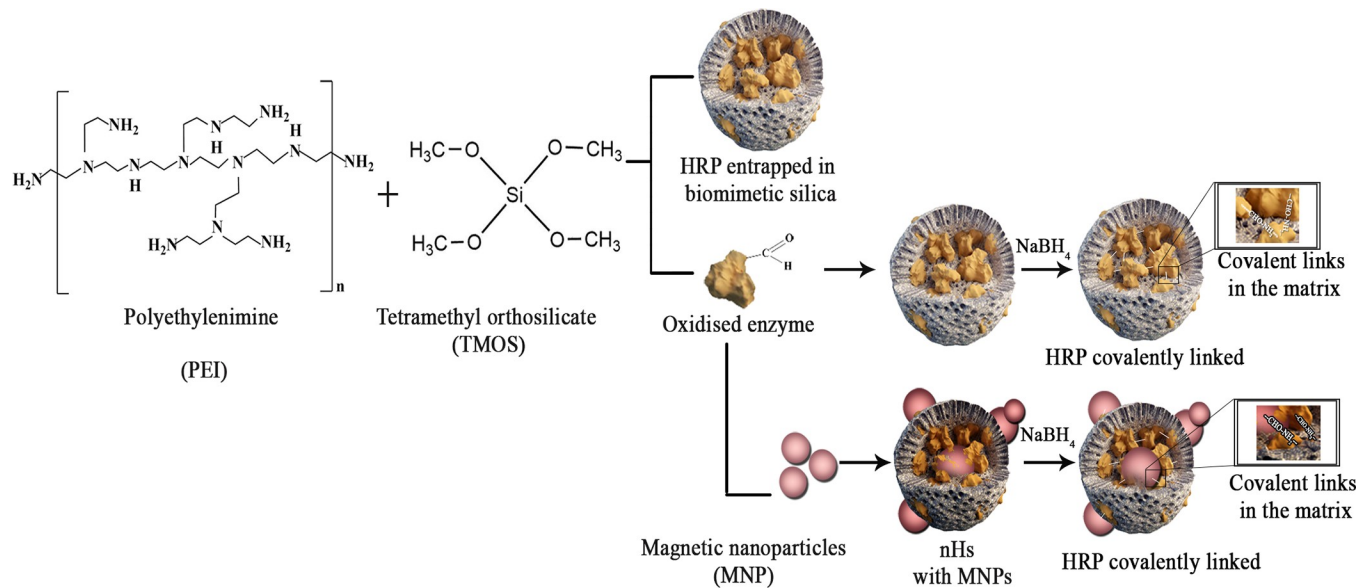


Fig 1. Schematic representation of different synthesis of silica and the co-entrapment of the enzyme with magnetic nanoparticles.

<https://doi.org/10.1371/journal.pone.0214004.g001>

of HRP immobilized preparations, we studied three different configurations of the immobilized enzyme [Fig 1](#).

We first studied the entrapment process of HRP solely in biomimetic Si and the properties of the obtained immobilized preparation. A range of HRP concentrations were used to evaluate the immobilization parameters in silica entrapment and select a minimal amount of enzyme that allowed the preparation of a high specific activity biocatalyst [S1 Table](#). In the light of the results obtained we chose 1 mg/mL HRP concentration for further experiments using different MW polyethylenimine (PEI) as a catalyst for the Si deposition. PEIs with MW of ~ 1300, 2000, 25000 and 60000 were used to study the role of the amine rich catalyst in the nanoparticle synthesis and HRP stabilization. PEI is a polymer containing primary, secondary and tertiary amino groups, having a strong anion exchange capacity under a broad range of conditions, and the capability to chemically react with different chemical groups on either an enzyme or a support. Difference in PEI sizes could not only affect biological aspects of the biocatalyst but also its physicochemical properties [8,36]. Additionally, post immobilization chemical strategies have often improved otherwise unstable immobilized enzyme preparations [37,38]. We therefore attempted to crosslink the enzyme once entrapped within the Si matrix via chemical connection of aldehyde groups of the enzyme to unreacted amino groups of the PEI [Fig 1](#). To the extent of our knowledge, there is no previous report on this approach for HRP immobilization in biomimetic Si nanoparticles (NPs). Considering the degree of glycosylation of this enzyme [39], we performed a standard mild oxidation via NaIO_4 of the enzyme. This treatment generates aldehyde groups on HRP sugar residues that could form Schiff's bases with amino groups of the PEI used as a catalyst for the Si deposition. Similar to the chemistry used to immobilize proteins on glyoxyl activated supports [40], a further reducing step via Na_2BH_4 , would transform the first reversible interaction between the enzyme and the matrix into a three dimensional multiple covalent attachment of HRP within the Si particles [Fig 1](#). The strategy was followed in the presence of trehalose, a common additive used to gain protein stability [12]. A direct correlation between the surface tension of trehalose solutions and the thermal stability of various proteins has been established and it is also known that

trehalose significantly increases the half-life of HRP [5]. No impact was observed in the immobilization percentage (%I) and immobilization yield (%Y) of the preparations after including the trehalose and the reduction step in the preparation of the nanobiocatalyst S2 Table.

Regarding the effect of the different PEI MW, except for the BioSi@T_HRP_PEI_60000, the immobilization percentage (%I) and immobilization yield (%Y) of the different HRP were above 60%. Protein immobilization yield was between 78±2% and 83±4% for all the preparations. The nanohybrid obtained with PEI MW 1300 displayed the higher results for %I and %Y Table 1. This preparation contained 1.33 mg HRP/g of wet support and 1.05 IU/g of wet support.

None of the immobilized preparations obtained showed enzyme leakage as measured in the supernatant of a suspension incubated at 4 °C for 1 month.

When adding MNPs to the synthetic mixture, we observed that for the nanohybrids with PEI MW 60000 there was an increase in the %Y from 33±5% to 57±5%. Probably, at higher PEI MWs a denser cover of Si could affect the partition of substrate/product through the solution thus yielding lower expressed activity of HRP after immobilization. The presence of MNPs could direct a Si deposition in a more compact polymeric shell, reducing mass transfer limitations.

Analysis by SEM showed that when entrapment of HRP using PEI MW 1300 was performed without chemical modification, biomimetic Si formed as preferentially disperse particles with a nanosized diameter range of ~ 300–550 nm with a sharp accumulation of ~ 400 nm diameter particles Fig 2A and 2B. When oxidized HRP was entrapped and the resulting particles submitted to NaBH₄ reduction, biomimetic Si formed as interconnected randomly agglutinated particles of approximately ~ 300–800 nm Fig 2C and 2D. In this case, the Gaussian fitting of the nanoparticle size histogram showed a wider size distribution of the material, demonstrating an effect of the chemical modification of the enzyme on the synthesis of biomimetic silica. The oxidation of enzymatic sugar residues may change the ionization state of the enzyme at pH 8.0 which could alter the Si deposition process. Previous reports have already conferred a fundamental role of the interplay of attractive/repulsive electrostatic interactions during Si synthesis on the particle size and distribution of the material [22,41]. The presence of trehalose during Si synthesis also affected the size distribution of the particles obtained with diameters ranging from 100 to 1000 nm. Moreover, trehalose significantly impacted the homogeneity of the sample Fig 2E and 2F. Given that the amount of protein used in all the entrapment experiments was the same (1 mg/mL), size dispersion can be attributed solely to trehalose. These results corroborate with Rodriguez et al [42] that found that the addition of carbohydrates to standard hydrostatic solutions altered the size of the spherical Si particles obtained from *in vitro* polycationic peptide-mediated biosilicification. Although their findings were obtained after Si precipitation without protein in the synthetic mixture, it became clear that sugar molecules imparted some degree of morphological control on the deposited silica.

Table 1. Immobilization parameters of nanohybrids with different sizes of PEI.

Entrapment	Immobilization (%)	Immobilization yield (%)	Protein immobilization yield (%)
BioSi@T_HRP_1300	60 ± 4	78 ± 1	82±1
BioSi@T_HRP_2000	61 ± 3	77 ± 2	80±2
BioSi@T_HRP_25000	64 ± 2	70 ± 5	77±1
BioSi@T_HRP_60000	70 ± 2	33 ± 5	77±4
BioSi@T_HRP_MNP_1300	83 ± 5	71 ± 2	78±1
BioSi@T_HRP_MNP_2000	76 ± 2	69 ± 4	78±3
BioSi@T_HRP_MNP_25000	77 ± 2	70 ± 5	83±4
BioSi@T_HRP_MNP_60000	69 ± 2	57 ± 5	78±2

<https://doi.org/10.1371/journal.pone.0214004.t001>

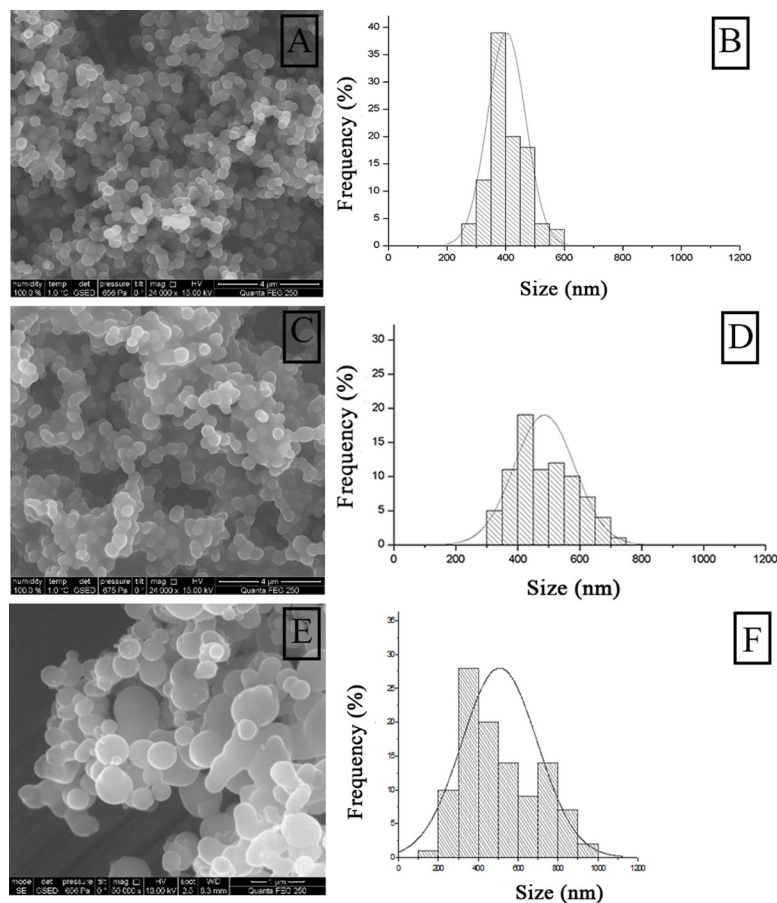


Fig 2. Analysis by scanning electron microscopy (SEM) of nanohybrids using PEI MW 1300. A) BioSi@HRP, C) BioSi@HRPox E) BioSi@T_HRP_1300. B, D y F) correspond to histograms of frequency of particles versus their particle size in each case.

<https://doi.org/10.1371/journal.pone.0214004.g002>

Table 2 shows the results for DLS analysis of the different nanohybrids with and without MNPs. Addition of MNP in the synthetic mixture provided nanohybrids with smaller hydrodynamic sizes making the final diameter of the hybrid independent of the size of the PEI used (~500–600 nm). This correlates with the results obtained for an increase in %Y after addition of MNPs and the analysis by SEM of the samples that included MNPs Fig 3. The samples that included MNPs showed again interconnected particles of a mean diameter of 400–450 nm Fig 3. The particle size distribution has a high dispersity that correlates with increased PDI results Table 2 that did not impact on the activity of the nanobiocatalysts.

Table 2. Dynamic light scattering and net charge analysis of nanohybrids.

Hybrids	Hydrodynamic size (nm)		Poly dispersity index (PDI)		Zeta potential (mV)	
	MNP (-)	MNP (+)	MNP (-)	MNP (+)	MNP (-)	MNP (+)
BioSi@THRP_1300	630 ± 26	684 ± 68	0.199 ± 0.136	0.311 ± 0.03	6.79 ± 0.791	23.4 ± 4.68
BioSi@THRP_2000	815 ± 52	589 ± 28	0.104 ± 0.067	0.321 ± 0.044	6.87 ± 0.701	21.5 ± 4.24
BioSi@THRP_25000	535 ± 23	491 ± 26	0.129 ± 0.063	0.402 ± 0.080	8.31 ± 0.701	11.6 ± 5.46
BioSi@T_HRP_60000	1026 ± 83	543 ± 21	0.207 ± 0.089	0.354 ± 0.059	9.81 ± 1.12	15.5 ± 4.00

<https://doi.org/10.1371/journal.pone.0214004.t002>

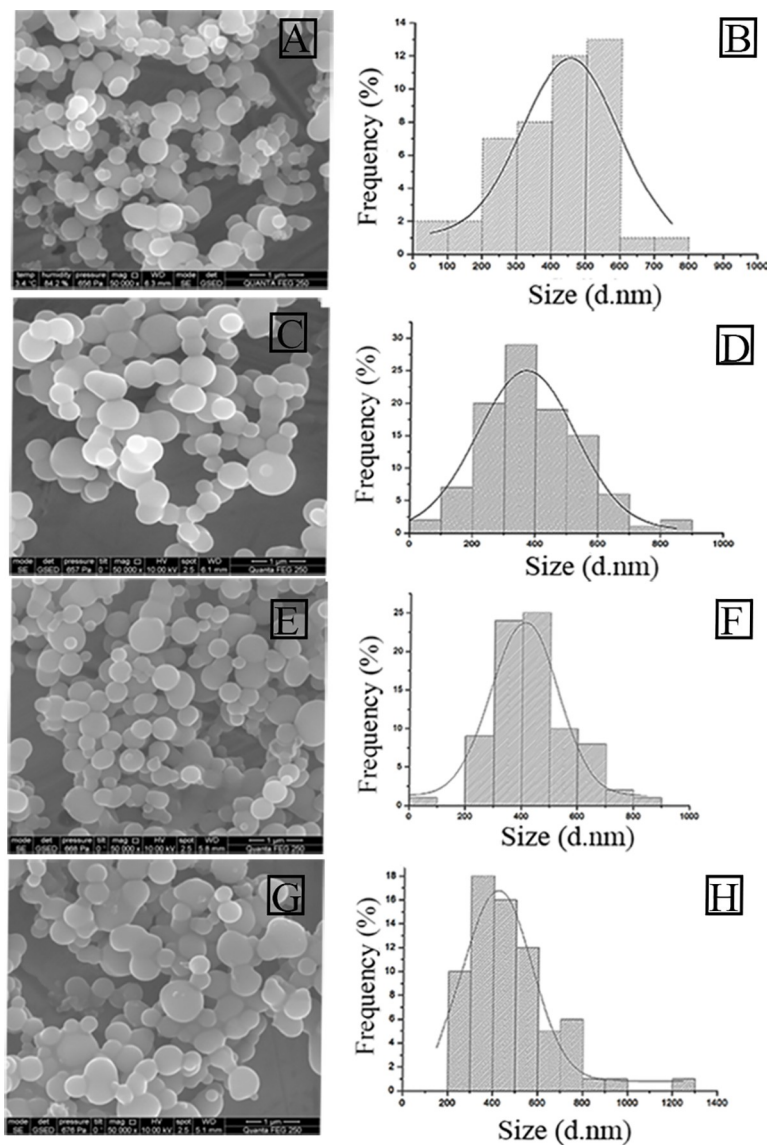


Fig 3. Analysis by SEM of nanohybrids with distinct PEIS. A) BioSi@T_HRP_MNP_1300. C) BioSi@T_HRP_MNP_2000. E) BioSi@T_HRP_MNP_25000 and G) BioSi@T_HRP_MNP_60000. Similarly, B, D, F, H correspond to their histograms analyzed using ImageJ and Origin 8 Pro.

<https://doi.org/10.1371/journal.pone.0214004.g003>

Stabilization of enzymes is a key factor to determine their full potential as biocatalysts. Our studies on thermal stability of the entrapped enzyme demonstrated that, after fitting the experimental data to the exponential model from Henley and Sadana [43], the physically entrapped HRP (BioSi@HRP) had a half-life time of 65.4 min at 50 °C compared to the soluble enzyme that reached 50% of its initial activity after only 2.4 min Fig 4. Thermal stabilization improved considerably after chemical modification of the nanobiocatalysts Fig 4B. When using PEI MW 1300, modified nanoparticles showed a half-life time of 150 min compared to 65.4 min of the unmodified entrapped HRP. The effect of trehalose and the chemical crosslinking on the thermal stability of the immobilized HRP was additive, as the preparation had a stabilization factor (SF) of 176 compared to the soluble HRP Fig 4B. Since the Si NP is a porous material, we excluded the possibility of trehalose leakage by incubating an immobilized preparation in

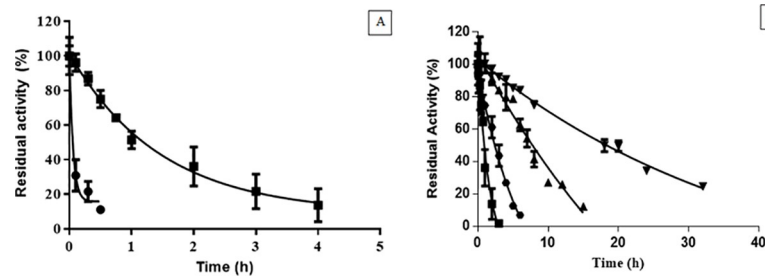


Fig 4. Thermal stability at 50°C of different HRP preparations. A) Soluble enzyme (HRP) (●), BioSi@HRP (■). Aliquots were taken at mentioned time intervals and measured spectrophotometrically at 405nm. The half-lives were determined as 0.04 h and 1.09 h for the soluble and immobilized preparations, respectively. B) Thermal stability of the BioSi@HRP (■), BioSi@HRPox (●), BioSi@T_HRP_1300(▲) and BioSi@T_HRP_MNP_1300 (▼) showing half-lives 1.09 h, 2.5 h, 7.02 h, 21.3 h.

<https://doi.org/10.1371/journal.pone.0214004.g004>

suspension at 4°C for 1 month and determination of reducing sugars in the supernatant. On measurement of the supernatant, no trehalose was detected under these conditions [S3 Table](#). Moreover, a suspension of BioSi@T_HRP_MNP_1300 containing 12.5 IU/mL in sodium phosphate buffer 0.1 M pH 8.0, retained 84%±3 (10.5±0.4 IU/mL) of its initial activity after 6 months of shelf storage at 4°C.

We believe these results demonstrate that a three-dimensional rigidification of the enzyme structure is a determinant factor to a drastic improvement in its stability. Some indications of this effect had been previously obtained by immobilization of enzymes on matrixes modified with polymeric molecules in which it was believed that regions of the biomolecules were embedded within the support, improving their stability [38]. However, an entrapment process assures that most of the enzymatic molecules lay within the matrix which is fundamental to reinforce our three-dimensional stabilization hypothesis.

When stability of nanohybrids including MNPs was studied at 50°C, we observed a 532 SF of the enzyme entrapped in Si with MNPs (BioSi@THRP_MNP_1300) compared to the soluble enzyme [Fig 4B](#).

Considering that the MNPs contain primary amino groups that could further react with the aldehyde generated upon mild oxidation in the HRP, we believe the presence of the MNPs provided an additional source of functional groups for multi-point covalent interaction. Moreover, the MNPs offer a more rigid surface to the enzyme to the flexible Si network formed as a shell of the nanohybrid. This may restrain enzyme distortion and contribute to a greater stabilization.

The nanohybrids with distinct PEIs showed an increase in the half-life similar to nanohybrids with PEI MW 1300 respect to the soluble with an exception of PEI MW 25000 which showed a SF of 20 with respect to the soluble enzyme [Fig 5](#). The branched nature of this PEI amplifies the loading enzyme but could leave the enzyme more exposed to degradation caused by temperature increase [44].

Reports for immobilization and stabilization of HRP are ubiquitous. The majority of these reports include inhouse fabricated supports and conditions for stability evaluation vary extensively. For instance, using commercially available biogenic porous silica, Sahare et al found a SF of 23[45] with an immobilized preparation with similar specific activity to the one used in our work. HRP immobilized onto PVA–PAAm nanofibers was found to retain 64% of its initial activity at 4°C after 55 days which represents a lower storage stability compared to the nanohybrid prepared herein[46]. For each of these examples it is important to highlight that the nature of the support used and the chemistry of HRP immobilization is different for that developed in this work. The different immobilization strategies might better suit precise applications, which eventually will make the stability results relevant.

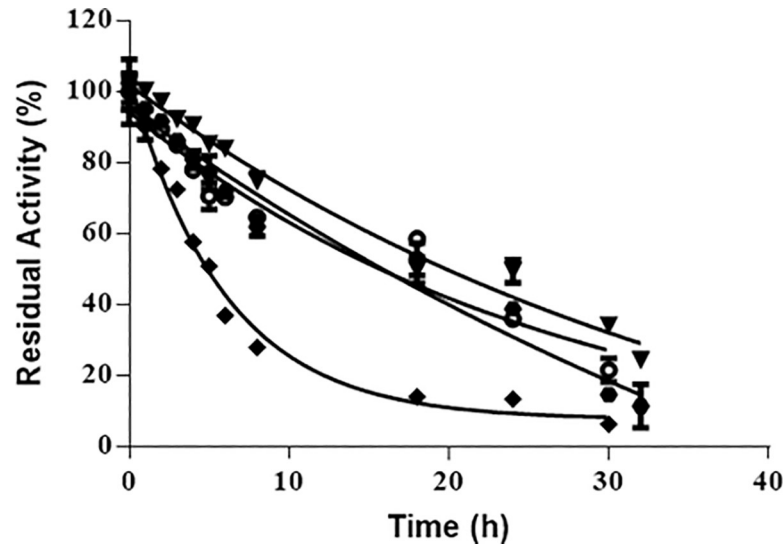


Fig 5. Thermal stability of the enzyme preparations with distinct polyethyleneimines (PEI). (BioSi@T_HRP_MNP_1300 (▼), BioSi@T_HRP_MNP_2000 (●), BioSi@T_HRP_MNP_25 000 (◆), BioSi@T_HRP_MNP_60 000 (○) entrapped in silica with a magnetic core. The half-lives were determined as 21 h, 20 h, 8 h, 22 h, respectively.

<https://doi.org/10.1371/journal.pone.0214004.g005>

We have selected BioSi@THRP_MNP_PEI_1300 for further experiments, under the premise that it was the most thermostable preparation obtained in our work with higher %Y and % I. We have studied the remaining activities of HRP preparations after 1 hour of incubation in several pHs [S1 Fig](#). pH stability often restrains the applicability of enzymatic preparations as it may have a profound impact on the loss of structural integrity of many proteins. Our results demonstrate that the nanohybrids were more stable under acidic pH. There was no observed effect of the MNPS on the pH stability. Additionally, no loss of integrity of the NPs was observed after 1 hour of incubation at the different pHs.

Optimal pH and optimal temperature of HRP did not change upon integration of the enzyme in the nanohybrids [S2A and S2B Fig](#).

It was important to demonstrate that after the Si modification, the nanohybrids maintained their superparamagnetic properties. [Fig 6](#) shows the field dependent magnetization of the BioSi@THRP_MNP_1300 at 300 K. The sample displayed superparamagnetic behaviour with negligible coercivity at zero field.

Operational stability of the BioSi@THRP_MNP_1300 was also assessed after several enzymatic cycles using the chromogenic substrate ABTS and hydrogen peroxide. In all studied cycles, the immobilized enzyme was magnetically separated and was assessed for its remnant catalytic activity. After 5 reuses the nanohybrids maintained 30% of its initial activity [Fig 7](#).

As a proof of its utility in a biotechnological relevant biotransformation, we studied the oxidation of 3-IAA. This non-toxic plant hormone has been examined as a prodrug candidate as, upon transformation to its oxidized species, it induces cellular apoptosis in cancerous lines. HRP has been proposed as oxidizing enzyme of this compound for the so-called direct enzyme prodrug therapy. The biocatalytic performance of the BioSi@THRP_MNP_1300 was tested in batch conversion of 3-IAA into its oxidized species. HPLC elution profiles showed that the nanohybrids catalysed the complete oxidation of a 500 mM prodrug solution within 30 min of reaction with the generation of at least five oxidized products [Fig 8A and 8B](#).

The major product is expected to be oxindol-3-yl carbinol for its distinctive spectra and matching retention time from previous works using the same HPLC analysis conditions. This

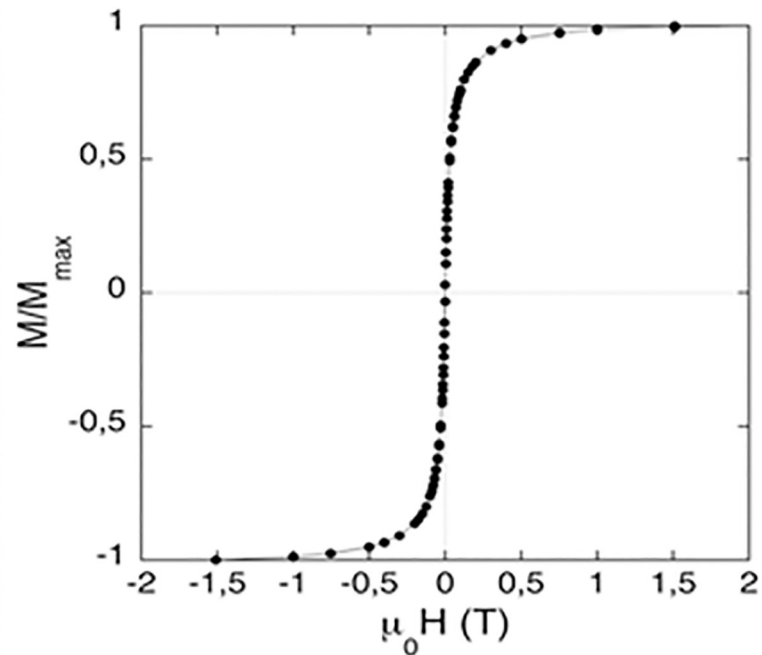


Fig 6. Field dependent magnetization of BioSi@T_HRP_MNP_1300. The measurements are shown at 300 K after diamagnetic correction.

<https://doi.org/10.1371/journal.pone.0214004.g006>

type of immobilized biocatalyst could be potentially applied to biotransformations such as *in situ* clean-up of contaminated environments [47,48], lignin polymerization for hydrophobicity enhancement of fibres [49] or other polymerization reactions applied in pharmaceuticals [50].

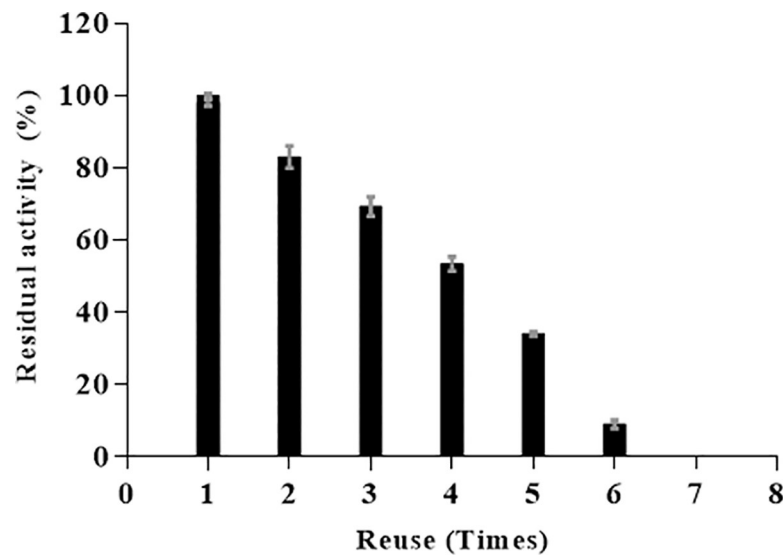


Fig 7. Operational stability of BioSi@T_HRP_MNP_1300. Residual enzyme activity after 6 reuses with substrates (ABTS and H₂O₂) and separation using a magnetic separator.

<https://doi.org/10.1371/journal.pone.0214004.g007>

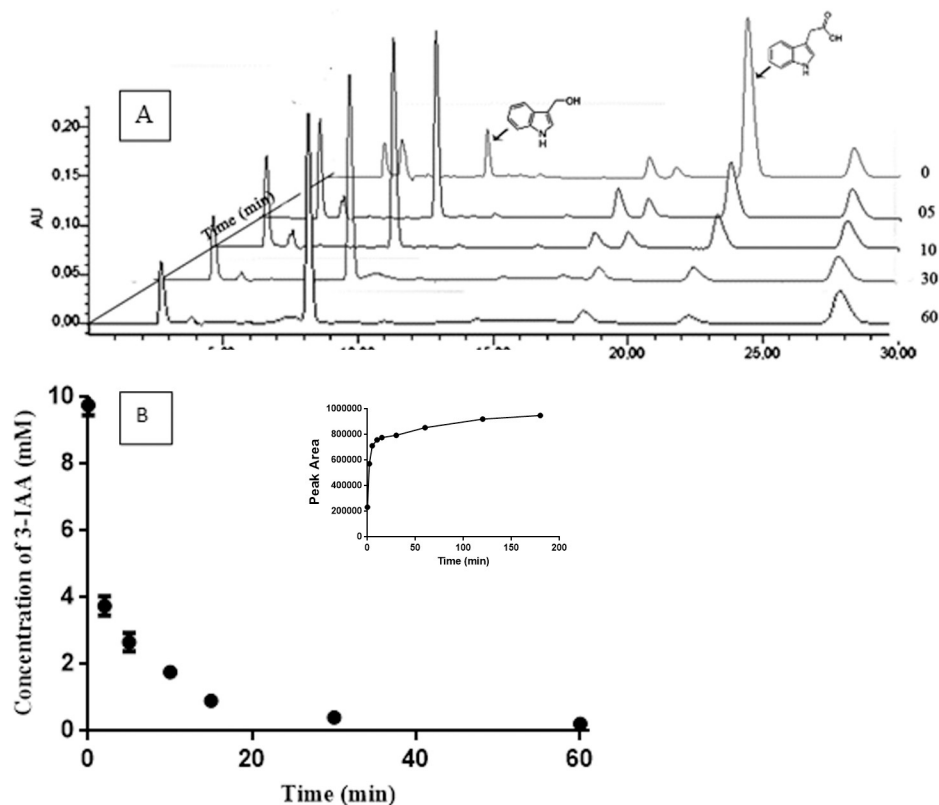


Fig 8. Oxidation of 3-IAA by the nanohybrids. A) Conversion of 3-IAA by nanohybrids BioSi@T_HRP_MNP_1300 at different intervals of time B) Conversion kinetic of 3-IAA by the nanohybrids. Reactions were carried at 25°C using 1 UI in a 100 mM sodium acetate buffer at pH 5.0 containing 500 mM of 3-IAA. Further details are described in Methods. Inset- Increment in the concentration (area) of the radical 3-ox-indol-carbinol.

<https://doi.org/10.1371/journal.pone.0214004.g008>

Anticipating a possible biomedical application of the HRP entrapped nanomaterial produced herein, we further investigated its cytotoxicity towards the model colorectal cancer cell line HCT 116 (ATCC) (Fig 9A and 9B). NPs may cause adverse health effects resulting from damage to membranes, changes in protein folding, DNA mutation, blood abnormalities and oxidative stress injuries. Measurements of cell viability and proliferation can provide an indication of the safety of nanomaterials.

The results show that after 6 hours in PBS, BioSi@THRP_MNP_PEI_1300 is well tolerated by the cells as not more than ~15% growth inhibition is observed in a range of concentrations of 5, 10 and 20 $\mu\text{g}/\text{mL}$. Besides, when incubating the cells solely with the free enzyme or with the prodrug no cytotoxicity effect was observed. However, cell death was observed when 3-IAA and nanohybrids were co-incubated with the cells. Increasing amounts of enzyme units (0.5–2 IU/mL) in the assay showed a correlated decrease in cell viability demonstrating that the optimized nanohybrid is efficient in the generation of toxic radicals. We can also see in the results that the two prodrug concentrations selected resulted in very similar cell viability values.

It is worth noting that the soluble enzyme showed a greater cytotoxic effect in the presence of the prodrug in comparison to the immobilized one, as it is free and easily available for the oxidation of the prodrug. The rate of conversion is slower in the nanohybrids as the substrate had to traverse through the Si matrix to access the enzyme entrapped thus decreasing the rapid conversion of the radicals in the assay. However, we have demonstrated that integration of the

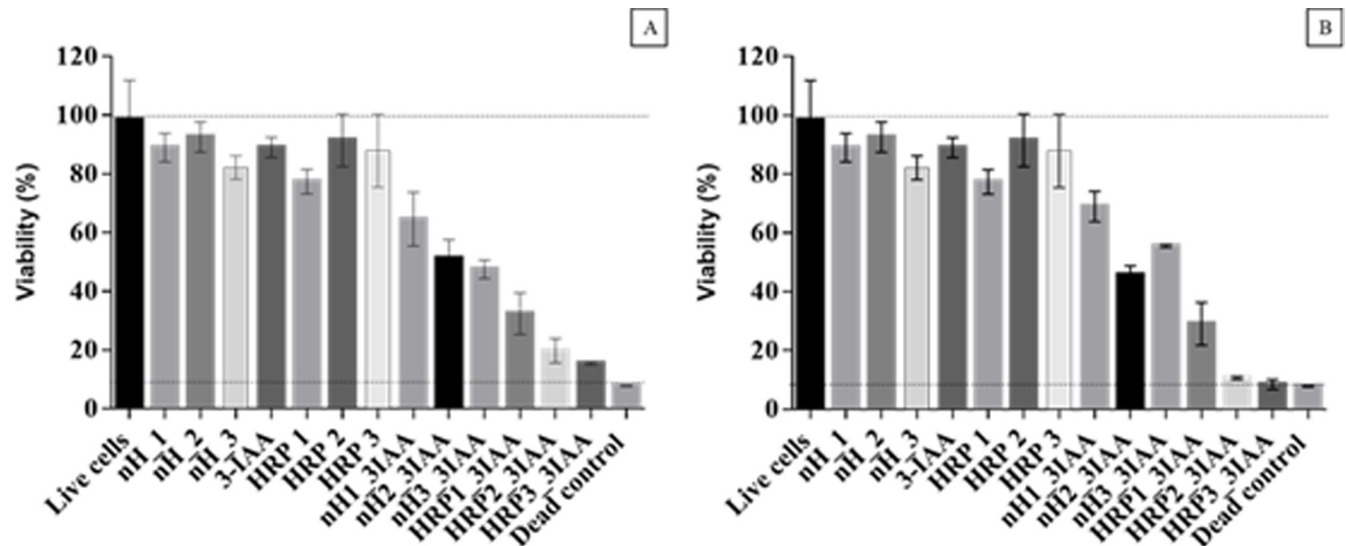


Fig 9. Effect of nanohybrids (BioSi@T_HRP_1300_MNP) on HCT 116 (ATCC) cell viability. Cytotoxicity studies using MTT were assayed. Cells were incubated for 6 h in PBS with concentrations of nanohybrids (0.5, 1 and 2 IU of Enzyme) and concentrations of prodrug 1 mM and 2mM. A) Corresponds to the data normalized against live control (cells with DMEM 10% FBS, considered as 100%) for an assay using 1 mM of 3-IAA. B) Corresponds to the data normalized against live control (cells with DMEM 10% FBS, considered as 100%) for an assay using 2 mM of 3-IAA. Results were expressed as the mean \pm SD of triplicates of a representative experiment. Live cells: Control of live cells, nH_1/2/3: control of nanohybrid at 5, 10, 20 μ g/mL containing 0.5, 1 and 2 IU/mL respectively, 3-IAA: Control of prodrug with concentrations of 1 and 2 mM, HRP1/2/3 ctrl: control with soluble enzyme at 0.5, 1 and 2 IU/mL; nH_1/2/3_3IAA: nanohybrids and prodrug combinations; HRP 1/2/3_3IAA: reaction mixture with soluble enzyme and prodrug combinations.

<https://doi.org/10.1371/journal.pone.0214004.g009>

enzyme in the composite material provided advantageous properties that counterbalance any decrease in the conversion rate of the prodrug 3-IAA.

Although extensive analysis is necessary to fully understand nanomaterials toxic effects, the results of MTT in this work confirmed the utility of BioSi@THRP_MNP_PEI_1300 in directed enzyme prodrug therapy (DEPT), which encourages further investigations into *in vitro* and *in vivo* effects of the material.

Conclusions

In this work we have prepared a new nanosized hybrid material that combined MNPs, biometric silica and the enzyme HRP. The diameter and polydispersity of the *in situ* prepared nanoparticles demonstrated a dependence on the size of the aminated polymer PEI used to deposit the siliceous material and the addition of the magnetic nanoparticles during synthesis. Addition of the disaccharide trehalose and a post immobilization chemical modification of the organic/inorganic material provided exceptional stability to the enzyme without compromising its activity. In fact, the immobilized enzyme showed a significantly higher thermal stabilization factor compared with previous reports for HRP [51,52]. The superparamagnetic properties of the nanohybrid facilitated its separation in repeated batch transformations of a synthetic substrate. Our findings demonstrate that the material is not cytotoxic while it enabled the cytotoxicity of cancerous cells upon transformation of the prodrug 3-IAA. In summary, the unprecedented approach for the preparation of a nanohybrid biocatalyst provided excellent properties that could enable a range of potential applications. Further experiments on conversion of alternate substrates of immobilized HRP will broaden the range of applications of the system. Moreover, the cytotoxic studies carried out with the nanohybrid prepared herein encourages additional experimentation for a better insight into its biomedical potential.

Supporting information

S1 Table. Entrapment of different concentrations of soluble HRP in biomimetic silica nanoparticles.

(DOCX)

S2 Table. Immobilization parameters of nHs with different immobilization strategies.

(DOCX)

S3 Table. Determination of Trehalose via DNS assay.

(DOCX)

S1 Fig. pH stability of different HRP preparations. pH stability of the enzyme preparations: soluble enzyme (black), BioSi@HRPox (gray), BioSi@T_HRP_MNP_1300 (white).

(TIF)

S2 Fig. Temperature profile of different HRP preparations. A) Optimal temperature of the enzyme preparations: soluble enzyme (black), BioSi@HRPox (gray), BioSi@T_HRP_MNP_1300 (white). B) Thermal stability of the enzyme preparations: soluble enzyme (black), BioSi@HRPox (gray), BioSi@T_HRP_MNP_1300 (white).

(TIF)

Acknowledgments

LB and SC acknowledge PEDECIBA Química, ANII and Universidad ORT Uruguay. We thank TD for helpful insight in the discussion of the results and Rodrigo Mila for help with the graphical abstract. The authors would like to acknowledge the use of Servicio General de Apoyo a la Investigación-SAI, Universidad de Zaragoza.

Author Contributions

Conceptualization: Valeria Grazú, Lorena Betancor.

Formal analysis: Sonali Correa, Laura Asín, Jesús Martínez de la Fuente.

Funding acquisition: Jesús Martínez de la Fuente, Valeria Grazú, Lorena Betancor.

Investigation: Sonali Correa, Sara Puertas, Lucía Gutiérrez, Laura Asín.

Methodology: Lorena Betancor.

Resources: Jesús Martínez de la Fuente.

Supervision: Lorena Betancor.

Validation: Sonali Correa, Sara Puertas, Lucía Gutiérrez.

Visualization: Sonali Correa.

Writing – original draft: Lorena Betancor.

Writing – review & editing: Valeria Grazú.

References

1. Sipponen MH, Farooq M, Koivisto J, Pellis A, Seitsonen J, Österberg M. Spatially confined lignin nanoparticles for biocatalytic ester synthesis in aqueous media. *Nat Commun*. Springer US;: 1–7. <https://doi.org/10.1038/s41467-018-04715-6> PMID: 29895870
2. Jackson E, Lopez FG, Guisan JM, Betancor L. Enhanced stability of l-lactate dehydrogenase through immobilization engineering. *Process Biochem*. 2016; <https://doi.org/10.1016/j.procbio.2016.03.002>

3. Romero-Fernández M, Moreno-Perez S, H. Orrego A, Martins de Oliveira S, I. Santamaría R, Díaz M, et al. Designing continuous flow reaction of xylan hydrolysis for xylooligosaccharides production in packed-bed reactors using xylanase immobilized on methacrylic polymer-based supports. *Bioresour Technol*. Elsevier; 2018; 266: 249–258. <https://doi.org/10.1016/j.biortech.2018.06.070> PMID: 29982045
4. Pavlovic M, Rouster P, Somosi Z, Szilagyi I. Horseradish peroxidase-nanoclay hybrid particles of high functional and colloidal stability. *J Colloid Interface Sci*. Elsevier Inc.; 2018; 524: 114–121. <https://doi.org/10.1016/j.jcis.2018.04.007> PMID: 29635084
5. Sharma SK, Leblanc RM. Biosensors based on β -galactosidase enzyme: Recent advances and perspectives. *Anal Biochem*. Elsevier Inc.; 2017; 535: 1–11. <https://doi.org/10.1016/j.ab.2017.07.019> PMID: 28735682
6. Rakhi RB, Nayuk P, Xia C, Alshareef HN. Novel amperometric glucose biosensor based on MXene nanocomposite. *Sci Rep*. Nature Publishing Group; 2016; 6: 1–10. <https://doi.org/10.1038/s41598-016-0001-8>
7. Consolati T, Bolivar JM, Petrasek Z, Berenguer J, Hidalgo A, Guisán JM, et al. Biobased, Internally pH-Sensitive Materials: Immobilized Yellow Fluorescent Protein as an Optical Sensor for Spatiotemporal Mapping of pH Inside Porous Matrices. *ACS Appl Mater Interfaces*. 2018; 10: 6858–6868. <https://doi.org/10.1021/acsami.7b16639> PMID: 29384355
8. Berne C, Betancor L, Luckarift HR, Spain JC. Application of a microfluidic reactor for screening cancer prodrug activation using silica-immobilized nitrobenzene nitroreductase. *Biomacromolecules*. 2006; 7: 2631–2636. <https://doi.org/10.1021/bm060166d> PMID: 16961327
9. Bolivar JM, Nidetzky B. Multiphase biotransformations in microstructured reactors: opportunities for biocatalytic process intensification and smart flow processing. *Green Process Synth*. 2013; 2. <https://doi.org/10.1515/gps-2013-0091>
10. Maximov V, Reukov V, Vertegel AA. Targeted delivery of therapeutic enzymes. *J Drug Deliv Sci Technol*. Elsevier Masson SAS; 2009; 19: 311–320. [https://doi.org/10.1016/S1773-2247\(09\)50066-4](https://doi.org/10.1016/S1773-2247(09)50066-4)
11. Fejerskov B, Jarlstad Olesen MT, Zelikin AN. Substrate mediated enzyme prodrug therapy. *Adv Drug Deliv Rev*. Elsevier B.V.; 2017; 118: 24–34. <https://doi.org/10.1016/j.addr.2017.04.013> PMID: 28457884
12. Jackson E, López-Gallego F, Guisán JM, Betancor L. Enhanced stability of l-lactate dehydrogenase through immobilization engineering. *Process Biochem*. 2016; <https://doi.org/10.1016/j.procbio.2016.03.002>
13. Cazaban D, Wilson L, Betancor L. Lipase Immobilization on Siliceous Supports: Application to Synthetic Reactions. *Curr Org Chem*. 2017; 21: 85–92. <https://doi.org/10.2174/1385272821666161108103>
14. Guisán JM. New opportunities for immobilization of enzymes. *Methods Mol Biol*. 2013; 1051: 1–13. https://doi.org/10.1007/978-1-62703-550-7_1 PMID: 23934794
15. Zdarta J, Meyer A, Jesionowski T, Pinelo M. A General Overview of Support Materials for Enzyme Immobilization: Characteristics, Properties, Practical Utility. *Catalysts*. 2018; 8: 92. <https://doi.org/10.3390/catal8020092>
16. Ribeiro LMO, Falleiros LNSS, de Resende MM, Ribeiro EJ, Almeida RMRG, da Silva AOS. Immobilization of the enzyme invertase in SBA-15 with surfaces functionalized by different organic compounds. *J Porous Mater*. Springer US; 2018; <https://doi.org/10.1007/s10934-018-0615-2>
17. Karthikeyan S, Kurt Z, Pandey G, Spain JC. Immobilized Biocatalyst for Detection and Destruction of the Insensitive Explosive, 2,4-Dinitroanisole (DNAN). *Environ Sci Technol*. 2016; 50: 11193–11199. <https://doi.org/10.1021/acs.est.6b03044> PMID: 27617621
18. Cao S-L, Li X-H, Lou W-Y, Zong M-H. Preparation of a novel magnetic cellulose nanocrystal and its efficient use for enzyme immobilization. *J Mater Chem B*. 2014; 2: 5522–5530. <https://doi.org/10.1039/C4TB00584H>
19. Betancor L, Luckarift HR. Bioinspired enzyme encapsulation for biocatalysis. *Trends Biotechnol*. Elsevier; 2008; 26: 566–72. Available: <http://www.cell.com/article/S016779908001972/fulltext> <https://doi.org/10.1016/j.tibtech.2008.06.009> PMID: 18757108
20. Johnson GR, Luckarift HR. Enzyme stabilization via bio-templated silicification reactions. *Methods in Molecular Biology*. 2017. https://doi.org/10.1007/978-1-4939-6499-4_6
21. Jackson E, Ferrari M, Cuestas-Ayllon C, Fernández-Pacheco R, Perez-Carvajal J, De La Fuente JM, et al. Protein-templated biomimetic silica nanoparticles. *Langmuir*. 2015; 31: 3687–3695. <https://doi.org/10.1021/la504978r> PMID: 25741589
22. Lechner C, Becker C. Silaffins in Silica Biomineralization and Biomimetic Silica Precipitation. *Mar Drugs*. 2015; 13: 5297–5333. <https://doi.org/10.3390/md13085297> PMID: 26295401

23. Liu J, Yang Q, Li C. Towards efficient chemical synthesis via engineering enzyme catalysis in biometric nanoreactors. *Chem Commun*. 2015; 51: 13731–13739. <https://doi.org/10.1039/C5CC04590H> PMID: 26208044
24. Johnson GR, Luckariff HR. Enzyme stabilization via bio-templated silicification reactions. *Methods in Molecular Biology*. 2017. https://doi.org/10.1007/978-1-4939-6499-4_6 PMID: 27770414
25. Betancor L, Berne C, Luckariff HR, Spain JC. Coimmobilization of a redox enzyme and a cofactor regeneration system. *Chem Commun (Camb)*. 2006; 3640–3642. <https://doi.org/10.1039/b604689d> PMID: 17047791
26. Seo JH, Betancor L, Demirci KS, Byun A, Spain J, Brand O. Liquid-phase biochemical sensing with disk-type resonant microsensors. *TRANSDUCERS and EUROSensors '07 - 4th International Conference on Solid-State Sensors, Actuators and Microsystems*. 2007. <https://doi.org/10.1109/SENSOR.2007.4300488>
27. Krainer FW, Glieder A. An updated view on horseradish peroxidases: recombinant production and biotechnological applications. *Appl Microbiol Biotechnol*. 2015; 99: 1611–1625. <https://doi.org/10.1007/s00253-014-6346-7> PMID: 25575885
28. Chiu YR, Ho WJ, Chao JS, Yuan CJ. Enzyme-encapsulated silica nanoparticle for cancer chemotherapy. *J Nanoparticle Res*. 2012; 14: 1–10. <https://doi.org/10.1007/s11051-012-0829-1>
29. Nanayakkara S, Zhao Z, Patti AF, He L, Saito K. Immobilized horseradish peroxidase (I-HRP) as biocatalyst for oxidative polymerization of 2,6-dimethylphenol. *ACS Sustain Chem Eng*. 2014; 2: 1947–1950. <https://doi.org/10.1021/sc500392k>
30. Ritter DW, Roberts JR, McShane MJ. Glycosylation site-targeted PEGylation of glucose oxidase retains native enzymatic activity. *Enzyme Microb Technol*. Elsevier Inc.; 2013; 52: 279–285. <https://doi.org/10.1016/j.enzmictec.2013.01.004> PMID: 23540931
31. Henley JP, Sadana A. Categorization of enzyme deactivations using a series-type mechanism. *Enzyme Microb Technol*. 1985; 7: 50–60. Available: <http://www.sciencedirect.com/science/article/pii/S0141022985900134>
32. Makizumi R, Yang WL, Owen RP, Sharma RR, Ravikumar TS. Alteration of Drug Sensitivity in Human Colon Cancer Cells after Exposure to Heat: Implications for Liver Metastasis Therapy using RFA and Chemotherapy. *Int J Clin Exp Med*. 2008; 1: 117–129. PMID: 19079666
33. Betancor L, Luckariff H. Co-immobilized coupled enzyme systems in biotechnology. *Biotechnol Genet Eng Rev*. 2010; 27: 95–114. PMID: 21415894
34. Zamora P, Narváez A, Domínguez E. Enzyme-modified nanoparticles using biomimetically synthesized silica. *Bioelectrochemistry*. Elsevier B.V.; 2009; 76: 100–106. <https://doi.org/10.1016/j.bioelechem.2009.05.006> PMID: 19540173
35. Cui J, Liang L, Han C, Lin Liu R. Stabilization of Phenylalanine Ammonia Lyase from *Rhodotorula glutinis* by Encapsulation in Polyethyleneimine-Mediated Biomimetic Silica. *Appl Biochem Biotechnol*. 2015; 176: 999–1011. <https://doi.org/10.1007/s12010-015-1624-0> PMID: 25906687
36. Bahulekar R, Ayyangar NR, Ponrathnam S. Polyethyleneimine in immobilization of biocatalysts. *Enzyme Microb Technol*. 1991; 13: 858–868. [https://doi.org/10.1016/0141-0229\(91\)90101-F](https://doi.org/10.1016/0141-0229(91)90101-F) PMID: 1367996
37. Palomo JM, Filice M, Romero O, Guisan JM. Improving lipase activity by immobilization and post-immobilization strategies. *Humana Press Inc.*; 2013; 1051: 255–273. https://doi.org/10.1007/978-1-62703-550-7_17 PMID: 23934810
38. Lopez-Gallego F, Betancor L, Hidalgo A, Dellamora-Ortiz G, Mateo C, Fernández-Lafuente R, et al. Stabilization of different alcohol oxidases via immobilization and post immobilization techniques. 2007; 40: 278–284. <https://doi.org/10.1016/j.enzmictec.2006.04.021>
39. Zakharova GS, Uporov I V., Tishkov VI. Horseradish peroxidase: Modulation of properties by chemical modification of protein and heme. *Biochem*. 2011; 76: 1391–1401. <https://doi.org/10.1134/S0006297911130037> PMID: 22339595
40. Ramírez Tapias YA, Rivero CW, Gallego FL, Guisán JM, Trelles JA. Stabilization by multipoint covalent attachment of a biocatalyst with polygalacturonase activity used for juice clarification. *Food Chem*. 2016; 208: 252–257. <https://doi.org/10.1016/j.foodchem.2016.03.086> PMID: 27132847
41. Hyde EDER, Seyfaee A, Neville F, Moreno-Atanasio R. Colloidal Silica Particle Synthesis and Future Industrial Manufacturing Pathways: A Review. *Ind Eng Chem Res*. 2016; 55: 8891–8913. <https://doi.org/10.1021/acs.iecr.6b01839>
42. Rodríguez F, Glawe DD, Naik RR, Hallinan KP, Stone MO. Study of the chemical and physical influences upon in vitro peptide-mediated silica formation. *Biomacromolecules*. 2004; 5: 261–265. <https://doi.org/10.1021/bm034232c> PMID: 15002982

43. Henley JP, Sadana A. Categorization of enzyme deactivations using a series-type mechanism. *Enzyme Microb Technol.* 1985; 7: 50–60.
44. Lungu CN, Diudea M V, Putz M V, Grudziński IP. Linear and Branched PEIs (Polyethylenimines) and Their Property Space. *Int J Mol Sci. Multidisciplinary Digital Publishing Institute (MDPI)*; 2016; 17: 555. <https://doi.org/10.3390/ijms17040555> PMID: 27089324
45. Sahare P, Ayala M, Vazquez-Duhalt R, Pal U, Loni A, Canham LT, et al. Enhancement of Peroxidase Stability Against Oxidative Self-Inactivation by Co-immobilization with a Redox-Active Protein in Mesoporous Silicon and Silica Microparticles. *Nanoscale Res Lett.* 2016; 11. <https://doi.org/10.1186/s11671-016-1605-4> PMID: 27650291
46. Temoçin Z, İnal M, Gökğöz M, Yiğitoğlu M. Immobilization of horseradish peroxidase on electrospun poly(vinyl alcohol)–polyacrylamide blend nanofiber membrane and its use in the conversion of phenol. *Polym Bull.* 2018; 75: 1843–1865. <https://doi.org/10.1007/s00289-017-2129-5>
47. Jiang Y, Tang W, Gao J, Zhou L, He Y. Immobilization of horseradish peroxidase in phospholipid-templated titania and its applications in phenolic compounds and dye removal. *Enzyme Microb Technol.* Elsevier Inc.; 2014; 55: 1–6. <https://doi.org/10.1016/j.enzmictec.2013.11.005> PMID: 24411438
48. Wang M, Abad D, Kickhoefer VA, Rome LH, Mahendra S. Vault Nanoparticles Packaged with Enzymes as an Efficient Pollutant Biodegradation Technology. *ACS Nano.* 2015; 9: 10931–10940. <https://doi.org/10.1021/acsnano.5b04073> PMID: 26493711
49. Liu R, Dong A, Fan X, Yu Y, Yuan J, Wang P, et al. Enzymatic Hydrophobic Modification of Jute Fibers via Grafting to Reinforce Composites. *Appl Biochem Biotechnol.* 2016; 178: 1612–1629. <https://doi.org/10.1007/s12010-015-1971-x> PMID: 26754422
50. Lončar N, Fraaije MW. Catalases as biocatalysts in technical applications: current state and perspectives. *Appl Microbiol Biotechnol.* 2015; 99: 3351–3357. <https://doi.org/10.1007/s00253-015-6512-6> PMID: 25761626
51. Sahare P, Ayala M, Vazquez-Duhalt R, Agrawal V. Immobilization of peroxidase enzyme onto the porous silicon structure for enhancing its activity and stability. *Nanoscale Res Lett.* 2014; 9: 1–9. <https://doi.org/10.1186/1556-276X-9-1>
52. Wu C, Böttcher C, Haag R. Enzymatically crosslinked dendritic polyglycerol nanogels for encapsulation of catalytically active proteins. *Soft Matter.* 2015; 11: 972–980. <https://doi.org/10.1039/c4sm01746c> PMID: 25519490



Cellulose-Based Nanosupports for Enzyme Immobilization

41

Erienne Jackson, Sonali Correa, and Lorena Betancor

Contents

1	Introduction	1236
2	Cellulose Architectures for Enzyme Immobilization	1237
2.1	Natural Cellulose Supports for Enzyme Immobilization	1237
2.2	Microfibrillated Cellulose	1238
2.3	Cellulose Nanocrystals	1238
2.4	Bacterial Cellulose Nanosupports	1239
2.5	Electrospun Cellulose	1239
2.6	Synthetic Supports	1241
3	Strategies for the Immobilization of Enzymes in Cellulose-Based Nanocarriers	1241
3.1	Immobilization by Cross-Linking	1241
3.2	Immobilization by Physical Adsorption	1243
3.3	Covalent Immobilization	1244
3.4	Combined Strategies	1245
3.5	Immobilization by Entrapment	1247
4	Cellulose-Based Nanobiocatalysts at Work	1247
4.1	Biomedical Applications	1247
4.2	Food Applications	1249
4.3	Environmental Applications	1249
5	Conclusion	1250
	References	1250

Abstract

Integration of biocatalysts and nanoscale materials offer multiple advantages over micro-scaled heterogeneous biocatalysts. Apart from providing reusability and sustainability of the enzyme, the use of nanosupports is aimed at increasing

E. Jackson · S. Correa · L. Betancor (✉)
Laboratorio de Biotecnología, Facultad de Ingeniería, Universidad ORT Uruguay,
Montevideo, Uruguay
e-mail: betancor@ort.edu.uy

© Springer Nature Switzerland AG 2019
Md. I. H. Mondal (ed.), *Cellulose-Based Superabsorbent Hydrogels*,
Polymers and Polymeric Composites: A Reference Series,
https://doi.org/10.1007/978-3-319-77830-3_42

1235

the surface area available for biocatalyst immobilization and improving the yields in bioconversions through better biocatalyst mobility and less diffusional problems. Among many nanomaterials for enzyme immobilization, cellulose stands out as biocompatible, biodegradable, and environmentally-friendly regarding its biological source. In this chapter, we discuss the steady advancement in utilizing different nanostructured cellulosic materials for enzyme immobilization. We address the use of hybrid materials that include cellulose and improve the properties of the heterogeneous biocatalyst. The methodologies for functionalization and integration of enzymes on nanocellulose hydrogels are discussed including covalent linkage through chemical modification, entrapment, and cross-linking. We consider its applications to biomedicine, food industry, and environmental science with a special emphasis on the impact of the enzymatic properties caused after immobilization on cellulosic supports.

Keywords

Enzyme immobilization · Cellulose · Nanosupports · Biocatalysis · Nanobiotechnology

1 Introduction

Nanobiocatalysis is a new frontier of emerging nanosized material supports in enzyme immobilization application. Enzymes are remarkable biocatalysts and have been used in biotechnology for many years because of their interesting characteristics such as substrate and product specificity, ease of preparation, and ability to function under mild conditions with no toxic by-products for more environmentally-friendly conversions.

Enzyme association to insoluble materials, commonly known as enzyme immobilization, provides a number of advantages to the applied use of enzymes: immobilized enzymes can be reused, minimizes costs and time of analysis, facilitates the continuous use of the biocatalyst, and may improve enzyme properties such as operational or thermal stability [1, 2]. A wide variety of techniques are now available for the preparation of immobilized enzymes that may include chemical or physical mechanisms, addition of aiding agents during immobilization, or combination of different strategies to obtain more active and stable preparations. Moreover, investigations on material science have contributed with a plethora of new supports compatible with enzyme activity and better physical and mechanical properties. Such is the case of nanosupports, rapidly adopted for enzyme immobilization, as they reduce diffusion limitations and maximize the functional surface area to increase enzyme loading. Active immobilized enzymes in nanomaterials, also known as nanobiocatalysts, have been studied for a wide variety of applications [3].

Cellulose, as a natural polymer resource is abundant, renewable, and biocompatible and has gained interest due to its optical, mechanical, chemical, and rheological properties that make it suitable for materials applications, actuators/sensors, drug delivery systems, biomedical science, and biotransformations [4]. As it is produced

from plants and bacteria, the nature of its structure varies and offers numerous possibilities for the attachment of enzymatic molecules and functionalization with non-natural reactive groups which further expands the possibility of associating biocatalysts to its structure. It was only in the last 10 years that researchers were able to develop and study strategies for the preparation of cellulose-based nanostructures. These studies have rampaged from a mere 4 articles in 2006 and 2007 related to “nanocellulose” to 365 articles published in 2016 (source Scopus). The recent interest on these materials is not fortuitous but the result of a slow unveiling of the opportunities that this material has on biotechnological applications. It is therefore timely to revise the piled evidence of nanocellulose materials that have been used in the immobilization of enzymes, the different methodological approaches to obtain them and their suitability for biocatalytic applications with a view of the future impact of these composites in biocatalysis.

2 Cellulose Architectures for Enzyme Immobilization

There are a number of cellulose nanostructures able to support enzyme immobilization: cellulose nanofibers (CNF), which can be electrospun, microfibrillated cellulose (MFC), nanocrystalline cellulose (CNC), or bacterial nanocellulose (BC). CNF can be produced from both cellulose I source, such as wood fibers, cotton, and agricultural crops, and cellulose II source, such as lyocell fibers using various techniques such as grinding, high-pressure homogenization, and sonication. There are four different polymorphs of cellulose: cellulose I, II, III, and IV. Cellulose I, native cellulose, is the form found in nature, and it occurs in two allomorphs, I α and I β . Cellulose II, or regenerated cellulose, the most stable crystalline form, emerges after recrystallization or mercerization with aqueous sodium hydroxide. The major distinction between these two forms of cellulose lies in the layout of their atoms: cellulose II has antiparallel packing, whereas the chains in cellulose I run in a parallel direction. Finally, cellulose III $_I$ and III $_{II}$ are obtained by ammonia treatment of cellulose I and II, respectively, and with the modification of cellulose III with glycerol, cellulose IV is finally produced [5].

The isolation of cellulose from its sources can be carried out by top-down or bottom-up method. The bottom-up approach is used to process material from small molecules into complex structures [6]. The top-down method usually involves various mechanical, chemical, and biological treatments, or a combination of two or more methods which is used for the removal of plant constituents apart from cellulose.

2.1 Natural Cellulose Supports for Enzyme Immobilization

Natural sources of cellulose could be generalized as rigid and partially crystalline. Cellulose is the main constituent in the most abundant organic compound on earth, especially within wood and natural fibers (kenaf, palm, cotton, hemp, flax, etc.). Almost 65–70% of cellulose compound is contained in plant fibers and comprised C,

H, and O elements [1, 7, 8]. Kenaf (*Hibiscus cannabinus* L.) is a lignocellulosic fiber having a high cellulose content, low specific gravity, and good mechanical properties along with good chemical characteristics, large surface area, and low coefficient thermal expansion. The isolation process of kenaf raw bast fiber has been done by using combinations of chemical and physical treatments which can remove matrix substances such as lignin and hemicellulose, and disintegrate the micron-sized cellulose fiber into nanofiber [9]. This process results in changes in the appearance of the material from micron-sized to nanosized fibers. It is organized as web-like network structure with long entangled cellulosic filaments with an average diameter ranged as less than 100 nm right up to less than 10 nm depending on the ultrasonication output power. Thus, ultrasonication disintegration plays an important role in the determination of the diameter of the fiber. The nanofibril has been successfully observed as an individual wire-like fiber [10], arranged in longitudinal direction as aggregated fibers with high specific surface area and strong association due to interfiber hydrogen bonding between hydroxyl groups of adjacent fibers.

2.2 Microfibrillated Cellulose

Microfibrillated cellulose (MFC) is a material derived by disintegrating digested cellulose through a homogenizing process in a reciprocating motion producing a high pressure drop. The strategy results in shearing and impact forces that in turn expose microfibrils regardless of the starting material [11]. The production of MFC by fibrillation of cellulose fibers involves intensive mechanical treatment. Additionally, it could involve prior chemical treatments to purify the cellulose depending on the raw material. MFC consists of aggregates of cellulose microfibrils. Its diameter is in the range 20–60 nm and it has a length of several micrometers. If we consider that the microfibrils have a 2–10 nm-thick fibrous cellulose structure and a length of several tens of microns, then MFC is composed of 10–50 microfibrils [5]. The raw materials and fibrillation techniques dictate the cellulose degree of polymerization, morphology, and nanofiber aspect ratio. MFC can further be subclassified depending on the treatment it undergoes. On transverse cleavage of the microfibrils along the amorphous regions and subsequent sonication, they form rod-like structures called “cellulose whiskers” with a typical diameter of 2–20 nm and wide length distribution of 100–600 nm. Their almost perfect crystalline arrangement makes them a potential reinforcing material [12].

2.3 Cellulose Nanocrystals

Cellulose nanocrystals (CNCs) are rod-like cellulose nanomaterials that can be economically prepared from various cellulosic materials by the elimination of amorphous regions of cellulose. This material is interesting as a nanofiller due to its nanoscale dimensions, high specific area, and highly rigid crystalline structure [11, 13]. Generally, CNCs are formed upon the elimination of disordered or amorphous regions of cellulose through several strategies, including acid hydrolysis,

microfluidization, and TEMPO-mediated oxidation. BC and cotton linter cellulose long fiber (CLC) can also produce cellulose nanocrystals (CNC) [14]. Reports from Roman et al. have shown that CNCs are much safer than other nanomaterials in use in biomedicine as targeted drug delivery systems. They have been used to immobilize various enzymes such as lysozyme, papain, and glucose oxidase [4, 13, 15]. The CNC-CLC and CNC-BC showed higher loading capacity of the protein, enhanced stability and activity, and overall a potential support for application in biomedicine, bioelectronic, and biocatalytic fields.

2.4 Bacterial Cellulose Nanosupports

Cellulose synthesized by bacteria is called bacterial cellulose (BC) or sometimes microbial cellulose and is obtained as a gel-like three-dimensional mat formed by entangled nanofibrils of cellulose [16]. Different from cellulose from wood pulp, BC is devoid of other contaminating polysaccharides which provide high crystallinity and purity to the material and its isolation and purification are relatively simple, not requiring energy- or chemical-intensive processes. The ability to naturally synthesize BC is restricted to a few genre of bacteria being the most common bacteria associated with the synthesis of cellulose *Gluconacetobacter xylinus* as it is the only one able to produce it at the industrial level [17]. After polymerization of glucose residues occurring in the cytoplasm, an extracellular secretion of the glucan chains occurs in a hierarchically linear arrangement favored by van der Waals forces and hydrogen bridges. Intra- and interfiber hydrogen bonding favor crystalline packing of the fiber for amorphous and crystalline regions [18]. The resulting microfibrils aggregate to produce a typical ribbon assembly with a lateral width of 40–60 nm. This structuration provides a specific density, tensile strength, and hydrophilicity that suit the material for functionalization and application to cosmetic industry, paper industry, food processing and packaging, and tissue engineering. Furthermore, the unique fibrillar nanostructure of BC (Fig. 1) determines its distinguished physical and mechanical properties such as high porosity, large surface area, excellent mechanical strength, and good biocompatibility [19]. BC-forming microorganisms can be cultivated in mannitol-based medium with alternative source of carbons and the supernatant freeze-dried to form a BC sponge after purification. Acid hydrolysis of BC form bacterial cellulose nanocrystals (BCNs) that have a higher hydrophilicity due to increased number of hydroxyl groups while being able to establish hydrophobic interactions due to its highly ordered crystalline organization (Fig. 1). This amphiphilic capacities can be applied to stabilize surfactant-free emulsions [20].

2.5 Electrospun Cellulose

Electrospinning is a simple, cost-effective, and scalable technique that utilizes electrical charge to form fine fibers from a polymer solution or polymer melt. In the past decades, electrospinning has emerged as a facile, economical, and scalable

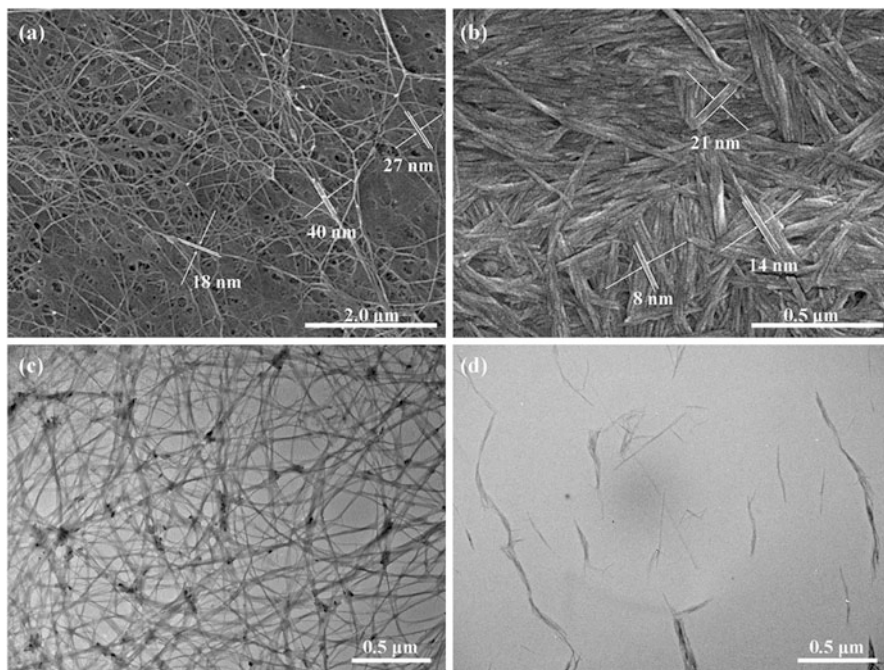


Fig. 1 An example of bacterial cellulose from *Acetobacter xylinum*. SEM images of (a) BC and (b) BCNs; TEM images of (c) BC and (d) BCNs. (Reproduced with permission from [20])

technique to produce polymeric fibers with a diameter ranging from micro- to nanometer scale. The biggest advantages of electrospun nanofibers are the high specific surface area, high porosity, and interconnectivity [21]. In biocatalysis, electrospun nanofibers could be used as the support for enzyme immobilization, and the immobilized enzyme could be reused and simultaneous biocatalytic reaction and enzyme-product separation is possible.

Substrates of this technique can be salts of cellulose such as cellulose acetate. The properties of the final material obtained can vary depending on the concentration and electrical conductivity of the starting solution, applied electrical potential, fiber collection distance and time, flow rate, and inner diameter of the reservoir during the process [6].

Electrospun cellulose has been used in a layer-by-layer self-assembled (LBL) configurations based on the electrostatic interactions of additional materials sequentially added to cellulose mats. This material was prepared by alternate adsorption of highly positively charged enzyme Naringinase (NA) and negatively charged alginate (ALG) from dilute solutions on the surface of negatively charged cellulose acetate nanofibrous mats via electrostatic attraction. The self-assembly of NA and ALG gave the reversal of the surface charge, demonstrating the successful polyelectrolyte multilayer deposited onto electrospun cellulose acetate nanofibers [21].

2.6 Synthetic Supports

In the recent years, the preparation of lignocellulose-based materials and biomimetic synthetic wood composites containing cellulose, hemicellulose, and lignin by using ionic liquids (ILs) as well as cellulose/starch/lignin film, lignocellulose aerogel, and all-wood composites have been reported [8, 22]. The major components of wood have been reported to be dissolved in ILs and successfully reconstituted as hydrogels, thin films, and electrospun materials. Fabrication of homogeneous composites from cellulose/hemicellulose/lignin has been achieved via an uncomplicated process by using in 1-ethyl-3-methylimidazolium acetate resulting in hydrogel beads composites with controllable properties [8]. The material shows a regular spherical shape and it is noted that the surface could be controlled by altering the ratio of cellulose, xylan, and lignin. When all three components were present, it was referred to as a wood mimetic composite which was a viable support for the entrapment of lipase and stabilization of its activity.

3 Strategies for the Immobilization of Enzymes in Cellulose-Based Nanocarriers

There are many enzyme immobilization approaches in cellulose-based nanocarriers already available and many more are being developed. Most of these approaches share the goals of finding a biocompatible support for enzyme immobilization, provide a higher surface area to increase the enzyme loading, and achieve high stability and reusability of the biocatalyst with a simple and mild methodology. In this regard, cellulose materials have been studied due to its low cost and biocompatibility [23, 24]. Cellulose materials have been proven to be environmentally friendly and are able to work under mild conditions [23, 25].

Among many strategies for enzyme immobilization, cellulose-based nanobiocatalysts have been developed mainly using four different approaches to retain the enzyme in the cellulosic support: entrapment, cross-linking, adsorption, and covalent immobilization.

In this chapter, we describe these four immobilization strategies in cellulosic-based nanosupports and examine the impact of the immobilization process on the biocatalyst activity and stability through several examples.

3.1 Immobilization by Cross-Linking

Chemical modification of enzymes after immobilization such as chemical cross-linking is a widely used strategy in the preparation of insoluble biocatalysts [26]. The enzyme is generally adsorbed to the nanosupport and then cross-linked with a bifunctional agent such as glutaraldehyde (Fig. 2). This approach can improve the enzyme stability as well as reduce enzyme leakage, a common problem in

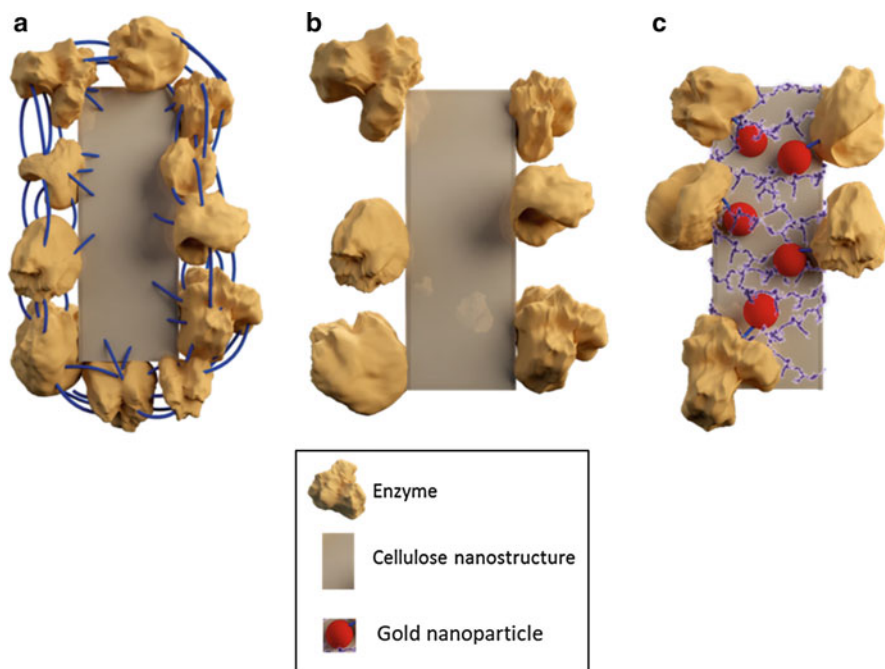


Fig. 2 Schematic representation of an enzyme immobilized on cellulose nanosupport via (a) adsorption and cross-linking, (b) physical adsorption, and (c) covalent immobilization to gold nanoparticles (AuNPs) attached to the support

noncovalently attached enzymes to supports. An alternative approach to a previous adsorption of the enzyme on a support is its precipitation and further cross-linking. Further advantages could be obtained if additives or other material are present during the precipitation. For instance, magnetic nanoparticles can be added to the mixture to form a hybrid nanobiocatalyst to ease its separation from reaction media.

Magnetic cellulose nanocrystals (MCNCs) have been used as a support for enzyme immobilization [13, 27]. The enzyme can be mixed with an aqueous suspension of MCNC and be deposited on its surface in the presence of a precipitant such as ethanol. Upon precipitation, addition of a cross-linking agent such as glutaraldehyde generates a chemical attachment between the immobilized molecules [23].

Immobilization on MCNCs via the described precipitation-cross-linking process was successfully accomplished with different types of enzymes [13, 27]. For instance, following this strategy, a nanobiocatalyst papain/MCNC has been prepared with high enzyme-loading capacity (333 mg protein/g MCNCs). The highest enzyme activity recovery was 80.1% at a mass ratio of 1:3 papain to MCNC. This could be attributable to the abundant active $-OH$ groups of the cellulose nanocrystals that contribute to the cross-linking of the enzymes on the MCNC. When comparing the nanobiocatalyst with the free enzyme, the optimal pH value increased from 6.5 to 7.0 and the temperature for the highest activity was 75 °C, 5 degrees higher

than that of the free enzyme. The change in optimal temperature was attributed to an increase in the enzyme conformational rigidity (seen in a secondary structure study). When comparing the kinetic behavior of free and immobilized papain, a higher V_{\max} (2.07×10^{-2} compared to 1.19×10^{-2} $\mu\text{mol/ml}\cdot\text{min}$) and lower K_M (0.85–1.27 mM) were found, thus demonstrating the increase in enzyme-substrate apparent affinity. This phenomenon could be attributable to the fact that the enzyme was anchored on the surface of MCNC, making the substrate accessible to the enzyme and in turn increasing the apparent affinity, or that the immobilization of papain onto the MCNC may have resulted in the conformational changes, helping the enzyme to suitably orient its active site toward the substrate. The immobilized enzyme was also proved to be more thermally stable. When comparing at the same temperature, the immobilized enzyme exhibited higher activity recovery than its free counterpart, 30% after 7 h incubation at 80 °C, while the free enzyme was inactivated after only 3 h. Moreover, the nanobiocatalyst showed no significant loss of activity when stored at 4 °C for 30 days. Finally, the reusability of the immobilized preparation was successful in maintaining 52.4% of its initial activity after 6 cycles.

3.2 Immobilization by Physical Adsorption

Physical adsorption of the enzymes on insoluble cellulose-based nanosupports has been reported elsewhere for the production of stable immobilized preparations that avoided leakage provided a strong enzyme-support interaction was established [28]. This immobilization approach has a major advantage considering the simplicity of the steps required, although functionalization of bare cellulose with ionizable/hydrophobic groups is sometimes necessary to achieve strong enzymatic adsorption of enzymes.

Physical adsorption of enzymes is feasible onto cellulose nanocrystals (CNCs) by incubating both the support and the enzyme under shaking at room temperature [13]. At neutral pH, a high fraction of sulfonate groups on the CNCs are ionized and the cationic sites or amino groups of the enzyme may have ionic interaction with anionic groups of CNCs (Fig. 2). The adsorption level of enzymes onto cellulose increases by the oxidation of cellulose primary hydroxyl groups to carboxyl groups; this strategy has been tested with cellulose fibers and could be translated to nanostructures [29].

When immobilizing a lipase from a *C. rugose* with this approach, an immobilization yield was low (51%) [13]. The decrease of lipase activity after immobilization may be due to the changes in spatial conformation of lipase and lower accessibility of substrate to the active site. However, the thermal stability can be enhanced by this approach. In the case of lipases, an immobilized enzyme to CNCs maintained over 50% of the residual activity when incubated at 60 °C for 1 h. Under the same conditions, the residual activity of the free lipase was only 11%. When comparing the half-lives, the immobilized enzyme was 27 times higher than of the free lipase. This increase in thermal stability may be associated to the enhanced ionic

interactions between anionic sulfonate groups of CNCs and the lipase, and the increased interactions caused by the higher surface area of the nanomaterial [13]. With this strategy, the pH profiles of free and immobilized lipase were similar, pH 8 being the optimal for both. A difference was found at pH 5, where the relative activity of immobilized lipase was 3.7 times higher than that of free lipase, and at pH 10, where free lipase showed no activity while the relative activity of immobilized lipase was 27.8%. The pH profiles for the stability of free and immobilized lipase were also very similar after a 5h incubation. The residual activities of immobilized lipase in buffers from pH 3 to pH 8 were approximately 140% higher than those of the free lipase. At alkaline pH, the stability of the lipase was significantly enhanced by immobilization on CNC (8.8 times higher at pH 10). Increased activity and stability in alkaline pH may be caused by increased ionic interaction between anionic groups of CNCs and the lipase since the anionic form of the sulfate half-ester in CNC is dominant at an alkaline pH.

Physical adsorption of lipase not always results in a more stable preparation. In a study where the adsorption of a *Candida rugosa* lipase was performed on a cellulose nanofiber membrane, the preparation demonstrated a low enzyme loading and poor enzyme stability [30]. These types of examples still prove the necessity of protocol optimization in order to tailor the immobilization strategy to a particular support or a desired enzyme.

Functionalization of nanocellulose-based supports for adsorption of enzymes has also been achieved via coverage of the cellulose surface with ionic polymers. Efficient immobilization of papain was achieved using CNCs associated to polyethyleneimine (PEI) modified Fe_3O_4 nanoparticles [16]. Magnetic nanoparticles embedded on CNCs facilitated the separation of the particles from a reaction mixture, simplifying the reuse of the biocatalysts. This support was successfully used for the immobilization and separation of papain from the reaction mixture which under optimal conditions resulted in a preparation with an enzyme activity of 227 $\mu\text{g}/\text{min.g}$. When studying the kinetic parameters of this preparation, the immobilized papain required higher substrate concentration compared to the free papain which could be explained by the increased steric hindrance and diffusion impediments. However, compared with free papain, the immobilized papain still demonstrated high catalytic efficiency.

Also, the immobilized papain exhibited higher relative activity in both acidic and alkaline pH ranges when compared to its free form. The immobilized enzyme retained over 90% of its original activity after incubation for 1 h at 40 °C, almost twice the activity measured for the free enzyme [16].

3.3 Covalent Immobilization

Covalent immobilization of enzymes is often chosen over adsorption strategies because it overcomes the primary disadvantage of adsorption which is enzyme dissociation (leakage) [28]. A number of functionalization strategies have been developed for cellulose nanomaterials for the covalent bonding of enzymes

[13, 31, 32]. One of this approaches involved functionalization of cellulose nanocrystals (CNCs) with cyanogen bromide, a functional group that is able to react with amino-terminal groups of enzymes under neutral pH [31]. Peroxidase has been immobilized in CNCs following this approach resulting in a highly active preparation (594 IU/g) with a higher catalytic efficiency when compared to the free enzyme.

Modification of CNCs can be also obtained via esterification with amino acids such as glycine through the abundant hydroxyl groups on the CNC surface. Lysozyme, for example, can be covalently immobilized via amide linkage of its glutamate and aspartate residues to the surfaces of amino-modified materials. In this case, lysozyme-amino-glycine-CNC conjugates were created using a carbodiimide-activated coupling reaction. The prepared nanobiocatalyst showed a high enzyme loading (604 mg/g CNCs) and high antimicrobial activity (1500 IU/mg biocatalyst) against *Micrococcus lysodeikticus* [32].

An alternative strategy for covalent immobilization can involve the addition of another material to the system. An approach described by Boluk et al. [33] involved the immobilization of a glucose oxidase (GOx) through the formation of covalent bonds between the enzyme and gold nanoparticles (AuNPs) attached to rod-like cellulose nanocrystals (Fig. 2). The AuNPs must be previously functionalized with thiol linkers and later activated, offering a multipoint attachment of GOx molecules to the nanocomposite surface. In this approach, the CNCs have been incubated with cationic PEI which covers the nanocrystals by ionic interactions; then negatively charged AuNPs were deposited on the CNC/PEI electrostatically resulting in a CNC/PEI/AuNPs nanocomposite. The enzyme (GOx) was covalently attached to the thiol-functionalized nanocomposite by activation of the $-\text{COOH}$ group using 1-ethyl-3-(3-dimethylaminopropyl) carbodiimide hydrochloride (EDC) and N-hydroxysuccinimide (NHS). The best case resulted in a 25.2 mg of GOx loaded per gram of support. Interestingly, the amount of GOx immobilized on this support increased with decreasing thiol-linker length. The difference could be attributed to their ability to access the AuNPs, as these particles are densely packed.

3.4 Combined Strategies

A new trend in the preparation of immobilized nanobiocatalysts is the combination of different strategies previous to, during, and/or after the immobilization process. The different strategies may have a synergistic effect on the desired properties of the final enzymatic preparation. To improve both loading and stability of enzymes, a three-step approach of enzyme precipitate coating (EPC), consisting of covalent enzyme attachment, enzyme precipitation, and crosslinking, has been successful in achieving both high enzyme loading and stability of enzymes on cellulose nanofibers (CNFs) (Fig. 3a) [34]. Such is the case of immobilization of α -chymotrypsin (CT) on CNFs by the EPC approach. In this approach, magnetic nanoparticles can be added to the enzyme mixture during the precipitation and cross-linking steps to produce

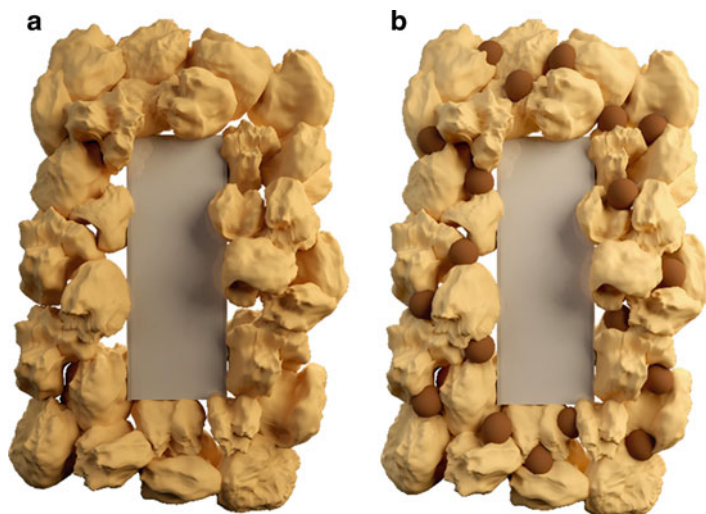


Fig. 3 Schematic representation of enzymes immobilized to cellulose nanofibers by (a) enzyme precipitate coating (EPC) and (b) magnetically separable EPC (Mag-EPC)

magnetically separable EPC (Mag-EPC) allowing for facile nanobiocatalyst separation (Fig. 3b).

As previously mentioned, this immobilization process consists of three steps. First, carboxyl groups of CNFs can be modified by EDC/NHS reaction for the covalent attachment between enzymes and CNFs, second, enzyme precipitation by ammonium sulfate, and third, enzyme cross-linking with glutaraldehyde treatment. The amine-functionalized magnetic nanoparticles can be added to enzyme solution in the step of enzyme precipitation (Fig. 3b).

The enzyme loadings with (Mag-EPC) and without (EPC) magnetic nanoparticles were estimated to be 3.5 and 3.0 mg CT/mg CNF, respectively. Interestingly, Mag-EPC showed two times higher activity than EPC. The efficiency of cross-linking between enzymes and magnetic nanoparticles was improved possibly due to a higher amount of amine groups on the surface of magnetic nanoparticles, resulting in an increased enzyme loading of Mag-EPC than EPC, as reflected in the activity data (0.43 and 0.74 IU/mg CT for EPC and Mag-EPC, respectively). After incubation under rigorous shaking for 30 days, EPC and Mag-EPC maintained 77% and 50% of their initial activities, respectively, while the free enzyme showed only 0.2%. High stability of EPC can be explained by ammonium sulfate precipitation and cross-linking of CTs. Enzyme precipitation by ammonium sulfate allows enzyme molecules to be closely packed based on “salting out” effect. Interestingly, the Mag-EPC residual activity was lower than that of EPC; this could be caused by the release of large aggregates of CTs and magnetic nanoparticles which would make the enzyme more vulnerable to denaturation under rigorous shaking [34].

3.5 Immobilization by Entrapment

Immobilization by entrapment involves the physical confinement of one or more enzymes in an insoluble matrix. In this strategy, the matrix is usually formed during the immobilization process. The bibliography related to immobilization by entrapment in cellulose nanosupports is scarce. The main drawback for this approach could be related to the very low solubility of cellulose in an aqueous solution since is highly crystalline. Nonetheless, there are successful cases using micro-sized supports. For example, a lipase from *C. rugose* was entrapped in a hydroxypropylmethyl-cellulose and chitosan matrix. Although this strategy involved many steps and over 48 h of synthesis, the result was a highly active and stable preparation [35].

Also, the rapid development of more and greener ionic liquids, which can dissolve cellulose, opens a new window of opportunities in this field. Again, successful examples can be found with cellulose-based micro-supports. Lipase from a *C. rugose* was entrapped into a cellulose–biopolymer using a biocompatible ionic liquid, 1-ethyl-3-methylimidazolium. This strategy also resulted in a preparation with good residual activity [36].

The technological approach employed on these successful cases could be applied for the development of similar strategies involving nanocellulose.

4 Cellulose-Based Nanobiocatalysts at Work

Application of immobilized enzymes on cellulose spans a wide variety of fields. The biodegradability of cellulosic materials has recently drawn the attention of researchers which boosted investigation of its potential in sensitive biotechnological areas such as biomedicine or environmental sciences. In this section, a few recent examples of cellulose-based nanobiocatalysts will be described to provide the reader with a sense of the applicability of these materials.

4.1 Biomedical Applications

Reactive oxygen species are implicated in cellular injuries, the initiation and progression of the aging process, and a vast variety of clinical abnormalities. In order to reduce the damage generated by these compounds, a nanofibrous cellulose mat containing attached catalase was prepared and tested in vitro on human umbilical vascular endothelial cells (HUVECs). The immobilized preparation based on electrospun nanofibers proved to have a protective effect on cells previously exposed to H₂O₂ which in turn pointed to a potential strategy to prevent cell damage by reactive oxygen species. The work also showed that the number of coating bilayers in the catalase-modified nanofibrous mats acted as important factor affecting their cytotoxicity and biocompatibility. This was an explorative work with potential to overcome H₂O₂-induced adverse effects at the cellular levels [37].

The antibacterial properties of lysozyme, a hydrolytic enzyme that catalyzes the breakdown of peptidoglycan polymers found in the bacterial cell wall, has been exploited and tested while using immobilized preparations on cellulosic materials. In comparison to many other antibacterial nanoparticles in use, lysozyme immobilized on cellulose possesses low toxicity, high biocompatibility, and selectivity. Researching its potential in a biomedical wound dressing, lysozyme was immobilized via different approaches to cellulose nanofibers aerogels (CNFs) [38]. The performance of the nanobiocatalysts was evaluated against nonimmobilized enzyme and silver nanoparticles. The antimicrobial activity of the preparations was tested against *Escherichia coli* and *Staphylococcus aureus* demonstrating the feasibility of using lysozyme-modified CNFs for this application. The preparation containing lysozyme was not only inhibitory of bacterial growth but was also more stable than the soluble enzyme, which amplifies the possibilities of its application considering the importance of shelf life of biological based products.

A work from Abouhmad et al. [39] also investigated the antibacterial properties of a lysozyme immobilized on CNC. Following different approaches for the integration of hen egg white- and T4 lysozyme, the work demonstrated that the surface modification and the mode of immobilization are critical for the retention of the enzymatic (lytic and hydrolytic) and antibacterial activity as well as stability of the immobilized enzymes. The positive charge on the nanocrystals and lysozyme activity improved the enzymatic action and broadened the scope to Gram-negative bacteria that are normally more challenging to inactivate.

Biosensors offer simple, portable, and disposable analytical devices applicable in clinical diagnosis, food quality control, and environmental monitoring. They depend on a biological recognition capable of being translated on a signal proportional to a target analyte. Particularly, paper-based sensors that offer affordability and ease of preparation although protein immobilization could be challenging to achieve an even distribution of oriented enzyme molecules that could increase the sensibility of the sensing device. A recent work on the development of a lactate biosensor has tackled this problem by using a recombinant lactate dehydrogenase fused with a cellulose-binding domain (CBD) which in nature promotes arbohydrate binding functionality for cellulases. The tag allowed a highly specific binding affinity on filter paper. Moreover, it enhanced enzyme binding capacity and stability, leading to much improved sensor sensitivity and lifetime. The one-step binding procedure using enzyme crude extract aimed at an efficient sensor fabrication strategy for production of high-performance paper sensors that could be extended to nanocellulosic materials for increased sensibility [40].

In another biosensing approach, glutamate dehydrogenase was immobilized on bacterial cellulosic nanofiber with a view on its application in artificial kidney machines and their dialysate liquid regeneration systems as a glutamate-sensing device. The study showed the success of cross-linked immobilization of glutamate dehydrogenase on 30–70 nm bacterial cellulosic nanofiber from *Gluconacetobacter xylinum*. The enzyme was cross-linked to the nanofibers using glutaraldehyde. The study provided an inexpensive, simple, efficient, and reliable technique for

immobilization of glutamate dehydrogenase on bacterial nanofiber which may contribute to find alternative for glutamate determination in solution [41].

4.2 Food Applications

Stem bromelain is a cysteine protease obtained from stems of pineapples (*Ananas comosus*). Although it finds some applications in medicine, this protease is widely used in food industries such as beer clarification, meat tenderization, and baking industries. Using casein as a model substrate, Talingtaisong et al. demonstrated that when the enzyme was immobilized on gauze-reinforced regenerated cellulose (RC) fibers, it became more heat resistant [42]. The enzyme was attached to the RC fibers through covalent immobilization via aldehyde groups introduced by activation with glutaraldehyde and was able to resist up to nine reuses in casein hydrolysis with 40% loss in activity. The results provide an opportunity for bromelain to be reused and used in other processing conditions.

Another interesting application of a cellulose-immobilized biocatalyst is that of naringinase. Naringin and limonin are two of the major compounds that contribute to a bitter taste in citrus juices. Enzymatic and physicochemical treatments have been applied to reduce bitterness, naringinase being one of the enzymes applied as it is able to break down naringin in flavorless products. Naringinase was immobilized within a hybrid layer-by-layer self-assembled material containing alginate and electrospun cellulose acetate nanofibers [21]. As expected, the activity of immobilized naringinase increased with multilayer increasing. The immobilized preparation was applied to remove the bitterness in the grapefruit juice. About 22.72% naringin and 60.71% limonin were removed from the grapefruit juice by adsorption and hydrolysis. The results demonstrated that naringinase-immobilized electrospun cellulose acetate nanofibrous mat are potential materials to remove bitterness for fruit juice.

4.3 Environmental Applications

Biobased treatments of contaminant compounds have received a great deal of interest due to their minimal impact on the ecosystem, their higher efficiency, and their cost effectiveness. Application of immobilized decontaminant biocatalysts is one of the approaches followed to treat, sense, or remove contaminant wastes from water and soil. Although the literature on cellulose-immobilized enzymes on decontamination is not abundant, a few recent examples have demonstrated the potential of cellulosic-supported enzymes for this application. For example, laccase, a well-known phenol/polyphenol decontaminant biocatalyst, was immobilized on cellulose nanofiber and utilized for reactive dyes and simulated dye effluent (SDE) decoloration [43]. After covalent immobilization on electrospun nanofibers, the immobilized preparation was able to decolorate solutions of six different reactive dyes. Optimization of the conversion was performed after statistical analysis revealing that both the concentration of immobilized enzyme and type of

mediator for the catalysis were determinant in the result of the decontamination reactions. The immobilized preparations could be recycled more than 10 times while maintaining more than 50% of its initial activity.

Another example that represents a promising application of immobilized enzymes in cellulosic materials is the utilization of an ether hydrolase enzyme for the decontamination of 2,4-dinitroanisole (DNAN) [44]. This compound is nowadays preferred to 2,4,6-trinitrotoluene (TNT) given that it is less heat and shock sensitive. Strategies to decontaminate firing ranges and wastes from manufacturing sites should comply with biosafety and environmental regulations and therefore there is a constant search for new strategies to remediate explosive components. Additionally, analytical devices for the evaluation of contamination levels are also needed. The work described by the group of Prof. J C Spain used a DNAN demethylase entrapped in biomimetic silica which was further attached to cellulose discs. The immobilized enzyme became more stable and was able to detect 15–500 μM DNAN concentration.

5 Conclusion

Ideal supports for enzyme immobilization should be biocompatible, easy to functionalize, inexpensive, and biodegradable. Additionally, immobilization strategies should provide advantages for enzyme applications over the use of soluble enzymes to counterbalance any additional cost in the preparation of the biocatalyst (i.e., stabilization, increased activity, possibility of reuse). We believe this chapter compiles evidence that proves the benefits of nanocellulosic materials as supports for enzyme immobilization. Moreover, the methodologies for enzyme immobilization on cellulose-based nanocarriers presented suggest that cellulose can be a viable and dynamic material for stable and efficient enzyme immobilization via different approaches. Finally, the variety of applications, which are now in a continuous growth phase, only serve to foretell a promising future for the development of technological solutions involving cellulose-immobilized nanobiocatalysts.

Acknowledgments The authors acknowledge ANII, PEDECIBA, and Universidad ORT Uruguay for providing financial support.

References

1. Sulaiman S, Mokhtar MN, Naim MN, Baharuddin AS, Sulaiman A (2014) A review: potential usage of cellulose nanofibers (CNF) for enzyme immobilization via covalent interactions. *Appl Biochem Biotechnol* 175:1817–1842. <https://doi.org/10.1007/s12010-014-1417-x>
2. Mateo C, Palomo JM, Fernandez-Lorente G, Guisan JM, Fernandez-Lafuente R (2007) Improvement of enzyme activity, stability and selectivity via immobilization techniques. *Enzym Microb Technol* 40:1451–1463. <https://doi.org/10.1016/j.enzmictec.2007.01.018>
3. Misson M, Zhang H, Jin B (2015) Nanobiocatalyst advancements and bioprocessing applications. *J R Soc Interf* 12:20140891

4. Esmaili C, Abdi MM, Mathew AP, Jonoobi M, Oksman K, Rezayi M (2015) Synergy effect of nanocrystalline cellulose for the biosensing detection of glucose. *Sensors (Switzerland)* 15:24681–24697. <https://doi.org/10.3390/s151024681>
5. Lavoine N, Desloges I, Dufresne A, Bras J (2012) Microfibrillated cellulose – its barrier properties and applications in cellulosic materials: a review. *Carbohydr Polym* 90:735–764. <https://doi.org/10.1016/j.carbpol.2012.05.026>
6. Panatadasirisuk W, Vongsetskul T, Sucharitakul J, Chaiyen P, Tangboriboonrat P (2015) Functionalized electrospun regenerated cellulose fibers for immobilizing pyranose 2-oxidase. *React Funct Polym* 86:47–51. <https://doi.org/10.1016/j.reactfunctpolym.2014.11.008>
7. Sulaiman S, Mokhtar MN, Naim MN, Baharuddin AS, Salleh MAM, Sulaiman A (2015) Study on the preparation of cellulose nanofibre (CNF) from Kenaf Bast fibre for enzyme immobilization application. *Sains Malaysiana* 44:1541–1550
8. Park S, Kim SH, Won K, Choi JW, Kim YH, Kim HJ, Yang YH, Lee SH (2015) Wood mimetic hydrogel beads for enzyme immobilization. *Carbohydr Polym* 115:223–229. <https://doi.org/10.1016/j.carbpol.2014.08.096>
9. Karimi S, Tahir PM, Karimi A, Dufresne A, Abdulkhani A (2014) Kenaf bast cellulosic fibers hierarchy: a comprehensive approach from micro to nano. *Carbohydr Polym* 101:878–885. <https://doi.org/10.1016/j.carbpol.2013.09.106>
10. Sulaiman S, Cieh NL, Mokhtar MN, Naim MN, Kamal SMM (2017) Covalent immobilization of cyclodextrin glucanotransferase on kenaf cellulose nanofiber and its application in ultrafiltration membrane system. *Process Biochem* 55:85–95. <https://doi.org/10.1016/j.procbio.2017.01.025>
11. Pandey JK, Takagi H, Nakagaito AN, Kim HJ (2015) Handbook of polymer nanocomposites. Processing, performance and application: volume C: polymer nanocomposites of cellulose nanoparticles. In: *Handb Polym Nanocomposites process perform Appl Vol C Polym nanocomposites Cellul nanoparticles C: 1–511*. <https://doi.org/10.1007/978-3-642-45232-1>
12. Shahrousvand M, Tabar FA, Shahrousvand E, Babaei A, Hasani-Sadrabadi MM, Sadeghi GMM, Jafari H, Salimi A (2017) High aspect ratio phospho-calcified rock candy-like cellulose nanowhiskers of wastepaper applicable in osteogenic differentiation of hMSCs. *Carbohydr Polym* 175:293–302. <https://doi.org/10.1016/j.carbpol.2017.08.001>
13. Kim HJ, Park S, Kim SH, Kim JH, Yu H, Kim HJ, Yang YH, Kan E, Kim YH, Lee SH (2015) Biocompatible cellulose nanocrystals as supports to immobilize lipase. *J Mol Catal B Enzym* 122:170–178. <https://doi.org/10.1016/j.molcatb.2015.09.007>
14. Uth C, Zielonka S, Hörner S, Rasche N, Plog A, Orelma H, Avrutina O, Zhang K, Kolmar H (2014) A Chemoenzymatic approach to protein immobilization onto crystalline cellulose Nanoscaffolds. *Angew Chemie Int Edgl* 53(46):12618–12623. <https://doi.org/10.1002/anie.201404616>
15. Mahmoud KA, Lam E, Hrapovic S, Luong JHT (2013) Preparation of well-dispersed gold/magnetite nanoparticles embedded on cellulose nanocrystals for efficient immobilization of papain enzyme. *ACS Appl Mater Interf* 5:4978–4985. <https://doi.org/10.1021/am4007534>
16. Pacheco G, Nogueira CR, Meneguín AB, Trovatti E, Silva MCC, Machado RTA, Ribeiro SJL, da Silva Filho EC, da S, Barud H (2017) Development and characterization of bacterial cellulose produced by cashew tree residues as alternative carbon source. *Ind Crop Prod* 107:13–19. <https://doi.org/10.1016/j.indcrop.2017.05.026>
17. Keshk SM (2014) Bacterial cellulose production and its industrial applications. *J Bioprocess Biotech* 4:150–160. <https://doi.org/10.4172/2155-9821.1000150>
18. Iris SL, Calvar L, Liu JMCJ, Cheng ADK (2013) Biosynthesis, production and applications of bacterial cellulose. *Cellulose* 20:2191–2219. <https://doi.org/10.1007/s10570-013-9994-3>
19. Sampaio LMP, Padrão J, Faria J, Silva JP, Silva CJ, Dourado F, Zille A (2016) Laccase immobilization on bacterial nanocellulose membranes: antimicrobial, kinetic and stability properties. *Carbohydr Polym* 145:1–12. <https://doi.org/10.1016/j.carbpol.2016.03.009>
20. Yan H, Chen X, Song H, Li J, Feng Y, Shi Z, Wang X, Lin Q (2017) Food hydrocolloids synthesis of bacterial cellulose and bacterial cellulose nanocrystals for their applications in

- the stabilization of olive oil Pickering emulsion. *Food Hydrocoll* 72:127–135. <https://doi.org/10.1016/j.foodhyd.2017.05.044>
21. Huang W, Zhan Y, Shi X, Chen J, Deng H, Du Y (2017) Controllable immobilization of naringinase on electrospun cellulose acetate nanofibers and their application to juice debittering. *Int J Biol Macromol* 98:630–636. <https://doi.org/10.1016/j.ijbiomac.2017.02.018>
 22. Kang Y, Ahn Y, Lee SH, Hong JH, Ku MK, Kim H (2013) Lignocellulosic nanofiber prepared by alkali treatment and electrospinning using ionic liquid. *Fibers Polym* 14:530–536. <https://doi.org/10.1007/s12221-013-0530-8>
 23. Cao S, Xu P, Ma Y, Yao X, Yao Y, Zong M, Li X, Lou W (2016) Recent advances in immobilized enzymes on nanocarriers. *Cuihua Xuebao/Chinese J Catal* 37:1814–1823. [https://doi.org/10.1016/S1872-2067\(16\)62528-7](https://doi.org/10.1016/S1872-2067(16)62528-7)
 24. Sulaiman S, Mokhtar MN, Naim MN, Baharuddin AS, Sulaiman A (2015) A review: potential usage of cellulose nanofibers (CNF) for enzyme immobilization via covalent interactions. *Appl Biochem Biotechnol* 175:1817–1842. <https://doi.org/10.1007/s12010-014-1417-x>
 25. Ayissi Eyebe G, Bideau B, Boubekour N, Loranger É, Domingue F (2017) Environmentally-friendly cellulose nanofibre sheets for humidity sensing in microwave frequencies. *Sensors Actuators B Chem* 245:484–492. <https://doi.org/10.1016/j.snb.2017.01.130>
 26. Barbosa O, Ortiz C, Berenguer-Murcia Á, Torres R, Rodrigues RC, Fernandez-Lafuente R (2014) Glutaraldehyde in bio-catalysts design: a useful crosslinker and a versatile tool in enzyme immobilization. *RSC Adv* 4:1583–1600. <https://doi.org/10.1039/c3ra45991h>
 27. Cao SL, Xu H, Li XH, Lou WY, Zong MH (2015) Papain@magnetic Nanocrystalline cellulose Nanobiocatalyst: a highly efficient biocatalyst for dipeptide biosynthesis in deep eutectic solvents. *ACS Sustain Chem Eng* 3:1589–1599. <https://doi.org/10.1021/acssuschemeng.5b00290>
 28. Liu Y, Chen JY (2016) Enzyme immobilization on cellulose matrixes. *J Bioact Compat Polym* 31:553–567. <https://doi.org/10.1177/0883911516637377>
 29. Karra-Châabouni M, Bouaziz I, Boufi S, Botelho Do Rego AM, Gargouri Y (2008) Physical immobilization of *Rhizopus oryzae* lipase onto cellulose substrate: activity and stability studies. *Colloids Surfaces B Biointerfaces* 66:168–177. <https://doi.org/10.1016/j.colsurfb.2008.06.010>
 30. Huang X-J, Chen P-C, Huang F, Ou Y, Chen M-R, Xu Z-K (2011) Immobilization of *Candida rugosa* lipase on electrospun cellulose nanofiber membrane. *J Mol Catal B Enzym* 70:95–100. <https://doi.org/10.1016/j.molcatb.2011.02.010>
 31. Yang R, Tan H, Wei F, Wang S (2008) Peroxidase conjugate of cellulose nanocrystals for the removal of chlorinated phenolic compounds in aqueous solution. *Biotechnology* 7:233–241. <https://doi.org/10.3923/biotech.2008.233.241>
 32. Edwards JV, Prevost NT, Condon B, French A, Wu Q (2012) Immobilization of lysozyme-cellulose amide-linked conjugates on cellulose I and II cotton nanocrystalline preparations. *Cellulose* 19:495–506. <https://doi.org/10.1007/s10570-011-9637-5>
 33. Incani V, Danumah C, Boluk Y (2013) Nanocomposites of nanocrystalline cellulose for enzyme immobilization. *Cellulose* 20:191–200. <https://doi.org/10.1007/s10570-012-9805-2>
 34. Je HH, Noh S, Hong SG, Ju Y, Kim J, Hwang DS (2017) Cellulose nanofibers for magnetically-separable and highly loaded enzyme immobilization. *Chem Eng J* 323:425–433. <https://doi.org/10.1016/j.cej.2017.04.110>
 35. Badgujar KC, Bhanage BM (2015) Carbohydrate base co-polymers as an efficient immobilization matrix to enhance lipase activity for potential biocatalytic applications. *Carbohydr Polym* 134:709–717. <https://doi.org/10.1016/j.carbpol.2015.08.036>
 36. Kim MH, An S, Won K, Kim HJ, Lee SH (2012) Entrapment of enzymes into cellulose-biopolymer composite hydrogel beads using biocompatible ionic liquid. *J Mol Catal B Enzym* 75:68–72. <https://doi.org/10.1016/j.molcatb.2011.11.011>
 37. Huang R, Deng H, Cai T, Zhan Y, Wang X, Chen X, Ji A, Li X (2014) Layer-by-layer immobilized catalase on electrospun Nanofibrous Mats protects against oxidative stress induced by hydrogen peroxide. *J Biomed Nanotechnol* 10:1346–1358. <https://doi.org/10.1166/jbn.2014.1802>

38. Uddin KMA, Orelma H, Mohammadi P, Borghei M, Laine J, Linder M, Rojas OJ (2017) Retention of lysozyme activity by physical immobilization in nanocellulose aerogels and antibacterial effects. *Cellulose* 24:2837–2848. <https://doi.org/10.1007/s10570-017-1311-0>
39. Abouhmad A, Dishisha T, Amin MA, Hatti-Kaul R (2017) Immobilization to positively charged cellulose nanocrystals enhances the antibacterial activity and stability of hen egg white and T4 lysozyme. *Biomacromolecules* 18:1600–1608. <https://doi.org/10.1021/acs.biomac.7b00219>
40. Dai G, Hu J, Zhao X, Wang P (2017) Sensors and actuators B : chemical a colorimetric paper sensor for lactate assay using a cellulose-binding recombinant enzyme. *Sensors Actuators B Chem* 238:138–144. <https://doi.org/10.1016/j.snb.2016.07.008>
41. Pesaran M, Amoabediny G (2017) Study on the stability and reusability of glutamate dehydrogenase immobilized on bacterial cellulose nanofiber. *Fibers Polym* 18:240–245. <https://doi.org/10.1007/s12221-017-6864-x>
42. Talingtaisong S, Vongsetskul T (2017) Gauze-reinforced electrospun regenerated cellulose ultrafine fibers for immobilizing bromelain. *Cellulose* 24:2967–2975. <https://doi.org/10.1007/s10570-017-1307-9>
43. Sathishkumar P, Kamala-Kannan S, Cho M, Kim JS, Hadibarata T, Salim MR, Oh BT (2014) Laccase immobilization on cellulose nanofiber: the catalytic efficiency and recyclic application for simulated dye effluent treatment. *J Mol Catal B Enzym* 100:111–120. <https://doi.org/10.1016/j.molcatb.2013.12.008>
44. Karthikeyan S, Kurt Z, Pandey G, Spain JC (2016) Immobilized biocatalyst for detection and destruction of the insensitive explosive, 2,4-Dinitroanisole (DNAN). *Environ Sci Technol* 50:11193–11199. <https://doi.org/10.1021/acs.est.6b03044>

Chapter

***In situ* immobilization of enzymes in biomimetic silica**

Erienne Jackson, Sonali Correa and Lorena Betancor*.

Laboratorio de Biotecnología, Facultad de Ingeniería, Universidad ORT Uruguay. Mercedes
1237, 11100, Montevideo, Uruguay

***Corresponding author**

Prof. Lorena Betancor

Laboratorio de Biotecnología

Facultad de Ingeniería,

Universidad ORT Uruguay

Mercedes 1237, 11100, Montevideo, Uruguay

betancor@ort.edu.uy

Abstract

In this chapter we describe different strategies for enzyme immobilization in biomimetic silica nanoparticles. Synthesis of this type of support is performed under mild and biocompatible conditions and has been proven suitable for the immobilization and stabilization of a range of enzymes and enzymatic systems in nanostructured particles. Immobilization occurs by entrapment while the silica matrix is formed *via* catalysis of a polyamine molecule and the presence of silicic acid. Parameters such as enzyme, polyamine molecule or source of Si concentration have been tailored in order to maximize enzymatic loads, stabilities and specific activities of the catalysts. We provide different approaches for the immobilization and co-immobilization of enzymes that could be potentially extensible to other biocatalysts.

Keywords: biomimetic silica, enzyme immobilization, entrapment.

1. Introduction

Enzyme encapsulation or entrapment refers to a non-covalent immobilization strategy where polymers self-assemble in the presence of soluble enzymes. Various matrices can be used for entrapment, such as chitosan, collagen, cellulose triacetate, poly acrylamide, agar, silicon rubber, polyvinyl alcohol, etc [1–3]. In any approach to immobilize enzymes, the goal is to achieve a high specific activity without compromising any other advantages of immobilization such as higher stability. In recent years, several methods have been reported that achieve higher volumetric activities. Silica sol-gel encapsulation of enzymes is an example of such methods and has been widely used for the immobilization of biocatalysts[4,5] One of the primary limitations of the sol-gel technique, however, is poor loading efficiency and enzyme leakage. Additionally, these methods often include harsh sol-gel processing conditions that result in the loss of enzyme activity. Inspired from silaffin proteins used by unicellular diatoms[6], the utilization of the so called biomimetic approaches in the production of organic-inorganic nanostructures is of great interest to the scientific and industrial community due to the relatively moderate physicochemical conditions needed for its synthesis[7]. Biomimetic silica can be synthesized within minutes under mild and green conditions, as nanostructured silica with divergent morphologies[8]. The synthesis necessitates a source of Si and an organic aminated small molecule or polymer in order to catalyze the precipitation of the nanoparticles in phosphate buffer at pH 8 (Scheme 1). Any material contained in the synthetic mixture may become entrapped within the biomimetic silica nanoparticles and therefore this strategy has been commonly used for enzyme immobilization[9–12].

A fundamental attribute of this immobilization methodology is its versatility which allows it to be widely applicable to a range of biomolecules. Since a primigenial work from Luckarift

et al[13] and due to its biocompatibility and facile and quick synthesis, this entrapment strategy has been used to immobilize oxidases, hydrolases and coupled enzyme systems.

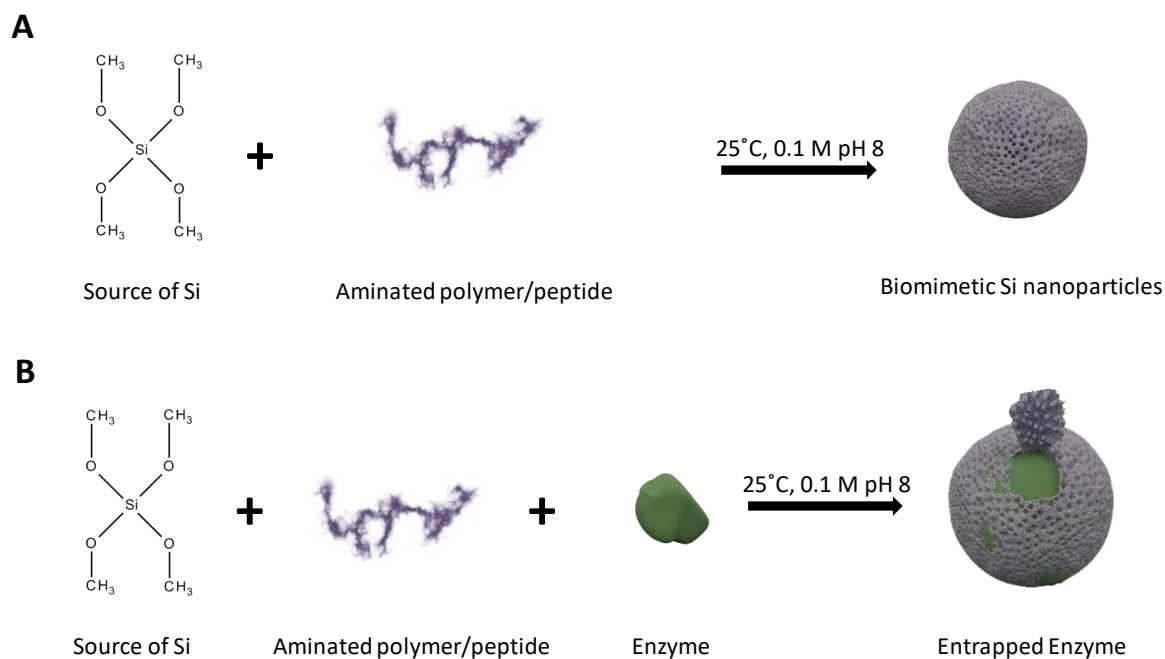
Co-immobilization of enzymes using *in situ* immobilization approaches benefit from the close proximity of the different biocatalysts which translates into higher catalytic efficiencies of the overall reaction. Biomimetic silica encapsulation has been used in the past for the co-entrapment of a variety of multienzyme configurations as well as the preparation of combi robust biocatalysts for bioconversions of biosensing applications. [14,15].

However, the synthetic strategy for biomimetic silica nanobiocatalysts can provide distinct properties to different enzymes and may be tailored to improve a desired attribute[13]. For instance, optimization of immobilized conditions to achieve active and stable nanobiocatalysts has included in the past studies of the synthetic precursors ratios, alternate aminated molecules or inclusion of organic solvents during synthesis. Addition of enzyme stabilization molecules for the *in situ* entrapment or post immobilization strategies such as crosslinking could further improve the stability of the biocatalysts.

Results on the biomimetic silica entrapment of different enzymes seem to indicate a dependence of the physical and textural properties of the Si nanoparticles with properties of such as size, shape or chemistry of the surface of the enzymatic molecule[16]. As in any other immobilization strategy, parameters such as loading capacity of the nanobiocatalysts or specific activity are also directed influenced by the properties of the enzyme to be immobilized. However, in *in situ* immobilization strategies they also play a fundamental role in the synthesis of the material support to the extent of preventing its formation under certain unbalanced ratios of the synthetic precursors and enzyme concentration[10].

In this chapter, we describe strategies for the *in situ* immobilization and co-immobilization of enzymes in biomimetic Si nanoparticles selecting a few examples that highlight the

potential of the technique and providing insight into the main parameters that should be considered when extending the strategy to other biomolecules.



Scheme 1. General procedure for the preparation of A) biomimetic Si nanoparticles and B) *in situ* immobilized enzymes in biomimetic SI nanoparticles.

2. Materials

1. Horseradish peroxidase (HRP), Type IV was from Sigma Aldrich (St. Louis, MO).
2. Lipase from *Rhizomucor miehei* (RML) was from Sigma Aldrich (St. Louis, MO).
3. Acyltransferase (BtrH) and γ -glutamyl cyclotransferase (BtrG) were recombinantly expressed in *E. coli* kindly donated by PFL group (Dept. Biochemistry, University of Cambridge)
4. β -Galactosidase (Grade VIII), from *Escherichia coli* was from Sigma Aldrich (St. Louis, MO).
5. Glucose oxidase (Type VII) from *Aspergillus oryzae* was from Sigma Aldrich (St. Louis, MO).

6. 2,2'-azino-bis(3-ethylbenzothiazoline-6-sulphonic acid) (ABTS), polyethyleneimine (PEI) and tetramethyl orthosilicate (TMOS) were from Merck (Darmstadt, Germany)

7. Other analytical reagents were purchased from SIGMA (St. Louis, MO)

3. Methods

3.1 Enzyme activity

1. Horseradish peroxidase activity assay contained 1.7 mL of 0.1 M potassium phosphate, pH 5.0 at 25°C, 0.1 mL of 9.1 mM ABTS ($\epsilon_M = 36.8 \text{ mM}^{-1}\text{cm}^{-1}$), 0.2 mL 0.3% (w/w) hydrogen peroxide solution (H_2O_2) in deionized water and 10 μl of enzyme (1mg/mL). The oxidation of ABTS was measured in a spectrophotometer at a wavelength of 405 nm for 2 min.

2. Lipase activity was performed by continuously measuring the increase in the absorbance at 348 nm produced by the released p-nitrophenol in the hydrolysis of 0.4 mM pNPP in 25mM sodium phosphate buffer at pH 7.0 and 30°C.

3. L-Lactate dehydrogenase (LDH) activity was measured in 2.5 mL containing 0,8 mM de piruvate, 0,2 mM of NADH in 25mM sodium phosphate buffer at pH 7.0 at 25°C. The reaction was started by addition of a 0.015 mg/mL solution of LDH and followed during 120 seconds at 340nm ($\epsilon_M = 6220 \text{ M}^{-1}\text{cm}^{-1}$).

4. The activity of the aciltransferase BtrH was measured in 108 μL containing 0.1mM ribostamycine, 0.5mM γ -Glu-AHBA-SNAC and 0.2mM de DTNB in buffer HEPES 50mM pH 7.0 at 25°C. The reaction was started by addition of 0.2mg of BtrH and the SNAC release was followed during 10 min at 412nm ($\epsilon_M = 14150 \text{ M}^{-1}\text{cm}^{-1}$).

The enzymatic unit is defined as the amount of enzyme able to produce 1 μmol of product per mL in the above-mentioned conditions.

5. β -Galactosidase activity was determined spectrophotometrically by following the increase in absorbance at 405 nm caused by the hydrolysis of *o*-nitrophenyl- β -D-galactopyranoside (oNPG). The reaction mixture contained 20 mM oNPG and 1 mM MgCl_2 in potassium phosphate buffer.

6. Glucose oxidase activity was determined spectrophotometrically by the increase in absorbance at 414 nm resulting from the oxidation of 2,2'-Azino-bis(3-ethylbenz-thiazoline-6-sulfonic acid) (ABTS) by a coupled peroxidase-catalyzed reaction. The reaction mixture consisted of 1 mL 100 mM sodium phosphate buffer pH 6.0, 0.5 mL 1 M glucose, 0.1 mL of 1 mg/mL ABTS in distilled water, and 0.1 mL of 2 mg/mL horse radish peroxidase in sodium phosphate buffer, pH 6.0.

One enzyme unit (IU) was defined as the amount of enzyme that catalyzes the formation of 1 μmol of product per minute under the specified conditions.

3.2 Oxidation of HRP

1. Dissolve 3 mg of the HRP in 1.8 mL of 154 mM sodium chloride in 10 mM sodium phosphate, pH 7.2.

2. Dissolve 8.6 mg of sodium periodate in 200 μL of distilled water (see Note 1) and add to the previously prepared enzyme solution.

3. Keep sample in gentle agitation in the dark for 1 h at 25°C. To stop the reaction, add 2.5 μL of glycerol and purified the oxidized enzyme using a desalting PD10 column equilibrated with 100 mM sodium phosphate pH 7.0 containing 154 mM sodium chloride.

4. Evaluate the activity of the enzyme to consider any activity loss after chemical modification.

3.3 In situ enzyme immobilization by entrapment in biomimetic silica.

The following is a general procedure with ratios of the component of the synthetic mixture (TMOS, aminated molecule, enzymatic solution) that usually provides good immobilization yields for a range of enzymes. However, the ratios may be varied to optimize the performance for a specific enzyme[10].

1. A stock solution of 10 % of polyethylenimine (PEI) or 12 mg/mL of spermidine (SP) is prepared in deionized water.
2. Silicic acid is prepared by hydrolyzing 157 μ L of tetramethyl orthosilicate (TMOS, 1 M) in 1 mL of 1 mM hydrochloric acid (see **Note 2**).
3. Prepare a 10 mL enzymatic solution with a desired concentration in 0.1 M sodium phosphate dibasic buffer pH 8.0, add 2.5 mL of PEI 10% or Spermidine 1mg/mL and mix.
4. Measure the activity of the enzymatic mixture to be immobilized.
5. Add 2.5 mL of hydrolyzed TMOS, mix the solution by inverting the tube several times and keep in agitation for 5 min at room temperature (see **Note 3**).
6. Centrifuge for 10 min at 4600g and wash once in sodium phosphate buffer 0.025 M, pH 7.0, 0.5 M NaCl (see **Note 4**) and twice with sodium phosphate buffer 0.025 M, pH 7.0.
7. Sonicate for 5 min to improve monodispersity.
8. Evaluate the activity of the immobilized suspension.

3.4 Cross-linking of entrapped HRP

1. HRP immobilization by entrapment is performed as previously described, using the oxidized enzyme.
2. Incubate 1 g of immobilized HRP in silica nanoparticles in 10 mL of sodium bicarbonate 25 mM at pH 10.0, 16 h at 4°C.
3. Finally, reduce the preparation by adding sodium borohydride (1 mg/ml) to the mixture under gentle agitation for 30 min (*see Note 5*). Centrifuge and resuspend in 0.025 M sodium phosphate buffer pH 7.0 for activity measurement.
4. Evaluate the activity of the immobilized cross-linking suspension.

4. Notes

1. Sodium periodate solution should be prepared fresh and keep protected from light.
2. Vortex until solution is clear. This solution should be freshly prepared.
3. Reagents should be added in the specified order.
4. NaCl is sometimes necessary to remove non-entrapped ionically adsorbed enzymatic molecules to the surface of the nanoparticles.
5. Keep the vessel open as small amounts of H₂ are formed during reduction.

5. Examples

1. *In situ* immobilization of enzymes in biomimetic silica nanoparticles.

- 1.1 Prepare solutions of enzyme of varying concentrations in 0.1 M sodium phosphate buffer pH 8.
- 1.2 Measured the activity of the different enzymatic preparations.
- 1.2 Perform the *in situ* immobilization described in 3.3 of the different enzymatic preparations using PEI 10% or Spermidine 12 mg/ml keeping the supernatant of the immobilization after the first centrifugation. It is worth mentioning that a number of

additional aminated molecules have been used for Si deposition. In fact, proteins with high amounts of Lys on their surface are able to auto catalyse their own Si entrapment [17].

1.3 Measure the activity of the supernatant after silica precipitation.

1.3 Measure the activity after resuspension of the biocatalysts in working buffer solution of the enzyme.

1.4 Weight the amount of biocatalyst formed after immobilization.

1.5 Evaluate the amount of enzyme immobilized by difference of activity in the starting enzymatic preparation and the supernatant after immobilization (Immobilization %). Measure the immobilization yield either in terms of protein (YP) and/or activity (YA) according to Eqs. (1) and (2), respectively:

$$Y_P(\%) = \frac{P}{P_0} \times 100 \quad (\text{Eq. 1})$$

$$Y_A(\%) = \frac{A}{A_0} \times 100 \quad (\text{Eq. 2})$$

where P_0 represents the amount of offered protein, P the amount of loaded protein in the biocatalyst, A_0 the offered enzyme activity and A the activity expressed in the biocatalyst.

1.6 Y_p and Y_a as well as the amount of Si nanoparticles of the biocatalysts obtained, and specific activity depend on multiple factors related to physico-chemical and biochemical nature of the enzyme to be immobilized. Table 1 shows the results obtained for the enzymes analyzed in this chapter and examples of previous works using PEI 10% for the Si deposition. It is worth noting that these results have been obtained under similar conditions from those described above.

Table 1. Examples of the results obtained for different enzymes immobilized by *in situ* entrapment in biomimetic silica.

Enzyme	Immobilization (%)	Y_A (%)	Source
Peroxidase from Horseradish	82 ± 4	49 ± 6	This work
Lipase from <i>Rizomucor miehei</i>	90 ± 1	24 ± 1	This work
Acyltransferase from <i>Bacillus circulans</i>	90 ± 2	20 ± 4	This work
Lipase from <i>Trametes versicolor</i>	82 ± 7	71 ± 1	[10]
β-galactosidase from <i>E. coli</i>	76 ± 7	42 ± 8	This work
Glucose oxidase from <i>Aspergillus niger</i>	50 ± 5	71 ± 2	This work
Enoate reductase recombinant from <i>E coli</i>	34	92	[18]
Papain from <i>Carica papaya</i>	83	83	[17]*
Nitroreductase from <i>Pseudomonas pseudoalcaligenes</i>	80 ± 5	60 ± 5	[19]

*No aminated molecule was needed for Si precipitation

1.7 Regarding stabilization, there are multiple examples of stabilized *in situ* entrapped enzymes. Figure 1 shows thermos stabilization achieved for β-galactosidase and glucose oxidase after immobilization using this approach.

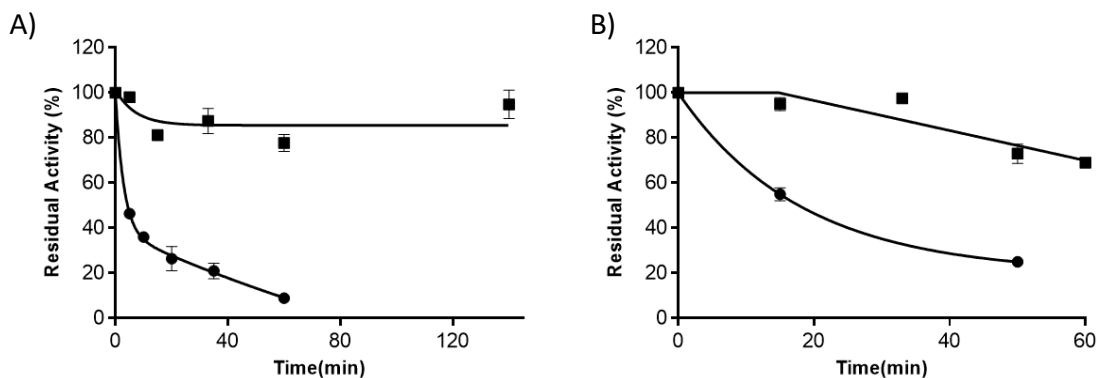


Fig 1. Thermal stability of soluble and *in situ* entrapped enzymes in biomimetic silica. A) β -galactosidase preparations at 54 °C, B) glucose oxidase preparations at 50 °C. In both graphs solid circles: PEI; open diamonds: soluble.

2. Stabilization of HRP through 3D cross-linking in biomimetic silica nanoparticles.

2.1 Perform a mild oxidation *via* NaIO_4 as previously described (*see* 3.2). This treatment generates aldehyde groups on the sugar moieties of this highly glycosylated enzyme. Any glycosylated protein could be crosslinked after *in situ* entrapment in biomimetic silica. Additionally, any other chemical modification of the enzyme surface protein to introduce aldehyde groups could also allow for a 3D multipoint covalent immobilization of the encapsulated enzyme.

2.2 Assay the catalytic activity of the preparation after gel filtration in a PD-10 column into phosphate buffer 0.1 M pH 8.0.

2.3 Entrap the oxidized enzyme in silica nanoparticles as described in 3.3 using PEI 10%.

2.4 Incubate the immobilized preparation at pH 10 as described in 3.4. This incubation promotes the formation of Schiff's bases between the aldehyde groups of the enzyme (obtained by its oxidation) and unreacted amino groups of the PEI near the entrapped enzymatic structure. The reducing step *via* NaBH_4 transform the first reversible interaction

between the enzyme and the matrix, into a three-dimensional multiple covalent attachment of HRP within the silica particles.

2.5 After reduction, wash twice with phosphate buffer by centrifugation for 10 min at 4500g and resuspend in 25 mM phosphate buffer pH 7.0. Optimal results in terms of specific activity are obtained when using 5-7.5 mg/mL as starting HRP concentration (Table 2).

Table 2. Results obtained after *in situ* immobilization of HRP in biomimetic silica nanoparticles.

HRP (mg/ml)	Immobilization (%)	Y _A (%)	UI (UI/mg)
0.5	94 ± 3	50 ± 2	1.042 ± 4E-03
1	85 ± 2	59 ± 2	1.025 ± 2E-03
3	83 ± 2	53 ± 3	1.286 ± 4E-03
5	82 ± 4	49 ± 6	1.700 ± 7E-03
7.5	63 ± 4	42 ± 2	2.125 ± 5E-03
10	54 ± 3	12 ± 3	1.887 ± 8E-03
20	34 ± 5	10 ± 5	1.900 ± 7E-03

2.6 The studies on thermal stability demonstrated that the entrapped and cross-linked enzyme preparation presented a half life time of 156 min, significantly higher compared to the solely entrapped enzyme or the non immobilized HRP (53 and 2.4 min for their half-life time respectively) (Fig. 2).

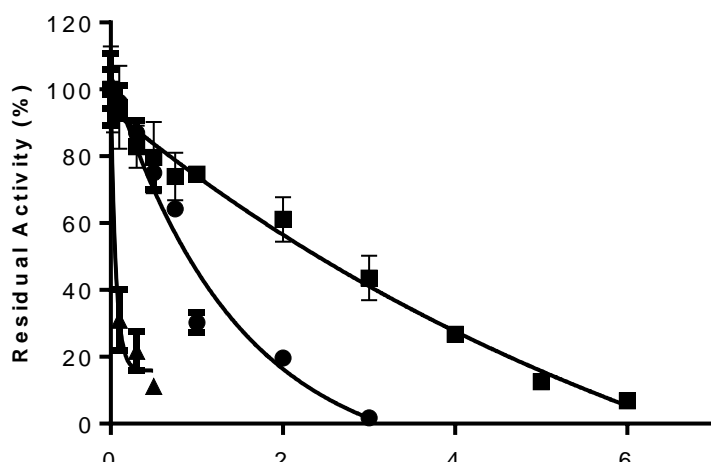


Fig 2. Graphical representation of the thermal stability at 50°C of the soluble (▲), entrapped enzyme (●) and the crosslinked entrapped enzyme (■). The half-life increased from 2.5 min to 53 min and 156 min, respectively. The experimental data was fitted to the exponential model from Henley and Sadana[20].

3. Use of alternate aminated catalysts for *in situ* entrapment of lipase from *Rygomucor miehei* (RML).

3.1 Perform a gel filtration of the commercial enzyme in a PD-10 column using sodium phosphate buffer 0.1 M pH 8.0. Measure the activity of the preparation.

Use of spermidine for *in situ* entrapment:

3.2 Prepare a 12 mg/mL solution of spermidine in sodium phosphate buffer 0.1 M pH 8.0 and a solution of silicic acid as described in the Methods section 3.3.

3.3 Mix 1 mL of gel filtrated RML with 0.5 mL spermidine solution.

3.4 Add 0.5 mL of silicic acid solution.

3.5 Centrifuge for 10 min at 4600g and wash once in sodium phosphate buffer 0.025 M, pH 7.0, 0.5 M NaCl and twice with sodium phosphate buffer 0.025 M, pH 7.0.

3.6 Measure the activity in the suspension.

Use of PEI for *in situ* entrapment:

3.7 Prepare a 10% PEI solution in sodium phosphate buffer 0.1 M pH 8.0 and a solution of silicic acid as described in the Methods section 3.3.

3.8 Mix 1 mL of gel filtrated RML with 0.1 mL of PEI solution.

3.9 Add 0.5 mL of silicic acid solution.

3.10 Centrifuge for 10 min at 4600g and wash once in sodium phosphate buffer 0.025 M, pH 7.0, 0.5 M NaCl and twice with sodium phosphate buffer 0.025 M, pH 7.0.

3.11 Measure the activity in the suspension.

3.12 Both immobilized preparations were significantly more stable than the soluble RML (Fig 3).

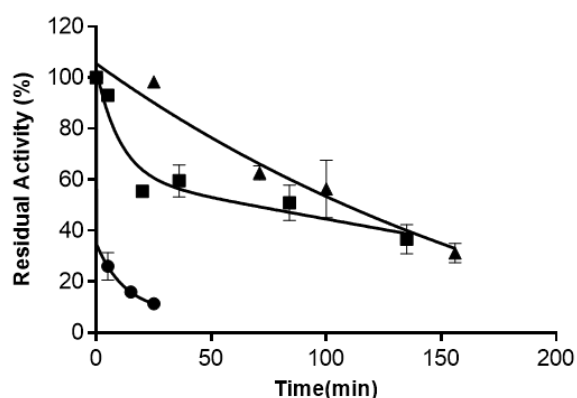


Fig 3. Thermal stability at 60°C of different RML preparations. Soluble enzyme (RML) (●), *in situ* entrapped enzyme using PEI (■), and *in situ* entrapped enzyme using spermidine (▲). The preparations were incubated in 25 mM sodium phosphate buffer pH 7.

4. Co-immobilization of the coupled enzyme system BtrH and BtrG.

The acyltransferase (BtrH) and γ -glutamyl cyclotransferase (BtrG) are two of the eight enzymes involved in the natural production of Butirosin B[21], a glycosidic antibiotic of relevance used to treat resistant infections. Previous works demonstrated the concerted action of these enzymes starting from synthetic precursors such as N-acetylcysteamine (SNAC) derivatives[22]. The following example involve the co-entrapment of both enzymes as a model of immobilized enzymatic system.

- 4.1 Prepare 1 mL solution of 0.2 mg of BtrH and 0.4 mg of BtrG in sodium phosphate buffer 0.1 M pH 8 and measure BtrH activity.
- 4.2 Add 0.25 mL of PEI 10% and mix.
- 4.3 Rapidly add 0.25 mL of previously hydrolyzed TMOS (silicic acid solution).
- 4.4 Mix the solution by inverting the tube three times.
- 4.5 Centrifuge for 10 min at 4600g and wash once in sodium phosphate buffer 0.1 M, pH 8.0, 0.5 M NaCl and twice with sodium phosphate buffer 0.1 M, pH 8.0.
- 4.6 Measure BtrH activity in the suspension to evaluate any possible loss in activity during immobilization.
- 4.7 *In situ* immobilization for the co-entrapment of BtrG and BtrH did not affect significantly the %I (Table 3).
- 4.8 Although the Y_A obtained for BtrH, the only activity that was possible to measure uncoupled with a chromogenic substrate, was low (Table 3), analysis by LC-MS using γ -Glu-AHBA-SNAC and ribostamycin as substrate showed the presence of butirosin B. This compound is the expected product of the concerted action of both enzymes which proved that BtrH was active in the nano-co-entrapped biocatalysts.

Table 3. Results obtained for the entrapment and co-entrapment of BtrH and BtrG

Encapsulated enzymes	Immobilization (%)	Y_A (%)
BtrG	$96.8 \pm 1.1^*$	ND
BtrH	89.7 ± 2.2	13.5 ± 2.01
BtrG and BtrH	75.2 ± 1.1	20 ± 3.5

*Determined using protein concentration

4.9 Characterization by scanning electron microscopy of the *in situ* co-entrapped preparation showed dispersed as well as interconnected nanoparticles of a mean diameter of ~110 nm (Fig 4). The shape and polydispersity obtained is similar for previously entrapped isolated proteins. However, the mean size obtained for the nanobiocatalyst is significantly smaller than reported entrapped proteins [16,17].

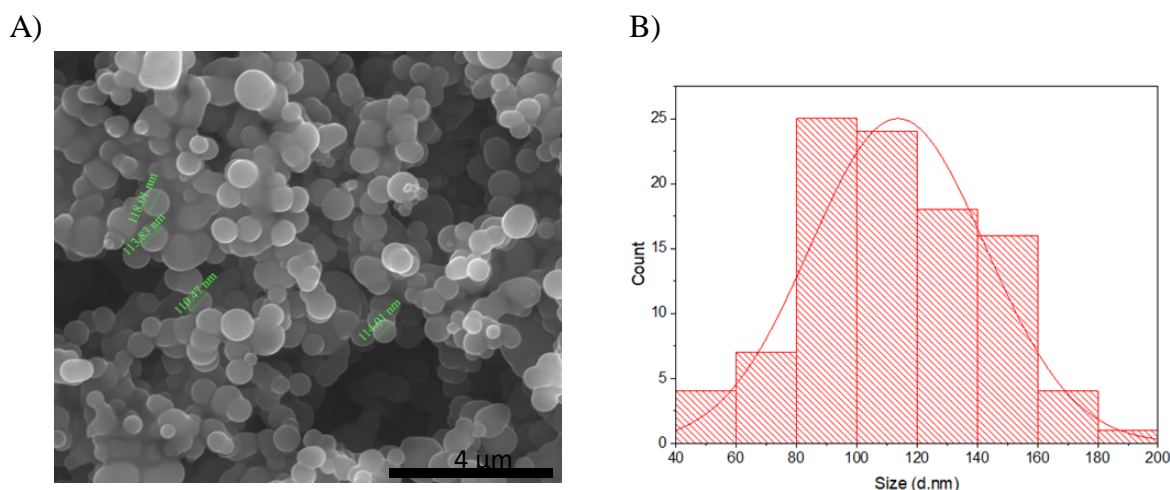


Fig 4. A) SEM analysis of *in situ* co-immobilized preparations of BtrH and BtrG. B) Histogram representation of nanoparticle diameters using Image J.

6. References

- [1] V. Krasňan, R. Stloukal, M. Rosenberg, M. Rebroš, Immobilization of cells and enzymes to LentiKats®, Appl. Microbiol. Biotechnol. 100 (2016) 2535–2553.
- [2] M. Monier, I. Youssef, D.A. Abdel-Latif, Synthesis of photo-responsive chitosan-cinnamate for efficient entrapment of β -galactosidase enzyme, React. Funct. Polym. 124 (2018) 129–138.
- [3] J. Zdarta, A. Meyer, T. Jesionowski, M. Pinelo, A General Overview of Support Materials for Enzyme Immobilization: Characteristics, Properties, Practical Utility, Catalysts. 8 (2018) 92-119.
- [4] D. Cazaban, L. Wilson, L. Betancor, Lipase immobilization on siliceous supports: Application to synthetic reactions, Curr. Org. Chem. 21 (2017) 96-103.
- [5] L. Ronda, S. Bruno, B. Campanini, A. Mozzarelli, S. Abbruzzetti, A. Cupane, M. Levantino, S. Bettati, Immobilization of Proteins in Silica Gel: Biochemical and

- Biophysical Properties 19 (2015) 1653–1668.
- [6] N. Kröger, N. Poulsen, Diatoms-from cell wall biogenesis to nanotechnology., *Annu. Rev. Genet.* 42 (2008) 83–107.
- [7] C. Lechner, C. Becker, Silaffins in Silica Biomineralization and Biomimetic Silica Precipitation, *Mar. Drugs.* 13 (2015) 5297–5333.
- [8] S.H. Yang, Biomimetic silica nanostructures on the surface, controlled by polyvalent counteranions, *Solid State Sci.* 23 (2013) 1–7.
- [9] L. Betancor, H.R. Luckarift, Bioinspired enzyme encapsulation for biocatalysis., *Trends Biotechnol.* 26 (2008) 566–572.
- [10] D. Cazaban, A. Illanes, L. Wilson, L. Betancor, Bio-inspired silica lipase nanobiocatalysts for the synthesis of fatty acid methyl esters, *Process Biochem.* (2018) In press.
- [11] S.K.S. Patel, S. V. Otari, Y. Chan Kang, J.-K. Lee, Protein–inorganic hybrid system for efficient his-tagged enzymes immobilization and its application in xylulose production, *RSC Adv.* 7 (2017) 3488–3494.
- [12] G.R. Johnson, H.R. Luckarift, Enzyme stabilization via bio-templated silicification reactions, *679* (2017) 85-97.
- [13] H.R. Luckarift, J.C. Spain, R.R. Naik, M.O. Stone, Enzyme immobilization in a biomimetic silica support, *Nat. Biotechnol.* 22 (2004) 211-213.
- [14] F. López-Gallego, E. Jackson, L. Betancor, Heterogeneous Systems Biocatalysis: The Path to the Fabrication of Self-Sufficient Artificial Metabolic Cells, *Chem. - A Eur. J.* 19 (2017) 17841-17849.
- [15] L. Betancor, G.R. Johnson, H.R. Luckarift, Stabilized Laccases as Heterogeneous Bioelectrocatalysts, *ChemCatChem.* 5 (2013) 46–60.
- [16] E. Jackson, M. Ferrari, C. Cuestas-Ayllon, R. Fernández-Pacheco, J. Perez-Carvajal, J.M. De La Fuente, V. Grazú, L. Betancor, Protein-templated biomimetic silica nanoparticles, *Langmuir.* 31 (2015) 3687–3695.
- [17] L. Zhou, C. Wang, Y. Jiang, J. Gao, Immobilization of papain in biosilica matrix and its catalytic property, *Chinese J. Chem. Eng.* 21 (2013) 670–675.
- [18] H. Li, W. Xiao, P. Xie, L. Zheng, Co-immobilization of enoate reductase with a cofactor-recycling partner enzyme, *Enzyme Microb. Technol.* 109 (2018) 66–73.
- [19] C. Berne, L. Betancor, H.R. Luckarift, J.C. Spain, Application of a microfluidic reactor for screening cancer prodrug activation using silica-immobilized nitrobenzene nitroreductase., *Biomacromolecules.* 7 (2006) 2631–2636.
- [20] J.P. Henley, A. Sadana, Categorization of enzyme deactivations using a series-type mechanism, *Enzyme Microb. Technol.* 7 (1985) 50–60.

- [21] Y. Li, N.M. Llewellyn, R. Giri, F. Huang, J.B. Spencer, Biosynthesis of the unique amino acid side chain of butirosin: Possible protective-group chemistry in an acyl carrier protein-mediated pathway, *Chem. Biol.* 12 (2005) 665–675.
- [22] N.M. Llewellyn, J.B. Spencer, Chemoenzymatic acylation of aminoglycoside antibiotics, *Chem. Commun.* (2008) 3786-3788.